THIN-FILM PHOTONIC CRYSTAL LEDS WITH ENHANCED DIRECTIONALITY

Krister Bergenek

A Thesis Submitted for the Degree of PhD
at the
University of St Andrews

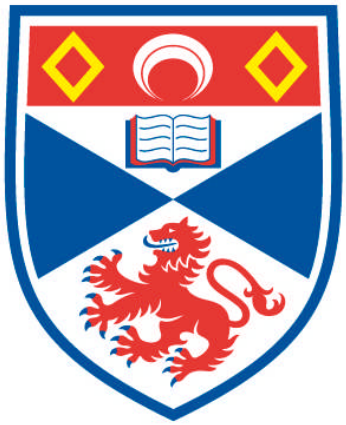

2009

Thin-film photonic crystal LEDs with enhanced directionality

Krister Bergenek

PhD Thesis

Date of submission: 2009-07-17

1st supervisor:

Professor Thomas F. Krauss

University of St Andrews, St Andrews, UK

2nd supervisor:

Dr. Ralph Wirth

Osram Opto Semiconductors GmbH, Regensburg, Germany

I, Krister Bergenek, hereby certify that none of the work contained in the books or papers in this portfolio, which record work substantially carried out by me, has been submitted by me for a higher degree in any other university.

Date: _____ Signature of candidate: _____

I was admitted as a research student in 25 September 2006 and as a candidate for the degree of PhC in 25 September 2006; the higher study for which this is a record was carried out between 2006 and 2009.

Date: _____ Signature of candidate: _____

I hereby certify that the candidate has fulfilled the conditions of the Resolution and Regulations appropriate for the degree of PhD in the University of St Andrews and that the candidate is qualified to submit this portfolio in application for that degree.

Date: _____ Signature of supervisor: _____

In submitting this portfolio to the University of St Andrews I understand that I am giving permission for it to be made available for use in accordance with the regulations of the University Library for the time being in force, subject to any copyright vested in the work not being affected thereby. I certify that I have obtained permission of all copyright holders for this action. I also understand that the title and abstract will be published, and that a copy of the work may be made and supplied to any bona fide library or research worker.

Date: _____ Signature of candidate: _____

The following is agreed request by candidate and supervisor regarding the publication of this thesis:

Embargo on both printed and electronic copy for the same fixed period of two years on the following ground: Publication would be commercially damaging to the researcher, or to the supervisor, or to the University.

Date: _____

Signature of candidate: _____ Signature of supervisor: _____

Directional photonic crystal thin-film light-emitting diodes

Krister Bergenek

Microphotonics Group, School of Physics and Astronomy, University of St Andrews, United Kingdom

The use of photonic crystals for light extraction from light-emitting diodes (LEDs) gives the possibility to shape the farfield emission pattern. This is of particular interest for étendue-limited LED applications that require a more directional farfield than state-of-the-art Lambertian emitters. However, the application of a photonic crystal in a LED results in directional emission only if the photonic crystal and the distribution of guided modes in the LED are tuned correctly. In this thesis, red- and blue-emitting thin-film PhC-LEDs in the AlGaInP and InGaN material systems were modelled, designed, fabricated and characterized. The first experimental results show that light extraction with photonic crystals from AlGaInP thin-film LEDs several microns thick is neither directional nor more efficient than state-of-the-art LEDs with a rough surface structure. Directional light extraction for AlGaInP PhC-LEDs is for the first time demonstrated in much thinner devices where the photonic crystal light extraction of guided modes is combined with the resonant-cavity effect. In an attempt to approach the ideal PhC-LED, strong photonic crystal farfield shaping is demonstrated in InGaN thin-film LEDs of sub-micron thickness. Analysis of their spectral farfields unexpectedly shows that high order diffraction contributes significantly to the light extraction efficiency if the mode absorption is sufficiently low. It is also demonstrated that directional photonic crystal light extraction is possible in InGaN thin-film LEDs several microns thick. The directionality stems from the modulation of the spontaneous emission caused by the proximity of the active region to the bottom mirror. Two new concepts for enhanced light extraction and high directionality are presented: Photonic crystals with two dominating lattice constants are found to outperform conventional photonic crystal LEDs. An alternative approach is the dielectric PhC-LED - FDTD simulations show that the high extraction efficiency of LEDs with surface roughness is combined with the higher directionality of photonic crystal light extraction.

ACKNOWLEDGEMENT

The work presented in this thesis would not have been possible without the support from many others. First of all I would like to thank my two supervisors: Prof. Thomas F. Krauss at the University of St Andrews and Dr. Ralph Wirth at Osram Opto Semiconductors GmbH in Regensburg. Thank you Thomas, for introducing me to the world of photonic crystals and for pushing the project forward with your knowledge, ideas and eagerness. *Danke* Ralph, for sharing your vast experience in how to make efficient LEDs and for supporting me in my daily work. I am also very grateful to Dr. Klaus Streubel, who offered me the opportunity to pursue my PhD project at Osram Opto Semiconductors in Regensburg in the first place. Furthermore, I would like to thank Christopher Wiesmann for all the simulations and the fruitful discussions about photonic crystal LEDs in the past three years. The discussions with Dr. Norbert Linder have also made an impact on the outcome of my work.

Several persons have been involved in the processing of my LED wafers. Dr. Petrus Sundgren, Dr. Rainer Butendeich and Dr. Hans-Jürgen Lugauer at Osram deserve credit for the epitaxial growth of my wafers as well as all process engineers from the department T PE at Osram for processing my wafers. A special thanks also to Nicole Stamm and Heike Fegerl for making sure that my lots always finally reached the end of front-of-line. Many hours have been spent in the measurement labs of the department T M – Dr. Siegmar Kugler and Jürgen Braun among others have helped when things have not worked as I wanted it. I would also like to express my gratitude to Dr. William Whelan-Curtin and all other colleagues in the Microphotonics Group in St Andrews, who introduced me to the e-beam lithography system and all other clean-room facilities. In 2007, the processing work carried out at MC2 Nanofabrication Laboratory, Chalmers University of Technology was financed by the FP6-Research Infrastructures program MC2ACCESS with Contract No: 026029. A special *tack* to Dr. Bengt Nilsson for helping me with the e-beam and to Dr. Ulf Södervall and Dr. Göran Alestig for all practical arrangements during my visits in Göteborg.

Finally, I would like to thank my family and friends in Germany and Sweden for giving me something else to think about than paper submissions and circles in the reciprocal plane. *Didi madloba* Sophia, for your daily support and for your patience while I have travelled around northern Europe to drill the all the holes that together constitute a photonic crystal.

LIST OF PAPERS

This portfolio thesis is based on the following papers:

I. Enhanced light extraction efficiency from AlGaInP thin-film light-emitting diodes with photonic crystals

K. Bergenek, Ch. Wiesmann, R. Wirth, L. O`Faolain, N. Linder, K. Streubel, T.F. Krauss, Applied Physics Letters 93, 041105 (2008)

II. Directional light extraction from thin-film resonant cavity light-emitting diodes with a photonic crystal

K. Bergenek, Ch. Wiesmann, H. Zull, R. Wirth, P. Sundgren, N. Linder, K. Streubel, T.F. Krauss, Applied Physics Letters 93, 231109 (2008)

III. Photonic crystal LEDs - designing light extraction

C. Wiesmann, K. Bergenek, N. Linder, U. T. Schwarz,
Laser & Photonics Review, Volume 3 Issue 3, 262-286 (2009)

IV. Beam-shaping properties of InGaN thin-film micro-cavity light-emitting diodes with photonic crystals

K. Bergenek, Ch. Wiesmann, H. Zull, C. Rumbolz, R. Wirth, N. Linder, K. Streubel, T. F. Krauss, SPIE Proceedings, Vol 7231, DOI: 10.1117/12.807617 (2009)

V. Strong high order diffraction of guided modes in micro-cavity light-emitting diodes with hexagonal photonic crystals

Krister Bergenek, Christopher Wiesmann, Heribert Zull, Christian Rumbolz, Ralph Wirth, Norbert Linder, Klaus Streubel and Thomas F. Krauss
Accepted for publication in IEEE Journal of Quantum Electronics on 23 April 2009

VI. Theoretical Investigation of the Radiation Pattern from LEDs Incorporating Shallow Photonic Crystals

Christopher Wiesmann, Krister Bergenek, Romauld Houdré, Ross P. Stanley, Norbert Linder and Ulrich T. Schwarz
Accepted for publication in IEEE Journal of Quantum Electronics on 14 May 2009

1. INTRODUCTION

The efficiency of light-emitting diodes (LEDs) that operate in the visible range has improved rapidly over the last decade and LED have now emerged as one of the most efficient among all light sources [1]. InGaN is the dominating material system for ultra-violet, blue and green LEDs, whereas AlGaInP-based devices cover the remaining visible spectrum from green to red. Blue-emitting InGaN LEDs are used together with phosphors to obtain highly efficient white light-emitters, enabling the replacement of the currently used incandescent and gas discharge lamps with solid state lighting (SSL) [2]. LEDs illuminate the LCD screens not only in small hand-held devices but lately also in notebooks and LCD TVs. Incandescent light sources are increasingly being replaced by LEDs also in automotive applications: initially used for dashboard backlighting, brake lights and signal lights, high-power LEDs are now also utilized for car head lights. Not only the energy efficiency, but also compactness, life-time and colour rendering are strong arguments for the replacement of incandescent and fluorescent lamps with LEDs.

The tremendous efficiency enhancement that has been achieved in recent years can be attributed to improved internal efficiency on the one hand, i.e. the light generation efficiency of the material, and on the other hand to improved light extraction efficiency of the generated light from the high index semiconductor. State-of-the-art LEDs are geometrically shaped to avoid total internal reflection and the top surface is randomly structured to scatter the light out of the LED. The random scattering results in a Lambertian emission pattern. Several optical systems using LEDs as light sources would gain efficiency if the light was emitted more directionally. Examples of such étendue limited optical systems are projectors, rear-projection TVs and car head lights. A more directional farfield could also be advantageous for white light applications since it increases the architectural freedom [2]. The objective of my work is to explore the potential of LEDs with photonic crystals for efficient and directional light extraction.

A photonic crystal is an artificial dielectric medium with a periodic variation of the refractive index and with a periodicity around the order of the wavelength of the light. The periodicity of the refractive index constrains the propagation of light. Photonic crystals were first proposed in 1987 with a view to inhibiting spontaneous emission in heterojunction bipolar transistors, semiconductor lasers and solar cells [3]. The

historical starting point of photonic crystal LEDs is usually dated to an article by Fan et al. [4] in 1997, although the concept of a single mode LED in a three-dimensional micro-cavity was suggested four years earlier [5]. The former was however based on a two-dimensional photonic crystal, shortly after the demonstration of a polarization-sensitive photonic bandgap at nearly visible wavelengths (*800-900nm*) using a two-dimensional photonic crystal [6]. The first weakly coupled photonic crystal LED design that did not influence the spontaneous emission but worked as a light extractor was demonstrated by Boroditsky et al [7] in 1999. It was found that the dominating effect in a shallow photonic crystal is Bragg diffraction [8]. It took until 2004 before the first electrically driven photonic crystal LEDs in the visible range were demonstrated [9]-[10]. In fact, the first electroluminescent organic LED with a diffracting Bragg grating was demonstrated three years earlier [11]. Very much progress was made in the field of InGaN PhC-LEDs in following years by David et al, which resulted in a series of published articles in late 2005 and early 2006 [12]-[15]. This includes the use of angular resolved spectra [12] for mode analysis (in this thesis referred to as spectrally resolved farfields) and the attempt to concentrate the spontaneous emission in a multi-mode LED mainly into one guided mode [13]. However, with the exception of [15], all published material until then dealt with photonic crystal light extraction from substrate LEDs. Meanwhile, commercial high-brightness LEDs were processed as thin-film LEDs with a highly reflecting metallic bottom mirror. The potential of PhC-LEDs in this form and how they compare to state-of-the-art LEDs using surface roughening was very much unknown when my project started in June 2006.

The objective of my work has been to design and fabricate PhC-LEDs in the visible range using the thin-film technology available for the AlGaInP as well as the InGaN material system. The unique ability of photonic crystals to shape the farfield radiation pattern of the LEDs has been the main focus of the work. However, directional emission can only be obtained when on the one hand the vertical layer stack of the LED itself is optimized for photonic crystal light extraction and on the other if the photonic crystal is adjusted to the right wavelength and resonant mode range.

My PhD project was conducted jointly between the University of St Andrews, UK and Osram Opto Semiconductors GmbH, Regensburg, Germany. My working place has primarily been in the department Conceptual Engineering at Osram and I have visited

St Andrews mainly for the processing of photonic crystals. The need to define photonic crystals on 100mm LED wafers led me back to my old home university Chalmers University of Technology, Göteborg, Sweden. This portfolio thesis is based on its six appended papers. The aim of the following text is to summarize, generalize and sometimes complement the conclusions that have been drawn from the experimental results and the simulation results in these publications. Example figures have been taken from the publications where appropriate to link the text to the published material. These figures have a dashed frame and a reference to the original paper is made in the caption. Chapter 2 gives a brief introduction to the light-emitting diode (2.1) and the spontaneous emission in a cavity is derived in 2.2. The different efficiency definitions for LEDs are presented (2.3) and the parameters influencing the internal efficiency (2.4) and the extraction efficiency (2.5) are discussed. The influence of the farfield radiation pattern on the efficiency for étendue limited optical systems is introduced in Section 2.6. The process flow for thin-film LEDs is sketched in Section 2.7 and the efficiency of state-of-the-art LEDs is thereafter presented in 2.8. The standard characterization methods of photonic crystal LEDs are described in Section 3.1 whereas the measurement and analysis of spectrally resolved farfields are dealt with in Section 3.2. The photonic crystal is introduced in 4.1 before its application in LEDs is discussed in 4.2. The diffraction type PhC-LED, which is the objective of this work, is discussed in more detail in Section 4.3. The single mode LED is the simplest and at the same time ideal case of a photonic crystal light extraction device. The extraction efficiency for this LED is calculated for different photonic crystal parameters and absorption regimes – this is a generalization of the extraction efficiency calculations in Paper V. Chapter 5 deals with the design of real (multi-mode) LEDs. The two simulation models developed by Christopher Wiesmann are described in Section 5.1. The design of the vertical layer stack to maximize the use of the photonic crystal is discussed in 5.2. Thereafter, we flip the coin and optimize the photonic crystals to maximize their use in the LED (5.3). The trends for AlGaInP and InGaN PhC-LEDs are then discussed separately in Section 5.4 and 5.5, respectively. A critical discussion of the potential of PhC-LEDs relative to state-of-the-art is included in these both sections. Two new concepts that are not mentioned in any of the appended papers are introduced in Chapter 6, namely the dual photonic lattice and the dielectric photonic crystal LED. The portfolio thesis is rounded up with my conclusions (Chapter 7), followed by a summary of the appended papers.

2. LIGHT-EMITTING DIODES

2.1 The light-emitting diode

A light-emitting diode (LED) transforms electrical energy into light emission through a radiative recombination of an electron-hole pair in the junction between a p-doped and a n-doped semiconductor material. With no applied bias the junction is depleted of carriers (electrons and holes). The depletion region is charged due to the ionized acceptors and donors with concentration N_A and N_D, which induces an electrical field. In equilibrium, the drift current caused by the electric field cancels the diffusion current across the junction (Fig. 1(a)). When a positive bias is applied, the voltage drops across the depletion region and the barriers seen by the electrons and holes are lowered. This enables majority carriers (electrons from the n-side, holes from the p-side) to diffuse into the depletion region where they can recombine (Fig. 1(b)). The diffusion current is governed by Boltzmann statistics and is described by the Shockley equation:

$$I = eA \cdot \left(\sqrt{\frac{D_p}{\tau_p}} \cdot \frac{n_i^2}{N_D} + \sqrt{\frac{D_n}{\tau_n}} \cdot \frac{n_i^2}{N_A} \right) \cdot \left(e^{eV/kT} - 1 \right) \tag{1}$$

$D_{n(p)}$ and $\tau_{n(p)}$ are the electron (hole) diffusion constant and the electron (hole) minority carrier lifetime, respectively and n_i is the intrinsic carrier concentration. The recombination can be radiative if the semiconductor has a direct band gap. The simplest form of an LED is the p-n homo-junction consisting of n-doped and p-doped material of the same material composition. The efficiency of such devices is very low since the minority carriers can diffuse far into the side of the junction, resulting in a low minority carrier density. In this regime, non-radiative recombination will dominate. This will be discussed further in Section 2.5.

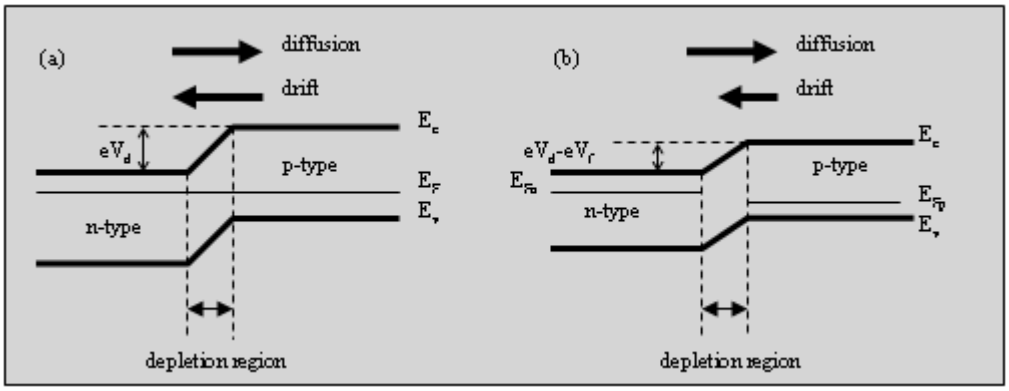

Fig. 1 A p-n homo-junction consists of a n-doped side and a p-doped side. The carriers near the interface have diffused to the other side, creating a charged depletion region with ionized atoms. At equilibrium (a) the diffusion current and the drift current caused by the electric field cancel each other. When a positive bias is applied, the barrier height is lowered and carriers can diffuse to the other side, where they recombine (b).

Higher carrier density can be obtained by sandwiching the active material between a semiconductor with a larger band gap. This confines the carriers to a small active region, since they cannot diffuse into the large band gap material. A further advantage with a heterostructure is that once the emitted photons have escaped out of the active region, they cannot be absorbed in the surrounding material, due to its larger bandgap. Even higher carrier density (resulting in higher radiative recombination rates) can be achieved in a quantum well (QW) that is typically thinner than 10 nm. The smaller volume of active material further reduces the re-absorption of emitted photons. Carrier overflow is typically avoided by employing a multiple quantum well (MQW) structure.

2.2 Spontaneous Emission in a Cavity

In this section we will derive the spontaneous emission from a dipole in a cavity (i.e. in a LED) and see how discrete guided modes and resonant Fabry-Perot modes are formed. The impact of the cavity on the dipole emission properties is of great importance since it alters the internal efficiency, the extraction efficiency and the farfield radiation pattern of the extracted light.

Here we follow the derivation of spontaneous emission in a cavity given in [16]. Consider a dipole situated in a cavity with length L between two mirrors/layer interfaces with reflectivity and transmittance (r_1,T_1) and (r_2,T_2) and at the distance d from the bottom mirror (Fig. 2) that emits light with the vacuum wavelength λ_0. The emitted intensity with the internal angle θ (see Fig. 2) out of mirror 1 is then given by:

$$I_{dipole}(\theta) = T_1 \cdot |(A_{dipole,up} + A_{dipole,down} \cdot r_2 \cdot e^{-j2\phi_{2,eff}}) \times \ldots \quad (2)$$

$$\ldots \times (1 + r_1 r_2 \cdot e^{-j2\phi} + (r_1 r_2 \cdot e^{-j2\phi})^2 + \ldots)|^2 =$$

$$= T_1 \cdot \frac{|A_{dipole,up} + A_{dipole,down} \cdot r_2 \cdot e^{-j2\phi_{2,eff}}|^2}{|1 - r_1 r_2 \cdot e^{-j2\phi_{eff}}|^2} \quad (3)$$

$A_{dipole,up/down}$ is here the dipole's plane wave component for light being emitted upwards and downwards, respectively. $2\Phi_{eff} = 2\Phi - \arg(r_1) - \arg(r_2)$ is the effective phase shift from one round-trip in the cavity and Φ is:

$$\phi = n \cdot k_0 \cdot L \cdot \cos\theta \quad (4)$$

$k_0 = 2\pi/\lambda_0$ is the vacuum wave-number of the light. Similarly, $2\Phi_{2,eff} = 2\Phi_2 - \arg(r_2)$, where $\Phi_2 = n \cdot k_0 \cdot d \cdot \cos\theta$. The expression in the first bracket in Eq. (2) corresponds to the sum of the dipole strength emitted upwards and the dipole strength emitted downwards, being reflected at the bottom mirror and propagated back to the source position with the following phase shift $e^{-j2\phi_{2,eff}}$. The expression in the second bracket in Eq. (2) sums up the intensity for all roundtrips in the cavity: 1 is the power that is transmitted when incident on mirror 1 for the first time. After one round-trip in the cavity the remaining power is $r_1 r_2 \cdot e^{-j2\phi_{eff}}$ and so on. The second bracket is a geometrical series so that the expression in Eq. (3) is obtained. The denominator is called the Airy factor which has minima for:

$$2\phi_{eff} \approx 2 \cdot n \cdot k_0 \cdot L \cdot \cos\theta - \arg(r_2) - \arg(r_1) = 2m\pi \quad (5)$$

As a result, the dipole emission is stronger for certain angles θ where Eq. (5) is fulfilled. The resonances that lie within the critical angle are extracted (i.e $T_1 \neq 0$) and these are called Fabry-Perot (FP) resonances or FP-modes. The guided mode distribution is obtained by omitting the T_1-factor in Eq. (2)-(3). With $r_1 = r_2 = 1$, Eq. (2) diverges at the resonance angles where Eq. (5) is fulfilled. Hence, light is only being emitted into a discrete set of guided modes with a propagation angle given by (here neglecting any reflection phase shifts):

$$\cos\theta = \left(\frac{m \cdot \pi}{n \cdot k_0 \cdot L}\right) = \left(\frac{m \cdot \lambda}{2 \cdot n \cdot L}\right) \quad (6)$$

The thickness L of the cavity determines the number of solutions to Eq. (6) and therefore the number of modes. The numerator of Eq. (3) is called the standing wave-factor. The reflected wave can either interfere constructively or destructively with the light wave emitted upwards. Hence, the light emission is cancelled for $\Phi_{2,eff} = (2m+1)\pi$

and constructive interference occurs for $\Phi_{2,eff} = 2m\pi$. The numerator does not depend on the cavity thickness but on the distance between the bottom mirror and the dipole source. In conclusion, the minima for the denominator give the propagation angles of the guided modes and the numerator determines to what degree the modes are filled, for the given dipole position. Emission occurs only to every second mode in a symmetric cavity with the dipole source in the centre of the cavity. It is convenient to express the guided modes in terms of in-plane k-vectors. In Fig. 2 we see that $\sin\theta = k_{||}/nk_0$ and we define the effective index of the mode as.[1]:

$$k_i = n_{eff} = \beta_i = n\sin\theta = k_{\parallel}/k_0 \qquad (7)$$

Modes with $k_i < 1$ correspond to Fabry-Perot modes. The range of guided modes is given by $k_i \in (1,n)$, where n is the refractive index seen by the radiating dipole.

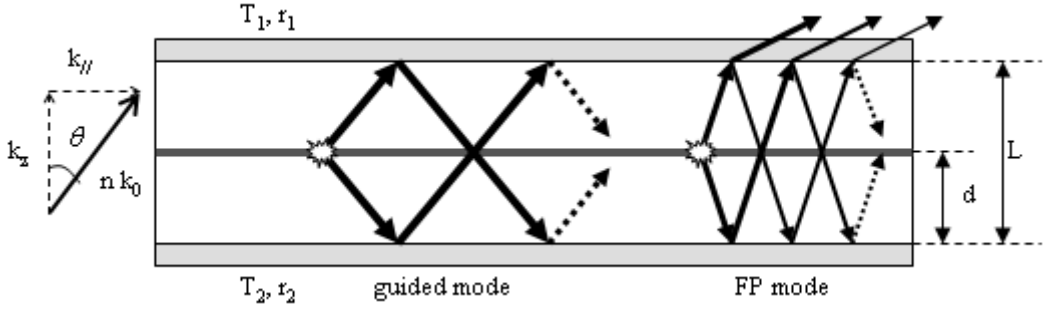

Fig. 2 Spontaneous emission from a dipole in a cavity to a guided mode and to a radiating FP mode. The distinction between the two is provided by the angle θ, i.e. whether θ is larger than the critical angle and the light is totally internally reflected to yield a guided mode or not.

The modification of the spontaneous emission in the cavity changes the internal efficiency, the extraction efficiency and the farfield radiation pattern. The internal efficiency is enhanced if the total radiative recombination rate in the cavity (integrated over all angles and dipoles) according to Eq. (2) is higher than in bulk material. This is called the Purcell effect [17]. The cavity effect on the extraction efficiency and the farfield radiation pattern will be discussed in Section 2.5.

[1] n_{eff} is used in Paper I and II and β_i is used in Paper III and VI. In this thesis we denote the effective index k_i like in Paper IV and V.

2.3 Efficiency definitions for light-emitting diodes

The efficiency of LEDs is usually expressed as the wall-plug efficiency η_{WP} or the external quantum efficiency η_{QE}. The former is of interest for the LED user since it simply expresses the ratio of the output optical power Φ_e (radiant flux) to the input electrical power:

$$\eta_{WP} = \frac{\Phi_e}{I \cdot U_f} \tag{8}$$

I is the current and U_f the forward voltage. The external quantum efficiency is more often used in science and it expresses the ratio

$$\eta_{QE} = \frac{\#emitted\_photons}{\#injected\_electrons} = \frac{\Phi_e / (h\upsilon)}{I / e} \tag{9}$$

where h is Planck's constant and $\upsilon = c/\lambda$ is the light frequency. The η_{QE} is 100% if every injected electron and hole recombine radiatively in the active region and the emitted photon escapes out of the LED. The difference between the two efficiencies (8) and (9) is that the latter does not consider the energy required for injecting an electron-hole pair. Ohmic losses are therefore not taken into account. The relation between η_{QE} and η_{WP} is given by:

$$\eta_{QE} = \eta_{WP} \cdot \frac{e \cdot U_f}{h\upsilon} \tag{10}$$

The external quantum efficiency can in turn be divided into injection efficiency η_{inj}, radiative efficiency η_{rad} and extraction efficiency η_{extr}:

$$\eta_{QE} = \eta_{inj} \cdot \eta_{rad} \cdot \eta_{extr} = \eta_{\text{int}} \cdot \eta_{extr} \tag{11}$$

The injection efficiency expresses the probability with which the carriers are injected into the active region, whereas the radiative efficiency is the probability that the carriers in the active region recombine radiatively. Since these efficiencies are closely interconnected, they are usually bundled into the internal quantum efficiency η_{int}.

2.4 Internal Efficiency

In order to deduce the internal efficiency of a LED, we start from a recombination rate equation as a function of the carrier concentration ∂n in the active region with width w [18]:

$$\frac{J - J_{leak}}{qw} = A \cdot \partial n + B \cdot \partial n^2 + C \cdot \partial n^3 \qquad (12)$$

q is here the elementary charge, A is the non-radiative Shockley-Read-Hall recombination rate, B is the radiative recombination rate and C is the non-radiative Auger recombination rate. At low currents densities J, the Auger term and the leakage current J_{leak} can be neglected and the internal efficiency can be expressed as:

$$\eta_{\text{int}} = \frac{B \cdot \partial n}{B \cdot \partial n + A} \qquad (13)$$

B can be enhanced with the Purcell effect as described in Section 2.2 whereas the non-radiative recombination via deep levels in the electronic bandgap is caused by defects in the crystal lattice. Eq. (13) shows that high carrier concentration is needed for high efficiency and thus, high doping of the p-type and n-type material is desired. On the other hand, high doping concentrations causes higher defect densities and therefore higher non-radiative recombination rates. The internal efficiency at low current density therefore depends very much on the quality of the epitaxially grown layers and their doping profile.

Current leakage and Auger recombination limit the internal efficiency at high current densities. The leakage current density J_{leak} also depends quadratically on ∂n [18] :

$$\frac{J_{leak}}{qw} = D \cdot \partial n^2 \cdot \exp\left(\frac{E_g^{active} - E_g^{conf}}{k_B T} \right) \qquad (14)$$

The Boltzmann factor in Eq. (14) results in high leakage current when the bandgap energy difference between the active material and the confinement layers is low and when the junction temperature is high. AlGaInP LEDs have rather low confinement energy and this makes them more prone to current leakage. The Auger term in Eq. (12) is only important at high current densities. Auger recombination is one of the proposed causes of the efficiency “droop” in InGaN LEDs at high current densities [19]-[20].

2.5 Extraction Efficiency

The low extraction efficiency of planar LEDs has been the largest obstacle towards obtaining high efficiencies and increasing this efficiency is still a lively field of research. Let us consider a light ray incident on the semiconductor-air interface with the angle θ_i to the surface normal. The angle of refraction θ_t is given by Snell's law:

$$n_{sc} \cdot \sin\theta_i = n_{air} \cdot \sin\theta_t \qquad (15)$$

For $\theta_t = 90°$ no light is extracted to air and the corresponding critical incident angle for total internal reflection (TIR) is:

$$\theta_c = \arcsin(n_{air} / n_{sc}) \qquad (16)$$

The critical angle is *17°* for AlGaInP ($n \approx 3.5$) and *24°* for GaN ($n \approx 2.5$). If we neglect Fresnel reflection and absorption of photons in the semiconductor, the extraction efficiency is given by the fraction of the totally emitted light within the critical angle. With isotropic internal emission this equals the fraction of the area element of the unity sphere with $\theta < \theta_c$ and the area of the unity sphere:

$$\eta_{extr} = \frac{dA}{A} = \frac{\int_0^{\theta_c} 2\pi \cdot r \cdot \sin\theta \cdot r \cdot d\theta}{4\pi \cdot r^2} = \frac{1}{2}\left(1 - \cos\theta_c\right) \approx \frac{1}{4n^2} \qquad (17)$$

The extraction efficiency from the top surface of a semiconductor slab is then *2%* (AlGaInP) and *4%* (InGaN).

Geometrical solutions to the light extraction problem

The very low extraction efficiency from the top surface can be improved in several ways:

By encapsulating the LED in epoxy or silicon with $n \approx 1.5$, the critical angle is shifted to *25°* and *37°* for AlGaInP and InGaN, respectively. Using Eq. (17), the extraction efficiency into the encapsulant is more than doubled to *5%* and *10%*, respectively. The extraction efficiency to air via the encapsulation does not change in a planar encapsulant design. The problem of TIR at the semiconductor-air interface is just divided between the two interfaces semiconductor-encapsulant and encapsulant-air. However, the encapsulant can easily be shaped like a dome to avoid TIR at the encapsulant-air interface.

Further improvement of the efficiency is obtained by removing the growth substrate (which is absorbing for AlGaInP LEDs) and by incorporating a metallic mirror that

reflects the light emitted downwards towards the top surface. Substrate removal is a key feature of the thin-film technology [21] described in Section 2.7.

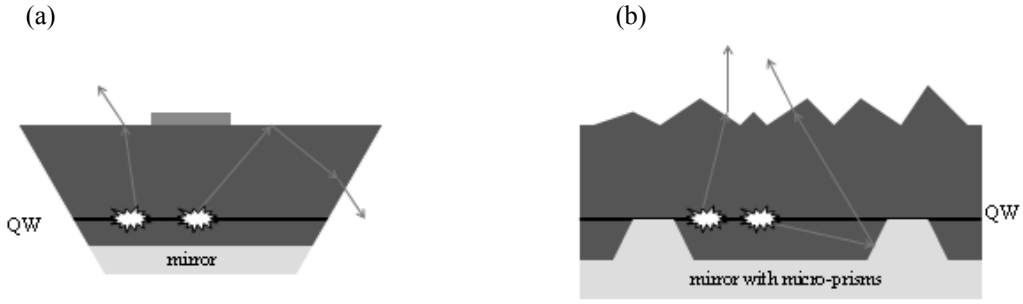

Fig. 3 The light extraction problem can be solved geometrically. TIP-LED (a) and thin-film LED with micro-prisms and a rough surface (b).

The laterally propagating light can be reflected towards the top surface by a slanted side-wall as in the TIP-LED (truncated inverted pyramid) [22] or by micro-prisms [23] in a thin-film LED (Fig. 3). The former method is not scalable since light is only reflected at the chip edge. Micro-prisms on the other hand can be incorporated in LEDs of any size.

Finally, the surface of the LED can be structured in order to avoid total internal reflection. This can be done with a random surface structure [24] or with a diffracting photonic crystal grating, which is the topic of this thesis. The random surface structure in a surface roughening LED (SR-LED) is typically on a micron or sub-micron scale and is most commonly used commercially today. The rough surface can look quite different as seen in Fig. 4 depending on how it is made.

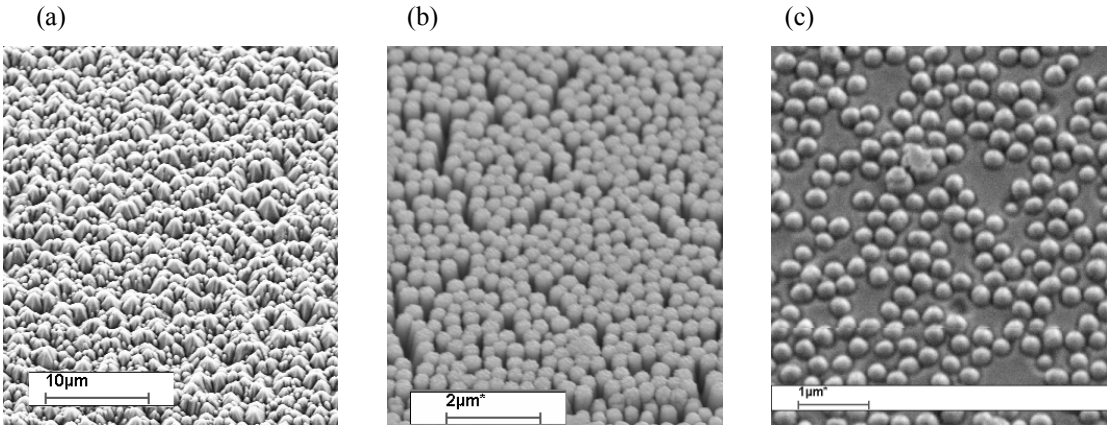

Fig. 4 Scanning electron images of three rough LED surfaces. The topology of the surface depends on the process used.

From a ray-optic point of view, the incident light ray "sees" multiple surfaces with different angles of incidence. The incident angle for one light ray is therefore randomized and the result is a random scattering mechanism of the light. A fraction of the incident light is then scattered to air and the light that is reflected back can be assumed to have a randomized propagation angle. In a thin-film design with a bottom mirror, this light will be reflected back towards the surface for another escape chance. In the absence of internal absorption, all light would be extracted to air after some propagation length, regardless of the strength of the extraction mechanism. But part of the back-reflected light is absorbed in the active region, the bulk semiconductor and at the mirror for every round-trip. The final extraction efficiency is therefore given by the relation between the absorption length L_{abs} and the extraction length L_{extr}:

$$\eta_{extr} = \frac{1/L_{extr}}{1/L_{extr} + 1/L_{abs}} = \frac{1}{1 + L_{extr}/L_{abs}} \tag{18}$$

This expression gives a good conceptual insight, although it is somewhat simplified. It should ideally be specified for every guided mode of the system, since each mode has a different absorption and extraction length.

The resonant-cavity LED

As discussed in Section 2.2, the extraction efficiency can be improved by changing the spontaneous emission in a resonant cavity [25]. A detailed discussion about the resonant-cavity LED can be found in [26]- [27]. In high finesse cavities, i.e. where the FWHM of the Airy factor resonances is small, the extraction efficiency is approximately

$$\eta_{extr} \approx \frac{1}{m_c} \tag{19}$$

where $m_c \approx (2 \cdot n \cdot L)/\lambda$ is the cavity order. If the dipole is situated in the centre of the cavity, this extraction efficiency can be enhanced by a factor two at most [16]. Absorption is neglected in this case. Hence, the extraction efficiency is enhanced in very thin cavities. Possible resonant-cavity LED designs are shown in Fig. 5. Distributed Bragg Reflectors (DBR) (a) or metallic mirrors (b-c) are commonly used as bottom mirror. A metal mirror has the advantage that it is reflecting omnidirectionally, whereas DBRs have high reflectivity only for a limited angle range and wavelength range. The top mirror is typically a DBR (a-b) or simply the semiconductor-air interface (c). The ideal reflectivity of the top mirror is an optimization problem and depends on

the absorption in the active region and in the bottom mirror. High intra-cavity losses require a rather low reflectivity so that the light escapes out of the cavity after just a few round-trips in the cavity. Additionally, high reflectivity DBRs requires a large number of periods which in turn increases the effective cavity length. The top DBR used for the AlGaInP PhC-RCLED in Paper II has seven periods and a reflectivity of just 35%. State-of-the-art LEDs have current spreading layers several microns thick to ensure homogenous current distribution over the LED chip. This layer must therefore be outside the cavity. The use of a transparent conductive oxide (TCO) on top of the RCLED enables a very thin vertical layer (c) stack while maintaining very good current spreading. This design was used in Paper II.

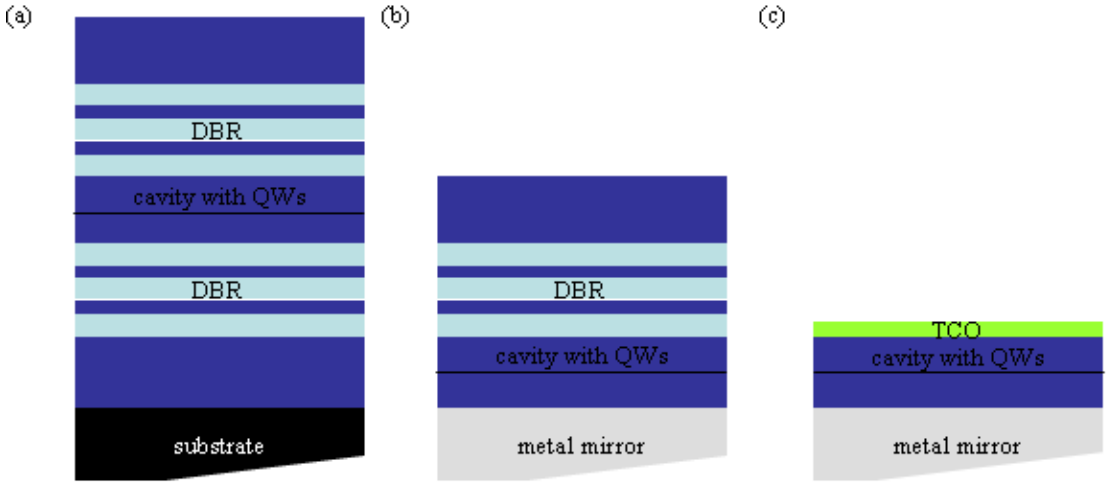

Fig. 5 Different resonant-cavity LED designs. The cavity is defined by two DBRs in a substrate LED (a). Thin-film RCLEDs (b-c) have a bottom metal mirror and an optional top DBR. Very thin LEDs require a transparent conductive oxide (TCO) to enable current spreading (c).

The available materials also set limits for the RCLED design. A top DBR on an InGaN RCLED would require the growth of AlGaN-layers with high Al content to get a reasonable refractive index contrast between the two materials in the DBR. The higher Al content induces strain to the material which reduces the internal efficiency of the subsequently grown active region. Furthermore, the electrical conductivity is much worse in high Al layers. AlGaN/GaN DBRs are therefore not a feasible alternative for InGaN RCLEDs. InGaN RCLEDs without a top DBR [28], with a dielectric DBR [29]-[30] and GaN/air-gap DBR [31] are alternatives found in literature.

The resonant-cavity LED has gained a lot of interest since the farfield radiation pattern can be tuned so that more light is emitted normal to the LED surface. Directional farfields [32] as well as batwing farfields [33], [34] have been demonstrated for AlGaInP RCLEDs. Batwing farfields yield the highest extraction efficiency but have lower directionality. Hence, there is a trade-off between high directionality and high extraction efficiency [26], [35]. The extraction efficiency and the farfield also change as the wavelength change with varying temperature or current [34]. Furthermore, RCLEDs cannot compete with surface-roughness LEDs regarding efficiency. Simulations have shown that even a close to ideal InGaN RCLED would have an extraction efficiency in encapsulation of $\eta_{extr} = 44\%$ [36] – much lower than for state-of-the-art InGaN LEDs that can achieve up to *85%* (see Section 2.8). Hence, the increase in extraction efficiency with the RCLED effect alone is not sufficient to outperform state-of-the-art LEDs. However, the directional emission from the RCLED is ideal in combination with a photonic crystal (Paper II) that diffracts the remaining guided modes to air.

Photon Recycling

Photons propagating in the LED can be re-absorbed in the active region and create a new electron-hole pair. The subsequent emission of a new photon occurs with the probability η_{int}. The re-absorption and re-emission processes are independent from each other and the photon is therefore emitted into any state given by Eq. (3). Since radiating modes escape quickly from the active region, they are less prone to re-absorption in the active region. Re-absorption therefore occurs mostly from guided modes. The net effect of this re-absorption – re-emission process called photon recycling is thus a re-distribution of light from guided modes to radiating modes. The extraction efficiency is therefore enhanced by photon recycling and is now a function of the internal quantum efficiency [27]:

$$\eta_{extr,eff} = \frac{\eta_{extr}}{1-(1-\eta_{extr})\cdot P_{abs}\cdot\eta_{\mathrm{int}}} \tag{20}$$

Here, η_{extr} is the extraction efficiency without photon recycling and P_{abs} is the re-absorption probability of the light emitted into guided modes. Photon recycling contributes significantly to the extraction efficiency in AlGaInP LEDs since they have high internal efficiency and rather thick active layers. Ray-tracing simulations in [18] showed that the extraction efficiency in AlGaInP LEDs can be enhanced by a factor larger than 3 due to photon-recycling. An even larger photon recycling enhancement

was found in Paper I: The simulated extraction efficiency without photon recycling and the measured external quantum efficiency for an unstructured AlGaInP LED in Paper I differed by almost a factor 4. Photon recycling is much less important for the extraction efficiency of InGaN LEDs. These have higher direct light extraction due to the lower refractive index compared to AlGaInP. The recycling probability is also much lower since the internal quantum efficiency is lower (see Section 2.8) and the active layer is much thinner than for AlGaInP LEDs.

2.6 Efficiency of étendue limited optical systems with LEDs

The efficiency of an optical system as a whole does not only depend on the efficiency of the light source. Many optical systems have a small étendue E_{sys}, which describes the phase space of light that can pass the system. In order to couple all the light to the optical system, the étendue of the light source E_{source} must be smaller or equal to the étendue of the optical system. A small emitting area A_E and a small extraction angle θ_E of the emitted light are needed to couple light to an optical system with a small étendue. Hence, the acceptance angle of the emitted light to the system is determined by the étendue E_{sys} of the system and the area A_E of the light-emitter and it reads [37]:

$$E_{source} = n^2 \cdot \pi \cdot \sin^2 \theta_E \cdot A_E \leq E_{sys} \qquad (21)$$

We assume that the refractive index n of the medium into which the light is emitted is 1 (e.g. emission to air). For optical systems with $E_{sys} >> \pi \cdot A_E$, light emitted from the LED surface in all directions $|\theta| < 90°$ can be used. The useful radiant flux is then

$$\Phi_E = M \cdot A_E \qquad (22)$$

M is here the radiant emittance (W/m^2) from the LED surface. If higher flux is required, the area of the light source can be increased. The useful radiant flux is linearly proportional to the surface area (assuming constant M, i.e. constant current density) until $E_{sys} = \pi \cdot A_E$. If the emitting area is made even larger, only light within the angle θ_E can be used according to Eq. (21). The useful radiant flux is now:

$$\Phi_E = M \cdot A_E \cdot D(\theta_E) \qquad (23)$$

$D(\theta_E)$ is the directionality and is defined as the fraction of the totally emitted flux that is emitted within the acceptance angle θ_E. The flux through the system decreases as the system étendue gets smaller, since more and more light is wasted. From Eq. (23) it is obvious that higher directionality leads to higher system efficiency. It is less obvious

that the étendue actually limits the flux Φ_E from a Lambertian emitter that can be coupled to the system. The directionality for a Lambertian emitter is $D_{Lam}(\theta) = \sin^2\theta$. The largest useful light-emitting area for a given E_{sys} and θ_E is calculated from Eq. (21):

$$A_{E,\max} = \frac{E_{sys}}{n^2 \cdot \pi \cdot \sin^2 \theta_E} \tag{24}$$

The insertion of Eq. (24) in Eq. (23) gives the highest possible radiant flux:

$$\Phi_E = M \cdot A_E \cdot D_{Lam}(\theta_E) = M \cdot \frac{E_{sys}}{n^2 \cdot \pi \cdot \sin^2 \theta_E} \cdot \sin^2 \theta_E = M \cdot \frac{E_{sys}}{n^2 \cdot \pi} \tag{25}$$

Eq. (25) shows that the additional flux obtained by using a larger area is exactly cancelled by the smaller acceptance angle so that Φ_E remains constant for a Lambertian emitter, independent of the area of the light emitter. A super-Lambertian radiation pattern ($D(\theta) > \sin^2\theta$) is required to further increase the useful flux.

Fig. 6 shows the flux to an optical system with étendue E_{sys} where the emitter area A_E and radiant emittance $M=1$ is held constant. The Lambertian emission pattern is compared with the farfield pattern from the ideal single-mode PhC-LED with $D(\theta) = \sin\theta$ as discussed later in Section 4.3 (and in Paper VI). The two LEDs perform equally well as long as all emitted light can be coupled to the system. But the ideal PhC-LED outperforms the Lambertian emitter as long as the étendue $E_{sys} < \pi \cdot A_E$.

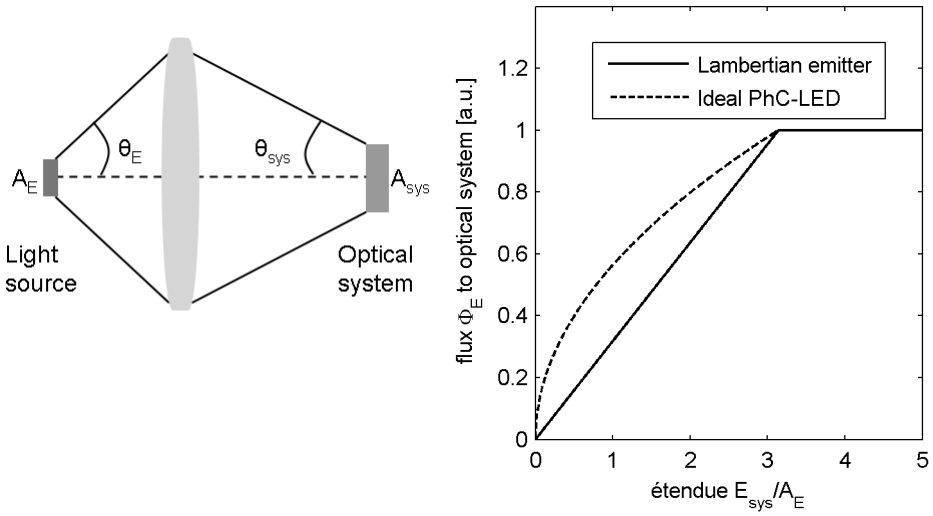

Fig. 6 Étendue limited optical system (a) [Figure 24 Paper III]. Only a fraction of the light emitted within $\theta < \theta_E$ can be coupled to the system on the right hand side of the figure. Total flux to an optical system with étendue E for a Lambertian emitter and for the ideal PhC-LED (see Section 4.3) (b). All light emitted light from the chip can be coupled to the system as long as $E_{sys} > \pi \cdot A_E$. The higher directionality for the ideal PhC-LEDs leads to higher flux in the optical system when the étendue $E_{sys} < \pi \cdot A_E$.

Let us go back to Eq. (21) and the role of the refractive index of the medium into which the light is emitted. The étendue grows with n^2, which limits the largest possible emitting area. The encapsulation of the LED in a dielectric is therefore counter-productive. The higher extraction efficiency (typically less than *50%*) obtained in encapsulation is more than compensated, since the area has to be reduced by a factor $n^2 \approx 1.5^2 = 2.25$ to conserve the étendue.

Examples of étendue limited optical systems where LEDs are used are projection based systems, such as rear-projection TVs, head-up displays and projectors as well as car head lights. Light coupling to an optical fibre is of course also strongly limited by the étendue.

In conclusion, we have seen that the system efficiency of an optical system with a small étendue depends on the farfield radiation pattern and the area of the light emitter. A Lambertian emitter is not suited for such applications, since the useful radiant flux cannot be increased by increasing the emitting area. A super-Lambertian emission pattern – for example from an ideal PhC-LED – enhances the system efficiency (for a

given LED chip size) and the highest possible radiant flux (by increasing the emitting area).

2.7 Fabrication of thin-film LEDs

The fabrication of thin-film LEDs is summarized in the following section. Almost identical LED chips can be produced with a large number of work-flows where each has advantages and disadvantages. The material system (InGaN or AlGaInP) requires different processing techniques and chemistry. The intention with this section is to give the reader an overview of the processing required to realize a thin-film LED rather than to give the complete picture of the processing for a single chip design. More detailed description of thin-film LED processing technology can be found in [21] and [38]. Information about the fabricated PhC-LEDs can also be found in the attached papers. A minimalistic thin-film processing flow is presented below:

The active LED material is grown on a n-doped substrate by metal-organic vapour phase epitaxy (MOVPE) which is also called metal-organic chemical vapour deposition (MOCVD). GaAs is used as growth substrate for AlGaInP LEDs whereas GaN/InGaN is grown on sapphire or silicon carbide. After the epitaxial growth, a metallic electrical contact and mirror is formed on the p-side. The wafer is thereafter bonded eutectically to a new substrate. The growth substrate is subsequently removed by grinding and wet chemical etching (AlGaInP) or laser lift-off (InGaN). The chip mesa is defined with photo-lithography followed by wet or dry etching. An electrical contact is formed on the n-side of the chip with photo-lithography, metallization and lift-off. A large number of contact designs exist, each optimized for the particular chip size, current working point and current distribution and so on. The small chips (*200-300μm* chip side) used for this thesis all have a centred circular bondpad. The LED chips are thereafter diced and mounted in a package or on a TO18 header for characterization.

In practice, several extra process steps are used to improve the electrical and optical properties of the LED chips: The chip surface and side-walls can be electrically isolated with a dielectric layer to avoid shunts and shorts. Transparent conductive oxides (TCOs) can be used to ensure a homogeneous current density over the whole chip area. Measures to increase the light extraction efficiency include the structuring of the LED

surface (for example surface roughening or photonic crystal) and the etching of micro-prisms prior to the bonding.

2.8 Efficiency of state-of-the-art LEDs

Two types of AlGaInP LEDs have demonstrated external quantum efficiency above *50%* for encapsulated devices: the TIP-LED [22] and the thin-film LED [23] as seen in Fig. 3(a)-(b). The thin-film LED uses micro-prisms as well as surface roughening to maximize the extraction efficiency. Photon-recycling also contributes to the light extraction. Since the internal efficiency for record devices is close to *100%*, the extraction efficiency is also around *50%*.

High efficiency InGaN LEDs are also thin-film LEDs and surface roughening is used to further enhance the extraction efficiency. At the time of writing (spring 2009), the highest efficiency reported from Osram [39] is $643mW$ at $I=350mA$ and $U_f = 3.24V$ and $\lambda = 440nm$ with a $1mm^2$-chip in an advanced package design. This corresponds to an external quantum efficiency of *65%*. The internal quantum efficiency at this working point is assumed to be *75%* and the extraction efficiency is thus *>85%*! Other large LED-companies have published similar performance. The same chips were also characterized without encapsulation. The external quantum efficiency and the extraction efficiency at the working point was then *54%* and *73%*, respectively! These excellent values were achieved mainly by minimizing the absorption losses and by improving the mirror reflectivity. The light extraction problem in InGaN LEDs can thus be considered as solved. There is, however, some room for improvement in directionality and, to some extent, in light extraction without encapsulation.

Records are achieved with excellent epitaxial material (the best chips from wafers with the highest efficiency). Our PhC-LEDs have been made from material taken for near the centre of the wafer – however without attempting to find the brightest area of the wafer in advance. The epitaxial quality of the material is also still variable. The performance of our devices can therefore not be compared to world record devices. Table 1 shows datasheet values for some products emitting in blue and red with and without encapsulation [40]. Encapsulated red LEDs approach *40%* quantum efficiency at the working point. Devices without encapsulation have efficiencies around just *20%*,

although at a very high drive current. The difference between encapsulated and non-encapsulated devices is smaller for InGaN LEDs. Their efficiency is, however, well below the records mentioned above.

Product	Encapsulated	λ_{peak} *[nm]*	Φ_e*[mW]*	*I[mA]*	η_{QE} *[%]*
Golden Dragon Plus (typical)	Yes	632 (RED)	340	400	43
Ostar Projection (typical)	No	627 (RED)	380	1000	19
Golden Dragon Plus (typical)	Yes	449 (BLUE)	420	350	43
Ostar Projection (typical)	No	460 (BLUE)	610	1000	23

Table 1 External quantum efficiency at the working point for some Osram products with and without encapsulation (April 2009).

3. MEASUREMENT AND ANALYSIS METHODS

In this chapter, I present the experimental characterization methods and the analysis of the measurement data. The standard methods are described in section 3.1 and the very revealing farfield measurements are discussed in detail in section 3.2.

3.1 Characterization methods

The devices are characterized by four types of measurements: integrating sphere measurements, measurement of the radiant intensity in a narrow tube with 3° acceptance angle, microscope imaging and farfield measurements. The former three are described below whereas the farfield measurements and the interpretation of them are explained in the following section.

The total emitted flux of light Φ_e is collected in an integrating sphere and spectrally analyzed in a spectrometer as a function of the current I. The system is calibrated to measure the flux in real units (mW or lm) and the spectra are saved together with information about the peak wavelength, FWHM and the forward voltage U_f. The efficiency of the devices can be calculated from this set of measurement data using Eq. (8) and Eq. (10). The performance of the devices is typically measured in the range of currents between $0.1mA$ and $30mA$. The Φ-U_f-I information gives an indication of the series resistance of the device and if shunts or short circuits spoil the performance. Non-radiative recombination in the active region has the largest impact for small current densities. Carrier leakage/escape and Auger-like losses on the other hand, dominate at high current densities. The dependence of the light emission efficiency on the current therefore gives an indication about what loss process dominates. All of these effects are considered when evaluating the PhC-LEDs in comparison to reference devices with or without surface roughening. For example, the emitted flux from devices with shunts or extremely high forward voltage is usually lower than the emitted flux from devices without these flaws. Such devices are then excluded from the evaluation of the optical properties.

The radiant intensity I_e [mW/sr] measures the light emitted within $0.01sr$ to the surface normal, corresponding to an acceptance angle of approximately $3°$. These measurements are performed in a radiant tube that only couples the light within this limited angular range to the spectrometer for analysis. The radiant intensity is mainly

interesting for applications with a very limited étendue, such as light coupling to an optical fibre. However, the ratio between Φ_e and I_e gives a hint about the directionality of the emitted light. Therefore the I_e for different PhC-LEDs are used to identify the devices that should be analyzed further with the very valuable, but time-consuming farfield measurements described below.

Microscope imaging of the LEDs during operation gives qualitative information about their performance. Of particular interest is the difference in brightness from areas with and without surface structure, the homogeneity of the light across the chip (current distribution) and the strength of the side emission.

3.2 Analysis of spectrally resolved farfields

Spectrally resolved farfields contain much important information that is especially useful for the analysis of PhC-LEDs [12]. The intensity $I(\theta,\varphi,\lambda)$ is collected with an optical fibre on a rotating arm, as seen in Fig. 7. The light coupled to the fibre is analysed in a spectrometer.

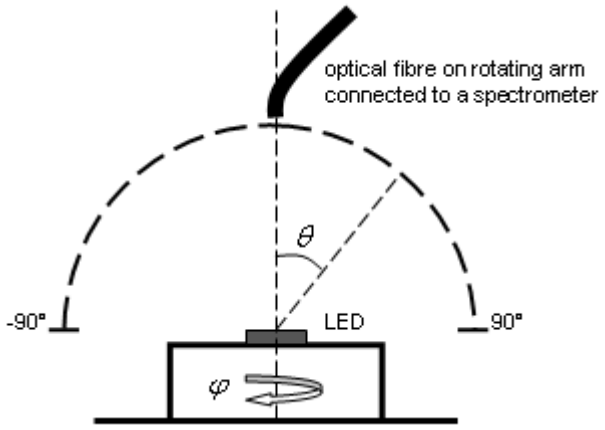

Fig. 7 Schematic farfield measurement setup. An optical fibre connected to a spectrometer is mounted on a rotating arm to measure the emitted intensity at the angle θ. The LED is rotated around the vertical axis in order to collect the farfield intensity along different azimuthal directions with angle φ.

The distance between the LED surface and the optical fibre is kept constant throughout the measurement. The distance is *190mm* for measurements with a multi-mode fibre of 3 mm diameter, which yields an angular resolution of ± *0.45*°. Occasionally, a single-mode fibre was also used, which yields an angular resolution below ± *0.1*° even though the fibre was mounted closer to the surface of the LED (*150mm*) to get a low noise signal. All farfields presented in this thesis were recorded with a step of $\Delta\theta = 1°$. The

LED itself is also rotated in the azimuthal plane in order to obtain the farfield along different photonic crystal directions. A small step size $\Delta\varphi = 3°$ was used to obtain azimuthal farfields. The collected spectra have a resolution of $\Delta\lambda = 0.7\text{-}0.8\ nm$ and spectra were recorded over a wavelength range of $\lambda_{peak} \pm 50nm$. Hence a typical azimuthal farfield consists of 11041 measurement points; given the 142 wavelength points, this multiplies to almost 1.6 million data points.

Visualization of spectrally resolved farfields

The spectrally resolved farfield $I(\theta, \varphi,\lambda)$ can of course not completely be visualized in a single two-dimensional diagram. By using two of the parameters $(\theta, \varphi,\lambda)$ as variables to the measured intensity I and keeping the third parameter constant, a colour scaled intensity plot can be made.

The most valuable plot is where φ is kept constant, typically along one of the symmetry directions of the photonic crystal, and the intensity is plotted as a function of θ and λ. Fig. 8(a) shows the spectral farfield from a thin-film InGaN LED without surface structure.

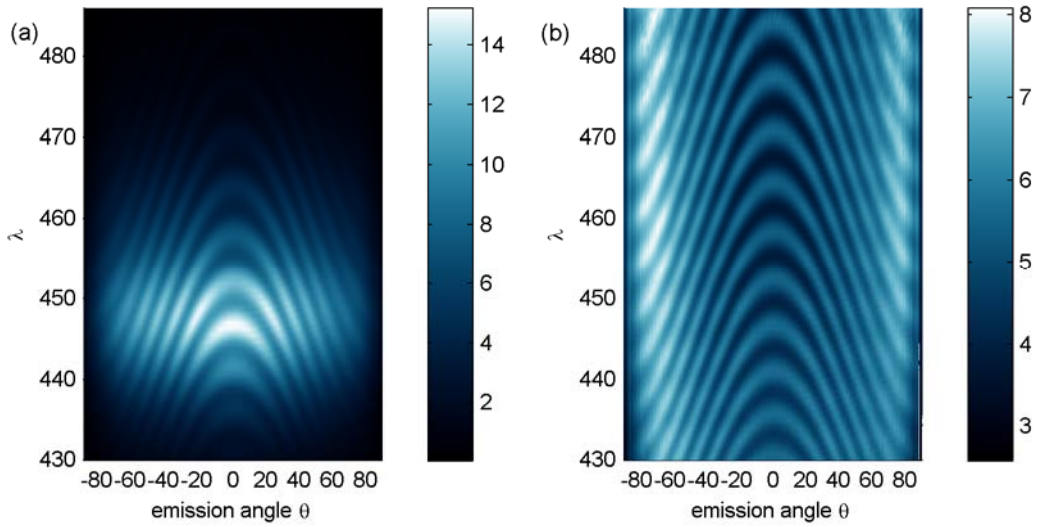

Fig. 8 Spectrally resolved farfield from a ~$6\mu m$ thick InGaN ThinGaN LED without surface structure (a). The boomerang shaped maxima are Fabry-Perot resonances. The spectral farfield in (b) is normalized with the overall emission spectrum of the LED and with a Lambertian-like function [4]. Deviations from the Lambertian emission pattern are therefore seen over a larger wavelength and angular range than in the original spectral farfield. This farfield is flatter than a Lambertian emitter due to the resonance with the bottom mirror. The FP-resonances are therefore brighter for angles larger than $60°$.

The boomerang shaped intensity pattern is caused by the Fabry-Perot resonances in the thick cavity formed between the bottom mirror and the semiconductor-air interface. The

spectral density of the Fabry-Perot resonances depends on the thickness of the cavity and it can be seen that for this approximately six µm thick LED, there are several resonances within the FWHM of the spectrum. However, resonances at large extraction angles and at wavelengths with low spontaneous emission cannot be seen in this colour-scaled intensity plot. Since most top-emitting LEDs are roughly Lambertian emitters, the farfield data can be normalized with a Lambertian-like function in order to visualize the farfield pattern at large angles better [3]. Furthermore the farfield can be normalized with the emission spectrum of the totally emitted light. Bright areas now correspond to a higher intensity than for a Lambertian emitter and vice versa. In the normalized spectral farfield (Fig. 8 (b)), features can be seen for all angles and over a large wavelength range. Fig. 9(a) and (b) show original and normalized spectral farfields from a thin-film LED with surface roughness.

[3] The farfield intensity from a Lambertian emitter is given by $I_{lam}(\theta) = \cos\theta$. Since the measured farfield at $I(\theta=90°) > 0$ and $\cos(90°) = 0$, a normalization $I_{norm} = I/I_{Lam}$ would give an indefinite value. The resulting farfield has very low colour contrast since the colour scale is determined by the highest and lowest value in the normalized farfield. Therefore a „Lambertian like" function $I_{„Lam"} = (\cos\theta + \mu)$ is used, where $\mu \in [0.1,1]$. These normalized farfields are just used for qualitative evaluation such as the identification of Fabry-Perot modes or diffracted guided modes from PhC-LEDs. Therefore, μ can be chosen to get the best possible contrast in the normalized farfield. The same colour-scale is used throughout this thesis. The lowest intensity point in the farfield is always chosen as the starting point of the colour scale in order to maximize the contrast.

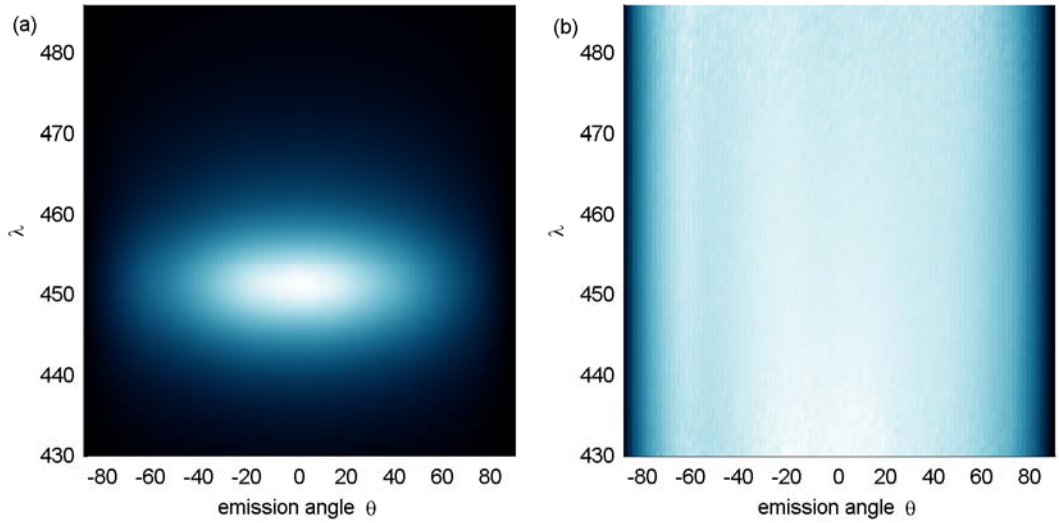

Fig. 9 Spectral farfield (a) and normalized spectral farfield (b) for a ~$6\mu m$ thick ThinGaN LED with surface roughness. No FP resonances can be seen and the vanishing contrast in (b) shows that the emission is almost perfectly Lambertian.

Such LEDs have a Lambertian emission pattern without Fabry-Perot resonances as seen in Fig. 9(a). The normalized farfield in Fig. 9(b) has consequently close to zero contrast. Fig. 10(a) and (b) finally show the spectral farfield from a thick InGaN PhC-LED. In these farfields, almost vertical lines are superimposed on the underlying FP resonance pattern. The mode dispersion for the guided modes causing the diffraction lines can be calculated using Eq. (36) in Section 4.3, presupposed that the azimuthal angle φ relative the PhC crystal direction is known.

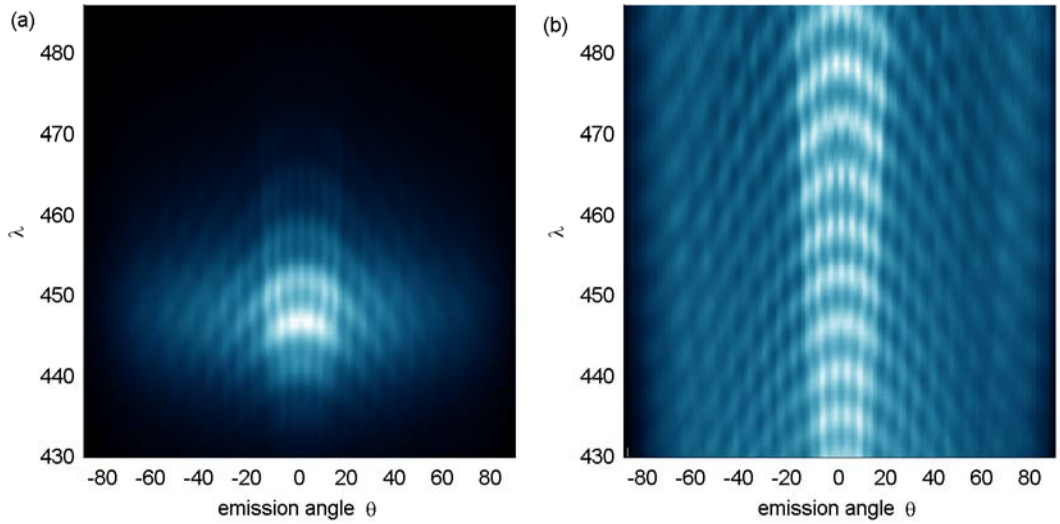

Fig. 10 Spectral farfield (a) and normalized spectral farfield (b) for a ~$6\mu m$ thick ThinGaN LED with a hexagonal photonic crystal. Almost vertical diffraction lines dominate the farfield – the FP resonances can however still be identified.

The azimuthal farfield is obtained by keeping the wavelength constant and plotting the farfield intensity after a transformation to Cartesian coordinates in the reciprocal plane:

$$k_x = \sin\theta \cdot \cos\varphi \tag{26}$$

$$k_y = \sin\theta \cdot \sin\varphi \tag{27}$$

Typical azimuthal farfields for a thick PhC-LED and a thin PhC-LED are seen in Fig. 11.

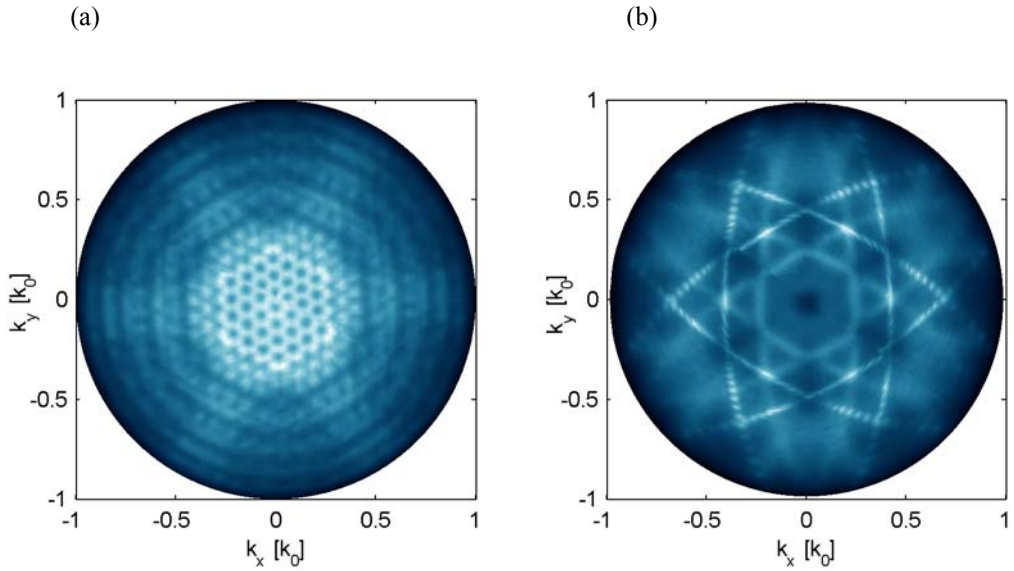

Fig. 11 Azimuthal monochromatic farfield from a *~6μm* thick (a) and *850 nm* thick InGaN thin-film PhC-LED (b).

The first displays a very complex emission pattern that can hardly be subjected to a modal analysis. However, a hexagonal symmetry can be identified that corresponds to the symmetry of the lattice. The figure to the right on the other hand, is from a much thinner device and is ideal for modal analysis. Since there are only two visible modes, the extraction strength along different crystal directions can easily be examined and the effective index of the modes can be determined. The missing dimension in these figures, the wavelength, can be visualized by playing a movie of azimuthal farfields with increasing wavelength.

Calculation of directionality from farfields

Finally, we turn to the shape of the farfield integrated over all wavelengths. The integrated intensity within the acceptance angle θ is calculated by approximating the integral below with the weighted sum of the discrete measurement points:

$$P(\theta) = 2\pi \cdot \int_0^{\theta} I(\theta') \cdot \sin\theta' \cdot d\theta' \approx 2\pi \sum_{\theta' < \theta} I(\theta') \cdot \sin\theta' \cdot \Delta\theta' \qquad (28)$$

Where *I(θ')* is the farfield intensity measured at the angle *θ'* averaged over all crystal directions of the photonic lattice, since the intensity varies slightly with φ in PhC-LEDs. The directionality is subsequently calculated as:

$$D(\theta) = P(\theta) / P(90°) \qquad (29)$$

P(θ) is the relevant value for étendue limited applications. The relative directionality value *D(θ)* indicates how strong the collimation of the emitted light is and it can be compared to devices without a surface structure or with surface roughening.

4. PHOTONIC CRYSTAL LEDs

In this chapter, I discuss the principle operation of photonic crystal LEDs (PhC-LEDs). Starting with an introduction to photonic crystals in Section 4.1, I turn to the use of photonic crystals in LEDs in Section 4.2. The diffraction-type PhC-LED, which is considered in this thesis, is discussed in detail in Section 4.3.

4.1 Photonic crystals

Understanding photonic crystals is a matter of intuition and analogy. There is no single textbook about photonic crystals that explains their function without referring to the analogy of the propagation of electrons in a crystal, such as in a semiconductor. This fact is historic, as photonic crystals were invented in the late 1980s, with the initial motivation of controlling the propagation of light in analogy to the controlled propagation of electrons in solid state crystals [41]. A photonic crystal is an artificial dielectric medium with a periodic variation of the refractive index (dielectric constant) and with a periodicity of the order of the wavelength of the light. The periodicity of the refractive index constrains the propagation of light and photonic band gaps can arise for some frequency bands, just like for electrons in a periodic electrical potential landscape. The photonic crystal is characterized by its lattice type, lattice constant a, and air filling factor F. All lattice points in a two-dimensional lattice can be described by its two lattice vectors $\vec{a}_1$ and $\vec{a}_2$. In the reciprocal plane, the reciprocal lattice vector $\vec{G}$ is given by $\vec{b}_1$ and $\vec{b}_2$:

$$\vec{G} = G_0 \cdot (m \cdot \vec{b}_1 + n \cdot \vec{b}_2) \tag{30}$$

Throughout this thesis I use normalized reciprocal lattice vectors with $|\vec{b}_i| = 1$. The relation between the lattice constant a and the reciprocal lattice constant G_0 for a hexagonal lattice, as seen in Fig. 12(a), is given by:

$$G_0 = \frac{4\pi}{\sqrt{3} \cdot a} \tag{31}$$

The Fourier transform for a photonic crystal with circular holes can be calculated with Bessel functions:

$$\tilde{\varepsilon}(G) = F \cdot \frac{J_1(GR)}{GR} \tag{32}$$

Here, F is the air filling factor of the PhC, J_1 is the first Bessel function of the first kind and R is the radius of the holes. For a hexagonal lattice, the air filling factor is given by:

$$F = \frac{2 \cdot \pi}{\sqrt{3}} \left(\frac{R}{a} \right)^2 \tag{33}$$

We can also assign the photonic crystal an average refractive index n_{PhC} calculated as:

$$\varepsilon_{PhC} = F \cdot \varepsilon_{air} + (1 - F) \cdot \varepsilon_{sc} \tag{34}$$

$$n_{PhC} = \sqrt{\varepsilon_{PhC}} \tag{35}$$

Fig. 12(b) shows the free photon dispersion for an artificial hexagonal lattice without refractive index contrast in a photonic band diagram. Starting at low reduced frequencies, the dispersion line of the guided mode along ΓM (in red) corresponds to the normal mode dispersion for a guided mode in an uncorrugated slab and follows a path between the semiconductor light line and the air light line (in black). The mode is then folded back at the edge of the first Brillouin zone (at the M-point and K-point) according to Bloch's theorem. At the Brillouin zone edge two degenerate states exist whose field profile are shifted by $a/2$ to another in real space [see Fig. 5 in Paper III]. When the dielectric constant contrast $\Delta\varepsilon \neq 0$, band splitting arises at the Brillouin zone edges. This can be understood intuitively since light that is mainly located in the semiconductor material "sees" another refractive index than the formerly degenerate state that is mainly located in the air holes due to the field profile shift by $a/2$ [44]. Hence, light propagation for example in the ΓM -direction is forbidden for a defined frequency range. A complete photonic bandgap exists if there is no allowed propagation direction at all for a certain frequency. The dispersion just below and above the band gap is flatter than the free mode dispersion. The higher density of photonic states at these frequencies can be utilized to enhance the radiative recombination rate, known as the Purcell effect. The reduced group velocity of the light $v_g = \partial\omega/\partial k$ near the band edges enables "slow light propagation" – a regime that enhances non-linear effects (see for example [45]). The reader is referred to [41], [44] for a more detailed description of photonic crystals and its applications. At higher reduced frequencies (here $\omega a/2\pi c$) the first Bloch harmonic crosses the light line given by $\omega = k_0 c$. This means that the guided mode now leaks to air – this is the principle of photonic crystal light extraction.

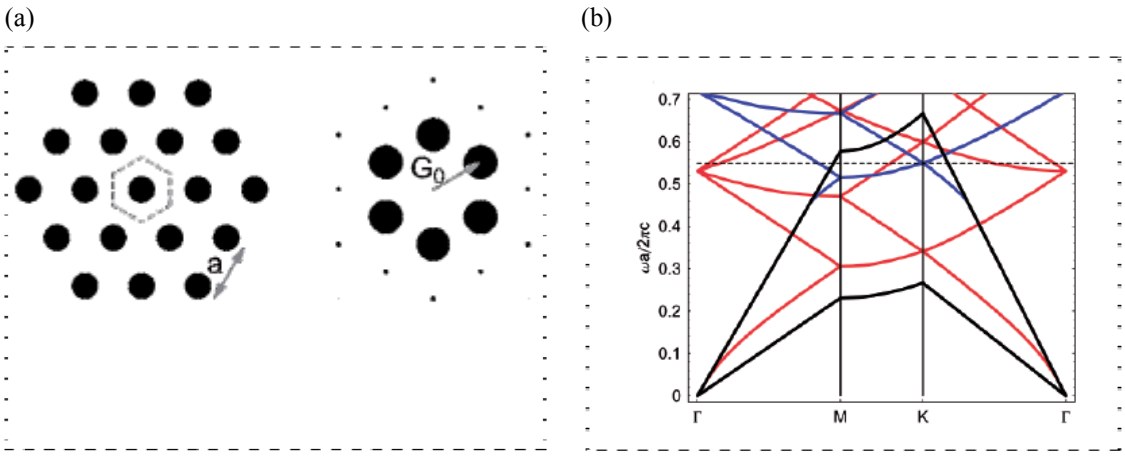

Fig. 12 Hexagonal photonic crystal with lattice constant a in the real plane and G_0 in the reciprocal plane. The diameter of the holes in the reciprocal plane corresponds to the squared modulus of the Fourier transform (a) [Figure 10(a) Paper III]. Photonic band-diagram for a slab with a hexagonal lattice with lattice constant a and zero refractive index contrast (b) [Figure 4(b) Paper III]. The fundamental TE mode in red is folded at the edges of the first Brillouin zone. A second TE mode (blue line) appears at the reduce frequency *0.46*. The lower and upper black line corresponds to the semiconductor light line and the air light line, respectively.

4.2 Application of photonic crystals in LED

Strongly coupled photonic crystal LEDs

If the light emission occurs in a photonic crystal, as shown in Fig. 13(a), a number of effects associated with photonic crystals can be utilized to change the spontaneous emission from the active layer. For example, the spontaneous emission rate from the radiating quantum wells can be enhanced by modifying the optical density of states available to the emitter. By operating the device at a frequency within a photonic bandgap, the emission into guided modes is inhibited [42]. In this way, the light is forced into radiating modes that escape the high-index semiconductor. Since etching through the emitting layer induces non-radiative surface recombination, this effect has only been demonstrated at cryogenic temperatures [43]. Alternatively, the lattice constant can be tuned such that all Bloch modes for the frequency of the emitted light lie above the light line are therefore extracted [4]. Both of these approaches suffer from a strongly reduced effective emitting area given by the air filling factor of the photonic crystal. The possible gain in directionality from PhC-LED for étendue limited optical systems (as discussed in Section 2.6) is then lost since the radiant emittance M is reduced. Making electrical contacts without shorts and enabling good current spreading

are other practical challenges. Strongly coupled PhC-LEDs are thus not a viable solution to the light extraction problem in high-efficiency LEDs.

Weakly coupled photonic crystal LEDs

The second approach is to apply a photonic crystal to enable diffraction of guided light into air. In this case, the spontaneous light emission and the light extraction can be considered as two separate problems. Two set-ups for diffraction type LEDs are seen in Fig. 13 (b)-(c). One can choose to separate the light generation region from the diffraction region (Fig. 13 (b)).

Fig. 13 Possible PhC-LED designs. Strongly coupled PhC-LED with the active layer within the PhC (a); Weakly coupled PhC-LED with the extraction region separated from the light generation (b); weakly coupled PhC-LED with a shallow PhC above the active layer (c)

The advantage with this approach is that one can etch through the entire LED and in this way make the diffraction strength stronger. However, this leads to a reduction of the effective light emitting area and thus the radiant emittance, just like for the strongly coupled PhC-LEDs. The setup with a shallow photonic crystal as seen in Fig. 13(c) is therefore preferable and I have only followed this approach throughout my work. The diffraction type PhC-LED is treated in more detail in the next section.

4.3 Diffraction type photonic crystal LEDs

In this section we will deal with photonic crystal light extraction by diffraction and in particular consider the extraction efficiency and the directionality of the diffracted light. First, the simplest and at the time ideal situation is considered: the diffraction of a single guided mode. The upper limit for the directionality will be defined and the choice of diffraction order of the lattice will be discussed.

The PhC-LEDs presented in this thesis are all working in the diffraction regime. The spontaneous emission into the guided modes is assumed to be unaffected by the PhC. This assumption holds since the active region is situated in the remaining unetched slab.

An incident mode with in-plane k-vector $\vec{k}_i$ (with effective index k_i) is diffracted by the PhC with reciprocal lattice vector $\vec{G}$ to the state $\vec{k}_d$ according to Bragg's law:

$$\vec{k}_d = \vec{k}_i + \vec{G} \tag{36}$$

All vectors have been normalized by $k_0 = 2\pi/\lambda$. The strength of the diffraction process is proportional to the Fourier intensity of the dielectric map of the photonic crystal (see Section 5.3). First (ΓM), second (ΓK) and third order ($2\cdot \Gamma M$) diffraction corresponds to the reciprocal lattice vector lengths G_0, $\sqrt{3}G_0$ and $2\cdot G_0$, respectively. Generally, the first order ($|\vec{G}| = G_0$) has the highest Fourier intensity. The light is extracted to air if $|\vec{k}_d| < 1$ and the extraction angle is given by $\theta = \arcsin(k_d)$. It is important to note that Eq. (36) is a vector relation and not scalar. Extraction normal to the surface, i.e. $|\vec{k}_d| = 0$, is therefore only obtained for $k_i = G$ if $\vec{k}_i$ and $\vec{G}$ are parallel. In other words, only light propagating parallel to the lattice vector can be extracted exactly normal to the surface.

One might wonder how Bragg diffraction is related to the photonic band-diagram. Bragg's law is equivalent to the band-folding of a guided mode for a photonic crystal without refractive index contrast as displayed in Fig. 12. The photonic band-diagram is however not very practical to visualize diffraction of guided modes to air. First of all, it only shows the behaviour along the main symmetry directions of the lattice. The spontaneous emission is however omnidirectional in the plane, which makes all in-plane directions equally important. Furthermore, the lines in the band diagram all look the same, regardless of the folding (diffraction) order. The diffraction order determines how strongly the light is extracted - or in other words how leaky the Bloch mode is. This information is not obtained in the band diagram. It is for example not obvious that Bloch modes with high reduced frequency (i.e. with a high diffraction order) only extract very weakly. We will therefore illustrate the diffraction according to Eq. (36) with Ewald diagrams, also called wave-vector diagrams [46].

Diffraction of a single guided mode

Ewald diagrams illustrating the diffraction of one guided mode by a hexagonal lattice are displayed in Fig. 14. We let the guided mode be represented by a vector with length $|\vec{k}_i|$ starting from a neighbouring reciprocal lattice point. Since the light emission is azimuthally isotropic, the vector can point in all in-plane directions, effectively forming

a circle in the reciprocal plane. The reciprocal lattice vector between two lattice points is shown in black. According to Bragg's law, the mode is diffracted according to Eq. (36) to the state $\vec{k}_d$. The mode is extracted if the diffracted state lies within the light extraction disc given by $|\vec{k}|<1$ (thick black circle). We see in Fig. 14(a) that the diffracted states for different incident azimuthal angles all lie along a circle arc. Fig. 14(b) shows the diffraction pattern from the six nearest reciprocal lattice points of a hexagonal lattice where $|\vec{k}_i|=|\vec{G}|$. A strong diffraction peak is obtained at $\theta = arcsin(0) = 0°$ since all diffraction lines meet at $|\vec{k}_d|=0$.

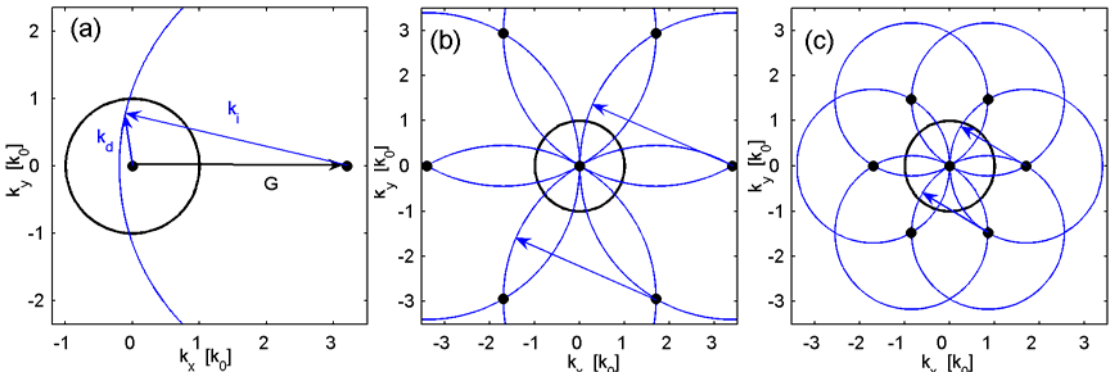

Fig. 14 Ewald diagrams showing diffraction according to Bragg's law in the reciprocal plane (a). The extraction of a mode forms a circle arc within the light extraction disk (thick black line). Very high peak intensity at $k_x = k_y = 0$ is obtained when $k_i = G_0 = 3.4$ (b). The arrows in (b) denote an in-plane propagation direction that cannot be extracted by any of the six nearest lattice points of the hexagonal lattice. Omnidirectional diffraction is possible for modes with lower effective index (c).

By comparing the circle arc length within $|\vec{k}_d|<1$ and $|\vec{k}_d|<\sin\theta$, the directionality of the diffracted light can be estimated. It is shown in Paper VI that the upper limit for the directionality of the diffracted light (according to Eq. (29)) is $D(\theta) \approx sin\ \theta$. For comparison, a Lambertian emitter has the directionality $D_{Lam}(\theta) \approx sin^2\ \theta$. The fraction of the emitted light within the angle θ is summarized in Table 2. The largest enhancements for this single-mode diffraction over Lambertian emitters are obtained for very small emission angles. *50%* of the diffracted light is within the 30°-disc which is twice as much as for Lambertian emission. Therefore, PhC-LEDs can in principle be much more directional than competing LEDs with surface roughness (and a Lambertian emission pattern).

Angle θ	Lambertian emission	Single-mode diffraction	Enhancement over Lambertian
3°	0.0027	0.052	1837%
10°	0.030	0.17	481%
30°	0.25	0.50	100%
45°	0.50	0.71	42%
60°	0.75	0.87	16%
75°	0.93	0.97	3.5%

Table 2 Directionality of emitted light within different emission angles for a Lambertian emitter and for diffracted light from a single-mode PhC-LED.

The spectral width of the spontaneous emission reduces the maximum directionality since the in-plane k-vector of the mode and the reciprocal lattice constant of the PhC match perfectly only for one wavelength.

Fig. 14(b) illustrates the importance of sufficiently high symmetry of the lattice. The arrows in the diagram correspond to an incident azimuthal angle that cannot be diffracted to the light extraction disk by any of the lattice points although $k_i = G$. Hence, a fraction of the guided mode is without reach and will never be extracted. This very unfortunate feature of PhC light extraction applies for modes with $k_i > 2$ for a hexagonal lattice. Modes with smaller effective index can on the other hand be completely extracted as seen in Fig. 14(c). The complete extraction of the modes with higher effective index requires the use of several diffraction orders. Fig. 15(a-d) shows how the guided modes with $k_i = 3.4$ and $k_i = 2.4$ can be extracted by combining the first and the second order (a,c) and the second and the third order (b,d).

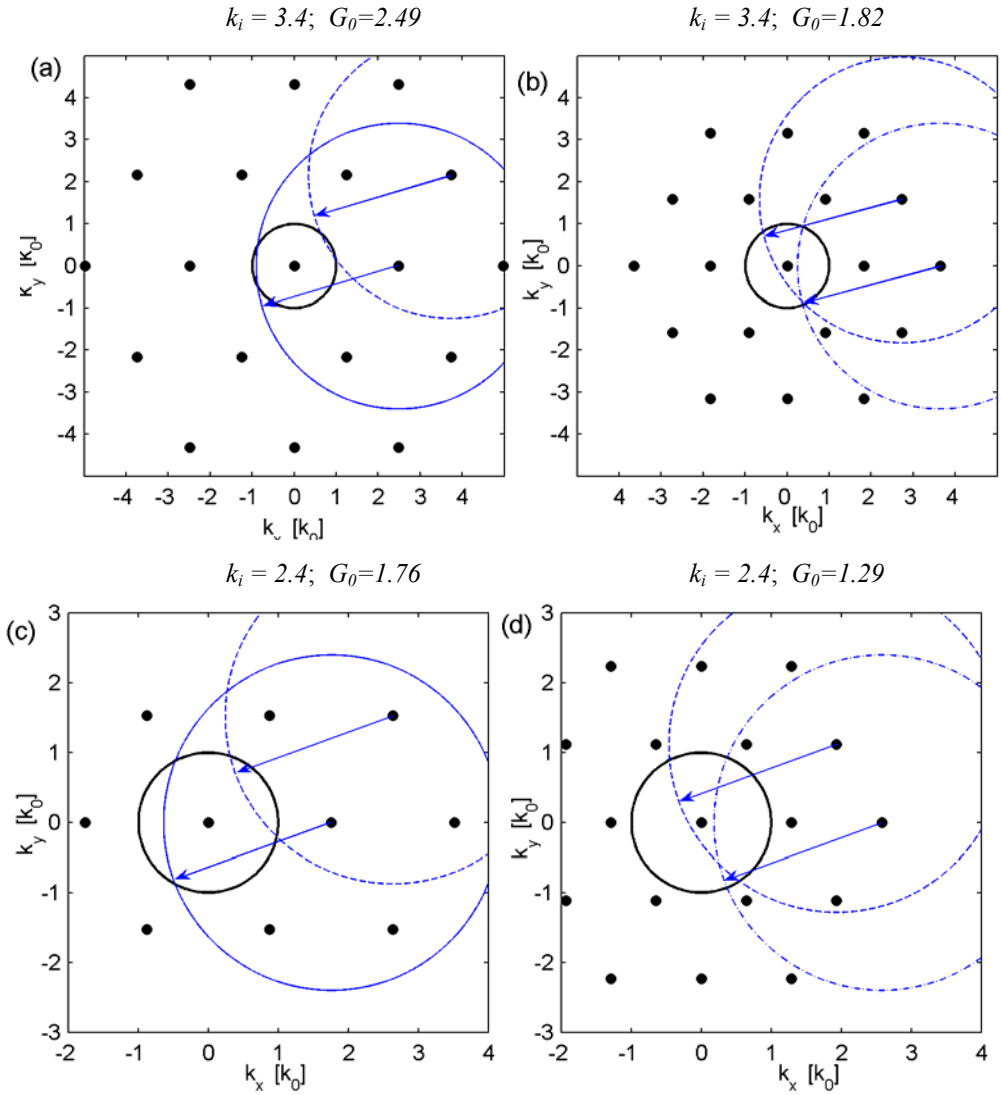

Fig. 15 Ewald diagrams for modes with k_i = *3.4* (a-b) and k_i = *2.4* (c-d) and G_0=2.49 (a), 1.82 (b), 1.76 (c) and 1.29 (d), respectively. The arrows outside the light extraction disk in (a) show that omnidirectional extraction is not possible by combining the first (solid circle) and second (dashed circle) diffraction order for the mode with higher effective index. A combination of the second and third order (dash-dotted circle) yields omnidirectional extraction (b). Both combinations are omnidirectional for the mode with k_i = *2.4* (c-d).

The former mode cannot be completely extracted by the first and second order (Fig. 15(a), G_0=*2.49*) but requires the second and third order (Fig. 15(b), G_0=*1.82*). The reason for this is that the difference in reciprocal vector length between the first order ($|\vec{G}| = G_0$) and the second order ($|\vec{G}| = \sqrt{3} \cdot G_0$) is larger than between the second and the third order ($|\vec{G}| = 2 \cdot G_0$). Hence, in the latter case both reciprocal lattice constants are reasonably well fitted to the guided mode. The second mode with smaller effective index can be fully extracted in both cases (Fig. 15(c) and (d), G_0=*1.76* and *1.29*, respectively).

Extraction efficiency of a single guided mode

We shall here calculate the extraction efficiency of a single guided mode in different diffraction and absorption regimes. This is a generalization of the calculation found in Paper V.

So far, we have neglected the diffraction strength β for different diffraction orders. This is proportional to the Fourier intensity of the dielectric map [47], as will be discussed later. We are now considering light propagating in all azimuthal directions for a mode with absorption strength α that can be diffracted by two diffraction orders i and j with diffraction strength β_i and β_j. The Ewald diagrams in Fig. 15 describe this situation. The extraction efficiency η is then:

$$\eta_i(\varphi) = \frac{\beta_i}{\beta_i + \beta_j + \alpha} \tag{37}$$

$$\eta_i(\varphi) = \frac{\beta_i}{\beta_i + \alpha} \tag{38}$$

Eq. (37) applies if two diffraction orders couple to air for the same in-plane angle φ whereas Eq. (38) applies if only one diffraction order i is possible for φ. The two cases are shown in Fig. 15 (c) and (a), respectively. Using Eq. (37) we get $\eta_i/\eta_j = \beta_i/\beta_j$ for light propagating with an in-plane angle where both diffraction orders are allowed. In the case where only one of the diffraction processes is allowed, however, Eq. (38) applies and the extraction efficiency with order i does not depend on the diffraction strength of order j anymore. The total extraction efficiency of the mode is obtained by integrating over all azimuthal angles φ. The optimal lattice constant (i.e the diffraction order) and PhC air filling factor is a function of the absorption. This is illustrated in Fig. 16 that shows the extraction efficiency of a single mode for three different absorption coefficients α. We limit the calculation to the three first diffraction orders of the hexagonal lattice. Let us first consider the extraction of a guided mode with $k_i = 2.4$ (a-c). When the absorption strength is much higher than the extraction strength (a), first order diffraction is most efficient due to its higher Fourier intensity and despite the lacking omnidirectionality. The optimal lattice constant is therefore close to the effective index of the mode: $G_0 = 2.2$. A filling factor $F = 0.4$ is better than $F = 0.5$ since this gives the highest Fourier intensity for this diffraction order. In Fig. 16(b), the absorption strength is an order of magnitude smaller than the first diffraction order and

first order diffraction still dominates. But second order diffraction also contributes since it can extract light out of reach of the first order. The optimal lattice constant is therefore found between the first and second diffraction order: $G_0 = 1.9$. Finally, the combination of the second and the third order is almost equally efficient as the combination of first and second order when the absorption strength is much smaller than the extraction strength (c). In the two latter cases, $F = 0.5$ is much more efficient, since the second and third diffraction order are relatively strong with this filling factor.

$k_i = 2.4$:

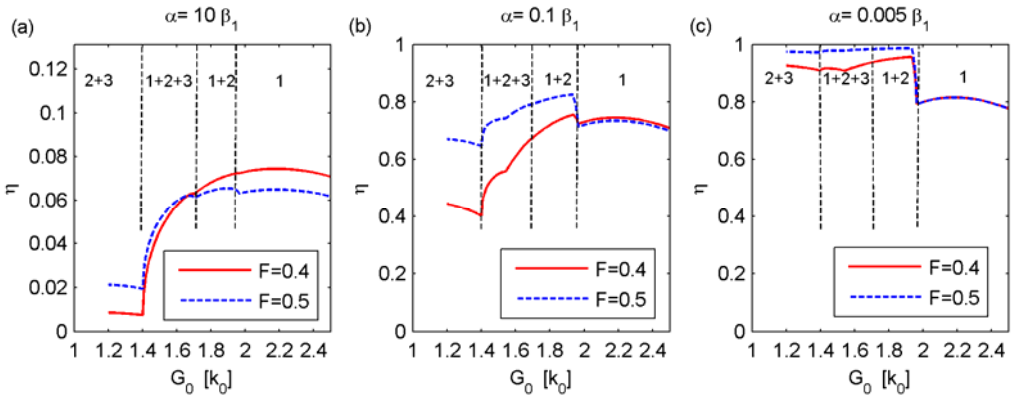

$k_i = 3.4$:

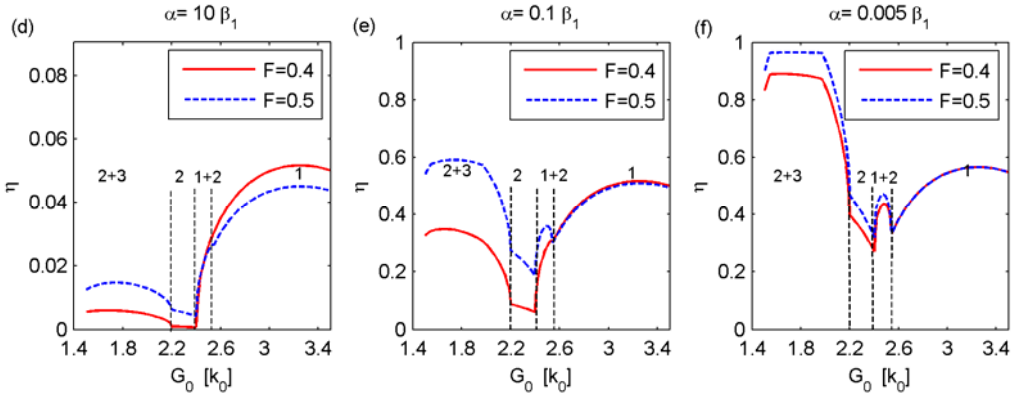

Fig. 16 Extraction efficiency of a single mode with effective index *2.4* (a-c) and *3.4* (d-f) as a function of the reciprocal lattice constant G_0 for different absorption coefficients α expressed in units of the diffraction strength of the first diffraction order β_1. The solid and dashed curves are calculated with an air filling factor $F = 0.4$ and $F = 0.5$ of the photonic crystal, respectively. The vertical dotted lines mark the domains with only first order diffraction (1), first and second (1+2), first and second and third (1+2+3) and so on. The optimal reciprocal lattice constant depends on the absorption coefficient. First order diffraction, i.e. large reciprocal lattice constants, extracts strongest in the high absorption regime (a and d). The combination of two diffraction orders (smaller G) yields highest extraction efficiency when the absorption coefficient is small.

The trend is somewhat different for the mode with $k_i = 3.4$ (d-f). First order diffraction is most efficient when the absorption is high (d). But choosing a reciprocal lattice constant between the first and the second diffraction order is never advantageous due to the large vector length difference between the first and second order, as seen in Fig. 15(a). Omnidirectional diffraction is obtained by combining the second and the third diffraction order, Fig. 16(f), and this is most efficient in the limit of vanishing absorption.

In summary, we have described photonic crystal light extraction using Bragg's diffraction law. We used Ewald diagrams to visualize the diffraction process in the reciprocal plane and identified lacking omnidirectionality as a limiting factor for efficient light extraction. The optimal reciprocal lattice constant was thereafter calculated for a single guided mode as a function of the effective index and the absorption coefficient of the mode.

5. DESIGN OF PHOTONIC CRYSTAL LEDs

In the previous chapter we have learned how a photonic crystal extracts light from LEDs by diffraction. For simplicity, the single-mode LED was studied in particular and we concluded that the extraction efficiency for such a LED is influenced by the effective index of the mode, the mode absorption, air filling factor and the used diffraction order (i.e. lattice constant). While the single-mode LED would be the ideal device for photonic crystal light extraction, realistic LEDs always contain several modes. We are now facing a much more complicated problem. Let us for simplicity consider two guided modes with effective index $k_1 = 3.4$ (type I) and $k_3 = 1.5$ (type III) in a AlGaInP thin-film LED with a hexagonal diffracting photonic crystal as seen in Fig. 17.

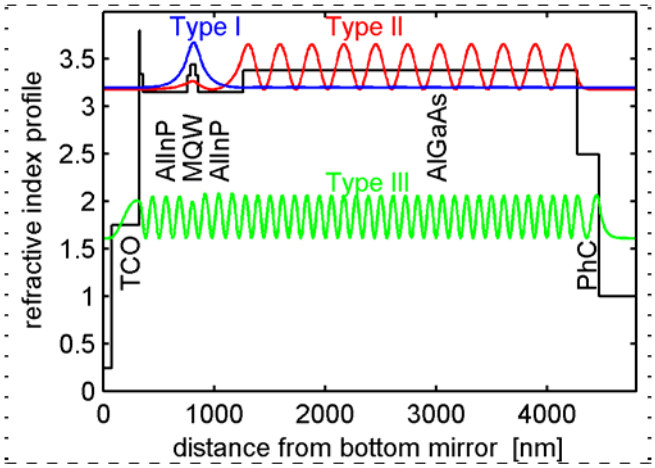

Fig. 17 Vertical refractive index profile and normalized guided mode intensity profiles for three types of modes in an AlGaInP thin-film LED. The vertical mode offset corresponds to the effective index of the modes. [Paper I, Fig 1]

They carry different amounts of energy, since the mode profile overlap with the active region is different. The mode k_1 with the highest effective index carries more energy than k_3. But since mode k_1 has a higher effective index than the average refractive index of the PhC, it is evanescent in the PhC. The impact of the PhC on the mode is therefore rather small. The second mode on the other hand, has a lower effective index and has a much larger overlap with the PhC. Furthermore, the low effective index enables omnidirectional light extraction. But this mode also "sees" the bottom mirror more often and is thus suffering from higher absorption losses. Both modes cannot be extracted by the same lattice constant and diffraction order. The question is now, what lattice constant and filling factor of the photonic crystal is optimal to get the highest possible

light extraction or the highest light extraction within a smaller extraction cone in air? The answer cannot be found intuitively – too many parameters influence the result.

In this chapter we will discuss how photonic crystal LEDs should be designed to maximize efficiency and directionality in this multi-mode case. Two simulation models of photonic crystal LEDs are introduced in Section 5.1. The conclusions from these simulations are used together with the experimental results obtained to discuss the design of the vertical layer stack in Section 5.2 and the photonic crystal in Section 5.3. The experimental results for AlGaInP PhC-LEDs (5.4) and InGaN PhC-LED (5.5) are thereafter discussed separately.

5.1 Simulation of multi-mode PhC-LEDs

The two numerical models of PhC-LEDs introduced here are also presented in Paper III and Paper VI. They were primarily developed by my colleague Ph.D. student Christopher Wiesmann at Osram Opto Semiconductors GmbH. The first one is based on coupled mode theory and is able to predict the farfield shape and the optimal lattice constant for a given LED design and choice of photonic crystal. Much of our understanding of photonic crystal LEDs are based on this conceptual framework. The relative low computation time enables variations of different parameters. The second model uses 3D finite-difference time-domain (FDTD) calculations to obtain the extraction efficiency as well as the farfield. The advantage with this model is that the extraction efficiency is obtained in real units and that also other light extraction mechanisms such as surface roughening can be simulated in the same way for comparisons. However, this brute force method does not give any insight about how PhC extraction works. A second disadvantage is the large computational power needed to simulate the rather slow extraction process in three dimensions. The FDTD model should therefore be considered a tool for calculating the extraction efficiency of already designed devices and to conduct a few comparisons rather than as an optimization tool.

The detailed derivation of the PhC-LED model based on coupled-mode theory is found in Paper VI. The starting point of the calculations is the guided mode distribution given by the vertical layer stack of the LED. The effective index of all guided modes k_i, their vertical mode profile and relative emission strength are obtained with a 1D transfer-

matrix algorithm. The inclusion of a thick air layer over the vertical layer stack yields a dense set of discrete radiating modes with $k_i < 1$ that represents the continuous radiating modes. The PhC is assumed to have an average refractive index depending on the filling factor for this calculation. The spontaneous emission B_i to the mode k_i is assumed to be proportional to the mode overlap with the active region. The extraction strength of the mode k_i to the state k_d is proportional to the product of the Fourier intensity of the photonic crystal $|\Delta\tilde{\varepsilon}_{ki\to kd}|^2$ that couples the guided mode k_i to the radiating mode k_d and the coupling integral κ_{id} between mode k_i and k_d in the photonic crystal. κ_{id} is calculated as:

$$\kappa_{id} = \int_{PhC} U_i^*(z) \cdot U_d(z) dz \tag{39}$$

Here, U_i and U_d are the vertical field profiles of the incident and diffracted mode, respectively. Hence, the coupling depends on the mode profile of both the guided mode and the radiating mode. The farfield intensity $I(\theta)$ is given by summing up the diffraction processes from all guided modes coupling to radiating modes with $k_d = \sin\theta$. The total diffraction strength of the mode is obtained by integrating over all in-plane wave-vectors inside the light extraction disk. In order to focus on the diffraction process and speed up calculations, absorption is not taken into account in this model. Hence, each diffraction process is proportional to the Fourier intensity of the reciprocal lattice vector causing the diffraction. If we once again consider Eqs. (37)-(38), we see that this proportionality is correct when the absorption coefficient is much larger than the extraction coefficient. Our PhC-LEDs model is thus calculating the diffracted intensity in a high absorption regime. The extraction efficiency for thin-film LEDs with photonic crystals is roughly between *20%* and *70%*. A quick look at Fig. 16 reveals that such values can only be achieved when the diffraction strength is of at least the same order of magnitude as the absorption strength. Hence, the diffraction model overestimates the impact of the photonic crystal Fourier intensity $|\Delta\tilde{\varepsilon}_{ki\to kd}|^2$ and therefore first order diffraction is overweighed. For the same reason, the impact of the coupling integral is exaggerated, which tends to favour modes with a low effective index. Nevertheless, this model predicts the ideal lattice constant for either highest extraction efficiency or directionality.

We now turn to the second model for PhC-LEDs based on the FDTD method. With this method the partial differential equations from the Maxwell's equations that govern the

propagation of the electromagnetic field is approximated by finite differences in time and space. A dipole located at the vertical position of the active region is used as a source. The FDTD algorithm offers the possibility to use periodic boundary conditions – at first glance an excellent idea for a periodic structure like a photonic crystal. The simulation volume could then be reduced in the two in-plane dimensions to one unit cell of the photonic crystal and the computation time could be reduced accordingly. However, this approach turned out to be impossible to use, since the spontaneous emission is then not modelled properly. The periodic boundary conditions lead also to a periodic set of dipole sources that interfere with each other, which yields unphysical farfield radiation patterns. It is therefore necessary to simulate a volume as large as reasonably possible with the given (powerful) computational resources. The extraction efficiency within this simulation area is obtained by calculating the relative Poynting flux through a disk in air above the LED with respect to the totally emitted flux from the dipole. Since the in-plane area of the simulations is much smaller than the actual area of a LED (the smallest being *~200µm x 200µm*) and the maximal propagation length in the model is comparable to the mode extraction length, a method must be found to estimate the real extraction efficiency from the simulated extraction efficiency. This was done by calculating the extraction efficiency as a function of the radius of the detection disk. The total extraction efficiency η of the LED was then calculated by fitting an exponential function to the extraction efficiency with different radii x. The exponential function is of the form:

$$\eta = \eta_0 + \frac{\beta}{\beta + \alpha} \cdot \left(1 - e^{-(\beta+\alpha)x}\right) \tag{40}$$

η_0 is the direct light extraction efficiency (without photonic crystal) and β and α are the extraction and absorption coefficients, respectively. These coefficients represent some average extraction and absorption strength for all light in the LED. They can therefore not be directly compared with the mode specific coefficients discussed earlier.

5.2 Optimization of the vertical layer stack

The vertical design of the PhC-LED determines the extraction efficiency and the directionality of the emitted light just as much as the photonic crystal itself. The perfect vertical design should:

1. hinder substrate losses
2. concentrate the light into a few guided modes that can be easily extracted by the photonic crystal
3. minimize absorption losses
4. shape the farfield of the directly emitted light

Several research papers on diffracting PhC-LEDs have focused on the correct choice of lattice or diffraction order to avoid losses to substrate modes [14], [49]. Since the substrate is at least an order of magnitude thicker than the LED itself, it supports a huge number of substrate modes in the range $k_i \in [1, n_{substrate}]$. Light diffracted to these modes are either absorbed (GaAs substrates) or will interact very weakly with the photonic crystal (sapphire substrate). For substrate LEDs it is therefore just as important to minimize diffraction to substrate modes, as it is to maximize diffraction to air. Such considerations are not necessary for thin-film LEDs. The incorporation of a metallic bottom mirror means that the light is confined to the epitaxial layers and interacts more strongly with the photonic crystal. The absence of substrate modes is probably the most important design feature to enable efficient light extraction with photonic crystals at all.

The most important aspect of the vertical stack optimization is the design of the guided mode distribution. A mismatch between G_0 and k_i is inevitable in a multi-mode LED, which first reduces the directionality and thereafter the extraction efficiency (see for example Fig. 3 in Paper VI). To put it simply, the goal is to resemble the ideal single guided mode case described in Section 4.3. Thin devices are therefore generally desirable, since this reduces the number of guided modes and enhances the mode coupling with the PhC. Attempts to reach the single guided mode regime led to the PhC-MCLEDs presented in Paper IV and V. However, these types of LEDs are difficult to realize for several reasons discussed later in Section 5.4 and 5.5. Let us have a look at the guided mode distribution in thin-film LEDs. Fig. 18(a) shows the amount of spontaneous emission for each guided mode of the the AlGaInP thin-film LED in Paper I. Apart from one guided mode with extreme intensity (which we will see, cannot be

extracted by the PhC), there is a quasi-continuum of guided modes. A weak periodicity in intensity can be seen. This variation is caused by the resonance with the bottom mirror. Light emitted upwards and light reflected at the bottom mirror interfere either constructively or destructively, according to Eq. (3). One can consider the numerator of Eq (3) as an envelope function that varies the spontaneous emission to the modes singled out by the denominator. The periodicity of this envelope function is determined by the distance between the active region and the bottom mirror. Here, the periodicity is small, since the optical distance ($\sim 3\lambda$) between the active region and the mirror is large. If we consider each modulation peak as a quasi-mode – the LED in Paper I has five quasi-modes spread over a large range of in-plane k-vectors. This is far from ideal for photonic crystal light extraction. Regardless of the choice of lattice constant, some of the quasi-modes will only be extracted to large extraction angles.

The starting point is much better in InGaN thin-film LEDs. The lower refractive index of InGaN compared to AlGaInP confines the guided modes to a smaller range. The active layer is also situated close to the bottom mirror (typically between a half and three quarters of a wavelength), which gives a much larger periodicity of the intensity modulation. The guided mode distribution for InGaN LEDs $\sim 6\mu m$ thick with a single quantum well is plotted in Fig. 18(b). There are two intensity maxima around $k_i = 2.3$ and $k_i = 1.1$. The distance between the maxima $\Delta k = 1.2$ is larger than the radius of the extraction cone ($r = 1$). If $G_0 = 1.1$ is chosen, the second mode will be diffracted directionally whereas the first mode is out of reach for the first diffraction order. In fact, this mode distribution is very advantageous, since second and third order diffraction can extract the second intensity maximum directionally. With the intensity modulation obtained by the source-mirror resonance, it is thus possible to extract the modes with highest intensity directionally if several diffraction orders are used. One could consider to further reduce the distance between the bottom mirror and the active layer to obtain only one intensity maximum (at $k_i \approx 2.2$) in the guided mode distribution as in Fig. 18(c). However, efficient extraction requires that these modes have a high overlap also with the PhC (Paper VI). This applies especially to guided modes with $k_i < n_{PhC}$ since the remaining guided modes with $k_i > n_{PhC}$ are evanescent in the PhC. The diffracted intensity from a LED with the guided mode distribution in Fig. 18(c) would therefore be low (see Fig 12-13 in Paper VI).

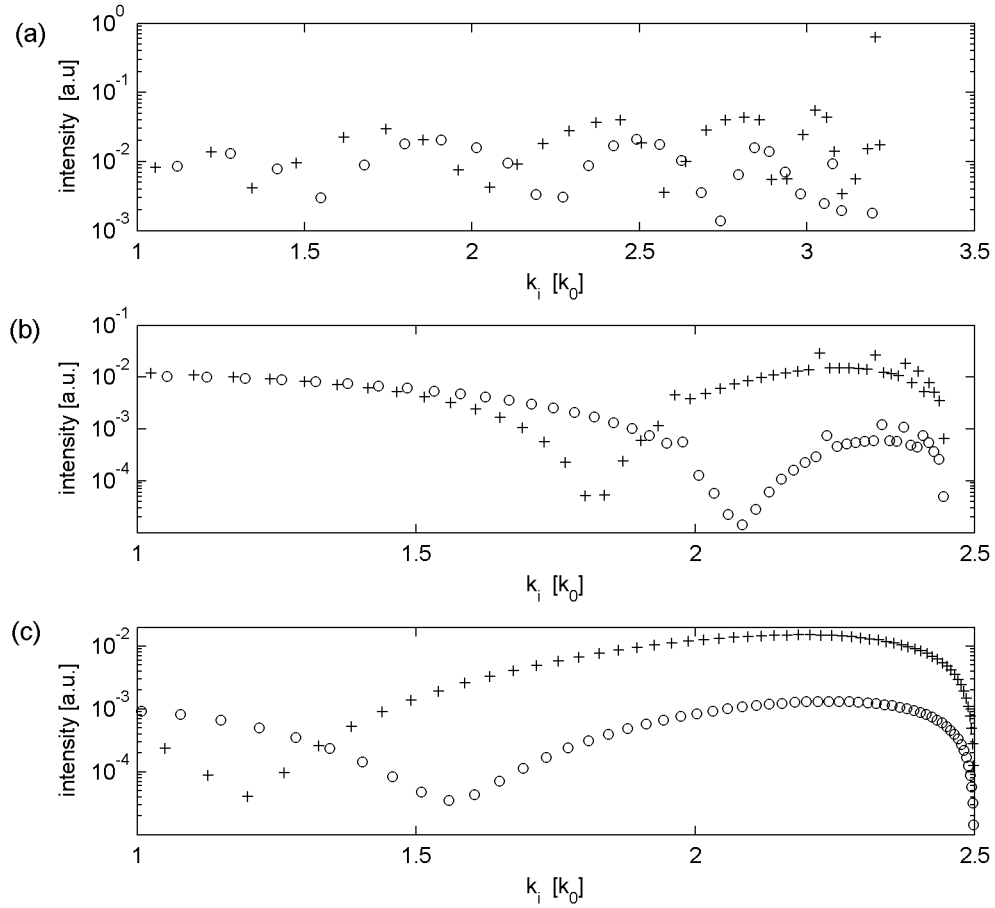

Fig. 18 Guided mode distribution (TE '+' and TM 'o' modes) for a AlGaInP thin-film LED (top), InGaN thin-film LED (centre) and InGaN thin-film LED with modified vertical layer design (bottom). Note the logarithmic scale on the y-axis.

The next aspect to consider for the vertical stack design is absorption. High extraction efficiency can never be achieved unless the absorption is reduced to a minimum. The absorption coefficient can differ by orders of magnitude between different modes and also for different LED designs with different epitaxial quality, active material thickness and mirror absorption. A thin device is advantageous when absorption in the semiconductor layers is significant. The mode can then interact more strongly with the PhC per unit propagation length in the bulk material. Mirror absorption is the dominating absorption mechanism in InGaN thin-film LEDs. The LED thickness is then of minor importance.

Finally, the vertical layer stack design determines the direct light extraction efficiency and the farfield radiation pattern of the directly emitted light. This aspect should not be neglected. With typical photonic crystal enhancement factors between *50%* and *200%*, *67%* and *33%* of the extracted light in PhC-LEDs is extracted without diffraction,

respectively. The simulated farfield radiation pattern for a ~*6μm* thick InGaN LED is plotted in Fig. 19(a). Strong FP resonances are seen in the monochromatic farfield (red). The exact position of the FP resonances is not important for the farfield in such a thick LED, since they are shifting along the spectral width of the emitted light. The flat farfield in (a) is caused by the resonance effect between the active layer and the bottom mirror, just like for the guided modes. Correctly tuned, it is possible to produce a Lambertian farfield radiation pattern by adjusting this distance, as seen in Fig. 19(b). Very thin devices or LEDs with the active layer situated in a resonant cavity have only one FP mode in the light extraction cone. The farfield can then be tuned freely; this is exemplified in Fig. 19(c) with the designed farfield for the PhC-RCLEDs in Paper II, optimized for emission within 30°.

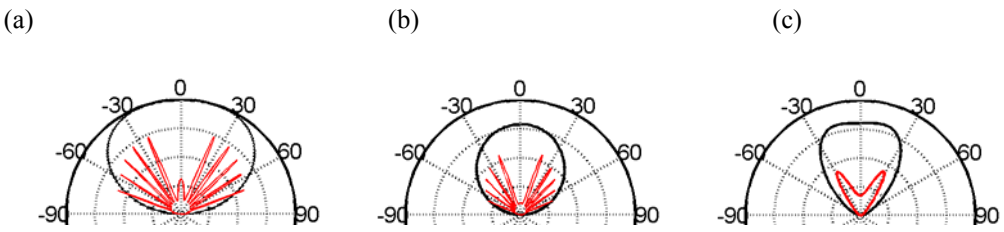

Fig. 19 Calculated farfield radiation pattern for a InGaN thin-film LED (a). The sharp FP-resonances in the monochromatic farfield (red) are averaged by the spectral width for all emitted light (black). The flat farfield is caused by the resonance between the active layer and the bottom mirror. The farfield shape can be tuned by changing this distance (b). The beam-shape can be tuned freely when there is only one FP resonance within the spectral width of the emitted light. The designed farfield for maximal emission within ~*30*° for the AlGaInP RCLED in Paper II is seen in (c).

In summary, thin-film LEDs without a substrate are ideal for photonic crystal light extraction. The primary goal with the optimization of the vertical layer stack is to approximate the single-mode LED. This can be done by reducing the slab thickness and/or by enhancing the spontaneous emission in a narrow guided mode range by placing the active layer close to the bottom mirror. The farfield radiation pattern of the directly extracted light (without the PhC) is also determined by the thickness of the slab and the QW position.

5.3 Optimization of the photonic crystal

In this section we will discuss how the photonic crystal properties influence the extraction efficiency. These are the lattice constant, the air filling factor, the etch depth and the symmetry order of the lattice. If not otherwise stated, we will deal with the

optimization of a hexagonal lattice, since this is the regular lattice with highest symmetry.

Lattice constant

The lattice constant a appears in Bragg's law (Eq.(36)) via its reciprocal counterpart G_0 and it therefore determines what modes can be diffracted at all and by what diffraction order. In the single-mode case, the lattice constant should be chosen so that G_0 is slightly smaller than the effective index of the mode since this maximizes the arc length of the diffraction line in the air disk. The choice of diffraction order in the case of a hexagonal lattice depends on the absorption coefficient as discussed earlier. The choice of optimal lattice constant for a multi-mode LED is an optimization problem with a unique solution for every guided mode distribution that can be solved with the model based on coupled-mode theory (Paper VI). As a rule of thumb, the optimal lattice constant for highest extraction efficiency is found in the range $1 < G_0 < n_{PhC}$. For red AlGaInP LEDs, this corresponds to $a = 300\text{-}750nm$. It seems plausible to aim at the centre of this mode range, which yields $a \approx 420nm$ ($\lambda = 650nm$). This trend is confirmed by the experimental results in Paper I (in Paper II, only lattice constants in this range were examined) as well as in several lattice constant variations made during this work that have not been published. Similarly, the range of interesting lattice constants for InGaN LEDs is found between $a = 270nm$ and $a = 520nm$. The reason for this is threefold. First of all, we have seen (in Paper VI) that modes with $k_i < n_{PhC}$ have a higher overlap with the PhC and thus couples stronger to the radiating modes. Secondly, most of these modes can be extracted omnidirectionally with a hexagonal lattice (applies for $k_i < 2$). Therefore, they are extracted more strongly than modes with higher effective index. Thirdly, the modes with high effective index can still be extracted by second and third order diffraction, e.g. by $\sqrt{G_0}$ and $2G_0$, as discussed in Section 4.3. If on the other hand G_0 was chosen to extract the low order modes by first order diffraction, the high order modes could not be extracted at all. The fact that low order modes can be extracted (by high order extraction) although $G_0 < n_{PhC}$ is very important. In a typical InGaN (AlGaInP) thin-film LED, approximately *50%* (*70%*) of the light is emitted into modes with $k_i > n_{PhC}$. A large part of this light must also be extracted in order to compete with LEDs with surface roughening.

It is worth noting that a larger G_0 than here suggested is used in the vast majority of all papers about InGaN LEDs [9]-[10], [12]-[14], [48]. The reason for this is that nearly all work on InGaN LEDs has been made on devices where the sapphire growth substrate has not been removed. In these LEDs, one can differ between sapphire modes with $k_i \in [1, n_{sapphire}]$ and modes guided in the InGaN LED with $k_i \in [n_{sapphire}, n_{GaN}]$. The former class of modes interact very weakly with the photonic crystal and is therefore extracted very slowly. The only interesting modes for PhC light extraction is then found in the latter quite narrow range. The range of modes that can be extracted in thin-film InGaN LEDs is larger: $k_i \in [1, n_{GaN}]$ and the optimum is therefore shifted towards smaller reciprocal lattice constants. The model based on couple mode theory [Paper VI] convincingly predicts the correct lattice constant for this type of LEDs. We also noted with interest that the excellent extraction efficiency to air from InGaN thin-film LEDs by Wierer et al [54] was achieved with a small G_0, close to the second and third diffraction order for the low order modes.

In this discussion we have neglected the directionality of the emitted light. Directionality can only be achieved if one mode or a narrow range of modes gets more spontaneous emission than the other modes. This was discussed in the previous section. The lattice constant should then be chosen so that these modes can be extracted by first order diffraction or by a combination of second and third order diffraction when the mode absorption is low and $k_i > 2$. An example for this is found in Paper V. A combination of the first and second diffraction order on the other hand can never bring directional extraction, due to the large difference in reciprocal lattice vector length. This case was shown in the Ewald diagrams in Fig. 15(a) and (c).

Air filling factor

The air filling factor affects the light extraction in two ways. It determines the diffraction strength for the different diffraction orders and it changes the effective refractive index of the PhC. The diffraction strength β is proportional to the squared Fourier transform of the photonic crystal dielectric map [47]:

$$\beta \propto |\tilde{\varepsilon}(G)|^2 \qquad (41)$$

We recall from Section 4.1 that for circular holes, the Fourier transform can be calculated with Bessel functions:

$$\tilde{\varepsilon}(G) = F \cdot \frac{J_1(GR)}{GR} \tag{42}$$

Here, F is the air filling factor of the PhC, J_1 is the first Bessel function of the first kind, G is the reciprocal wave-vector length and R is the radius of the holes. First (ΓM), second (ΓK) and third order ($2\Gamma M$) diffraction corresponds to the reciprocal lattice vector lengths G_0, $\sqrt{3}G_0$ and $2 \cdot G_0$, respectively. The diffraction strength and the relative diffraction strength for the first three diffraction orders is shown in Fig. 20 (a)-(b) as a function of the filling factor. First order (ΓM) diffraction is maximized for $F = 0.4$ whereas the sum of the three first diffraction orders is maximized for $F = 0.5$. Hence, $F = 0.4$ is preferable when first order diffraction dominates (for example with high absorption) whereas $F = 0.5$ is better when high order diffraction also contributes to the light extraction efficiency.

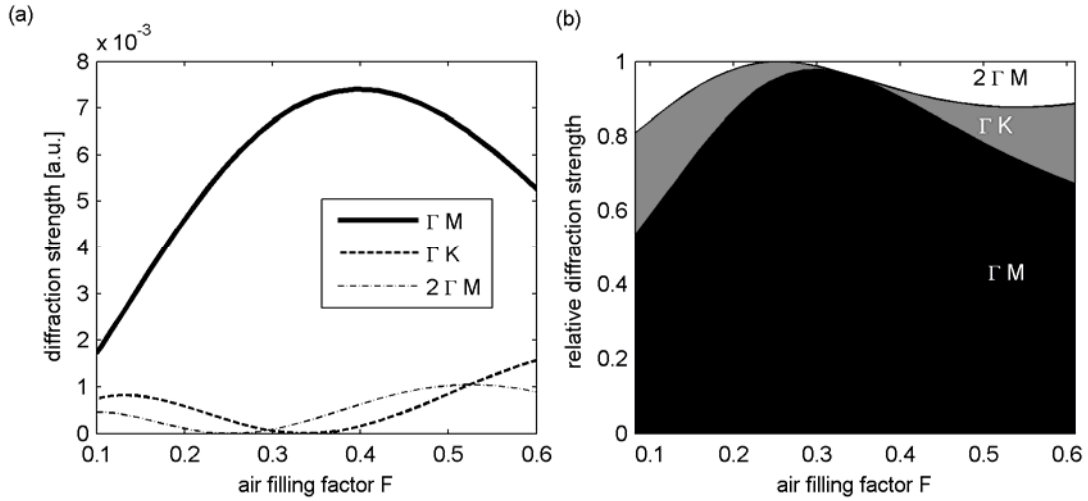

Fig. 20 Diffraction strength (a) and relative diffraction strength (b) for the first three diffraction orders of a hexagonal lattice as a function of the air filling factor F.

The second aspect of the filling factor is the average refractive index of the PhC, given by Eq. (33). Modes with $k_i > n_{PhC}$ are evanescent in the PhC and the diffraction strength for these modes is therefore very weak (Paper VI). A small filling factor results in a higher effective refractive index, which increases the guided mode overlap with the PhC.

In summary, the diffraction strength speaks for a rather high filling factor between *0.4* and *0.5* whereas the mode coupling is stronger the smaller the filling fraction is. Therefore, it is not intuitive what filling factor should be used in general. FDTD simulations by Christopher Wiesmann [55] show that the problem is relaxed in a multi-

mode LED. The extraction efficiency is not changed at all in the range *0.3-0.5* and the loss is less than *10%* between $F = 0.2$ and $F = 0.6$. This very broad optimum should get narrower in the single-mode case, as discussed in Section 4.3. Nevertheless, we can conclude that the variations in air filling factor do not change the extraction efficiency very much for multimode LEDs. The photonic crystals I have fabricated have been designed to have an air filling factor between *0.4* and *0.5*.

Etch depth

The thickness of the PhC (i.e. the etch depth) plays an important role since it determines the coupling strength between the guided and radiant mode. The extraction efficiency dependency on the etch depth was investigated experimentally in Paper I. A fourfold increase of the etch depth from *200nm* to *800nm* resulted in approximately *50%* stronger diffraction. A detailed analysis of the etch depth using the model based on coupled mode theory can be found in Paper VI. For a mode with $k_i > n_{PhC}$, the coupling integral κ_{id} that determines the diffraction strength, initially increases strongly with the etch depth as long as the thickness is smaller than the attenuation length of the mode in the PhC (Fig. 21). The attenuation length is typically one or a few hundred *nm*. Etching even deeper leads to even higher diffraction strength but the increase is more moderate. The increased diffraction strength for etch depths exceeding the attenuation length of the mode is attributed to the thinner remaining slab thickness t rather than the thicker PhC. It is shown in Paper VI that the diffraction strength is proportional to t^{-3}, a reproduction of the analytical result in [47].

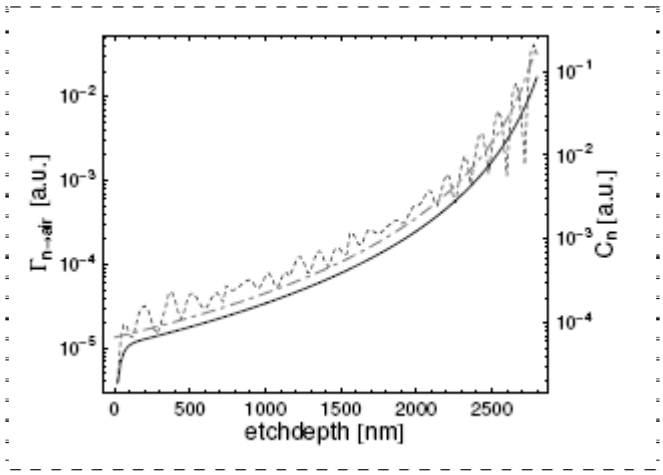

Fig. 21 Diffraction strength (dashed line) of the lowest order guided mode to air for an InGaN thin-film LED with overall thickness of *3μm*. A good agreement with a fit according to t^{-3} (dash-dotted line), where t is the remaining slab thickness, is attributed to the overlap of the guided mode with the PhC (solid line). [Fig. 6 in Paper VI]

In conclusion, the etch depth should be "sufficiently" large which means a few hundred *nm*. For a pre-defined total LED thickness, the diffraction strength is further enhanced with even larger etch depths, but this is rather the result of the thinner remaining slab than the etch depth itself. It should however be noted that the mode overlap with the mirror also increases when the thickness of the unetched slab is reduced. Both the extraction strength and the absorption strength are thus increased. The light will therefore be extracted or absorbed faster, while the extraction efficiency may remain the same (Paper VI).

Lattice symmetry

When treating the single mode diffraction case in Section 4.3, we mentioned that modes with an effective index $k_i > 2$ can not be completely extracted by first order diffraction with a hexagonal lattice. Light propagating near the ΓK-direction is out of reach for the six nearest lattice points in the reciprocal plane. The number of first order lattice points needed for omnidirectional extraction is plotted in Fig. 9 in Paper III. At least 8 points are required for InGaN ($k_i < 2.5$) and 11 points are required for AlGaInP ($k_i < 3.5$). The problem with the lacking number of first order lattice points for the hexagonal lattice can be circumvented by applying a smaller reciprocal lattice constant G_0 and use the second and third diffraction order, as previously discussed. But the efficiency is high enough only when the mode absorption is low (as demonstrated in Paper V). It would be more convenient to use only one diffraction order that has more reciprocal lattice points than the hexagonal lattice. Ideally, one would like only one diffraction order that has a ring-shaped Fourier transform. This was recognized by Rattier et al in [56] and Archimedean tilings [14], [49], [56] have been proposed for this purpose. The A7 and the A13 lattices are the most commonly used lattices and the former is plotted in Fig. 22 together with its Fourier transform. Both lattices have 12 main reciprocal lattice points which is enough to enable omnidirectional light extraction for all modes in InGaN and AlGaInP LEDs. The higher symmetry should thus in principle increase the light extraction efficiency compared to devices with hexagonal lattices.

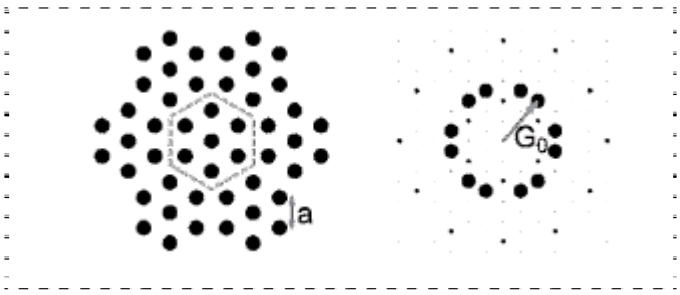

Fig. 22 Archimedean A7 lattice with lattice constant a in the real plane (left) and G_0 in the reciprocal plane (right). The diameter of the points in the reciprocal plane corresponds to the squared modulus of the Fourier transform. The A7 lattice has 12 main reciprocal lattice points – twice as many as the hexagonal lattice. [Paper III Fig 10(b)]

Throughout my work, I have used the Archimedean A7 lattice for comparisons with the hexagonal lattice. Experimental comparisons between the A7 lattice and the hexagonal lattice are presented in Paper I and in Paper IV. In both cases, the A7 lattice was more efficient although the difference between the two lattices was marginal. The radiant intensity for InGaN PhC-MCLEDs on the other hand, was found to be much lower than for the hexagonal lattices in Paper V. Is this representative for A7 lattices in thin-film LEDs? A trend can be seen when considering all experiments made throughout my work. In the AlGaInP material system five comparisons can be made whereas for InGaN LEDs only three different experiments exist. The experiments differ in terms of the epitaxial layer design and/or PhC etch depth. In each experiment, a number of hexagonal and A7 lattices with varying lattice constants were fabricated. The best A7 and hexagonal lattice constant was selected and compared to another. The enhancement for the best A7 lattice over the best hexagonal lattice was calculated. The average enhancement value for the radiant flux and the radiant intensity is listed in Table 3.

Material system	**peak wavelength range *[nm]***	**# of comparisons**	**average A7 enhancement in Φ_e**	**Average A7 enhancement in I_e**
AlGaInP	630-660 nm	5	+4%	-2%
InGaN	450-460	3	0%	-22%

Table 3: Average enhancement in emitted flux Φ_e and radiant intensity I_e for the A7 lattice compared to the hexagonal lattice. A small positive enhancement in flux is observed for AlGaInP LEDs. The radiant intensity is however higher for hexagonal lattices.

The radiant flux from AlGaInP LEDs is enhanced with *4%* on average whereas the radiant intensity is marginally reduced. No flux improvement at all is observed for InGaN LEDs but the radiant intensity is drastically reduced by *22%*. Let us first discuss the emitted flux. Modes with a high effective index gain most from the larger number of

lattice points and it is thus logical that an enhancement is obtained for AlGaInP LEDs. The problem with lacking omnidirectionality is smaller for InGaN LEDs and apparently, no enhancement at all is obtained regarding total light extraction.

The disappointing performance for the A7 lattice is in line with the experimental results of A7 lattices in GaAs heterostructures [49]. The worse performance of the Archimedean lattices compared to a hexagonal lattice in this paper is attributed to the halved diffraction strength of each of the 12 main lattice points compared to the six lattice points in the hexagonal lattice. The lower diffraction strength of each point compensates for the omnidirectional extraction in a high absorption regime, whereas a net positive gain compared to the hexagonal lattice is expected with negligible absorption. This trend is also seen for hexagonal lattices in Fig. 16. In this figure, strong first diffraction order of a hexagonal lattice is compared with omnidirectional extraction using the second and third diffraction with much lower diffraction strength. However, a halved diffraction strength is not enough to explain the much lower radiant intensity observed for the A7 lattices in Table 3. The reason for the lower radiant intensity may instead be found in Paper III (Fig 12b). The Fourier intensity for the first diffraction order of the A7 lattice (i.e the sum of the 12 main lattice points) is *25%* lower than for a hexagonal lattice (the sum of the six nearest lattice points). The Fourier intensity for all lattice vectors with length $G < 2 \cdot G_0$ (i.e. corresponding to the three lowest diffraction orders for the hexagonal lattice) is reduced by *13%*. Hence, the diffraction strength for the Archimedean lattice is distributed over more diffraction orders. This results in weaker beam-shaping for Archimedean lattices. The radiant intensity for different lattice constants in Fig 4(a) in Paper V is a typical example for this. Hexagonal lattices have the highest as well as the lowest radiant intensity, whereas the variation for different lattice constants with the A7 lattice is smaller.

In summary it is found that the use of Archimedean lattices gives slightly higher light extraction for AlGaInP LEDs whereas no enhancement over hexagonal lattices could be found for InGaN LEDs. The radiant intensity is however reduced, since the Fourier intensity of the dielectric map of the Archimedean lattice is distributed over more diffraction orders than for the hexagonal lattice. The most important feature of PhC-LEDs, namely the beam-shaping properties – is thus weakened.

5.4 AlGaInP photonic crystal LEDs

In this section we will analyze the potential of PhC-LEDs in the AlGaInP material system. The work has resulted in Paper I and II and these results will be discussed together with unpublished experimental results. The two main questions are if photonic crystals can help improve the total efficiency of red LEDs and if the directionality of the emitted light can be enhanced to improve the system efficiency of étendue limited optical system. When we started with this work in June 2006, there was no single publication on AlGaInP LEDs with photonic crystals and the first article about thin-film photonic crystal LEDs had just been published [15]. The aim with the first thin-film PhC-LEDs was therefore to find out how they compare with LEDs with surface roughening and to find the best photonic crystal parameters. PhC-LEDs with a wide range of lattice constants were fabricated with two etch depths: *200nm* and *800nm*. The high refractive index for AlGaInP made quasi-crystals particularly interesting since hexagonal lattices cannot extract most modes omnidirectionally. We therefore choose to compare the hexagonal lattices with Archimedean A7 lattices. The results are presented in Paper I.

The extraction efficiency enhancement for the thin-film PhC-LEDs is plotted in Fig. 23 (left). The lattice constant scan between *224nm* and *490nm* shows very clearly that large lattice constants (i.e. small G_0) are most efficient. This confirmed the simulation results based on coupled mode theory. Hence, high order modes with a small effective index (called type III modes) could be extracted more easily than modes with a high effective index (type II modes). The mode profiles for the different types are plotted in Fig. 17.

The very low enhancement of about *5%* for the lattices with $G_0 = 3.4$ is quite remarkable – despite good PhC quality and regardless of the etch depth! This definitely shows that the photonic crystal is something else than any random surface structure. Spectral farfield measurements (Fig. 23 right) for this lattice constant showed two strong diffraction lines that completely disappear below the peak wavelength. Bragg's law, Eq. (25), was used to confirm that the line is caused by a mode with very high overlap with the active region, see Fig. 18(a). This mode is guided in the high index active region and evanescent in the surrounding thick AlInP electrical confinement layers with lower refractive index. Very dense diffraction lines are seen in the spectral farfield for a hexagonal lattice with $G_0 = 1.7$ in Fig. 23 (b). The thickness ($\sim 4\mu m$) of the

LED results in a large number of modes with no favourable mode range as seen in Fig. 18(a). It is therefore very difficult to achieve directional light extraction.

Two very important conclusions could be drawn about the efficiency of these devices. First of all, the external efficiency of the reference devices without any PhC is much higher than one can predict with 1D extraction efficiency calculation. This is explained by the very strong photon recycling (i.e re-absorption and subsequent re-emission of light) that effectively redistribute light from guided modes to the light extraction cone. Secondly, the efficiency enhancement achieved with PhC (less than *50%*) is much lower than for standard devices with surface roughening (approximately *100%*). The ability to extract modes in a narrow mode range in terms of effective index is clearly not advantageous for standard thin-film LEDs with a quasi-continuum of guided modes in a wide range.

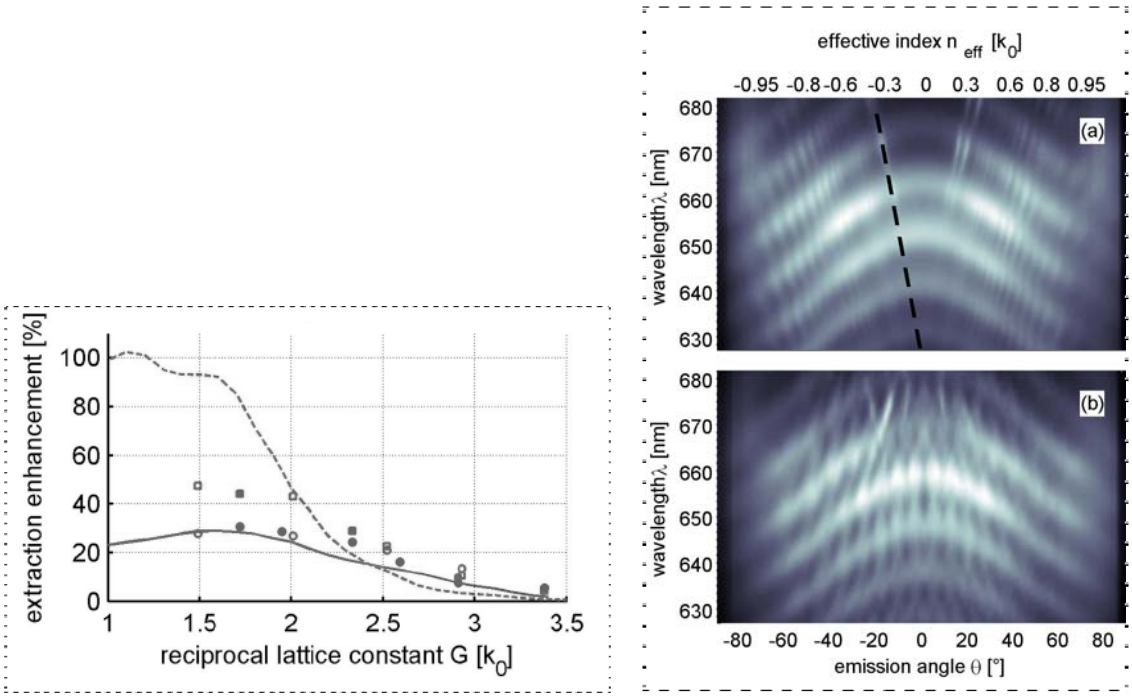

Fig. 23 Left: Experimental PhC enhancements for hexagonal (filled) and A7 (open) lattices with *200nm* (circles) and *800nm* (squares) etch depth together with simulated diffraction intensity in [a.u.] for *200 nm* (solid line) and *800nm* etch depth (dashed line) [Fig 2(d) in Paper I]. Right: Normalized spectral resolved farfields for hexagonal PhC-LEDs in the ΓM direction (a) $G_0 = 3.4$; The calculated type I mode with highest intensity has been inserted (dashed line). (b) $G_0 = 1.7$; Strong diffraction of type III modes at all wavelengths. [Fig 3 Paper I]

These limitations for directional light extraction were addressed in Paper II. The aim was to combine directional light extraction from a resonant cavity with directional PhC diffraction. The total epitaxial thickness was reduced to *1.4μm* in order to reduce the

number of guided modes in the LED. Furthermore, a top DBR was incorporated so that the MQW region was situated in a *5λ/2*-cavity. This helped improving the direct light extraction efficiency from *3.5%* for the reference devices in Paper I to *6.6%* with high directionality for the unstructured RCLED in Paper II according to a 1D mode solver calculation [50]. The realization of the thin resonant cavity was only possible by thinning down the AlInP electrical confinement layers to *90nm* on each side. The usual n-side current spreading layer was also omitted and replaced by a *290nm* thick transparent conductive oxide. Fig. 24 shows the external quantum efficiency as a function of the lattice constant for devices mounted on TO18 headers (extraction to air) and LEDs in a PowerTOPLED package. The dependency on the lattice constant was less pronounced for the AlGaInP RCLEDs than in the previous experiment since only lattice constants mainly extracting high order (type III) modes were fabricated. The extraction enhancement was *120-160%* for extraction to air – excellent values exceeding extraction enhancements normally achieved with surface roughening. Unstructured reference devices as well as devices with $G_0 = 1.5$ showed directional light extraction – their directionality within *30°* was *31%* and *29%*, respectively. This should be compared to Lambertian emission with *25%* directionality. The directional emission for the PhC-RCLED was made possible since only three guided modes were strongly extracted Fig. 25(b).

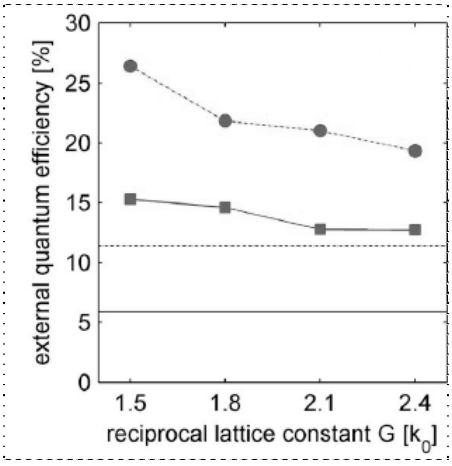

Fig. 24 External quantum efficiency at *30mA* as a function of the reciprocal lattice constant of the PhC for extraction to air (squares) and for encapsulated chips (circles). The efficiency for unstructured RCLEDs is plotted as horizontal lines (solid line to air and dotted line for encapsulation) [Fig 1(d) Paper II]

The re-design of the epitaxial layers did however also result in lower internal efficiency. The strong extraction contribution from photon-recycling found for the standard thin-film LEDs in Paper I has completely vanished. The low internal efficiency is probably

caused by high non-radiative recombination. This assumption is enforced by the high current density (*63-95A/cm*^{2}) for which the peak external quantum efficiency is reached. Non-radiative recombination is dominant at low current densities (see Section 2.4) and accordingly, high non-radiative recombination rates push the efficiency peak towards higher current densities. A possible explanation for the high non-radiative recombination is diffusion of dopants from the extremely thin p-side (i.e. mirror side) into the active MQW region. The very thin electrical confinement layers can also have resulted in higher current leakage across the MQW region at high current densities and therefore contributed to the lower internal efficiency. But this effect is clearly not dominating since this would have pushed the peak quantum efficiency to small current densities.

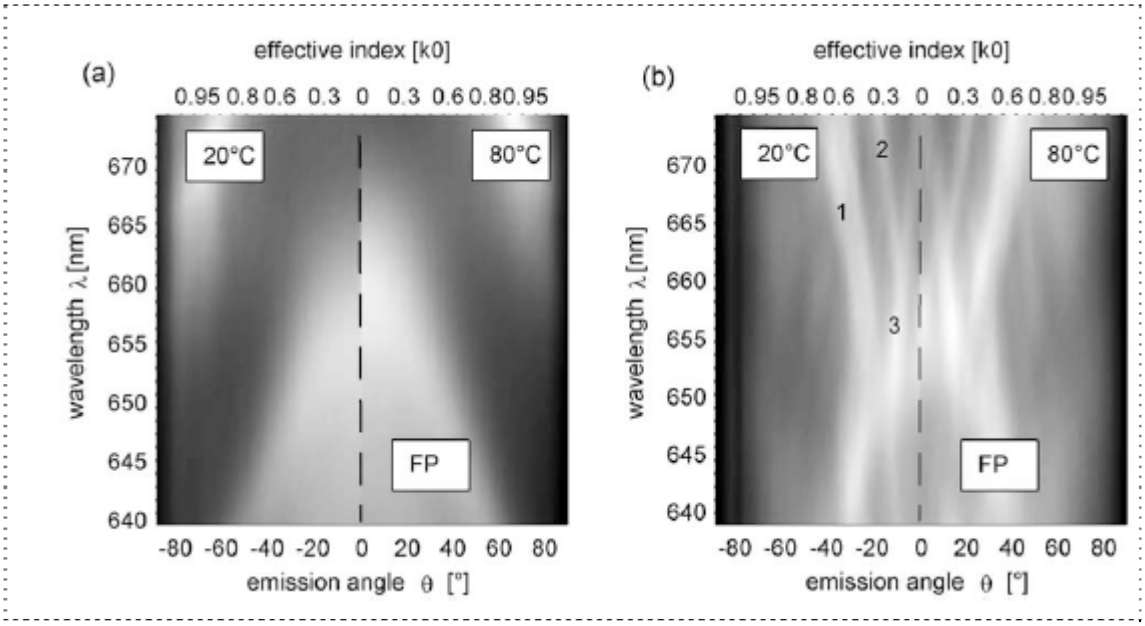

Fig. 25 Normalized spectral farfield for an unstructured RCLED (a) and for a PhC-RCLED with $G_0 = 1.5$ (b) measured at *20°C* (left side) and *80°C* (right side). Three strong diffraction lines can be seen together with the boomerang-shaped Fabry-Perot mode for the PhC-RCLED [Fig. 2 Paper II].

In conclusion, it is shown in Paper II that the directional emission from the resonant cavity can be combined with directional light extraction with a PhC in the AlGaInP material system. Directional light extraction from AlGaInP PhC-LEDs is thus demonstrated for the first time. But the re-design of the epitaxial layers can easily lead to reduced internal efficiency. The very non-linear response to this reduction, which is caused by the onset/reduction of photon recycling, is detrimental for the external quantum efficiency. It remains unclear from these results if the reduction of the internal

efficiency is inevitable for such thin devices or if it is just a question of optimization of the epitaxial growth.

Comparison with thin-film surface roughening LEDs

The enhancements stated in this section have all been made in comparison with LEDs with an unstructured surface. The external quantum efficiency as well as the PhC enhancement factor achieved are better than for any other AlGaInP PhC-LEDs found in the literature [51], [52], [53] at the time of writing (2009). However, state-of-the-art LEDs have a rough surface and the real test is therefore how PhC-LEDs perform in relation to these. Such comparisons can not be found in literature today. In total three AlGaInP wafers with different epitaxial designs have been processed with a large variation of PhC-LEDs side by side with unstructured LEDs and LEDs with surface roughening. In two out of three comparisons, the best PhC-LEDs have outperformed the LEDs with surface roughness by *20-30%,* whereas rough LEDs were slightly more efficient in the last comparison. The enhancement factor compared with unstructured references for the thin-film RCLEDs in Paper II was also much higher than reported enhancements achieved with surface roughening for AlGaInP LEDs in literature [57]-[58]. It is therefore tempting to conclude that photonic crystals are generally more efficient light extractors in AlGaInP thin-film LEDs. There is however some reason to believe that these results are not representative.

First of all, the PhC enhancement (*47%*) for the PhC-LEDs in Paper I was quite moderate. No surface roughening LEDs (SR-LEDs) were processed for comparison in this experiment, but the external quantum efficiency was lower than one could typically expect from SR-LEDs. These PhC-LEDs have most similarities with SR-LEDs in production regarding epitaxial design and chip design. The conclusion is thus that the use of photonic crystals is less efficient than surface roughness for LEDs with a thick epitaxial film.

The comparison between surface roughening and photonic crystals was made with thin epitaxial designs and two transparent contacts. A surface roughening process similar but not identical to the process used in production has been used that normally gives an identical result. The quality of this process step was given less attention than for

example the etching of the photonic crystal. SEM images have then shown that parts of the LED surface are still smooth. The quality of the surface roughness can thus be questioned. The only conclusion we can draw from the direct comparisons is thus that a good photonic crystal is better than poor surface roughening. We will see in the next section that the results are more conclusive regarding InGaN-LEDs.

5.5 InGaN photonic crystal-LEDs

The InGaN LEDs were grown on sapphire substrates and processed as thin-film LEDs. The lattice mismatch between sapphire and InGaN requires the growth of a thick buffer layer to be able to grow the active layers of the LED with high crystal quality. The active region is situated near the bottom mirror and the spontaneous emission can therefore be strongly modulated. With the exception for a AlGaN electronic buffer layer on the p-side and the thin Indium-containing quantum wells, all epitaxial layers can be assumed to have the same refractive index $n \approx 2.5$. Standard thin-film LEDs are *5-6μm* thick. As already discussed, thick epitaxial layers result in weak interaction of the light with the PhC and the light extraction process is therefore slow. The buffer layers have no function in the processed LED except for lateral current spreading and can therefore in principle be removed by etching. This opens the way for ultra-thin devices that have a very low number of modes. The slow extraction in thick InGaN LEDs should however affect LEDs with surface roughening equally – and they are highly efficient. It is therefore of principal interest how PhCs perform in thick LEDs compared to devices with surface roughening. Two sets of InGaN PhC-LEDs were fabricated and analyzed – *850nm* thick micro-cavity LEDs on the one hand and LEDs with standard thickness on the other hand. The results for the first approach are presented in Paper IV and Paper V. The simulation results in Paper III and Paper VI also deal primarily with InGaN PhC-LEDs.

Thin-film InGaN micro-cavity LEDs

The InGaN thin-film micro-cavity LEDs with photonic crystals were fabricated to minimize the number of guided modes in the LED in order to maximize the farfield shaping with the photonic crystals. A further requirement was a single FP-mode within the spectral width of the emitted light to enable directional direct light extraction. As previously discussed, the ideal LED would support only one guided mode. The thick n-doped buffer layer was dry etched to the final thickness *850nm*, as confirmed by an

image of a vertical layer cross-section made with a focused ion-beam (FIB). LEDs were patterned with hexagonal, A7 and 1D photonic crystals of *400nm* etch depth with different lattice constants. A *135nm* thick ITO layer was deposited on the patterned chip surface to ensure good current spreading in the absence of the thick buffer layer. This non-optimized process led to a high forward voltage around *4.5V* at *20mA*. The spectral farfield radiation patterns revealed that only three guided mode contributed to the light extraction. This made it possible to study the light extraction of one mode alone, rather than that of a bunch of modes. The performance of these devices is documented in Paper IV whereas the influence of high order diffraction is analyzed in Paper V. The findings are briefly summarized in the following:

- The radiant flux was found to be almost independent of lattice type and lattice constant. The absolute values for encapsulated devices (*15.8mW* at *20mA*, $\eta_{QE}^{peak} = 36\%$ for the best device) are approximately *10% - 20%* below the expectation value for a SR-LED with the same epitaxial quality. This can partly be explained by the introduction of the ITO layer that is not absorption free. Shunts at small currents for many PhC-MCLEDs may also have influenced the radiant flux negatively.
- The radiant intensity was varying strongly with the lattice constant and lattice type. The enhancement over unstructured MCLEDs was *330%*, much more than the flux enhancement of *85%*.
- The optimal lattice constant depends on the acceptance angle of the optical system with a shift to larger G with increasing acceptance angle. For the hexagonal lattices, the highest flux within small acceptance angles of $\theta < 18°$ is obtained for $G_0 = 1.2$, a slightly larger $G_0 = 1.3$ is optimal between *18°* and *30°* and $G_0 = 1.5$ is best between *30°* and *55°* (Figure 4(b) in Paper V).
- The very high enhancements for small extraction angles are not only caused by the directional PhC light extraction but also because the background farfield is anti-directional. The p-side thickness for these devices is better suited for emission to encapsulation rather than to air. Attempts were of course made to realize similar devices with a modified p-side thickness but for various reasons these wafers could not be processed into working LEDs.
- The large number of lattice constants fabricated allowed me to map the mode dispersion over a large reduced frequency range, see Fig. 26(a). The same guided modes can be identified for devices with different lattice constants, thus

convincingly confirming that light extraction with PhC can be described by Bragg's law. The azimuthal farfields were used to identify the crystal direction of the lattice relative to the measurement axis. Fig. 26(b) shows the azimuthally resolved farfield at $a/\lambda \sim 0.64$. The shift of $30°$ of line 1b relative to line 1 proves that the former is caused by second order diffraction. The repeated use of Bragg's law for the two diffraction orders confirmed that the two sets of lines are caused by the same mode I. In the same way it can be shown that line 1c, which appears at $a/\lambda \sim 0.95$, is shifted $30°$ in the plane relative to line 1b (not shown) and that it is caused by third order diffraction with $|\vec{G}| = 2 \cdot G_0$, e.g. by $\vec{G} = G_0 \cdot 2 \cdot \vec{b}_1$. Finally, line 1d is identified as mode I diffracted by the fourth order with $|\vec{G}| = \sqrt{7} \cdot G_0$, e.g. by $\vec{G} = G_0 \cdot (2 \cdot \vec{b}_1 + \vec{b}_2)$. The observation of several high diffraction orders was very much unexpected because of their lower Fourier intensity. Due to the low number of modes present is this LED, it was possible to extract the line intensity for the first and second diffraction order and it was found that $\eta_1/\eta_2 = 1.6 \pm 0.2$ in favour of first order diffraction. A model was introduced to understand these results. I have already used the same model to calculate the extraction efficiency of a single guided mode in Section 4.3.

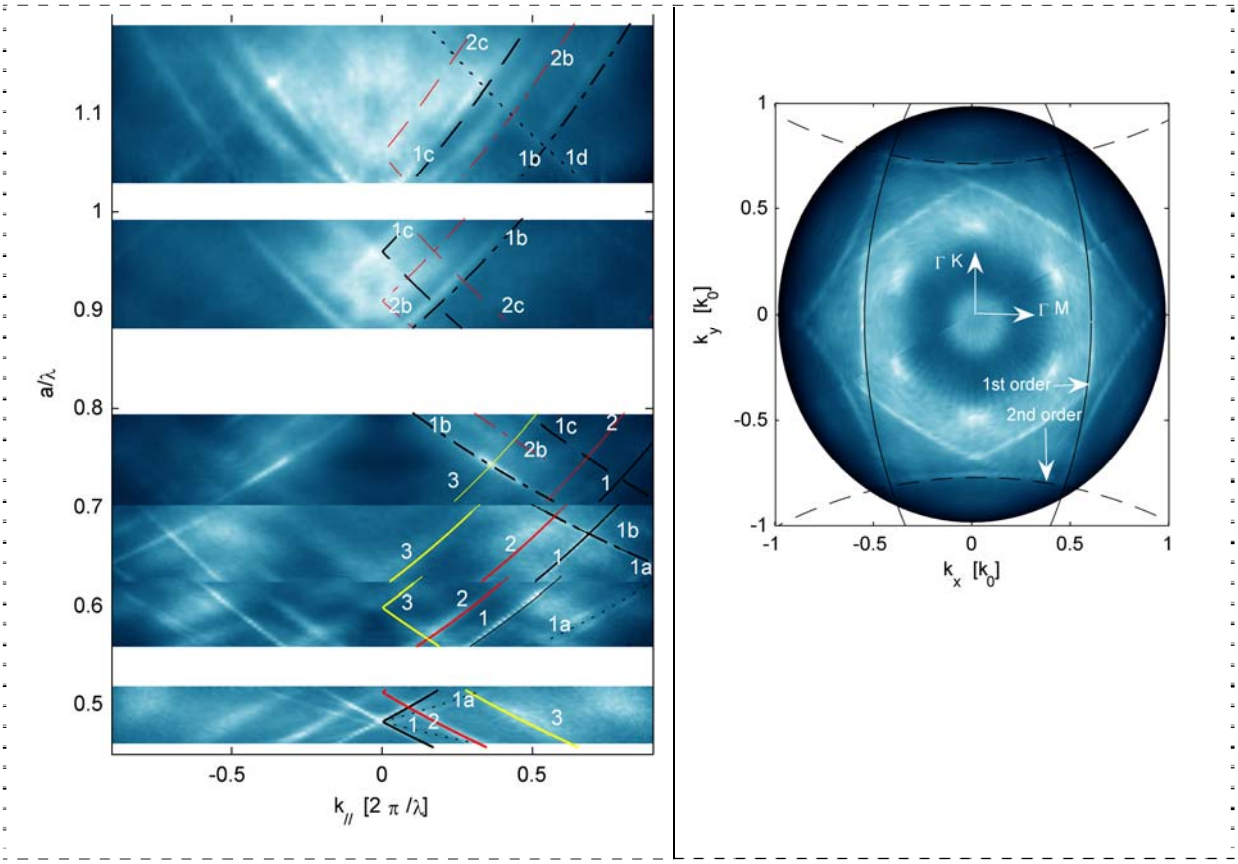

Fig. 26: "Photonic band diagram" (left): Spectral resolved farfields for TE polarized light collected in the ΓM-direction for different lattice constants. Three modes are detected altogether. Predicted diffraction lines from modes I-III are superimposed. b-,c- and d-lines are caused by diffraction of second, third and fourth order, respectively [Fig. 2 Paper V]. Azimuthally resolved farfield of the emitted light (λ=*475nm*) for a PhC-MCLED with $a/\lambda = 0.644$ ($G_0 = 1.7$) measured with a polarizer (right). Diffraction lines from first order and second order diffraction are shifted by *30°*. For simplicity, only two predicted lines for each diffraction order are superimposed [Fig. 4 Paper V].

Comparison with surface roughness LEDs

The demonstration of PhC MCLEDs was followed up by a more conservative approach where the thickness of the epitaxial layers was left unchanged at ~*6μm*. This makes a comparison with surface roughness LEDs (SR-LEDs) possible. We stayed with the chip design with a top ITO contact to enable a comparison also with the thin PhC-MCLEDs in Paper IV and V. The distance between the active layer and the bottom mirror was reduced to *112nm* in order to maximize the direct light extraction to air. Thick devices are generally unsuited for PhC light extraction since the light is distributed over a large number of modes. The spontaneous emission into the guided modes is however strongly modulated in thin-film InGaN LEDs due to the interference with light reflected at the bottom mirror. The guided mode distribution for the thick thin-film LED with two

intensity maxima at $k_i = 2.3$ and $k_i = 1.1$ is plotted in Fig. 18(b). Efficient light extraction is only possible if both maxima are efficiently extracted. Highest directionality of the emitted light should be obtained by choosing $G_0 = 1.1$, since this lattice constant extracts the first set of guided modes by first order diffraction. The second set of modes is then out of reach for first order diffraction but can be extracted slowly and rather directional with second and third order diffraction, since $2G_0$ approximately equals the effective index of the modes in the second maxima. Alternatively, $G_0 \approx 1.7$ could be used to extract some of the light from both mode regions with first order diffraction. However, the directionality with this lattice constant is low since the mismatch between G_0 and the modulation peaks is large. Hexagonal and A7 lattices were fabricated but the latter is left out of the discussion since they neither give higher flux nor radiant intensity compared to the hexagonal lattice in this experiment. The difference in radiant flux among the hexagonal lattices was small but $G_0 = 1.7$ has the highest radiant flux. $G_0 = 1.2$ has the highest radiant intensity – in good agreement with our expectation.

LEDs with surface roughening were processed in the same way as the thick PhC-LEDs and the wafer was from the same epitaxial run. The results are summarized in Table 4. The internal efficiency for the wafers used for this experiment was approximately 1/3 lower than for the record devices in Section 2.8, i. e. $\eta_{int} = 47.5\%$. The extraction efficiency to air and in encapsulation for the thick PhC-LEDs is then *50%* and *67%,* respectively. The corresponding value to air for the SR-LED is *57%*. The encapsulated SR-LEDs had electrical flaws so we will omit a comparison for encapsulated devices to avoid misleading conclusions. It is nevertheless clear that surface roughening is more efficient for thin-film LEDs with standard thickness. The results are in line with the FDTD simulation results in Paper III. A further experimental proof for this conclusion is that the emission from the chip side was higher for the PhC-LEDs. The side emission results in a flatter farfield than designed. The extraction strength is thus not sufficiently large for the photonic crystal to extract all light in this small chip. The higher directionality of the PhC-LEDs compensates for the lower efficiency so that the radiant intensity is slightly higher than for the SR-LEDs.

How do the thin PhC-MCLEDs from Paper IV and V compare to these values? We start by analyzing the internal efficiency for these devices. The radiant flux is plotted as a

function of the current in Fig. 27 where the thick devices have been used to normalize the curve. The MCLEDs perform worse than the thick LEDs at small currents as well as at higher currents. The U_f- I-curve shows that at least the best PhC-MCLEDs are shunt-free (data not shown). The poor performance at low currents is therefore attributed to higher non-radiative recombination. The worse linearity at higher currents is known as the "droop"-phenomenon. The PhC-MCLEDs were grown 15 months before the thicker LEDs at a stage where effectively only one or two of the quantum wells were active. The improved MQW operation for the thick LEDs [39] results in a lower current density per quantum well. For this comparison we assume that the peak internal efficiency is identical for thin MCLEDs and the thick LEDs. The internal efficiency of the PhC-MCLEDs at *20mA* is then *42.6%*. The reduction corresponds to the relative efficiency droop between *3mA* and *20mA* compared with the thick devices. The impact of the higher non-radiative recombination is thus neglected.

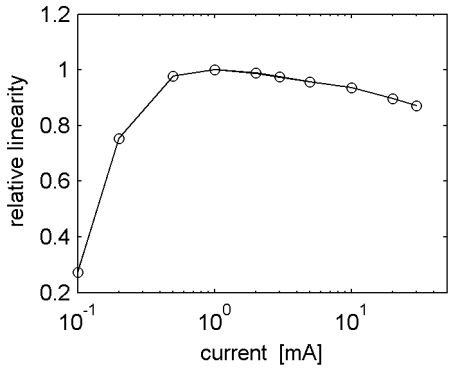

Fig. 27 Radiant flux from the best PhC-MCLED normalized with the average flux from the thick PhC-LEDs. Stronger droop at high currents as well as stronger non-radiative recombination. at low currents.

With this estimation of the internal efficiency, the extraction efficiency to air and in encapsulation for the PhC-MCLEDs is close to the corresponding values for the thick PhC-LEDs: *47%* and *68%*, respectively. The SR-LED has thus higher extraction efficiency than all PhC-LEDs. The strong beam-shaping in the PhC-MCLEDs gives strong variations in radiant intensity and the most directional device has the same radiant intensity as the SR-LED and the thick PhC-LED. The enhancement of radiant intensity with the same internal efficiency would have been *12%*. As previously discussed, the improvement had been much higher with a directional or at least Lambertian background farfield for the MCLEDs.

InGaN-LEDs	Encapsulated	η_{QE} [%]	Deviation from thick SR-LED [%]	η_{int} [%] est.	η_{extr} [%] est.	Deviation from thick SR-LED [%]	Radiant intensity [*mW/sr*]	Deviation from thick SR-LED [%]
Thick SR-LED	No	27	-	47.5	57	-	4.36	-
Thick PhC-LED	No	24	-11	47.5	50	-11	3.24	-26
Thick PhC-LED directional	No	22 (25)	-18 (-8)	47.5	46 (53)	-18 (-8)	4.37 (4.40)	0.2 (0.9)
Thick PhC-LED	Yes	32 (32)	-	47.5	67 (67)	-	-	-
PhC-MCLED efficient	No	20	-26	42.6	47	-18	2.41	-45
PhC-MCLED directional	No	18	-33	42.6	43	-25	4.38	0.5
PhC-MCLED	Yes	29	-	42.6	68	-	-	

Table 4 Efficiency of thick PhC-LEDs, thin PhC-MCLEDs and SR-LEDs with and without encapsulation. The extraction efficiency is calculated by estimating the internal efficiency. All PhC-LEDs have lower extraction efficiency than the SR-LEDs. The radiant intensity is slightly higher for the directional PhC-LEDs.

How directional can InGaN PhC-LEDs get?

The geometrical limit for the directionality $D(\theta)$ of the diffracted light from PhC-LED was found to be $D(\theta) = \sin\theta$ [Paper VI]. Hence, *50%* of the emitted light should theoretically be emitted into a 30°-cone for the ideal single mode PhC-LED which would be a factor 2 improvement over Lambertian emission. How do the fabricated PhC-LEDs compare to this limit? The farfields for the diffracted light from the PhC-MCLEDs (a) and the thick PhC-LEDs (b) are plotted in Fig. 28 and the directionality in 30° for the totally emitted light and the diffracted light is listed in Table 5 and Table 6, respectively. The diffracted light was obtained by subtracting the farfield for a LED without PhC from the farfield from the PhC-MCLED. We are thus making the assumption that the background farfield stemming from the directly emitted light in the

PhC-MCLED is not influenced by the photonic crystal. The diffracted directionality in *30°* is *43-44%* for directional PhC-MCLEDs. Note that the rabbit-ear shaped farfield for $G_0 = 1.5$ has higher directionality than the farfield from $G_0 = 1.2$. The directionality for the totally emitted light is however only *25% - 27%* in the 30°-cone. The very flat background farfield compensates for the directional PhC light extraction for these devices. The same trend is seen for the thick PhC-LEDs in Fig. 28 (b): only *25%* lies in the 30°-cone despite almost *41%* directionality for the diffracted light. The experimental diffracted directionality is thus quite close to the geometrical limit and large improvements regarding directionality cannot be expected. The main limitation is instead the background farfield!

(a)

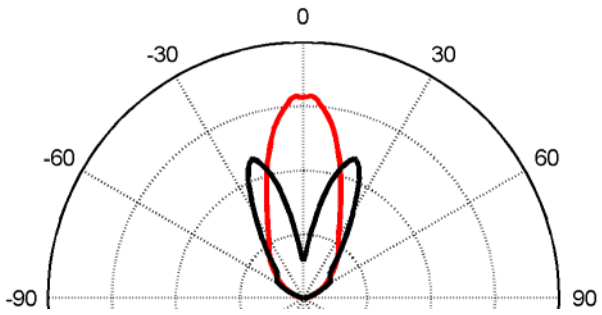

(b)

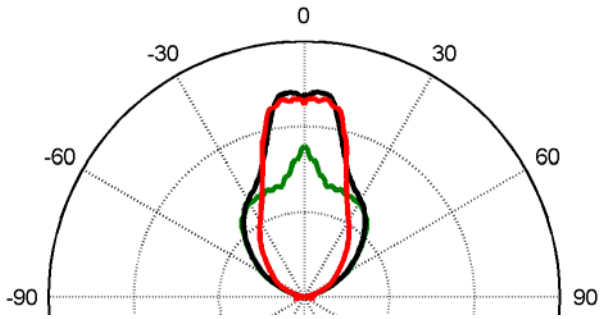

Thin InGaN MCLEDs (Paper IV-V)

G_0	**D(30°)**	**D(30°) diffracted**
1.2	27%	43%
1.5	25%	44%
reference	17%	-

Table 5 Directionality for thin PhC-MCLEDs within 30° for the totally emitted light and the diffracted light, respectively.

Thick InGaN LEDs (unpublished)

G_0	**D(30°)**	**D(30°) diffracted**
1.2	25%	41%
1.2/2.3	24%	35%
reference	19%	-

Table 6 Directionality for PhC-LEDs within 30° for the totally emitted light and the diffracted light, respectively.

Fig. 28 Diffracted farfields for InGaN *850nm* thin PhC-MCLEDs (a) and *~6μm* thick InGaN PhC-LEDs (b). The farfield for an unstructured reference has been subtracted from the original farfields.

What directionality can realistically be achieved from thin-film InGaN PhC-LEDs? As already discussed, the background farfield is determined by the optical length between the active layer and the bottom mirror. For the thick PhC-LEDs, the side emission was additionally influencing the farfield shape negatively. Let us assume that we can design a LED with at least a Lambertian background farfield without efficiency loss compared to the present design. An even more directional background farfield yields lower

extraction efficiency. Furthermore, we assume that the light extraction by diffraction enhances the light extraction by *100%* and that the directionality of the diffracted light is *41%* like for the thick PhC-LEDs. Since the Lambertian emitter has the directionality $D_{Lam}(30°) = \sin^2(30°) = 0.25$, the directionality of the totally emitted light is $0.5 \cdot (0.25 + 0.41) = 0.33$. Hence, the light extraction into the 30°-cone is a factor *1.32* higher than for a Lambertian emitter like a SR-LED. As already mentioned, side-emission must be avoided to obtain the Lambertian background. Large chip dies (for example 1 mm^2) that are typically used for étendue-limited applications do not have this problem since the top surface area to side surface area ratio is much smaller. In order to reach the *100%* extraction enhancement by the photonic crystal, the extraction strength must be higher and/or the absorption lower than for the InGaN PhC-LEDs in this thesis. Recent improvements in mirror reflectivity that contributed to the record values presented in Section 2.8 would thus help to increase the amount of diffracted light and therefore also the directionality.

In conclusion, we have seen that the directionality of the diffracted light is quite close to the ideal LED whereas the direct light emission reduces the directionality. For a realistic optimized PhC-LED, the directionality in the 30°-cone could be increased by a factor *1.32* compared to state-of-the-art Lambertian emitters.

6 NOVEL PHOTONIC CRYSTAL LED DESIGNS

In this chapter, two alternative ways are presented to reach the ultimate goal of efficient and directional light extraction. These results have not been published and they are therefore dedicated a separate chapter. The dual photonic crystal lattice in Section 6.1 is introduced to tailor the dielectric map of the photonic crystal to fit the guided mode distribution in real LEDs. The dielectric PhC-LED in Section 6.2 does the opposite: the guided mode distribution is fitted to the capability of a conventional photonic crystal lattice.

6.1 The dual photonic crystal lattice

The difference between photonic crystals and surface roughness is that the former extracts a limited range of guided modes strongly whereas the latter extracts all modes with the same (presumably lower) strength. It is this selectiveness of the photonic crystal that enables directional light extraction. But for most LEDs, this also means that a large remaining set of modes is out of range of the strong first diffraction order of the photonic crystal. These modes can only be extracted by high order diffraction or through mode mixing via multiple diffraction processes. Both alternatives require larger propagation lengths and most of the light is absorbed before it is extracted. Is it possible to maintain the mode selectivity of the photonic crystal but at the same time extract light in a broader mode range? What we need is two diffraction orders with approximately the same diffraction strength. This can be achieved by adding a second periodicity to the hexagonal lattice. One way is to introduce a hole-size variation as seen in Fig. 29. The second periodicity is given by the periodicity of large holes. In this case the second periodicity equals $a' = 2 \cdot a$ and six new reciprocal lattice points with length $G' = G_0/2$ are introduced. The relative strength of this diffraction order is determined by the hole size contrast as seen in Fig. 29 (b). It is therefore possible to tune the relative diffraction strength freely between the two diffraction orders and at for example $r_1/a = 0.21$ and $r_1/a = 0.49$ they are equally strong.

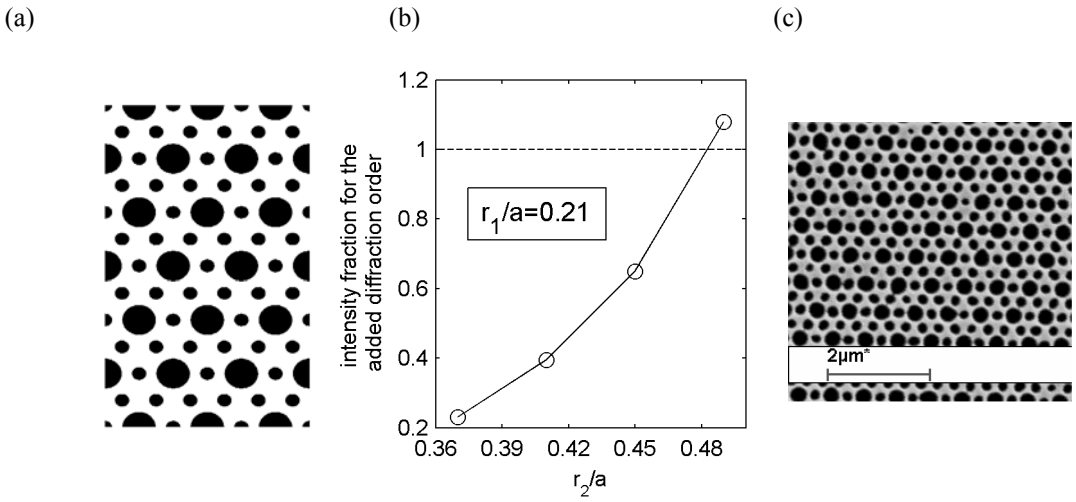

Fig. 29 Photonic crystal lattice with a hole size variation (a). The periodicity of the larger holes introduces a new diffraction order $G' = G_0/2$. The relative strength of this diffraction order is plotted as a function of the reduced radius r_2/a of the larger holes (b). The small holes have a constant radius $r_1/a = 0.21$. Scanning electron image of a fabricated lattice (c).

An alternative approach to the hole-size variation is to superimpose two lattices on each other. This can easily be realized experimentally by exposing two hexagonal lattices on the E-beam resist below the clearing dose. Only double-exposed areas will then be etched to form a complex periodic structure as seen in Fig. 30(a). Two diffraction orders can in this way get approximately the same intensity, see Fig. 30(b).

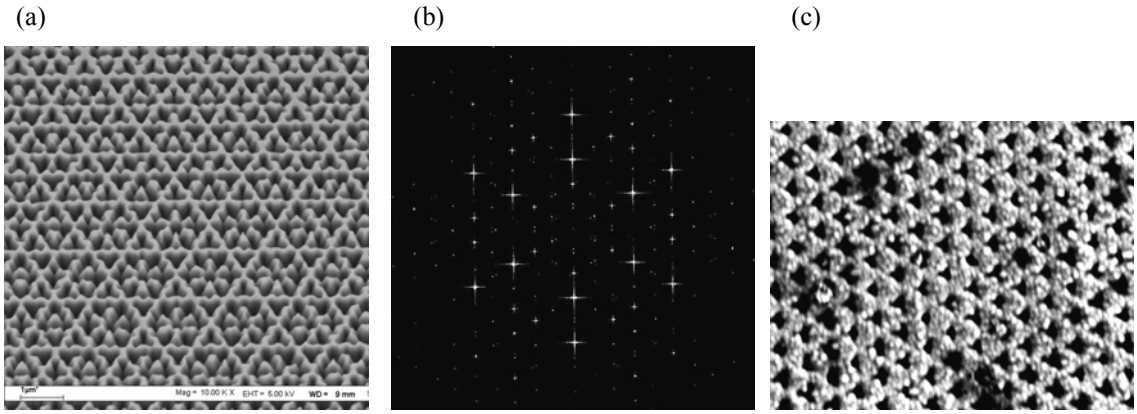

Fig. 30 Scanning electron microscope image of a superimposed photonic crystal (a). The Fourier transform of this lattice (b) shows that two diffraction orders have approximately the same intensity. SEM image of a superimposed lattice covered with ITO where one periodicity dominates (c).

Experimental evaluation of dual photonic lattices

The above mentioned lattices have been implemented in three test series for LEDs emitting at *450nm*, *630nm* and *850nm*, respectively. In all three experiments, one or both of the dual lattices have outperformed all hexagonal and Archimedean lattices regarding both radiant flux and radiant intensity.

Fig. 31 shows the spectral farfield for a conventional hexagonal lattice and a hole-size variation lattice with the same lattice constant for infra-red thin-film PhC-LEDs. These GaAs-based LEDs were chosen for this comparison since it is possible to grow highly efficient ($\eta_{QE} = 21\%$ to air) LEDs with a very thin epitaxial film (*~800nm*) at this wavelength. A small number of guided modes are supported in these LEDs, which makes the mode analysis easier. The two diffraction lines forming a "V" are visible in both lattices. The diffraction lines at larger angles for the conventional lattice can hardly be identified in the farfield from the dual lattice that is more blurry for large angles. But additional diffraction lines appear near $\theta = 0$ for $\lambda > 830nm$ in the latter farfield. This proves that the induced hole-size variation enhances a second diffraction order.

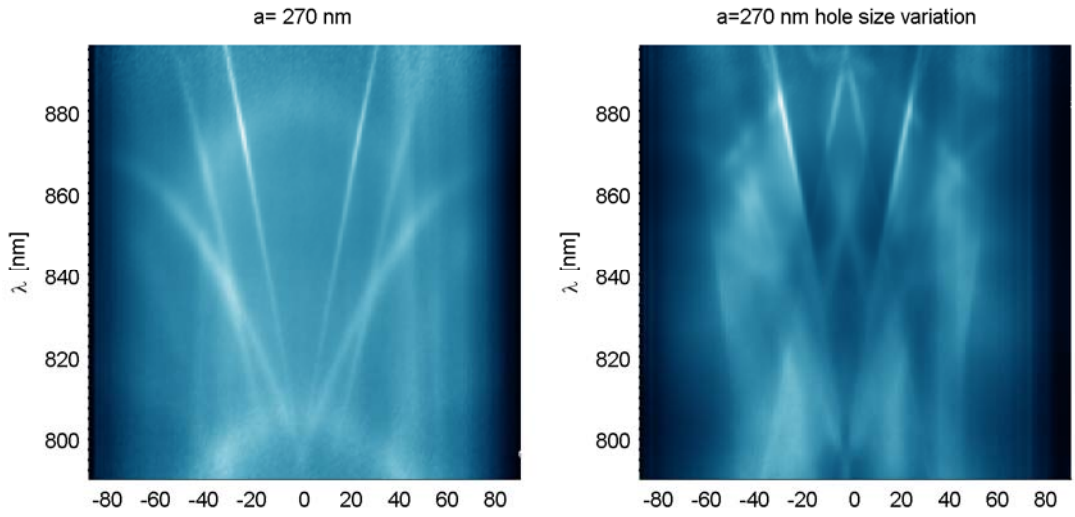

Fig. 31 Spectral farfields from infra-red thin-film LEDs with a normal hexagonal lattice (left) and a lattice with hole-size variation (right). Note the additional lines around $\theta = 0$ in the right figure from $\lambda > 830nm$.

Dual photonic lattices with the two main diffraction orders $G_1 = 2.3$ and $G_2 = 1.15$ were processed on the InGaN LED with a thick epitaxial film discussed in Section 5.5. The two diffraction orders were chosen to fit the guided mode distribution seen in Fig. 18(b). The super-imposed lattice had higher radiant flux and radiant intensity at *20mA*

than any of the reference hexagonal single lattices with $G_0 = 2.3$ ($\Delta\Phi_e = +3\%$ and $\Delta I_e = +25\%$) and $G_0 = 1.2$ ($\Delta\Phi_e = +5\%$ and $\Delta I_e = +1\%$), respectively. The extraction efficiency and radiant flux for this lattice is included in brackets in Table 4. The integrated farfields for these three lattices are plotted in Fig. 28(b). The farfield from the dual lattice (black line) looks like a combination of the two hexagonal lattices: it follows the farfield for $G_0 = 1.2$ for small extraction angles and the farfield for $G_0 = 2.3$ for large extraction angles. The spectral farfields for the hexagonal lattices with $G_0 = 1.2$ and $G_0 = 2.3$ are shown in Fig. 10(b) and Fig. 32(a), respectively and can be compared with the farfield from the dual lattice in Fig. 32(b). The latter is very similar to the hexagonal lattice with $G_0 = 1.2$. However, the strongest diffraction lines from the second maxima would be extracted to the same angle range so it is difficult to draw any conclusions about whether the superimposed PhC works as a dual lattice or not. The SEM image in Fig. 30(c) of the dual lattice covered with ITO reveals that the larger lattice $G_0 = 1.15$ dominates over the smaller lattice ($G_0 = 2.3$) so that the lattice is mere a single hexagonal lattice with perturbed hole shape rather than a dual lattice.

It can thus be questioned if the dual lattice in this experiment truly works with the two lattice constants or if the dominating lattice constant alone diffracts the light. The improved light extraction would in this case be caused by additional scattering due to the perturbed hole shape.

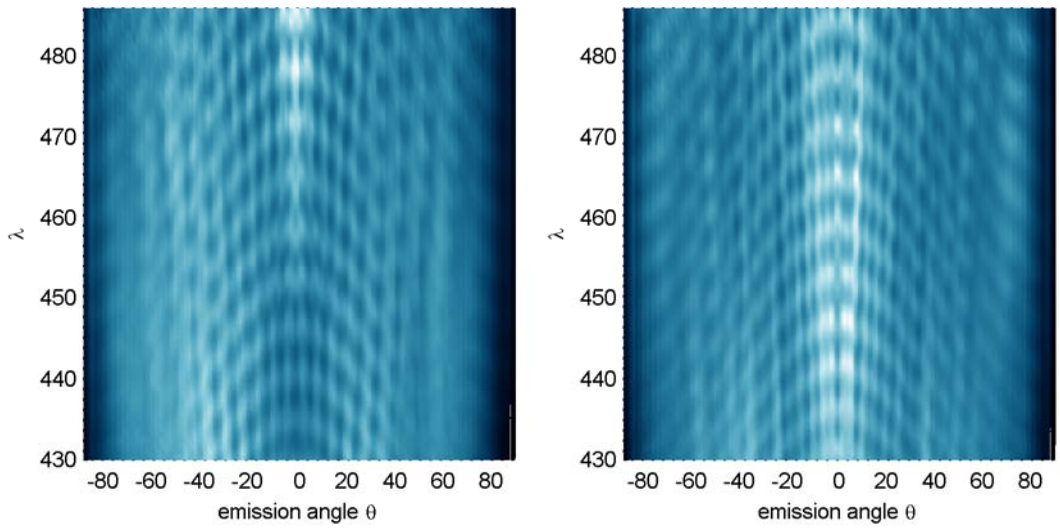

Fig. 32 Spectral farfields for a thick PhC-LED with a hexagonal lattice with $G_0 = 2.3$ (a) and a superimposed lattice with $G_1 = 2.3$ and $G_2 = 1.15$. The farfield from $G_0 = 1.2$ is plotted in Fig. 10.

The improvement made with the super-imposed lattice was even larger for red AlGaInP LEDs. The lattice with $G_1 = 2.3$ and $G_2 = 1.1$ was chosen to extract all high order

modes that couple strongly with the photonic crystal. The difference in radiant flux and radiant intensity was ($\Delta\Phi_e = +13\%$, $\Delta I_e = +14\%$) and ($\Delta\Phi_e = +13\%$, $\Delta I_e = +54\%$) compared with the hexagonal lattices with $G_0 = 1.1$ and $G_0 = 2.3$, respectively. The spectral farfield of the LED with the super-imposed lattice resembles the farfield from the hexagonal PhC-LED with the smaller reciprocal lattice constant (not shown).

In conclusion we have introduced a new type of photonic crystals that have two equally strong diffraction orders. More experiments and analysis is needed to finally assess these lattices. However, it has been shown here that they are efficient, rely on diffraction and are potentially directional.

6.2 Leaving mode design behind: the dielectric PhC-LED

The ideal case for directional PhC light extraction is the single-mode LED and it was presented in Section 4.3. It was shown that the upper limit for the directionality for such a device is $D(\theta) = \sin\theta$, which is much higher than for Lambertian emitters such as LEDs with surface roughening. An attempt to realize such an ideal PhC-LED led to the InGaN PhC-MCLED presented in Paper IV and V. However, such devices are difficult to fabricate since it requires the precise control of the back-etching of the thick InGaN buffer growth layer. It also requires that the epitaxial layer growth is extremely homogeneous on each wafer and for all wafers in the reactor. It is not foreseeable that such devices can be successfully produced commercially with today's growth techniques. High-efficiency single-mode LEDs in the AlGaInP material system are unthinkable – the active region and the electrical confinement layers alone support several modes. In the following section a new type of PhC-LEDs is proposed that combines the high extraction efficiency provided by surface roughening with the directionality that PhC-LEDs are capable of.

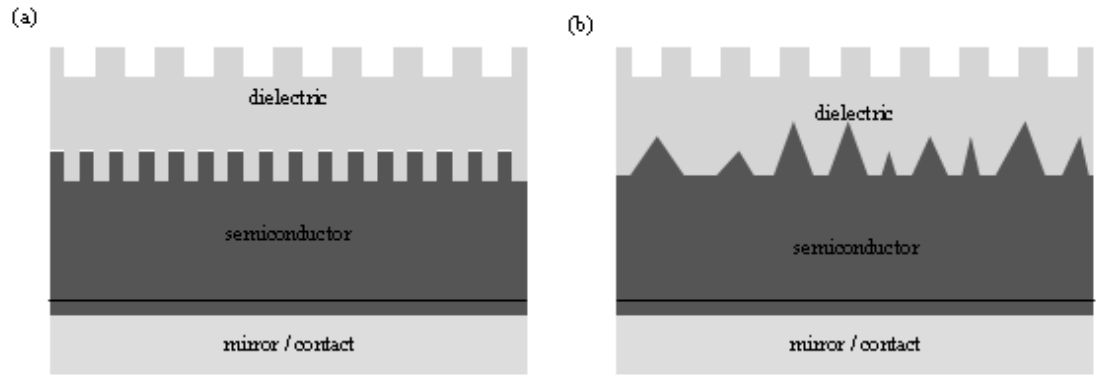

Fig. 33 Dielectric photonic crystal LEDs. The light is first extracted from the semiconductor material to the dielectric with lower refractive index by either a photonic crystal (a) or a rough surface (b). The guided light in the dielectric is confined to a smaller mode range and can be extracted directionally by the photonic crystal.

The dielectric PhC-LED is a result of the conclusions drawn throughout this work: directional extraction with photonic crystal is strongest when the light is confined to a narrow range in the reciprocal plane. The range of states in the reciprocal plane is determined by the refractive index n of the material since only guided modes with $k_i \in [1,n_{sc}]$ can propagate in this medium. In for example SiO2 with $n=1.5$, all guided modes propagating in the ΓM direction can be diffracted by a photonic crystal with $G_0 = 1.25$ within $\pm 15°$. The light extraction is omnidirectional for a hexagonal lattice since the effective index of all light is small. The corresponding Ewald diagram is shown in Fig. 34(a). One could therefore consider a PhC-LED where the PhC is etched into an extra dielectric layer instead of into the semiconductor material with high refractive index. However, such a device would have low extraction efficiency since light is still emitted into guided modes with $k_i > 1.5$. These modes are totally internally reflected at the semiconductor-dielectric interface and would therefore not "see" the photonic crystal at all. Hence, a scattering mechanism is needed to redistribute the modes with $k_i \in [n_{diel}, n_{sc}]$ to modes with $k_i \in [1,n_{diel}]$. This could be achieved either with another photonic crystal or with a rough interface between the semiconductor and the dielectric. These two possible designs are shown in Fig. 33. Since my experimental results in Section 5.5 as well as FDTD simulations in Paper III have shown that surface roughening extracts light more efficiently than photonic crystals, the latter design seems more promising. This type of PhC-LED could be used for any material system and regardless of the epitaxial design. Hence, the epitaxial layers can be optimized for internal efficiency.

The proposed design has the potential to combine the high extraction efficiency for LEDs with surface roughening with the directionality of PhC-LEDs. FDTD simulations show that this design actually works. The normalized farfields, the extraction efficiency as a function of the integration radius and the integrated light within a limited acceptance angle are shown in Fig. 34-Fig. 35. We use the simulation results in Paper III for green-emitting InGaN LEDs as reference: one LED with surface roughening and one conventional PhC-LED with $G_0 = 1.3$. Fig. 34(b) shows that the farfield from the dielectric PhC-LED (with the same $G_0 = 1.3$ and *300nm* etch depth) is much more directional than the LED with surface roughening that has a Lambertian emission pattern. Also the conventional PhC-LED is directional but its extraction efficiency is much lower (Fig. 35(a)): *42%* instead of *59%* for the SR-LED. The efficiency gap between PhC-LEDs and SR-LEDs is almost closed with the dielectric PhC-LED – the extraction efficiency with this design is *53%*. The light extraction is slower for the dielectric PhC-LED, due to the larger total thickness. It should be noted that this simulation was performed with a bottom mirror with only *90%* reflectivity at normal incidence. This is a rather pessimistic assumption and therefore the efficiency gap can be even smaller between SR-LEDs and dielectric PhC-LEDs in real devices.

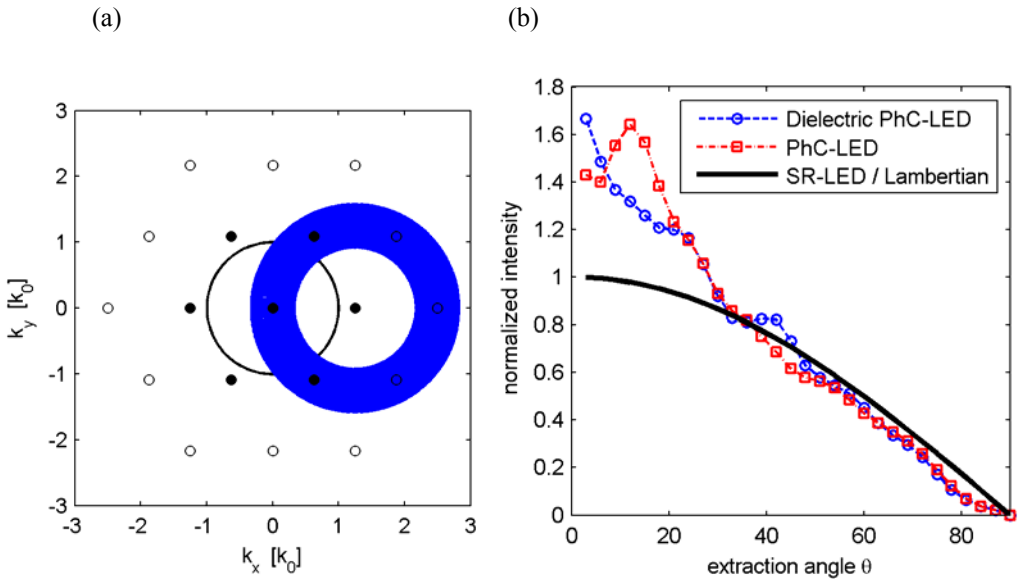

Fig. 34 Ewald diagram displaying directional diffraction of the the propagating modes in SiO_2, defined by the blue circle (a). Normalized farfields for a dielectric PhC-LED (circles), a normal PhC-LED and a SR-LED (Lambertian emitter) as simulated with FDTD. Both PhC-LEDs have a super-Lambertian emission pattern.

Fig. 35(b) shows how the farfield and extraction efficiency affect the emitted flux within a limited acceptance angle. The enhancement for the dielectric PhC-LED compared to the SR-LED within *3°* is *70%* and at *30°* it is still *16%*. The gain is positive until *54°*.

(a) (b)

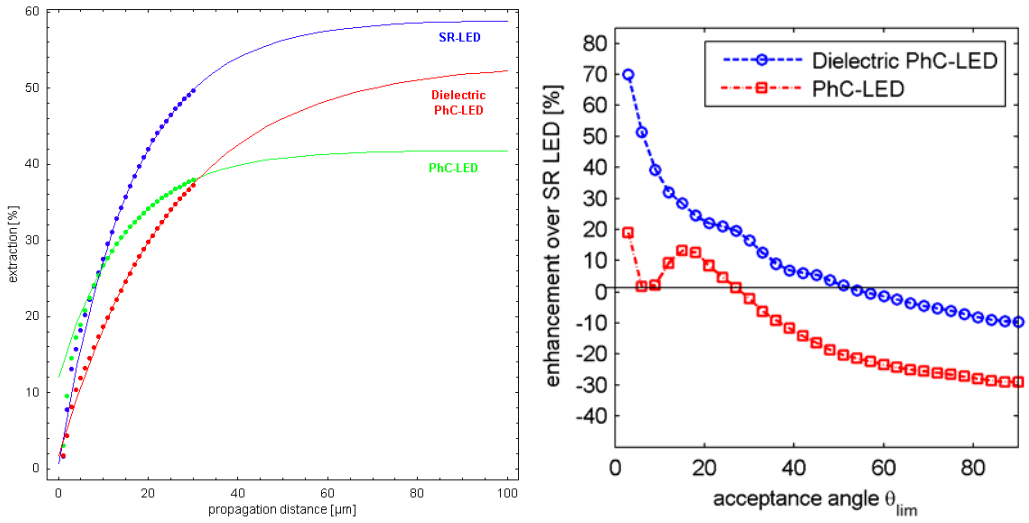

Fig. 35 Extraction efficiency simulated with FDTD as a function of the integration radius for the dielectric PhC-LED, the normal PhC-LED and a SR-LED. The circles correspond to FDTD simulation points, lines are fitted exponential functions (a). Light extraction enhancement within the acceptance angle θ_{lim} compared to the SR-LED (b). A positive enhancement is achieved within 54° for the dielectric PhC-LED.

In conclusion it has been shown that the advantages of highest extraction efficiency for SR-LEDs can be combined with high directionality characteristic for PhC-LEDs in the combined dielectric PhC-LED. This type of structure should also be easier to fabricate than devices that rely on precise layer thicknesses to get a desired guided mode distribution. It remains to demonstrate experimentally that dielectric PhC-LEDs are as efficient and directional as the simulations suggest.

7. CONCLUSION AND OUTLOOK

In this thesis photonic crystal LEDs have been designed, fabricated and characterized to answer the question if light extraction with photonic crystals yields higher efficiency and/or directionality than state-of-the-art LEDs with surface roughening. The fundamental advantage with photonic crystal light extraction is that light in a guided mode is extracted in a controlled and predictable way (given by Bragg's law) that can be directional if the photonic crystal has the right lattice constant. Real LEDs have several modes and the first challenge is to design the vertical layer stack so that the majority of the guided modes can be extracted by one and the same photonic crystal in a directional way. The second challenge is to optimize the properties of the photonic crystal for the particular LED. This includes choosing the right lattice constant, lattice type and air filling factor together with a sufficiently large etch depth. Below I will summarize some general design rules for multi-mode PhC-LEDs. Thereafter I will discuss the choice of lattice type and the experimental results for AlGaInP PhC-LEDs and InGaN PhC-LEDs.

Design rules

In Section 4.3 we concluded that the optimal lattice constant and air filling factor varies strongly even for a single mode depending on the absorption strength. A few design rules can however be made that applies for all multi-mode PhC-LEDs.

1. The use of the thin-film technology is very advantageous for photonic crystal light extraction. All emitted light stays in the LED slab confined at the bottom by a metallic mirror until it is extracted by the photonic crystal or absorbed.
2. The active region should be placed as close to the bottom mirror as possible to induce a modulation of the spontaneous emission. In this way, directional light extraction with a photonic crystal is possible even for LEDs several microns thick. The position of the active region must at the same time give a directional farfield for the directly extracted light. However, the internal quantum efficiency and the direct light extraction must not be negatively affected by the proximity to the mirror.
3. The LED thickness should be as small as possible without affecting the internal efficiency and the lateral current spreading. This reduces the number of guided modes which generally makes beam-shaping with the photonic crystal easier. The extraction length in a thin LED is also shorter due to the stronger coupling

with the photonic crystal. Ideally, there should be only one Fabry Perot resonance in the light extraction cone to enable directional direct light extraction.

4. The etch depth of the photonic crystal should be at least as large as the attenuation length of guided modes. This typically corresponds to *100nm*.
5. Directional light extraction of a single mode (or a single resonant mode range) with a hexagonal lattice can be realized by using the first diffraction order (i.e. $G_0 \sim k_i$) or a combination of the second and third diffraction order ($k_i/2 < G_0 < k_i/\sqrt{3}$). The latter yields omnidirectional extraction but requires low absorption in order to be efficient.
6. In the case of a quasi-continuum of guided modes, the most efficient lattice constant is found in the range $1 < G_0 < n_{PhC}$. A reciprocal lattice constant in this range extracts the modes that couples most strongly with the photonic crystal by first order diffraction.

Hexagonal lattice vs. Archimedean lattice

The hexagonal lattice – the regular 2D crystal with highest symmetry – has been used as the standard lattice throughout my work. Drawbacks with the hexagonal lattice have been identified and alternative lattices have been investigated. The hexagonal lattice has an insufficient number of first order diffraction points to enable omnidirectional diffraction of modes with effective index $k_i > 2$. The Archimedean lattices such as the A7 lattice proposed in literature have enough lattice points. The experimental results in this thesis show that a minor extraction efficiency improvement is obtained for AlGaInP LEDs whereas the performance in InGaN LEDs is similar to hexagonal lattices. The radiant intensity (and directionality) is however reduced. A possible explanation for this experimental result is the lower diffraction strength for the lower diffraction orders in the A7 lattice compared with a hexagonal lattice. The biggest advantage with photonic crystals compared to surface roughening – the ability to shape the farfield – is thus less pronounced when Archimedean lattices are used.

AlGaInP thin-film photonic crystal LEDs

The external quantum efficiency as well as the PhC enhancement factor demonstrated with AlGaInP photonic crystal LEDs are better than for any other AlGaInP PhC-LEDs found in literature. Several important conclusions have been drawn regarding the

potential of thin-film AlGaInP PhC-LEDs. First of all, the range of guided modes present expressed in terms of effective index is much too large for a photonic crystal with one dominating diffraction order. This is a fundamental problem, since the allowed mode range is given by the refractive index of AlGaInP. The quasi-continuum of guided modes found in standard thin-film LEDs results in a dense net of diffraction lines at all emission angles which makes directional light extraction very difficult. One must choose between trying to extract low order modes with much light but very small interaction with the photonic crystal or to extract high order modes that have higher mode overlap but less energy. Experimental results as well as simulations show that the latter alternative is better. To reach the ultimate goal of *100%* extraction efficiency, the remaining modes must then be extracted via photon recycling, high order diffraction or multiple diffraction processes. Strong photon recycling requires an internal efficiency close to *100%*, which sets high demands on the epitaxial quality as well as on the electrical bandgap engineering. It is however the only way to extract the (type I) modes that are guided between the electrical confinement layers. These modes do hardly experience the extracting surface structure – whether it is a photonic crystal or surface roughness. High order diffraction and multiple diffraction processes are slow processes that require that the mode absorption in the remaining low order modes is low. The direct comparisons made between PhC-LEDs and LEDs with surface roughening have not been clarifying – the quality of the surface roughness for the reference devices can be questioned. It highlights the fact that there is no such thing as "one piece surface roughening" – the topography varies between different processes and material systems.

The main objective of my work has been to realize directional LEDs. Efforts to reduce the total thickness of the AlGaInP LED and to form a resonant cavity resulted in directional light extraction and higher PhC enhancement factors than for previous experiments with thicker PhC-LEDs. The thinner LED supported less modes and the farfield of the most directional devices was dominated by only three guided modes. It was thus shown that a sufficiently strong modulation of the spontaneous emission to the guided modes to achieve directional emission is possible. The super-position of the FP-resonance formed by the resonant cavity and the diffraction lines also showed that these two light extraction mechanisms can be combined. This principally important demonstration of directional light extraction from AlGaInP LEDs was however achieved at the cost of lower internal efficiency and the absence of photon recycling.

This reduction of the internal efficiency is not believed to be inevitable. But it shows how sensitive the overall efficiency of AlGaInP LEDs is to changes in layer composition and thicknesses that reduces the internal efficiency. It remains to show that a vertical layer design suited for photonic crystal light extraction can be just as efficient as standard LEDs with thicker epitaxial layers.

InGaN thin-film photonic crystal LEDs

Thin-film InGaN LEDs are better suited for photonic crystal light extraction due to the low refractive index of InGaN. The ideal single-mode PhC-LED was approached with the *850nm* thick micro-cavity LED with *400nm* deeply etched photonic crystals. It was shown that the farfield radiation pattern can be varied strongly by changing the lattice constant of the PhC in these LEDs that contained only three guided modes. Even higher directionality would have been achieved if the directly emitted light had also been tuned correctly. This part of the vertical layer stack design should not be neglected, since a large fraction of the light is extracted without being diffracted by the photonic crystal. The realization of sub-micron PhC-MCLEDs is however very difficult with current epitaxial growth technology on sapphire substrates. A very precise control of the back-etching of the GaN buffer layer is necessary. Growth thickness fluctuations on the wafer will always result in a variety of final cavity thicknesses. The mode dispersion will change accordingly and fine-tuning of the lattice constant will therefore be impossible. It was however shown that farfield shaping with photonic crystals is also possible in thick InGaN LEDs. The proximity of the active region to the bottom mirror strongly modulates the spontaneous emission into the guided modes. This enables beam-shaping even in devices several microns thick. The weaker diffraction strength in these thick LEDs does however result in unwanted side-emission which reduces the directionality. The light extraction in InGaN PhC-LEDs of standard thin-film thickness is thus not fast enough whereas ultra-thin PhC-MCLEDs are at least not viable for industrial production today. A practical optimum may exist in between. InGaN LEDs *~2μm* thick with a fairly deeply etched photonic crystal would be easier to fabricate and the current spreading would be sufficiently good to allow lateral current spreading without using an absorbing ITO-contact. The mode overlap with the photonic crystal is enhanced and the extraction length thus shorter.

A direct comparison between InGaN-LEDs with surface roughness and photonic crystals showed that the high directionality achieved with photonic crystals is compensated by lower extraction efficiency – for thick as well as thin LEDs. The absolute enhancement achieved within a certain acceptance angle θ has therefore been positive only for very small angles. Is this the end of story for PhC-LEDs in the InGaN material system – no! The extraction efficiency is simply given by the relation between the extraction strength β and the absorption strength α: $\eta = \beta/(\beta + \alpha)$. Even if the PhC extraction strength remains at a somewhat lower level compared to surface roughening, the *efficiency* gap will be reduced as the absorption is minimized in future chip concepts. The difference in directionality on the other hand is fundamental: LEDs with surface roughening will keep being Lambertian whereas PhC-LEDs will stay directional also when the absorption is minimized. It is therefore foreseeable that the use of PhC-LEDs will yield higher system efficiency for étendue limited optical systems corresponding to their higher directionality.

Novel concepts

Two new concepts that might help to close the efficiency gap faster were presented in Chapter 6. The dual lattices are alternative photonic crystals that address a weakness of the hexagonal lattice: it can only extract light efficiently in a mode range smaller than the mode range in InGaN and AlGaInP LEDs. Dual lattices – here realized either as a hole-size variation or a superposition of two lattices – distribute the diffraction strength more evenly between two reciprocal lattice vector lengths. It can therefore in principle extract two mode ranges with moderate diffraction strength rather than one mode range with high diffraction strength. It has been shown that this in principle works and the first experimental results are promising. The key issue here is to ensure that the high directionality for PhC-LEDs is maintained while extracting more light from a wider mode range.

A complete different PhC-LED approach was suggested in Section 6.2. The photonic crystal is here etched into a dielectric with lower refractive index than the semiconductor material. The guided modes are confined to a smaller effective index range in this material. This is the ideal case for photonic crystal light extraction and directional emission is thus possible. A scattering mechanism is required to extract the light from the semiconductor material to the low index dielectric. This could be either a

second photonic crystal or a conventional rough surface. 3D FDTD simulations showed that this design works. The extraction efficiency approaches the efficiency of state-of-the-art LEDs with surface roughening whereas the directionality is high like for a PhC-LED. Another advantage with this design is that changes of the epitaxial design to improve the internal efficiency can be made without changing the directional light extraction. Precise control of the layer thickness to design the guided mode distribution is thus not necessary. The dielectric PhC-LED design could bring directional emission for AlGaInP as well as InGaN LEDs.

Finally, strongly coupled PhC-LEDs deserve a comment. This type of PhC-LED was ruled out as a viable alternative in Section 4.2 since etching of the active layer induces non-radiative surface recombination and the active material volume is reduced. Nanorod LEDs [59]-[60] are however also in principle strongly coupled photonic crystal LEDs. Epitaxial grown nano-rods are potentially defect-free and core-shell growth [61] would allow for a large active volume per area unit. Effects typically associated with photonic crystals like the Purcell effect, inhibited spontaneous emission in bandgaps and flat bands could then be used to increase the internal efficiency as well as the extraction efficiency. However, there is a long and challenging way to go before nano-rod LEDs can be grown with a material quality that gives them a performance comparable to state-of-the-art LEDs.

8. SUMMARY OF PAPERS

This thesis contains six appended papers sorted after publication date. Paper I and II deal with photonic crystal LEDs in the AlGaInP material system, whereas the rest mainly deal with InGaN devices. In Paper I, PhCs are for the first time applied to an AlGaInP thin-film LED with a design close to commercial devices. The resonant cavity effect is used together with PhC light extraction to obtain directional emission from a thin-film PhC resonant cavity LED in Paper II. Paper III is an extensive review paper about photonic crystal LEDs with emphasis on theoretical considerations and simulations. Strong farfield shaping from very thin InGaN micro-cavity LEDs with photonic crystals is observed in Paper IV. In Paper V it is shown that high order diffraction contributes significantly to the light extraction in these very thin InGaN PhC-MCLEDs and a model is presented to explain this surprising result. A theoretical model of PhC-LEDs based on coupled mode theory to predict the diffraction strength and the farfield radiation pattern is presented in Paper VI.

I. Enhanced light extraction efficiency from AlGaInP thin-film light-emitting diodes with photonic crystals

For the first time PhCs with varying lattice constants, lattice types and etch depths were applied on a AlGaInP thin-film LED emitting at *650nm*. Highest extraction enhancement compared to unstructured devices was *47%* for a *800nm* deeply etched Archimedean A7 quasi-crystal with $G_0=1.5$ that mainly extracts high order modes with a low effective index. Three characteristic mode types are identified in the complex wave-guide structure in this thin-film LEDs and their contribution to the PhC light extraction and to photon recycling in the active region is discussed. The extraction dependency on the lattice constant is predicted by a model based on coupled mode theory (see Paper VI).

II. Directional light extraction from thin-film resonant cavity light-emitting diodes with a photonic crystal

Two directional light extraction schemes, namely the resonant-cavity LED and photonic crystal light extraction are successfully combined in one AlGaInP device emitting at *650nm*. Furthermore, the use of transparent conductive oxides as current spreading layers enables a thin vertical design that improves the photonic crystal light extraction. The light extraction efficiency is increased by a factor *2.6* – an excellent value – while

the farfield radiation pattern is more directional than for Lambertian emitters. Due to the additional extraction channel given by the PhC, the PhC-RCLEDs are also more stable to a temperature induced wavelength shift compared to unstructured RCLEDs. The farfields show that the diffraction of the light works also with PhCs with very poor quality.

III. Photonic crystal LEDs - designing light extraction

In this review article, the physics behind PhC-LEDs is explained in detail and recent published results are summarized. The efficiency and farfield radiation patterns of PhC-LEDs are compared with state-of-the art thin-film LEDs with a rough surface structure using a 3D FDTD algorithm. It is shown that the direct replacement of the rough surface structure on a standard LED several microns thick with an optimized PhC results in lower extraction efficiency and only a moderate improvement of the directionality of the emitted light. On the other hand, if the vertical layer stack is optimized for PhC light extraction, the extraction efficiency is equally good as with surface roughening but with a superior farfield radiation pattern. It is shown that the higher directionality can be used to either increase the system efficiency or to maximize the total flux coupled to an étendue limited optical system.

The first author of this article is Christopher Wiesmann, who has written the article and performed the simulations therein himself. Apart from improving the text quality and content of the article and providing some farfield measurement data from the PhC-MCLEDs described in Paper IV and V, my main contribution has been the very fruitful discussions with Christopher Wiesmann and the other co-authors about the topic. These discussions have improved not only this article, but also the experimental results presented in the other papers with myself as the first author. Examples of discussed topics are the importance of the photonic crystal lattice symmetry versus the effective index of the mode, the classification of different types of modes and their contribution to the light extraction and the link between photonic band-diagrams on the one hand and wave-vector diagrams and azimuthal farfields on the other hand.

IV. Beam-shaping properties of InGaN thin-film micro-cavity light-emitting diodes with photonic crystals

Aiming towards the ideal single-mode diffraction PhC-LED, InGaN PhC micro-cavity LEDs (MCLEDs) with *850nm* GaN thickness was fabricated. The radiant intensity is increased by a factor *4.3* whereas the enhancement in emitted flux is *1.85* compared with MCLEDs without PhCs. Twofold, sixfold and twelvefold symmetries are found in the azimuthal farfields from devices with a 1D lattice, a hexagonal lattice and an Archimedean A7 lattice, respectively. These patterns confirm that PhC light extraction can be described as a diffraction phenomenon without considering typical effect associated with PhCs such as photonic band gaps or flat bands. The emitted flux for the best PhC-MCLED in a radial lens is found to be approximately *20%* lower than for state-of-the-art devices with surface roughening. Simulations show that the lower efficiency can partly be attributed to absorption in the ITO-layer incorporated in the absence of a thick current spreading layer.

V. Strong high order diffraction of guided modes in micro-cavity light-emitting diodes with hexagonal photonic crystals

By gathering spectrally resolved farfields from InGaN hexagonal PhC-MCLEDs with different lattice constants, an experimental photonic band-diagram can be constructed. Analysis of the photonic band-diagram and monochromatic azimuthal farfields reveals that only three guided modes exist in these LEDs. Unexpectedly, it is found that high-order diffraction contributes significantly to the light extraction in these devices. We use a model including the absorption and the lifted in-plane degeneracy of the guided modes in order to explain these experimental results.

VI. Theoretical Investigation of the Radiation Pattern from LEDs Incorporating Shallow Photonic Crystals

A theoretical model based on coupled-mode theory is presented that is able to determine the farfield radiation pattern of LEDs with shallow photonic crystals. The lattice type, pitch and air filling factor is taken into account as well as the guided mode distribution in the LED. An upper limit for the directionality of a single-mode PhC-LED is derived. The model is compared with the experimental results from Paper I and with a set of green-emitting PhC-LEDs. It is shown that guided modes with a low effective index can most easily be diffracted to air because of their higher overlap with the PhC.

This paper was written by Christopher Wiesmann, who has also implemented the presented model and performed the calculations. The early conception of this diffraction model based on coupled mode theory was made early in year 2006 without my participation. My contribution has been the vivid discussion thereafter, including but not limited to the influence of the mismatch between reciprocal lattice constant and the effective index of the guided mode on the directionality, the validity of the model and assumptions being made, and the interpretation of the results in the presence of absorption. Experimental data from Paper I are used for validation of the model.

BIBLIOGRAPHY

[1] M. R. Krames, O. B. Shcekin, R. Mueller-Mach, G. O. Mueller, L. Zhou, G. Harbers and M. G. Craford, "Status and Future of High-Power Light-Emitting Diodes for Solid-State Lighting", IEEE J. Display Technol. 3(2), 160-175 (2007)

[2] J. M. Phillips, M.E. Coltrin, M. H. Crawford, A. J. Fischer, M. R. Krames, R. Mueller-Mach, G. O Mueller, Y. Ohno, L. E. S. Rohwer, J. A. Simmons and J. Y. Tsao, "Research challenges to ultra-efficient inorganic solid-state lighting", Laser & Photon. Rev. 1 No 4, 307-333 (2007)

[3] E. Yablonovitch, "Inhibited Spontaneous Emission in Solid-State Physics and Electronics", Phys. Rev. Lett. 58, 2059 (1987)

[4] S. Fan, P. R. Villeneuve and J. D. Joannopoulos, "High extraction efficiency of spontaneous emission from slabs of photonic crystals", Phys. Rev. Lett. 78, 3294 (1997)

[5] E. Yablonovitch, "Photonic band-gap crystals", J. Phys. Condens. Matter 5, 2443-2460 (1993)

[6] T. F. Krauss, R. M. De La Rue and S. Brand, "Two-dimensional photonic-bandgap structures operating at near-infrared wavelengths", Nature 383, 6602 (1996)

[7] M. Boroditsky, T. F. Krauss, R. Coccioli, R. Vrijen, R. Bhat and E. Yablonovitch, "Light extraction from optically pumped light-emitting diode by thin-slab photonic crystals", Appl. Phys. Lett. 75, 8 (1999)

[8] M. Boroditsky, R. Vrijen, T. F. Krauss, R. Coccioli, R. Bhat and E. Yablonovitch, "Spontaneous Emission Extraction and Purcell Enhancement from Thin-Film 2-D Photonic Crystals", J. Lightwave Techn. 17(11) 2096-2112 (1999)

[9] T. N. Oder, K. H. Kim, J. Y. Lin and H. X. Jiang, "III-nitride blue and ultraviolet photonic crystal light emitting diodes", Appl. Phys. Lett. 84(4) 46-468 (2004)

[10] J. J. Wierer, M. R. Krames, J. E. Epler, N. F. Gardner, M. G. Craford, J. R. Wendt, J. A. Simmons and M. M. Sigalas, "InGaN/GaN quantum-well heterostructure light-emitting diodes employing photonic crystal structures", Appl. Phys. Lett. 84, 3885-3887 (2004)

[11] J. M. Lupton, B. J. Matterson, I. D. W. Samuel, M. J. Jory and W. L. Barnes, "Bragg scattering from periodically microstructured light emitting diodes", Appl. Phys. Lett. 77(21) 3340-3342 (2000)

[12] A. David, C., Meier, R. Sharma, F.S. Diana, S. P. DenBaars, E. Hu, S. Nakamura, C. Weisbuch and H. Benisty, "Photonic bands in two-dimensionally patterned multimode GaN waveguides for light extraction", Appl. Phys. Lett. 87, 101107 (2005)

[13] A. David, T. Fujii, R. Sharma, K. McGroddy, S. Nakamura, S. P. DenBaars, E. L. Hu, C. Weisbuch and H. Benisty, "Photonic-crystal GaN light-emitting diodes with tailored guided modes distribution", Appl. Phys. Lett. 88, 061124 (2006).

[14] A. David, T. Fuji, E. Matioli, R. Sharma, S. Nakamura, S. P. DenBaars, C. Weisbuch and H. Benisty, "GaN light-emitting diodes with Archimedean lattice photonic crystals", Appl. Phys. Lett. 88, 073510 (2006)

[15] A. David, T. Fujii, B. Moran, S. Nakamura, S. P. DenBaars, C. Weisbuch and H. Benisty, "Photonic crystal laser lift-off GaN light-emitting diodes", Appl. Phys. Lett. 88, 133514 (2006)

[16] D. Delbeke, R. Bockstaele, P. Bienstman, R. Baets and H. Benisty, "High-Efficiency Semiconductor Resonant-Cavity Light-Emitting Diodes: A Review", IEEE J. Sel. Top. Quant. 8 189-206 (2002)

[17] E. M. Purcell, "Spontaneous emission probabilities at radio frequencies", Phys. Rev. Lett. 69(681) (1946)

[18] P. Altieri, A. Jäger, R. Windisch, N. Linder, P. Stauss, R. Oberschmid and K. Streubel, "Internal quantum efficiency of high-brightness AlGaInP light-emitting devices", J. Appl. Phys. 98 1-3 (2005)

[19] N. Gardner, G. Mueller, Y. Shen, G. Chen, S. Watanabe, W. Goetz and M. Krames, "Blue-emitting InGaN/GaN double-heterostructure light-emitting diodes reaching maximum quantum efficiency above 200A/cm^2" , Appl. Phys. Lett. 91, 243506 (2007)

[20] A. Laubsch, W. Bergbauer, M. Sabathil, M. Strassburg, H. Lugauer, M. Peter, T. Meyer, G. Brüderl, J. Wagner, N. Linder, K. Streubel and B. Hahn, "Luminescence properties of thick InGaN quantum-wells", phys. stat. sol. (c) DOI: 10.1002/pssc.200880893 (2009)

[21] K. Streubel, N. Linder, R. Wirth and A. Jaeger, "High Brightness AlGaInP Light-Emitting Diodes", J. Select. Topics Quantum Electron. 8 321-332 (2002)

[22] M. R. Krames, M. Ochinai-Holocomb, G. E. Höfler, C. Carter-Coman, E. I. Chen, I. - H. Tan, P. Grillot, N. F. Gardner, H. C. Chui, J-W. Huang, S. A. Stockman,
F. A. Kish and M. G. Craford, "High-power truncated-inverted-pyramid $(Al_xGa_{1-x})_{0.5}In_{0.5}P$/GaP light-emitting diode exhibiting >50% external quantum efficiency", Appl. Phys. Lett. 75, 2365-2367 (1999)

[23] R. Windisch, R. Butendeich, S. Illek, S. Kugler, R. Wirth, H. Zull and K. Streubel,

"100-lm/W InGaAlP Thin-Film Light-Emitting Diodes With Buried Microreflectors", IEEE Photonic Tech. L. 19, 774-776 (2007)

[24] I. Schnitzer, E. Yablonivitch, C. Caneau, T. J. Gmitter and A. Scherer, "30% external quantum efficiency from surface textured, thin-film light-emitting diodes", Appl. Phys. Lett. 63, 2174-2176 (1993)

[25] E. F. Schubert, Y. –H. Wang, A. Y. Cho, L.-W. Tu and G. J. Zydzik, "Resonant cavity light-emitting diode", Appl. Phys. Lett. 60, 921 (1992)

[26] H. Benisty, H. De Neve and C. Weisbuch, "Impact of Planar Microcavity Effects on Light Extraction - Part I: Basic Concepts and Analytical Tends", IEEE J. Quantum Electron. 34, 1612-1631 (1998)

[27] H. Benisty, H. De Neve and C. Weisbuch, "Impact of Planar Microcavity Effects on Light Extraction - Part II: Selected Exact Simulations and Role of Photon Recycling", IEEE J. Quantum Electron. 34, 1632-1643 (1998)

[28] T. Fujii, A. David, C. Schwach, P. M. Pattison, R. Sharma, K. Fujito, T. Margalith, S. P. DenBaars, C. Weisbuch and S. Nakamura, "Micro Cavity Effect in GaN-Based Light-Emitting Diodes Formed by Laser Lift-Off and Etch-Back Technique", Jpn J Appl. Phys. 43(3B), L411-413 (2004)

[29] G. S. Huang, T. C. Lu, H. C. Kuo, S. C. Wang and H.-G. Chen, "Fabrication of Microcavity Light-Emitting Diodes Using Highly Reflective AlN-GaN and Ta_2O_5-SiO_2 Distributed Bragg Mirrors", IEEE Photonics Tech. L. 19(13), 999-1001 (2007)

[30] F. Rizzi, P. R. Edwards, K. Betjka, F. Semond, X. N. Kang, G. Y. Zhang, E. Gu, M. D. Dawson, I. M. Watson and R. W. Martin, "(In,Ga)N/GaN microcavities with double dielectric mirrors fabricated by selective removal of an (Al,In)N sacrificial layer," Appl. Phys. Lett. 90, 111112 (2007)

[31] R. Sharma, Y.-S. Choi, C.-F. Wang, A. David, C. Weisbuch, S. Nakamura and E. L. Hu, "Gallium-nitride-based microcavity light-emitting diodes with air-gap distributed Bragg reflectors", Appl. Phys. Lett. 91, 211108 (2007)

[32] R. Joray, M. Ilegems, R. P. Stanley, W. Schmid, R. Butendeich, R. Wirth, A. Jaeger and K. Streubel, "Far-Field Radiation Pattern of Red Emitting Thin-Film Resonant Cavity LEDs", IEEE Photonics Tech. L. 18(9), 1052–1054 (2006)

[33] P. Modak, M. D'Hondt, D. Delbeke, I. Moerman, P. VanDaele, R. Baets, P. Demester and P. Mijlemans, "AlGaInP Microcavity Light-Emitting Diodes at 650 nm on Ge Substrates", IEEE Photonics Tech. L. 12 (8), 957-959 (2000)

[34] R. Wirth, C. Karnutsch, S. Kugler and K. Streubel, “High-Efficiency Resonant-Cavity LEDs Emitting at 650 nm”, IEEE Photonics Tech. L. 13 (5), 421–423 (2001)

[35] D. Delbeke, P. Bienstman, R. Bockstaele and R. Baets, “Rigorous electromagnetic analysis of dipole emission in periodically corrugated layers: the grating-assisted resonant-cavity light-emitting diode”, J. Opt. Soc. Am. A 19, 871-880 (2002)

[36] C. Weisbuch, A. David, T. Fujii, C. Schwach, S. P. DenBaars, S. Nakamura, M. Rattier, H. Benisty, R. Houdré, R. P. Stanley, J. F. Carlin, T. F. Krauss and C. J. M. Smith, “Recent results and latest views on microcavities LED”, Proc. SPIE 5366, 1-19 (2004)

[37] G. Harbers, S. J. Bierhuizen and M. R. Krames, “Performance of High Power Light Emitting Diodes in Display Illumination Applications”, IEEE J. Display Technol. 3(2), 98-109 (2007)

[38] V. Härle, B. Hahn, S. Kaiser, A. Weimar, S. Bader, A. Plössl and F. Eberhard, “Light extraction technologies for high efficiency GaInN-LED devices”, Proc. SPIE 4996, 133-138 (2003)

[39] J. Baur, F. Baumann, M. Peter, K. Engl, U. Zehnder, J. Off, V. Kuemmler, M. Kirsch, J. Strauss, R. Wirth, K. Streubel and B. Hahn, “Status of high efficiency and high power ThinGaN®-LED development”, phys. stat. sol. (c) DOI: 10.1002/pssc.200880936 (2009)

[40] Updated product data sheets can be found at **www.osram-os.com**

[41] J.-M. Lourtioz, H. Benisty, V. Berger, J.-M. Gerard, D. Maystre and A. Tchelnokov, “Photonic crystals: Towards nanoscale photonic devices”, (Springer, Berlin 2008)

[42] R. K. Lee, Y. Xu and A. Yariv, “Modified spontaneous emission from a two-dimensional photonic bandgap crystal slab”, J. Opt. Soc. Am. B 17(8), 1438-1442 (2000)

[43] M. Fujita, S. Takahashi, Y. Tanaka, T. Asano and S. Noda, “Simultaneous Inhibition and Redistribution of Spontaneous Light Emission in Photonic Crystals”, Science 308, 1296-1298 (2005)

[44] J. D. Joannopoulos, S. G. Johnson, J. N. Winn and R. D. Meade, “Photonic crystals – Molding the flow of light”, (Princeton University Press, 2008)

[45] T. F. Krauss, “Slow light in photonic crystal waveguides”, J. Phys. D: Appl. Phys. 40 2666-2670 (2007)

[46] P. St. J. Russell, T. A. Birks and F. D. Lloyd-Lucas, Chapter "Photonic bloch waves and photonic bandgaps" p. 585-634, in "Confined Electrons and Photons: New Physics and Applications", ed. E. Burstein and C. Weisbuch (Plenum Press, New York 1995)

[47] A. David, H. Benisty and C. Weisbuch, "Optimization of Light-Diffracting Photonic-Crystals for High Extraction Efficiency LEDs", IEEE J Display Technol. 3(2), 133-148 (2007)

[48] K. McGroddy, A. David, E. Matioli, M. Iza, S. Nakamura, S. P. DenBaars, J. S. Speck, C. Weisbuch and E. L. Hu, "Directional emission control and increased light extraction in GaN photonic crystal light emitting diodes", Appl. Phys. Lett. 93, 103502 (2008)

[49] H. Benisty, J. Danglot, A. Talneau, S. Enoch, J. M. Pottage and A. David, "Investigation of Extracting Photonic Crystal Lattices for Guided Modes of GaAs-Based Heterostructures", IEEE J. Quantum Electronics 44, 777-789 (2008)

[50] J. A. E. Wasey and W. L. Barnes, "Efficiency of spontaneous emission from planar microcavities", J Mod Optics 47(5), 725-741 (2000)

[51] T. Kim, A. J. Danner, P. Leisher, K. D. Choquette, R. Wirth and K. Streubel, "Photonic crystal structure effect on the enhancement in the external quantum efficiency of a red LED", IEEE Photonic Tech. L. 18, 1876-1878 (2006)

[52] **http://www.luminus.com/** : The PhlatLight LEDs from Luminus use photonic crystal for light extraction. The external quantum efficiency can be calculated with the data sheet values for the product CBT-40: *400mW, 1400mA,* λ_{peak}*=625nm, 1.8V* gives η_{QE} *= 14%* (30 June 2009).

[53] S.-K. Kim, H. D. Song, H.-S. Ee, H. M. Choi, H. K. Cho, Y.-H. Lee, H.-G. Park, "Metal mirror assisting light extraction from patterned AlGaInP light-emitting diodes" Appl. Phys. Lett. 94 101102 (2009)

[54] J. J. Wierer, A. David and M. M. Megens, "III-nitride photonic crystal light-emitting diodes with high extraction efficiency", Nature Photon. 3, 163-169 (2009)

[55] C. Wiesmann, "Nano-structured LEDs – Light Extraction Mechanisms and Applications, Dissertation zur Erlangung des Doktorgrades der Naturwissenschaften", Universität Regensburg (To be published 2009)

[56] M. Rattier, H. Benisty, E. Schwoob, C. Weisbuch, T. F. Krauss, C. J. M. Smith, R: Houdré and U. Oesterle, "Omnidirectional and compact guided light extraction from Archimedean photonic lattices", Appl. Phys. Lett. 83, 1283-1285 (2003)

[57] R. Wirth, S. Illek, C. Karnutsch, I. Pietzonka, A. Plössl, P. Stauss, W. Stein, W. Wegleiter, R. Windisch, H. Zull and K. Streubel, "Recent Progress of AlGaInP Thinfilm Light Emitting Diodes", Proc. SPIE 4996 1-9 (2003)

[58] R. Windisch, C. Rooman, S. Meinlschmidt, P. Kiesel, D. Zipperer, G. H. Döhler, B. Dutta, M. Kuijk, G. Borghs and P. Heremans, "Impact of texture-enhanced transmission on high-efficiency surface-textured light-emitting diodes", Appl. Phys. Lett. 79, 2315 (2001)

[59] W. Han, S. Fan, Q. Li and Y. Hu, "Synthesis of gallium nitride nanorods through a carbon nanotube-confined reaction", Science 277, 1287 (1997)

[60] S. D. Hersee, X. Sun and X. Wang, "The controlled growth of GaN nanowires", Nano Lett. 6, 1808 (2006)

[61] F. Qian, S. Gradecak, Y. Li, C.-Y. Wen and C. M. Lieber, "Core/multishell nanowire heterostructures as multicolour, high efficiency light-emitting diodes", Nano Lett. 5, 2287 (2005)

ATTACHED PAPERS

Paper I

Enhanced light extraction efficiency from AlGaInP thin-film light-emitting diodes with photonic crystals

K. Bergenek, Ch. Wiesmann, R. Wirth, L. O`Faolain, N. Linder, K. Streubel, T.F. Krauss

Applied Physics Letters 93, 041105 (2008)

Enhanced light extraction efficiency from AlGaInP thin-film light-emitting diodes with photonic crystals

K. Bergenek,[1,2,a] Ch. Wiesmann,[1] R. Wirth,[1] L. O'Faolain,[2] N. Linder,[1] K. Streubel,[1] and T. F. Krauss[2]
[1]*OSRAM Opto Semiconductors GmbH, Leibnizstr. 4, 93055 Regensburg, Germany*
[2]*University of St Andrews, School of Physics and Astronomy, St. Andrews, Fife KY16 9SS, United Kingdom*

(Received 16 May 2008; accepted 2 July 2008; published online 29 July 2008)

We investigate the use of photonic crystals for light extraction from high-brightness thin-film AlGaInP light-emitting diodes with different etch depths, lattice constants, and two types of lattices (hexagonal and Archimedean). Both simulations and experimental results show that the extraction of high order modes with a low effective index n_{eff} is most efficient. The highest external quantum efficiency without encapsulation is 19% with an Archimedean A7 lattice with reciprocal lattice constant $G=1.5\ k_0$, which is 47% better than an unstructured reference device. © *2008 American Institute of Physics*. [DOI: 10.1063/1.2963030]

Total internal reflection at the semiconductor-air interface results in poor light extraction efficiency from light-emitting diodes (LEDs). Photonic crystals (PhC) have already been applied to extract the guided light.[1] Following initial concentration on infrared PhC-LEDs,[2,3] recent developments have focussed on GaN-based LEDs.[4–6] Furthermore, quasicrystals, such as Archimedean lattices, have also been implemented to allow for omnidirectional light extraction.[3] It is still uncertain, however, whether PhC-LEDs can outperform state-of-the-art LEDs in terms of external quantum efficiency η_{QE}. Here, we investigate the use of PhCs for light extraction from high efficiency thin-film LEDs in the AlGaInP material system emitting at 650 nm and compare the experimental results with simulations.

The PhC diffracts guided modes with in-plane wave vector $k_i=|n_{\mathrm{eff},i}|k_0$ $(1<|n_{\mathrm{eff},i}|<n_{\mathrm{QW}})$ as seen in Fig. 2(a) according to Bragg's law

$$\mathbf{n}_{\mathrm{eff},d}(k_x,k_y)=\mathbf{n}_{\mathrm{eff},i}(k_x,k_y)+\mathbf{G}/k_0, \tag{1}$$

where n_{eff} is the effective index of the mode, G is a reciprocal lattice vector of the PhC, and k_0 is the vacuum wavenumber. Diffracted modes with $0<|n_{\mathrm{eff},d}|<1$ are extracted to air with the farfield angle $\theta=\sin^{-1}(n_{\mathrm{eff},d})$. Hence, a mismatch $\Delta=|\mathbf{n}_{\mathrm{eff},i}-\mathbf{G}/k_0|<1$ is allowed for first order diffraction to air but the extraction efficiency for large Δ is low as it is proportional to $\sqrt{1-\Delta^2}$.[7] Since guided modes in AlGaInP have $n_{\mathrm{eff}}\in[1,3.4]$, the optimal reciprocal lattice constant must be sought in the range $1<G/k_0<3.4$.

Our LEDs were grown by metal-organic vapor phase epitaxy on a GaAs substrate and processed according to the scheme described elsewhere.[8] The vertical refractive index structure of the LED can be seen in Fig. 1. It has a combined transparent conductive oxide/Au mirror and p contact. The active region consists of five GaInP quantum wells (QWs) with $(Al_{0.5}Ga_{0.5})_{0.5}In_{0.5}P$ barriers embedded between 400 nm thick AlInP electrical confinement layers. A 3.8 μm thick n-$Al_{0.6}Ga_{0.4}As$ current spreading layer ensures sufficient current spreading onto the $250\times250\ \mu m^2$ chip. The PhCs were defined on 400 nm thick ZEP-520A resist by e-beam lithography and subsequently etched with chlorine-based chemically assisted ion beam etching into the n-$Al_{0.6}Ga_{0.4}As$ current spreading layer using only the ZEP resist as a mask. Two sets of samples were etched to an etch depth of 200 and 800 nm, respectively. We fabricated hexagonal lattices and Archimedean A7 lattices with reciprocal lattice constant G between 1.5 k_0 and 3.4 k_0, corresponding to lattice constants between 490 and 224 nm, respectively [Figs. 2(b) and 2(c)]. The PhC-LEDs and unpatterned reference LEDs were mounted on TO18 headers for characterization. The total flux from the fabricated LEDs was measured in an integrating sphere. The PhC enhancement at 10 mA drive current was given by dividing the PhC-LED intensity with an unpatterned reference LED intensity and is plotted in Fig. 2(d).

The experimental extraction efficiency dependence on G can be compared with a model based on coupled mode theory, where we treat the PhC as a perturbation of the unpatterned LED. Hence, we assume that the internal emission pattern is similar to the emission pattern in an unpatterned LED, where the PhC region has an effective refractive index n_{PhC}. The diffracted intensity from mode n to mode m is given by

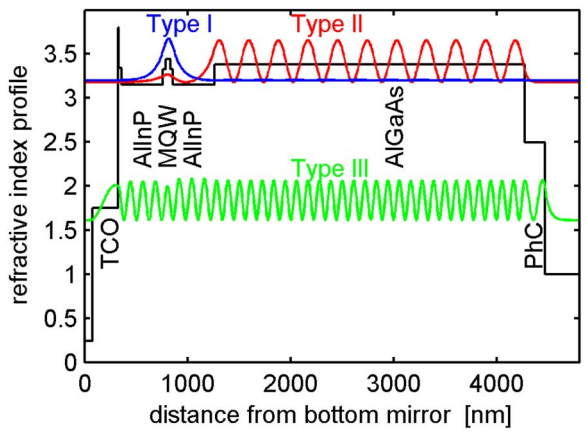

FIG. 1. (Color online) Vertical refractive index profile of the characterized LED (black thick line) and normalized guided mode intensity profiles. The high intensity type I mode is confined to the MQW region. Type II modes are evanescent in the PhC region whereas type III modes can propagate in the PhC region.

[a]Electronic mail: krister.bergenek@osram-os.com.

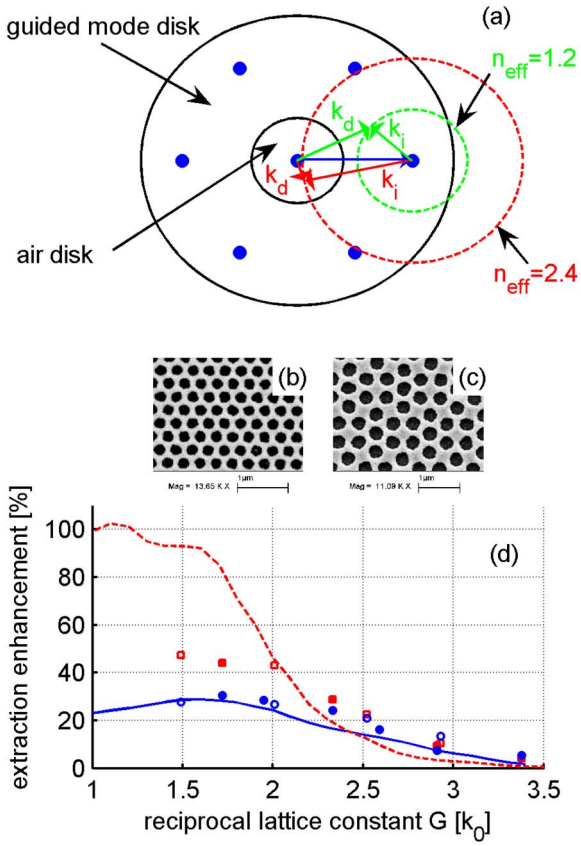

FIG. 2. (Color online) (a) Diffraction of incident in-plane k vectors k_i to k_d by the reciprocal lattice vector $G=2.5$. Both modes cannot be extracted by the same PhC. [(b) and (c)] Scanning electron microscope images of LED surfaces with a hexagonal PhC and an Archimedean A7 lattice. (d) Experimental PhC enhancements for hexagonal (filled) and A7 (open) lattices with 200 nm (circles) and 800 nm (squares) etch depth together with simulated diffraction intensity in a.u. for 200 nm (solid line) and 800 nm etch depth (dashed line).

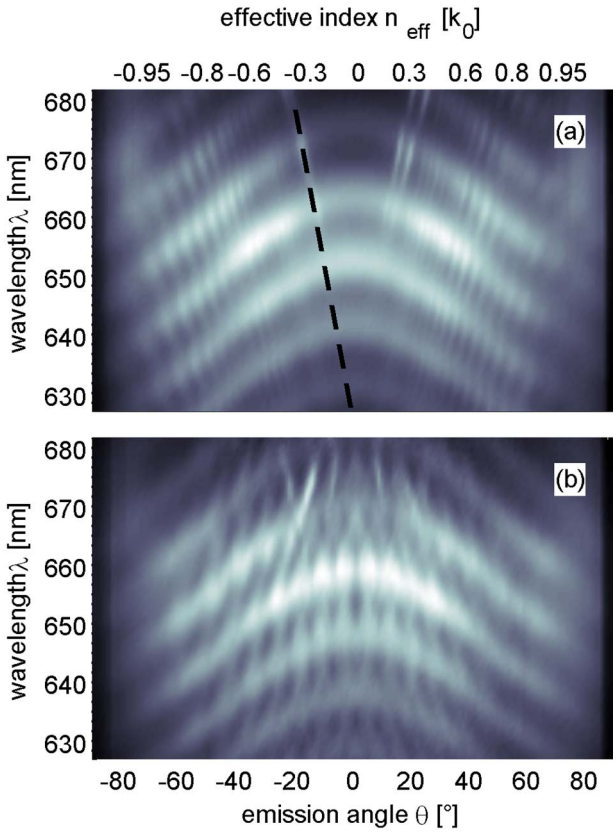

FIG. 3. (Color online) (a) Normalized spectral resolved farfields for hexagonal PhC-LEDs in the ΓM direction (a) $G=3.4\ k_0$. The calculated type I mode with highest intensity has been inserted (dashed line). (b) $G=1.7\ k_0$. Strong diffraction of type III modes at all wavelengths. NB The θ-λ representation used here is similar to the commonly used ω-k representation for guided modes.

$$I_d(n \rightarrow m) \propto I_n |\Delta\tilde{\varepsilon}_{mn}|^2 |\kappa_{mn}|^2, \tag{2}$$

where I_n is the spontaneous emission into the nth mode, $|\Delta\tilde{\varepsilon}_{mn}|^2$ is the Fourier amplitude of the reciprocal lattice vector G that couples mode n to m, and κ_{mn} represents the coupling strength and is calculated as

$$\kappa_{mn} = \int_{\mathrm{PhC}} E_m^*(z) \cdot E_n(z) dz. \tag{3}$$

The diffracted intensity into air is given by summing up all diffraction events for radiating modes with $n_{\mathrm{eff}}<1$. The strength of this model[7] is that the real undisturbed mode distribution is taken into account as well as all diffraction orders. Naturally, the validity of this perturbative approach decreases as the PhC etch depth increases, which is also evident from the comparison of experimental and simulated diffraction efficiencies presented in Fig. 2(d). There is good agreement for 200 nm etch depth, but less so for 800 nm. For the 200 nm curve (solid line), maximum diffraction to air is obtained for $G=1.6$. This can be understood by considering the vertical guided mode intensity profile for different types of modes in the LED (Fig 1). A few modes with $n_{\mathrm{eff}} > n_{\mathrm{AlInP}}$ are resonant in the waveguide created by the high index multiple QW (MQW) region surrounded by the lower index AlInP electrical confinement layers. These so called type I modes have a very high intensity but they are hardly affected by the distant PhC and so will only extract weakly. A second type (II) of modes with $n_{\mathrm{PhC}}<n_{\mathrm{eff}}<n_{\mathrm{MQW}}$ are guided within the whole LED. These modes also interact only weakly with the PhC since they are evanescent within the PhC. A third range of modes (III) with $1<n_{\mathrm{eff}}<n_{\mathrm{PhC}}$ interacts more strongly with the PhC. The simulation shows that this third type of modes is the most promising to extract due to its high coupling strength with the PhC, which explains the maximum extraction efficiency observed for $G/k_0 \approx n_{\mathrm{eff}}=1.6$, as this effective index falls within the range of type III modes.

Spectrally resolved farfield patterns (Fig. 3) were collected with a scan step of 1° and 0.9° angular resolution. The farfields were normalized with the integrated emission spectrum and divided by a lambertian emission profile to visualize the PhC effect for all wavelengths and angles. In addition to the Fabry–Pérot resonances evidenced by the broad "boomerang"-shaped lines, the PhC-LED farfields have steep diffraction lines [Figs. 3(a) and 3(b)] that correspond to extracted guided modes. In the farfield pattern from a hexagonal PhC-LED with $G=3.4\ k_0$ [Fig. 3(a)], two strong lines can be also observed near the top of the graph, around 670 nm. These lines disappear for wavelengths shorter than $\lambda_{\mathrm{peak}}=658$ nm, indicating that these modes are reabsorbed in the active region much faster than they are extracted by the PhC. These lines should therefore correspond to type I modes and this is confirmed by the good agreement with the diffraction line (inserted dashed line) from the type I mode with highest

intensity calculated with a one-dimensional mode solver. Extracted type II and type III modes on the other hand, suffer less from reabsorption, since they have a lower overlap with the active region and the diffraction lines can be observed over the whole spectrum [Fig. 3(b)]. The slope of the diffraction lines shows that the extraction angle is almost independent of the wavelength within the emission spectrum, which highlights the fact that the diffraction strength is not sensitive to wavelength shifts that can be induced by heating or high current densities.

The highest PhC extraction enhancement at 10 mA compared to an unstructured reference is 47% for a 800 nm deep A7 lattice with $G=1.5\ k_0$. Hexagonal and A7 PhCs do generally have very similar enhancement factors, as shown in Fig. 2(d). This was also observed in Ref. 9, suggesting that the total extraction efficiency is not enhanced by the A7 lattice despite its omnidirectional diffraction properties. The external quantum efficiency for this PhC-LED is 19% without encapsulation.

For comparison, the extraction efficiency for an unpatterned LED calculated with the formalism given in Ref. 10 is just $\eta_{\mathrm{extr}}=3.5\%$. The measured $\eta_{\mathrm{QE}}=\eta_{\mathrm{int}}\eta_{\mathrm{extr}}$ is 13%, however, where $\eta_{\mathrm{int}}\leqslant 100\%$ is the internal quantum efficiency. This significant discrepancy between simulation and experiment can only be explained by photon recycling. In fact, simulations have shown that the light extraction efficiency can indeed be enhanced by a factor of this magnitude when η_{int} is close to 100%.[11] The mechanism for this almost fourfold enhancement is the reabsorption of preferentially guided modes in the active MQW region followed by re-emission into any mode. Hence, photon recycling redistributes the mode intensity such that more light is emitted into the light extraction cone. Type I modes are absorbed most strongly due to their high overlap with the MQW region but recycling also occurs for type II and type III modes.

Even though the extraction enhancement of 47% facilitated by the PhC is significant, much higher enhancements have been reported by other researchers, e.g., values >100% (Ref. 12) have already been achieved. These high values have been reported for AlGaInP LEDs with absorbing GaAs substrates and small emission windows, however, i.e., the high relative enhancement was obtained for devices with low absolute efficiency. Our results, in contrast, highlight the fact that significant enhancements can also be achieved for devices with high absolute efficiency.

Compared to surface roughening,[13,14] our enhancement values are also lower. Surface roughening effectively scatters incident light randomly into all directions. Hence, a fraction of the light is extracted regardless of the effective index of the incident light. In contrast, the PhC extracts a limited mode range with high efficiency but the remaining modes are not extracted at all [Fig. 2(a)]. In principle, this enables the extraction of light into a limited extraction cone, i.e., the creation of a more directional beam. Therefore, a much thinner device with a tailored mode distribution[4] is expected to show higher PhC enhancements.

In summary, we have fabricated and characterized AlGaInP thin-film LEDs with 200 and 800 nm deep hexagonal and Archimedean A7 PhCs with different lattice constants. Spectral farfield measurements show the multimode extraction and that the extraction angle of a single mode is almost constant over the spectral emission width. The highest extraction enhancement of 47% is obtained for extraction of high-order type III modes, which is in agreement with simulations based on coupled mode theory. The main achievement reported here is the demonstration of high PhC-based extraction enhancement combined with a high absolute external quantum efficiency.

[1] S. Fan, P. R. Villeneuve, J. D. Joannopoulos, and E. F. Schubert, Phys. Rev. Lett. **78**, 3294 (1997).
[2] A. A. Erchak, D. J. Ripin, S. Fan, P. Rakich, J. D. Joannopoulos, E. P. Ippen, G. S. Petrich, and L. A. Kolodziejski, Appl. Phys. Lett. **78**, 563 (2001).
[3] M. Rattier, H. Benisty, E. Schwoob, C. Weisbuch, T. F. Krauss, C. J. M. Smith, R. Houdre, and U. Oesterle, Appl. Phys. Lett. **83**, 1283 (2003).
[4] A. David, T. Fujii, R. Sharma, K. McGroddy, S. Nakamura, S. P. DenBaars, E. L. Hu, C. Weisbuch, and H. Benisty, Appl. Phys. Lett. **88**, 061124 (2006).
[5] J. J. Wierer, M. R. Krames, J. E. Epler, N. F. Gardner, M. G. Craford, J. R. Wendt, J. A. Simmons, and M. M. Sigalas, Appl. Phys. Lett. **84**, 3885 (2004).
[6] D.-H. Kim, C.-O. Cho, Y.-G. Roh, H. Jeon, Y. S. Park, J. Cho, J. S. Im, C. Sone, Y. Park, W. J. Choi, and Q.-H. Park, Appl. Phys. Lett. **87**, 203508-1 (2005).
[7] C. Wiesmann, K. Bergenek, N. Linder, and U. T. Schwarz (unpublished).
[8] K. Streubel, N. Linder, R. Wirth, and A. Jaeger, IEEE J. Sel. Top. Quantum Electron. **8**, 321 (2002).
[9] A. David, T. Fuji, E. Matioli, R. Sharma, S. Nakamura, S. P. DenBaars, C. Weisbuch, and H. Benisty, Appl. Phys. Lett. **88**, 073510 (2006).
[10] J. A. E. Wasey and W. L. Barnes, J. Mod. Opt. **47**, 725 (2000).
[11] P. Altieri, A. Jäger, R. Windisch, N. Linder, P. Stauss, R. Oberschmid, and K. Streubel, J. Appl. Phys. **98**, 1 (2005).
[12] T. Kim, A. J. Danner, P. Leisher, K. D. Choquette, R. Wirth, and K. Streubel, IEEE Photonics Technol. Lett. **18**, 1876 (2006).
[13] R. Wirth, S. Illek, C. Karnutsch, I. Pietzonka, A. Plössl, P. Stauss, W. Stein, W. Wegleiter, R. Windisch, H. Zull, and K. Streubel, Proc. SPIE **4996**, 1 (2003).
[14] R. Windisch, C. Rooman, S. Meinlschmidt, P. Kiesel, D. Zipperer, G. H. Döhler, B. Dutta, M. Kuijk, G. Borghs, and P. Heremans, Appl. Phys. Lett. **79**, 2315 (2001).

Paper II

Directional light extraction from thin-film resonant cavity light-emitting diodes with a photonic crystal

K. Bergenek, Ch. Wiesmann, H. Zull, R. Wirth, P. Sundgren, N. Linder, K. Streubel, T.F. Krauss

Applied Physics Letters 93, 231109 (2008)

Directional light extraction from thin-film resonant cavity light-emitting diodes with a photonic crystal

K. Bergenek,[1,2,a)] Ch. Wiesmann,[1] H. Zull,[1] R. Wirth,[1] P. Sundgren,[1] N. Linder,[1] K. Streubel,[1] and T. F. Krauss[2]
[1]*OSRAM Opto Semiconductors GmbH, Leibnizstr. 4, 93055 Regensburg, Germany*
[2]*School of Physics and Astronomy, University of St Andrews, St. Andrews, Fife KY16 9SS, United Kingdom*

(Received 13 October 2008; accepted 18 November 2008; published online 10 December 2008)

We report directional light extraction from AlGaInP thin-film resonant cavity light emitting diodes (RCLEDs) with shallow photonic crystals (PhCs). Diffraction of guided modes into the light extraction cone enhances the light extraction by a factor of 2.6 compared to unstructured RCLEDs, where the farfields still show higher directionality than Lambertian emitters. The external quantum efficiency is 15.5% to air and 26% with encapsulation, respectively. The PhC-RCLEDs are also more stable to a temperature induced wavelength shift than unstructured RCLEDs. © *2008 American Institute of Physics*. [DOI: 10.1063/1.3046130]

The efficiency of red AlGaInP light-emitting diodes (LEDs) is limited by poor light extraction caused by the high refractive index contrast between AlGaInP and air. In the past decade, several methods have been developed to increase the external quantum efficiency from below 3% for AlGaInP LEDs on an absorbing GaAs substrate to above 50% for emission at 650 nm.[1,2] One of the successful solutions is the thin-film LED, where epitaxial layers are mounted on a carrier wafer with an intermediate metal mirror and contact. The subsequent removal of the absorbing substrate results in a thick cavity with losses only in the active region and at the contacts. The light extraction efficiency can be improved significantly by incorporating buried microreflectors and random surface texturing.[2] The latter measure results in a Lambertian farfield emission pattern where the directionality is $D(\theta)=(\sin\theta)^2$. The directionality is defined as

$$D(\theta) = P(\theta)/P(90^\circ) = \int_0^\theta I(\theta')\sin\theta' d\theta' \Big/ \int_0^{90} I(\theta')\sin\theta' d\theta', \quad (1)$$

where $I(\theta')$ is the measured intensity at the angle θ'. While this yields high overall extraction efficiency, a more directional emission profile is desirable for many applications as it increases the coupling efficiency to an external optical system with a limited numerical aperture. Such directional emission can be achieved with resonant cavity LEDs[3–5] (RCLEDs) first proposed by Schubert *et al.*[6] and have been investigated thoroughly theoretically.[7–9] However, the higher directionality in AlGaInP RCLEDs has been obtained with an external quantum efficiency of only 23% in encapsulation at its best.[3] Furthermore, the efficiency dependence on temperature is worse for resonant cavity based devices, since the emission spectrum and the cavity detune as the temperature increases.[4] Photonic crystals (PhCs) have been applied to LEDs with the purpose of diffracting guided light into the light extraction cone by a number of authors,[10–16] and it has been shown that the directionality of the emitted light for GaN LEDs can be enhanced.[17] Recent work on PhCs applied to a AlGaInP thin-film LED did indeed show that the extraction efficiency can be enhanced by almost 50% compared with a flat surface by extracting high order modes with an effective index $n_{\mathrm{eff}}<n_{\mathrm{PhC}}$, where n_{PhC} is the effective refractive index of the PhC.[16] However, the large number of guided modes in the thick (>4 μm) epitaxial film left little room for a directionality enhancement of the farfield.

In this letter, we show that the light extraction from AlGaInP RCLEDs can be greatly enhanced by using a thinner epitaxial film and applying a shallow PhC, while maintaining a super-Lambertian emission pattern and at the same time improving the temperature stability. This reduction in layer thickness can be achieved without loss of carrier injection uniformity because we introduce a transparent conductive oxide (TCO) layer that acts as the current spreading layer. The total thickness of the epitaxial layers is 1.4 μm, which results in fewer modes with higher intensity. Furthermore, the formation of a $5\lambda/2$ cavity between the bottom metal mirror and the top distributed Bragg reflector (DBR) enhances the light extraction efficiency and provides higher directionality of the directly emitted light. The DBR impact on the guided mode distribution on the other hand is negligible. Our approach is analog to the grating-assisted RCLED treated in Ref. 18, but with the major difference that the PhC is placed on top of the cavity and not within it. In this way, the Fabry–Pérot (FP) resonance is less sensitive to deviations of the PhC etch depth and air filling factor.

The PhC diffracts guided modes with in-plane wave vector $\vec{k}_i=|\vec{n}_{\mathrm{eff},i}|k_0$ $(1<|\vec{n}_{\mathrm{eff},i}|<n_{\mathrm{QW}})$ according to Bragg's law,

$$\vec{n}_{\mathrm{eff},d}(k_x,k_y) = \vec{n}_{\mathrm{eff},i}(k_x,k_y) + \vec{G}/k_0. \quad (2)$$

Since extraction to air requires that $|\vec{n}_{\mathrm{eff},d}|<1$, the allowed mismatch between a reciprocal lattice vector $\vec{G}$ and the effective index of the incident guided mode is $\Delta=|\vec{n}_{\mathrm{eff},i}-\vec{G}/k_0|<1$, where k_0 is the vacuum wave number. Hence, the PhC extracts only a limited range of the guided modes expressed in terms of effective index $n_{\mathrm{eff}}=|\vec{n}_{\mathrm{eff}}|$. More generally, the allowed mismatch for extraction within a limited external extraction angle θ_{ext} requires that $\Delta=|\vec{n}_{\mathrm{eff},i}-\vec{G}/k_0|<\sin\theta_{\mathrm{ext}}$. We choose lattice constants a in the range 310–500 nm, corresponding to $G/k_0=1.5-2.4$, in order to diffract

a)Electronic mail: krister.bergenek@osram-os.com.

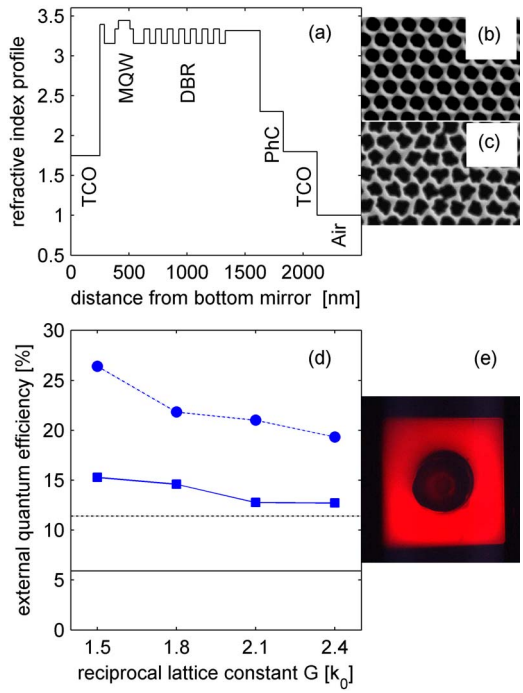

FIG. 1. (Color online) (a) Refractive index profile of the PhC-RCLED. Scanning electron microscope image of the PhC on an (b) etch test sample and on the (c) characterized sample. External quantum efficiency at 30 mA as a function of the reciprocal lattice constant of the PhC for extraction to air (squares) and for encapsulated chips (circles). (d) Efficiency for unstructured RCLEDs plotted as horizontal lines (solid line to air and dotted line for encapsulation). (e) Microscope image of PhC-RCLED under operation.

high order modes with a high overlap with the PhC.

The RCLEDs were grown by metal-organic vapor phase epitaxy on a GaAs substrate. The vertical refractive index structure of the processed RCLEDs can be seen in Fig. 1(a). It has a combined TCO/Au mirror and *p*-contact. The active region consists of five GaInP quantum wells emitting at 650 nm with $(Al_{0.5}Ga_{0.5})_{0.5}In_{0.5}P$ barriers embedded between 90 nm thick AlInP electrical confinement layers. The DBR consists of seven pairs of $\lambda/4n$ thick $(Al_{0.95}Ga_{0.05})_{0.5}In_{0.5}P$ and $(Al_{0.5}Ga_{0.5})_{0.5}In_{0.5}P$ layers. The refractive index contrast between the two DBR material components is only $\Delta n=0.16$, which results in a calculated reflectivity of 35% with a full width at half maximum (FWHM) of 36 nm. The hexagonal PhCs were defined on 400 nm thick ZEP520A resist by e-beam lithography and subsequently etched via a hard mask with chlorine-based inductively coupled plasma to a depth of 200 nm. After removal of the hard mask, the PhC was covered with 290 nm TCO that connects the whole chip with 210 μm side length to the central bondpad. The hole shape of the fabricated PhCs on the characterized devices was irregular since the hard mask eroded during etching [see Figs. 1(b) and 1(c)]. The simulated extraction efficiency η_{extr} with the method is given in Ref. 19 for a RCLED without a PhC is 6.6% to air when emission from all quantum well positions and the spectral width of the internal emission is taken into account. However, the redistribution of light from guided modes to radiating modes through photon recycling is not included in Ref. 19. For devices with high internal efficiency, this effect can cause an extraction efficiency enhancement of several hundreds of percent.[16,20]

The efficiency of the PhC-RCLEDs was measured in an integrating sphere and is plotted as a function of the reciprocal lattice constant of the PhC in Fig. 1(d). The highest external quantum efficiency η_{QE} is 15.5% for PhC-RCLEDs mounted on TO18 headers and 26% for encapsulated PhC-RCLEDs. The latter efficiency is higher than the highest reported efficiency of unstructured AlGaInP RCLEDs. The corresponding values for the unstructured reference RCLEDs is 5.9% and 11.6%. A comparison between the experimental η_{QE} and the simulated extraction efficiency η_{extr}, where $\eta_{QE}=\eta_{int}\eta_{extr}$, shows that the internal efficiency η_{int} is well below 90%, which indicates that photon recycling does not contribute substantially to the external efficiency. The highest quantum efficiency η_{QE} is obtained between 20 and 30 mA, corresponding to 63–95 A/cm^2. This remarkably high current density for which η_{QE} reaches its maximum is a further indicator of high nonradiative recombination, as nonradiative effects have most impact at low current densities. On the other hand, excellent current distribution over the whole chip area via the TCO contacts as seen in Fig. 1(e) ensures the lowest possible local current density, which minimizes current leakage over the thin confinement layers at high currents. The PhC enhancement factor for extraction to air measured at 30 mA is in the range of 2.2–2.6, with highest extraction efficiency for the smallest reciprocal lattice constant $G=1.5k_0$ ($a=500$ nm). It is worth noting that this dependency on G is similar to the results in Ref. 16. To determine the directionality of the emitted light, spectral farfields were measured with an optical fiber mounted on a rotating arm (step size 1°) connected to a spectrometer and they are shown in Figs. 2(a) and 2(b). The farfields are normalized with the integrated emission spectrum and a Lambertian emission profile. The $5\lambda/2$ cavity is thin enough to allow for only one FP resonance in the farfield within the spectral width as seen in Fig. 2(a) for the unstructured RCLED. The directionality $D(30°)=31\%\pm1\%$ of the emitted light is considerably better than for a Lambertian emitter, which has $D(30°)=(\sin 30°)^2=25\%$.

We now turn to the temperature dependence of the unstructured and structured emitters, respectively. The right-

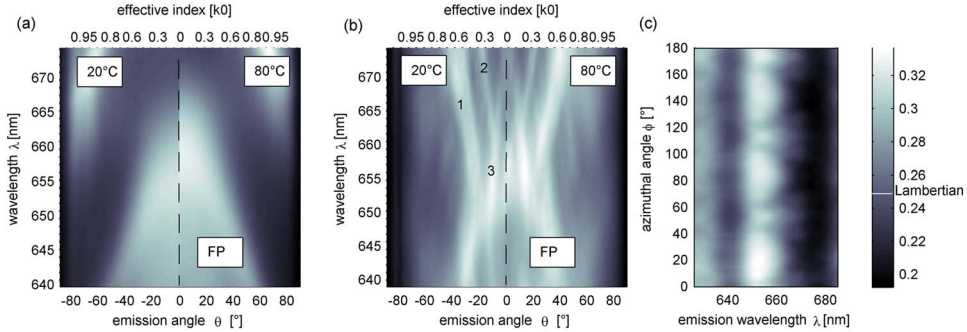

FIG. 2. (Color online) Normalized spectral farfield for an (a) unstructured RCLED and for a (b) PhC-RCLED with $G=1.5k_0$ measured at 20 °C (left side) and 80 °C (right side). Three strong diffraction lines can be seen together with the boomerang-shaped FP mode for the PhC-RCLED. (c) Directionality D (30°) as a function of emission wavelength and azimuthal angle for the same PhC-RCLED.

hand side of Fig. 2(a) shows the farfield measured at 80 °C for the unstructured emitter. The redshift of the spectrum is 7 nm and the FWHM is increased from 18 to 23 nm. The emitted flux drops by $30\% \pm 1.1\%$ between 20 °C, and 80 °C, which is due to the thermal wavelength detuning from the FP resonance and a drop in internal efficiency. Simulations suggest that the extraction efficiency drop is 20% and the internal efficiency drop contributes 10% to this figure. In comparison, the farfield for the PhC-RCLEDs is slightly less directional than the bare RCLEDs, but varies less with temperature; the most efficient PhC-RCLED with $G=1.5k_0$ has also the highest directionality with $29\% \pm 1\%$ in a 30° cone. The farfield in the ΓM-direction measured at 20 °C is seen on the left-hand side in Fig. 2(b). The boomerang-shaped FP-mode can still be recognized. Three additional diffraction lines labeled 1–3 in Fig. 2(b) apparently contribute to the light extraction. The effective index of the corresponding modes is 1.19, 1.47, and 1.74 for $\lambda = 650$ nm from Eq. (2). The right hand side of Fig. 2(b) then shows the farfield of the PhC-RCLED at 80 °C. The diffraction lines are almost identical for the two different temperatures and the temperature induced emission drop is reduced to $27\% \pm 1.5\%$. Assuming that the internal efficiency drop is similar to the bare RCLED, we calculate the extraction efficiency drop to be 17%. This improved temperature stability of the PhC-RCLED is explained by the reduced light extraction dependency on the FP-resonance; instead, the extraction is dominated by the PhC extraction channels that have weaker temperature dependence.

Finally, we assess the impact of the hexagonal nature of the lattice on the directionality. Figure 2(c) shows the fraction of the emitted light within a ±30° cone as a function of the azimuthal angle Φ (azimuthal step size 3°) and the wavelength λ of the PhC-RCLED. The directionality depends most strongly on λ with a maximum close to the peak wavelength. The strong λ-dependence is mainly caused by the FP resonance as seen in Fig. 2(b) but also because the strongest diffracted mode [mode 1 in Fig. 2(b)] falls outside the 30° cone for $\lambda > 660$ nm. The extraction of this mode would have been more directional with a smaller reciprocal lattice constant. A 60° periodicity is seen in the directionality dependence on the azimuthal angle Φ as expected from a hexagonal lattice. However, the azimuthal contrast $[P(30°)]^{\max} - P[(30°)^{\min}]/[P(30°)]^{\max} + P[(30°)^{\min}] < 7\%$ within the FWHM of the emission spectrum is quite small. Although such in-plane nonuniformity may be unwanted for some applications, we conclude that it is of minor importance for the directionality.

In summary we fabricated thin AlGaInP thin-film PhC-RCLEDs emitting at 650 nm. The measured external quantum efficiency up to 26% at high current density exceeds previous records for AlGaInP RCLEDs without PhCs. Analysis of spectral farfields shows that PhCs can enhance the extraction efficiency from resonant-cavity LEDs by 160% while still maintaining higher directionality than Lambertian emitters. It is also noteworthy that the quality of the etched lattice, which is relatively poor as seen in Fig. 1(c), has little impact on the extraction efficiency, as the relevant modes can be clearly distinguished.

Part of the processing work was done at MC2 Nanofabrication Laboratory, Chalmers University of Technology, Göteborg, Sweden and was financed by the FP6-Research Infrastructures Program MC2ACCESS with Contract No. 026029.

[1] M. R. Krames, M. Ochinai-Holocomb, G. E. Höfler, C. Carter-Coman, E. I. Chen, I-H. Tan, P. Grillot, N. F. Gardner, H. C. Chui, J-W. Huang, S. A. Stockman, F. A. Kish, and M. G. Craford, Appl. Phys. Lett. **75**, 2365 (1999).
[2] R. Windisch, R. Butendeich, S. Illek, S. Kugler, R. Wirth, H. Zull, and K. Streubel, IEEE Photon. Technol. Lett. **19**, 774 (2007).
[3] R. Joray, M. Ilegems, R. P. Stanley, W. Schmid, R. Butendeich, R. Wirth, A. Jaeger, and K. Streubel, IEEE Photon. Technol. Lett. **18**, 1052 (2006).
[4] R. Wirth, C. Karnutsch, S. Kugler, and K. Streubel, IEEE Photon. Technol. Lett. **13**, 421 (2001).
[5] P. Modak, M. D'Hondt, D. Delbeke, I. Moerman, P. VanDaele, R. Baets, P. Demester, and P. Mijlemans, IEEE Photon. Technol. Lett. **12**, 957 (2000).
[6] E. F. Schubert, Y.-H. Wang, A. Y. Cho, L.-W. Tu, and G. J. Zydzik, Appl. Phys. Lett. **60**, 921 (1992).
[7] H. Benisty, H. De Neve, and C. Weisbuch, IEEE J. Quantum Electron. **34**, 1612 (1998).
[8] H. Benisty, H. De Neve, and C. Weisbuch, IEEE J. Quantum Electron. **34**, 1632 (1998).
[9] D. Delbeke, R. Bockstaele, P. Bienstman, R. Baets, and H. Benisty, IEEE J. Sel. Top. Quantum Electron. **8**, 189 (2002).
[10] S. Fan, P. R. Villeneuve, J. D. Joannopoulos, and E. F. Schubert, Phys. Rev. Lett. **78**, 3294 (1997).
[11] A. A. Erchak, D. J. Ripin, S. Fan, P. Rakich, J. D. Joannopoulos, E. P. Ippen, G. S. Petrich, and L. A. Kolodziejski, Appl. Phys. Lett. **78**, 563 (2001).
[12] M. Rattier, H. Benisty, E. Schwoob, C. Weisbuch, T. F. Krauss, C. J. M. Smith, R. Houdre, and U. Oesterle, Appl. Phys. Lett. **83**, 1283 (2003).
[13] A. David, T. Fujii, R. Sharma, K. McGroddy, S. Nakamura, S. P. DenBaars, E. L. Hu, C. Weisbuch, and H. Benisty, Appl. Phys. Lett. **88**, 061124 (2006).
[14] D.-H. Kim, C.-O. Cho, Y.-G Roh, H. Jeon, Y. S. Park, J. Cho, J. S. Im, C. Sone, Y. Park, W. J. Choi, and Q.-H. Park, Appl. Phys. Lett. **87**, 203508 (2005).
[15] T. Kim, A. J. Danner, P. Leisher, K. D. Choquette, R. Wirth, and K. Streubel, IEEE Photon. Technol. Lett. **18**, 1876 (2006).
[16] K. Bergenek, Ch. Wiesmann, R. Wirth, L. O'Faolain, N. Linder, K. Streubel, and T. F. Krauss, Appl. Phys. Lett. **93**, 041105 (2008).
[17] J. J. Wierer, M. R. Krames, J. E. Epler, N. F. Gardner, M. G. Craford, J. R. Wendt, J. A. Simmons, and M. M. Sigalas, Appl. Phys. Lett. **84**, 3885 (2004).
[18] D. Delbeke, P. Bienstman, R. Bockstaele, and R. Baets, J. Opt. Soc. Am. A **19**, 871 (2002).
[19] J. A. E. Wasey and W. L. Barnes, J. Mod. Opt. **47**, 725 (2000).
[20] P. Altieri, A. Jäger, R. Windisch, N. Linder, P. Stauss, R. Oberschmid, and K. Streubel, J. Appl. Phys. **98**, 086101 (2005).

Paper III

Photonic crystal LEDs - designing light extraction

C. Wiesmann, K. Bergenek, N. Linder, U. T. Schwarz,

This is the pre-peer reviewed version of the following article:
Laser & Photonics Review, Volume 3 Issue 3, 262-286 (2009)

This is the pre-peer reviewed version of the following article: Laser & Photonics Review, Volume 3 Issue 3, 262-286 (2009)

Photonic Crystal LEDs – Designing Light Extraction

Christopher Wiesmann[1a,b], *Krister Bergenek*[a], *Norbert Linder*[a], *and Ulrich T. Schwarz*[b]
[a]*Osram Opto Semiconductors GmbH, Leibnizstr. 4, 93055 Regensburg, Germany*
[b]*Department of Physics, University of Regensburg, 93040 Regensburg, Germany*

Abstract
Photonic Crystals (PhCs) have attracted much attention during the last decade as a solution to overcome the low extraction efficiency of as-grown light-emitting diodes (LEDs). In this review we describe the underlying physics and summarize recent results obtained with PhC LEDs. Here, the main focus is on diffracting PhC. In order to quantify the benefit from the incorporation of PhCs for diffracting light a comparison by simulations between a PhC LED and a standard state-of-the-art LED is carried out. Finally, the impact of the PhC on the LEDs emission characteristics will be discussed with respect to étendue-limited applications.

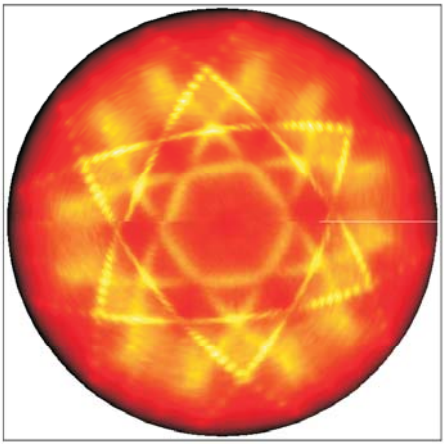

Azimuthal emission pattern of an InGaN/GaN LED with hexagonal PhC at a single wavelength

1. Introduction

From the very beginnings of light emitting diodes (LEDs) in the 1960's a continuous increase in their efficiency was achieved. Due to this enhancement LEDs were able to find their way into a wide field of applications ranging from their roots as indicators and display signs to high-performance applications like automotive head lamps or projection systems. Furthermore, owing to their efficiency, reliability, low power consumption and long lifetime LEDs are supposed to be the upcoming light source for general lighting [1]. One precondition for the introduction of LEDs into these new application areas was overcoming the low extraction efficiency of light from as-grown LEDs due to total internal reflection. In recent years numerous publications [2]-[24] investigated the application of photonic crystals (PhCs) for addressing this issue. Enhancements ranging from 1.5 [8][21] to 2.5 [9] compared to unstructured references reveal that PhCs have the potential to increase the extraction efficiency of LEDs. However, a commercial application of PhCs will additionally depend on the properties of state-of-the-art devices. First of all, the performance of PhC LEDs has to compete with standard LEDs already addressing the problem of total internal reflection, like volume emitters or thin-film LEDs. The latter almost reaches 80% extraction efficiency [26]. But also their manufacturing has to be as marketable as that of standard techniques. However, PhCs offer advantages beyond the pure extraction enhancement. Due to their periodicity it is possible to shape the emission profile of a LED [8]. This could be of great advantage for applications based on imaging or non-imaging optics as their overall efficiency is étendue

[1] christopher.wiesmann@osram-os.com; phone +49 941 850-3533; fax +49 941 850-1090; osram-os.com

In general, the benefits of PhC for LEDs stem from their influence on the dispersion relation of light, i.e. band-folding due to Bloch's theorem. However, due to technological limitations altering the dispersion of light within a PhC LED is restricted. In order to achieve reasonable electrical performance and homogeneous current distribution the epitaxial structure has to contain sufficient thick un-perforated current spreading layers. Thus, most PhC LEDs only incorporate shallow etched holes. In this case of weak PhCs the in general three dimensional problem can be separated into a 2D+1D problem. The two-dimensional part covers the lateral properties of the PhC and the one dimensional part consists of the vertical layer composition of the LED including the etch-depth of the PhC. This separation enables a clear insight into the mechanisms determining the extraction efficiency and gives a route for optimising PhC LEDs. Hence, we focus in this review on weak PhCs. The case of strongly coupled PhCs, i.e. PhCs etched vertically through the whole LED, has to be addressed separately. Here, the most popular property of PhCs, the photonic band-gap, has to be taken into account. But apart from the electrical issues a loss of active area equal to the area of holes has to be overcome.
Apart from enhancing the extraction efficiency of LEDs PhCs could also be incorporated into the LED as omni-directional mirrors for decreasing the absorption losses. Additionally, the use of metallic gratings in the vicinity of the LED's active region enables the use of surface plasmon polaritons for enhancing the efficiency of light generation.
In the upcoming section we will summarize briefly some basics on LEDs and discuss the problem of light extraction from unstructured LEDs along with traditional approaches to improve light extraction. These approaches are the benchmark for PhC LEDs. In section 3 first of all the influence of PhCs on the light propagation inside a LED will be investigated and from this the main mechanisms for enhancing the performance of LEDs will be derived.
Here, two regimes can be distinguished: the weakly and the strongly coupled PhC. Apart from the direct use of PhCs for light extraction its application as an omni-directional mirror will be summarized in section 6.1. In section 6.2 we will focus on the specific use of metallic PhCs in combination with surface plasmons for enhancing the internal quantum efficiency. In section 7 the most widely used patterning techniques will be briefly summarized for manufacturing of PhCs for the visible range of the spectrum. Thereafter, in section 8 a comparison between a state-of-the-art LED and a PhC LED will be carried out in order to investigate the potential of PhC LEDs by using three-dimensional finite-difference time-domain (FDTD) simulations [29]. Furthermore, a detailed investigation on the use of PhC LEDs in étendue-limited applications will be given in section 9.

2. LED's Basics

In general, LEDs cover the whole range of visible wavelengths. For the near-UV to green, Gallium-Nitride (GaN) based LEDs are used, where the emission wavelength is defined by the amount of Indium (In) content within the active region – the more In the longer the emission wavelength. For yellow up to the red emission the quaternary system $(Al_xGa_{1-x})_yIn_{1-y}P$ is common. The infrared part of the spectrum is opened by the $Al_xGa_{1-x}As$ system. But regardless of the emission wavelength, the overall power conversion efficiency or wall-plug efficiency of a LED is one of the most important properties and is given by emitted flux with respect to electrical input power, both quantities measured in Watts [W]. Four main loss mechanisms that cause heating of the LED determine its wall-plug efficiency

$$\eta_{wall} = \eta_{el} \cdot \underbrace{\eta_{inj} \cdot \eta_{IQE} \cdot \eta_{extr}}_{\eta_{EQE}}. \tag{1}$$

Here, η_{el} describes the electrical efficiency and the external quantum efficiency η_{EQE} is given by the product of the injection efficiency η_{inj}, the internal quantum efficiency η_{IQE} and the extraction efficiency η_{extr}.

The electrical efficiency η_{el} is determined by ohmic losses that come with applying voltage across the p-n-junction due to the resistance of the contacts and the epitaxial layers. For the nitrides losses due to piezoelectric barriers are included, too. The injection efficiency η_{inj} takes into account the efficiency of capturing the electrons and holes within the p-n-junction (the active region). The internal quantum efficiency η_{IQE} of photon generation from electron-hole-pairs depends on the ratio between the radiative recombination rate Λ_{rad} (a photon is generated in the active region) and the non-radiative recombination rates Λ_{nrad} (no photon is generated):

$$\eta_{IQE} = \frac{\Lambda_{rad}}{\Lambda_{rad} + \Lambda_{nrad}}. \tag{2}$$

For instance, non-radiative recombination can be caused by defects within the semiconductor, the so called Shockley-Read-Hall recombination [30][31], or by Auger recombination [32]. Finally, not every photon is emitted into the ambient medium but gets absorbed inside the LED (η_{extr}). Experimentally, the external quantum efficiency is defined by the number of emitted photons divided by the number of injected electrons and serves as an upper boundary for the extraction efficiency with the assumption of $\eta_{IQE}=\eta_{inj}=1$.

The internal quantum efficiency is mostly determined by the epitaxial quality and the electronic band engineering of the active region. Nevertheless, it is not an intrinsic property of the semiconductor but is related to the optical environment. Both the photon density of states and the local electromagnetic field amplitudes alter the radiative recombination rate – this is called the Purcell effect [33] – according to Fermi's Golden Rule

$$\Lambda_{rad}(\omega, \mathbf{r}) = \frac{2\pi}{\hbar} \left\langle \boldsymbol{d} \cdot \boldsymbol{E}(\mathbf{r}) \right\rangle^2 \rho(\omega) \tag{3}$$

with **d** the electric dipole of the electron-hole-transition, **E**(**r**) the local electric field strength and $\rho(\omega)$ the local density of photon states. Due to the dispersion relation of light $\omega(\mathbf{k})$ the radiative recombination rate is consequently dependent on the propagation direction of light. As we will see during this review, both the extraction efficiency and the internal quantum efficiency can be affected by photonic crystals.

The main limitation for an as-grown LED comes from the low extraction efficiency due to the high refractive index of the semiconductor (n_{SC}=2.5-3.5) relative to the ambient medium (typ. air with n_{amb}=1). With Snell's law ($n_{SC}\sin\theta_{SC}=n_{amb}\sin\theta_{amb}$) in mind, only light with incident angle smaller than the critical angle $\theta_{SC}<\theta_c=\text{asin}(n_{amb}/n_{SC})$ can radiate into the ambient medium, whereas the remaining light is total internally reflected and never escapes from the structure as depicted in Fig. 1. Snell's law is equivalent to the conservation of the in-plane k-vector length β at the interface as can be seen by multiplying with the vacuum k-vector length $k_0=2\pi/\lambda_0$. Therefore, only light with in-plane k-vector smaller than $\beta<k_0 n_{SC}\sin\theta_c=n_{amb}k_0$ can radiate into the ambient medium. Light with $\beta>n_{amb}k_0$ is called evanescent in the ambient medium as the corresponding angle θ_{amb} is imaginary. The in-plane k-vector is related to the total k-vector k by $k^2=(nk_0)^2=\beta^2+\gamma^2$, with γ the k-vector component perpendicular to β.

For an isotropic light source integrating over all possible directions while neglecting losses due to Fresnel reflection at the boundary (i.e. perfect anti-reflection coating)

$$\eta_{extr} = \frac{1}{2}\int_0^{\theta_c} \sin\theta d\theta \quad (4)$$

reveals an extraction efficiency of typically 2% for AlGaAs/AlGaInP material systems with n_{SC}=3.5 and 4% for GaN based ones with n_{SC}=2.5 to air (in the following the ambient medium will be assumed as air, n_{amb}=1). So even with 100% internal quantum efficiency the external quantum efficiency of the LED is limited to 4% in the best case. An early idea for enhancing the extraction efficiency is to encapsulate the LED with a high index hemispherical dome [34]. In order to obtain a large critical angle the encapsulation should be index matched to the semiconductor. In commercial devices silicon is widely used with a refractive index of n≈1.5 as it is easy to process and remains transparent over the life-time of the LED. But still 90% for the nitrides and 95% for the arsenides/phosphids of the generated light are trapped within the semiconductor.

Another way for enhancing the extraction efficiency uses five of the six facets of the LED chip for extracting light, as shown in Fig. 2a). For achieving reasonable efficiencies, highly transparent substrates or window layers have to be used in order to avoid absorption losses. Thus, it is possible to obtain 10% and 20% extraction efficiency to air, respectively. The limitation of the extraction efficiency in this case stems from the rectangular cross-section of the LED. Hence, the total internally reflected light cannot change its incident angle upon any of the facets. Therefore, additionally tilting the angle between these facets enables high extraction efficiencies, e.g. of up to 50% for GaN-based LEDs [35] and 55% for AlGaInP LEDs [36], as rays total internally reflected at one facet have the chance to escape from the LED at another facet as the incident angle is changed; see Fig. 2b). However, the overall size of these LEDs is limited as only the facets redistribute the light and the extraction competes with the absorption losses within the chip. Furthermore, in this set-up the light output is spread over the whole chip surface implying a volume-emitting LED along with strong side-emission. Therefore, special packaging has to redirect the light into the forward direction.

Another way to break the paths of the light is by incorporating a scattering mechanism on top of the LED like the rough surface shown in Fig. 2c) [37][38]. This has two advantages: light can escape partially from the structure more or less independent of its incident angle due to scattering at the rough surface and the reflected light gets redistributed (similar effect to the tilted facets). With the incorporation of a mirror at the opposite side of the LED the reflected light has several chances to escape from the LED through one single facet after hitting the mirror. These so-called thin-film LEDs are processed by bonding a second substrate, for instance Ge, Si or GaAs, on top of the last epitaxial layer. Between the two a metallization like Au, Ag or Al forms the mirror. The removal of the primary substrate is accomplished by either wet-etching in the AlGaInP/AlGaAs material system [39] or laser lift-off in the GaN material system [40][41]. Thin-film LEDs have shown high extraction efficiencies of 75-80% for blue GaN-based LEDs [25][26] and 50% external efficiency for AlGaInP [42]. Both values are obtained from encapsulated chips. Secondly, this efficiently generates a surface emitting LED rather than a volume emitting with an increased radiant emittance. The radiant emittance describes the power per area [W/m²] emitted from the LED's surface. A further advantage especially of interest for projection applications – where large chip areas are favourable – is the scalability of surface emitters [43]. Besides surface roughening there are some additional solutions for scattering the light internally, like patterned substrates [44] or buried micro-reflectors [43].

In general, the extraction mechanisms have to compete with absorption losses within the epitaxial layers, at the mirror, or at the contacts. Thus the extraction efficiency reads

$$\eta_{extr} = \frac{\kappa}{\kappa + \alpha} \tag{5}$$

with κ the extraction coefficient due to the extraction mechanism and α the absorption coefficient. Any redistribution of internal propagating light, either surface texturing or tilted facets, results in 100% extraction efficiency in the limit of vanishing absorption. Therefore, the route to high-performance LEDs is to reduce the absorption within the LED to a negligible amount while simultaneously pulling the light out of the LED as fast as possible (see Fig. 3).
Apart from these redistribution techniques, in resonant-cavity LEDs (RCLEDs) [45]-[47] as much light as possible is generated internally within the extraction cone by means of interference in order to obtain high extraction efficiencies, as sketched in Fig. 2d). The vertical cavity of the LED is tailored in a way that the radiative recombination rate according to Eq. (3) is increased within the extraction cone and decreased for the trapped light. The formation of the interferences is typically achieved by embedding the active layer between two mirrors (metallic mirrors, Bragg reflectors, or just the semiconductor-to-air interface). With this set-up extraction efficiencies of 22% (GaN material system) [48], 23% (AlGaInP material system and encapsulated) [49], and 30% (AlGaAs material system) [50] have been demonstrated. But as the layer composition of RCLEDs is optimised for a specific emission spectrum of the active layer, their performance is heavily temperature dependent [51]. Typically, with increasing temperature the emission of semiconductor based active layers tends to shift to longer wavelengths (due to a decreased electronic band-gap) causing a temperature dependent mismatch between the emission and the surrounding cavity. For the nitrides the wavelength shifts to shorter wavelength with increasing current density due to screening of the piezo-electric fields.

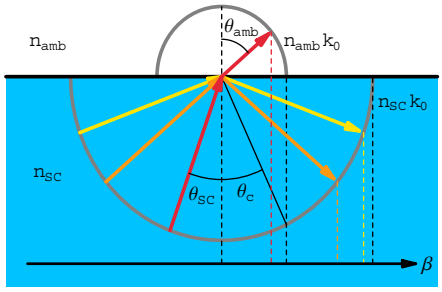

Fig. 1: Only light within a narrow escape cone of $\theta_{SC}<\theta_c$ can radiate from the semiconductor to the ambient medium. Along with the different k-vectors also their projection on the plane parallel to the interface ($\beta=n_{SC}k_0\sin\theta_{SC}$) is illustrated.

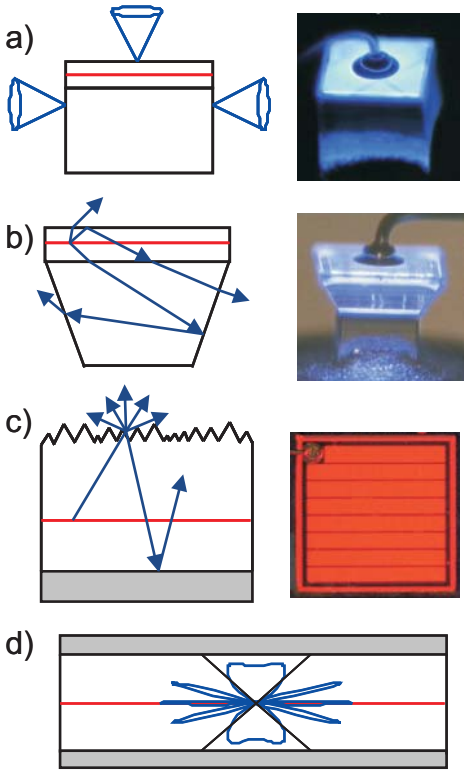

Fig. 2: Summary of standard LED set-ups for overcoming the low extraction efficiency along with images of real devices under operation. a) Five facets of the chip contribute to the extraction of light. The image shows a GaN-based LED grown on SiC-substrate. b) A further improvement of a) with tilted angles. The image is taken from a GaN-based LED grown on sapphire substrate. c) A typical set-up of a thin-film LED with a rough surface and back-mirror (gray area). The image shows a red-emitting AlGaInP thin-film LED. The bars for current injection are visible as horizontal black lines. d) Schematic illustration of the altered internal emission due to the mirrors of a RCLED. The extraction cone is depicted by the straight black lines.

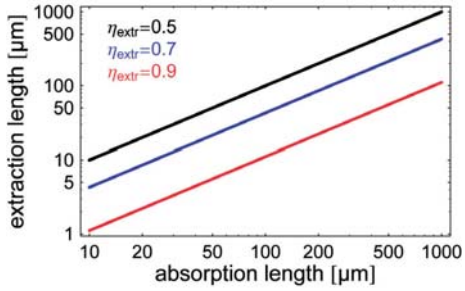

Fig. 3: Required extraction length $1/\kappa$ as a function of the absorption length $1/\alpha$ in order to achieve 50% (black), 70% (blue) or 90% (red) extraction efficiency.

3. Photonic Crystals

A PhC[2] in general is a one-, two-, or three-dimensional periodic arrangement of materials with different refractive index, where the characteristic length scale is in the order of the wavelength. Therefore, similar to the electronic bands in quantum mechanics that are generated by the periodic potential offered by the atoms in a crystal, a periodic refractive index alters the propagation behaviour of photons in a photonic crystal. The propagation properties of photons within any system are summarized by its dispersion relation $\omega(\mathbf{k})$ relating the allowed photon energies to the corresponding propagation directions. In free space the dispersion relation simply reads $\omega=k_0c$. In Fig. 4a) this so called light line for free space propagation (steep black line) is plotted as a function of the in-plane k-vector length β.

[2] For a more detailed description of PhCs the reader is referred to [52]-[55].

This is convenient for systems with either continuous or discrete translational invariance in the lateral directions[3] x and y. According to Fig. 1 light with a given frequency and in-plane k-vector $\beta<k_0$ is able to propagate in air. For instance, the part of the dashed horizontal line in Fig. 4a) left to the intersection with the light line contains all propagating states at the reduced frequency $\omega a/2\pi c=0.55$, where a is some characteristic length defined later. In contrast to this, light with $\beta>k_0$ is evanescent in air but propagating inside the semiconductor as long as $\beta<n_{SC}k_0$. This second boundary is given by the semiconductor light line $\omega=k_0c/n_{SC}$. Light with $\beta>n_{SC}k_0$ is evanescent in the semiconductor, therefore non-propagating, and is not taken into account. This is valid as long as there is no material with higher refractive index present or material supporting surface modes like surface plasmons.

In the case of a semi-infinite air slab on top of a semi-infinite semiconductor slab an infinite number of states with $k_0<\beta<n_{SC}k_0$ exist. By truncating the semiconductor slab to a finite thickness and introducing a material with lower refractive index, e.g. air, at the bottom, only a discrete number of states are allowed depending on the thickness and the refractive index of the slab. This is similar to the finite number of allowed electronic states in a potential well of finite depth. The dispersion of these so called guided modes is shown in Fig. 4a) for TE-polarized light (electric field parallel to the x-y-plane also often referred to as p-polarization). The solution for this symmetric slab is given for example in [56], and a general solution for an arbitrary structure can be found in [57]. At this point the reader should keep in mind that in such a vertical layer stack a guided mode with in-plane k-vector β consists of an infinite number of modes propagating with different in-plane directions $\boldsymbol{\beta}/\beta$ due the homogeneity of the slab in x and y direction. But for convenience this degenerate set of modes is referred to as a single mode.

After these general remarks on dispersion relations, let's introduce a periodicity offered by a PhC. For the sake of simplicity, we first deal with an artificial hexagonal lattice with lattice constant a; no refractive index contrast defines the periodicity. The resulting dispersion relation is often referred to as free-photon dispersion. According to Bloch's theorem the modes of the slab are folded at the edges of the first Brillouin zone (BZ). Typically, in a dispersion relation only k-vectors along the edges of the irreducible BZ are considered representing the main directions of the lattice. The formation of the different bands is simply derived from the dispersion of the un-corrugated slab and the geometrical consideration as shown in Fig. 4c. Starting from $\omega=0$ the dispersion for the corrugated slab is equal to that of the un-corrugated slab as the first BZ encloses the mode's circle in k-space. As soon as the in-plane k-vector of the mode is larger than the first BZ, e.g. the dashed blue circle around (0,0) in Fig. 4c), circles from the neighbouring BZ enter the first one. Due to Bloch's theorem these are equivalent to the mode starting from (0,0). In the dispersion relation for the corrugated slab the evolution of the intersections of the different mode circles with the irreducible BZ edges are drawn. Now, the formerly guided mode lies above the light-line for reduced frequencies $\omega a/2\pi c>0.38$. Therefore, the periodicity enables this mode to be radiative in the ambient medium and extracts guided light. An equivalent description of the process is given by Bragg's Law of diffraction $\boldsymbol{\beta}_d=\boldsymbol{\beta}_i+\mathbf{G}$, where the sum of the incident k-vector $\boldsymbol{\beta}_i$ and a reciprocal lattice vector $\mathbf{G}$ yields the diffracted k-vector $\boldsymbol{\beta}_d$. The reciprocal lattice vectors $\mathbf{G}$ can be derived analytically or by Fourier transformation of the real lattice. As soon as $\beta_d<k_0$ some parts of the mode with in-plane k-vector $\boldsymbol{\beta}_i$ are diffracted into air.

[3] Please note the axes labelling. As Maxwell's equations are invariant under scaling – there is no fundamental length scale like Bohr's radius in quantum-mechanics – it is convenient to use the reduced frequency $\omega L/2\pi c=L/\lambda_0$ and the reduced k-vector $kL/2\pi$ with L a characteristic length of the system. Therefore, photons with wavelength λ_1 propagating in a system 1 with a characteristic length L_1 behave exactly the same way as photons with λ_2 in a system 2 with L_2 as long as $L_1/\lambda_1=L_2/\lambda_2$. But as the characteristic length is an arbitrary choice all spatial dimensions in both systems have to satisfy the above equation. Typically, in the case of PhCs the pitch a of the lattice is used as the characteristic length L, i.e. $L=a$.

The dispersion within the extraction cone is directly accessible from the spectrally and angle resolved measurement of emitted light of a PhC LED [11]. The folding of the guided modes due to the hexagonal PhC results for a single frequency in a Star-of-David-shaped pattern, as shown in the title figure. This pattern directly reflects the dispersion around the Γ point, as seen in Fig. 4c). The measurement was performed on a GaN-based LED with ~1µm thickness including a more than 400nm deep PhC with 274 nm pitch and an ITO cover layer. The diffracted mode corresponds to an in-plane k-vector length of $\beta_i \approx 2.4 k_0$.

Recapitulating the basics of band-gaps for electrons in solid state physics, the two degenerate photonic states at e.g. the M-point do have the same periodicity but their field profiles are shifted by half of the lattice constant. A refractive index contrast as depicted in Fig. 5 for a one-dimensional grating lifts the degeneracy as the modes "see" different refractive indices. The mode mainly located within the high-index material has lower frequency. The corresponding band is often called the dielectric band (as the high-index material is typically a dielectric), whereas the band related to the mode mainly located in the low-index material (having higher frequency) is referred to as the air band.

An intuitive interpretation of this degeneracy-lift and the associated shift in frequency is given in [58]. Consider for instance a material with refractive index n that is perturbed in some regions with a refractive index shift Δn. The associated shift in frequency can be estimated in first order to be

$$\frac{\Delta\omega}{\omega} = -\frac{\Delta n}{n} \cdot \left(\text{fraction of } \int n^2 |E|^2 \text{ in perturbed regions} \right) \tag{6}$$

with E the electric field amplitude of the modes and ω the frequency. This shift causes band-bending at the symmetry points resulting in a band-gap. Therefore, propagation of photons at this frequency and the corresponding k-vector is inhibited. If the propagation is inhibited for k-vectors in all directions, a complete band-gap arises. Additionally to the band-gap, the band-bending causes a change of the photonic density of states as the number of available k-vectors within a given frequency range is altered. As a consequence of Eq. (3) the spontaneous emission is enhanced for certain frequencies and directions and suppressed for others.

As long as either the index shift is small or the depth of the PhC's holes is small compared to the slab's thickness, the band-bending effects can be neglected as the frequency shift is tiny and the formation of the dispersion relation as shown in Fig. 4b) is still valid. Hence, from Eq. (6) naturally two extremes of PhC LEDs can be distinguished:

a) The PhC is a perturbation of the LED and acts as a diffraction grating but does not alter the photonic density of states. This is valid in most PhC LEDs and we mainly remain with our treatment of PhCs in this limit.
b) The PhC introduces a large modulation into the LED and band-bending effects cannot be neglected. Therefore, the density of photonic states can be altered drastically and band-gaps play an important role. This will be discussed in section 5.

In general, a PhC LED is a three-dimensional problem requiring the solution of Maxwell's equations fully vectorial in three dimensions due to the feature size of the PhC. Here, the FDTD method [29] is widely used. To achieve reliable results, the dimension of the simulated volume has to be of the order of the third power of extraction or absorption length, resulting in a tremendous demand on computational resources. For the huge parameter space of PhC LEDs – covering different material systems, the vertical layer composition, the PhC lattice itself etc. – a general optimisation procedure is hardly obtainable. On the other hand, methods like scattering matrix algorithms [18][59][60] taking advantage of the periodicity of the PhC are more suitable for the solution of PhC LEDs but are restricted to periodical systems. Nevertheless, these methods enable a clear insight into the mechanisms of arbitrary PhC LED

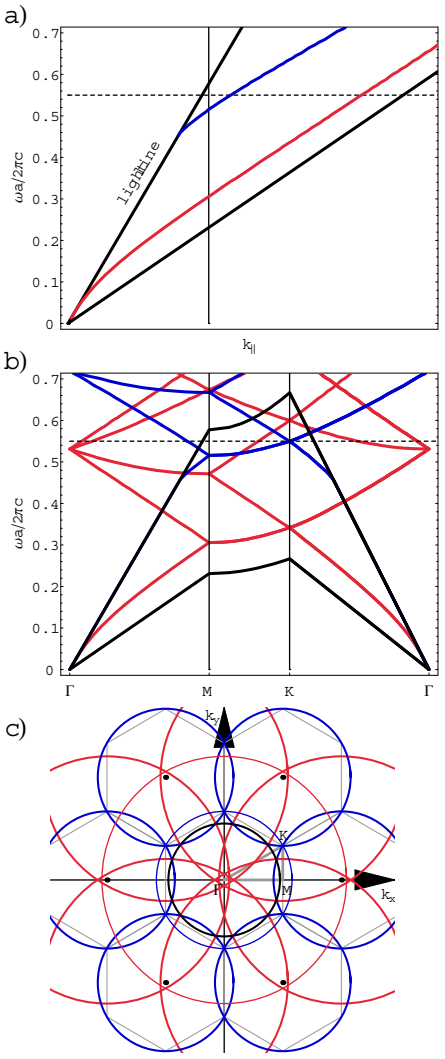

Fig. 4: a) Dispersion of the two fundamental TE-modes for a slab of thickness 0.5*a*, with *a* an arbitrary length within the system and the slab's refractive index of *n*=2.5. The steep black line illustrates the light line and the second less steep line the semiconductor light line. The dispersion of the fundamental TE-polarized guided mode and the following higher order mode are shown in red and blue, respectively. The horizontal dashed line at $\omega a/2\pi c$=0.55 corresponds to the k_x-k_y-diagram shown in c). The straight vertical line depicts the edge of the 1. BZ in ΓM direction of the hexagonal lattice used in b). b) Dispersion relation of the slab in a) with a hexagonal lattice with lattice constant *a* in the limit of infinitely weak perturbation. c) Illustration of the folding according to Bloch's theorem for the frequency corresponding to the dashed horizontal line in a) and b). The red and blue circles have radius equal to the in-plane k-vector obtained from a) and the centres are located at the reciprocal lattice points (black dots). The thin gray lines indicate the BZs and the thick gray lines enclose the irreducible BZ with the symmetry points Γ, M and K. The evolution of the intersection of the red and blue circles with the edges of the irreducible BZ gives the dispersion relation as shown in b). The black circle represents the light line and encloses the extraction cone.

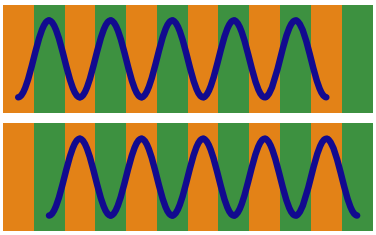

Fig. 5: Intensity profiles of two modes at the BZ edge in the case of an one-dimensional grating. When the refractive indices of the green and orange regions are different the degeneracy at the BZ edge is lifted.

4. Weak Photonic Crystals – Diffraction of Light

A general set-up for this regime is shown in Fig. 6 for two cases, a thin-film LED with a back-mirror and a LED with transparent substrate. The PhC is typically etched into the top-surface of the LED. Certainly, the PhC can be positioned arbitrarily within the vertical LED stack as long as it is technological feasible [16][19]. In any case the generated light can either escape from the structure directly without the help of the PhC (roughly 2-4% depending on the refractive index of the semiconductor) or gets diffracted by the PhC according to Fig. 4c. As soon as the bands of guided modes are folded above the light line they are accessible by measuring the farfield of the PhC LED [11]. Hence, it is possible to prove the operating regime of the PhC LED, whether the PhC is weak or not. Fig. 7 shows a spectrally resolved farfield of a PhC LED [23] with the in-plane k-vector $\beta=k_0\sin\theta_{air}$ as the x-coordinate instead of the farfield angle θ_{air}. The four lines intersecting the y-axis at $\omega a/2\pi c=0.485$ agree with the dispersion relation close to the dashed line in Fig. 4b). In both cases the bands stem from folding of a single guided mode. The next higher order branches intersect with the y-axis at $\omega a/2\pi c=0.515$. As band bending or splitting at the Γ-point is hardly observed, the PhC can be considered weak and the dispersion is related to the band folding of the free photon dispersion as shown in Fig. 4 (see also [12]). Also in the azimuthal farfield as shown in the abstract figure no local band-gaps appear, but the Star-of-David-shaped diffraction pattern similar to Fig. 4c).

After the operation principle of this regime – diffraction – has been proven, the question arises, what LED structure and what PhC lattice should be chosen in order to obtain as much extraction as possible. As the weak PhC can be handled as a perturbation, we can separate the whole 3D problem into a 2D+1D problem that facilitates the interpretation. The two-dimensional part is represented by the two-dimensional PhC and describes the diffraction process. Here, the parameters of the PhC, i.e. the lattice type, the lattice constant and the filling fraction, have to be taken into account. In contrast, the one-dimensional part arises from the vertical layer stack of the LED and contains the etch-depth of the PhC. The two-dimensional and the one-dimensional part are coupled to each other by the filling fraction F of the PhC. For the one-dimensional calculation the effective refractive index of the PhC is approximated by $n_{PhC}^2 = Fn_{amb}^2 + (1-F)n_{SC}^2$.

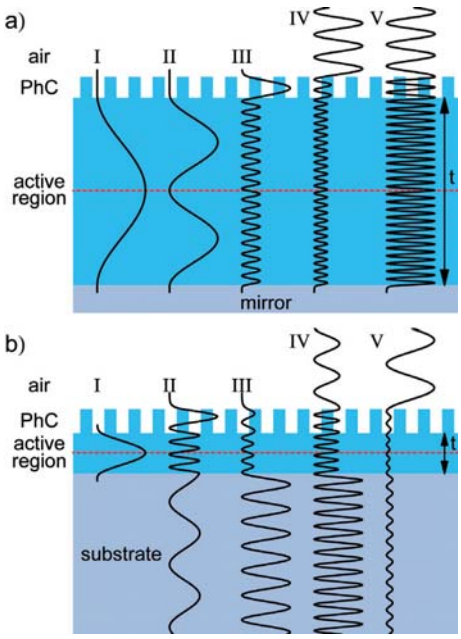

Fig. 6: Schematic for a general PhC LED in the case of diffraction. a) Thin-film LED with back-mirror; b) LED with transparent substrate. The intensity profiles (black curves) of the different modes will be discussed in section 4.2. The un-etched core thickness is *t*.

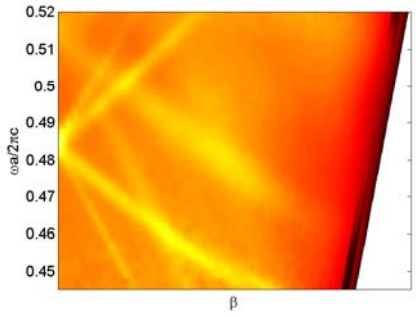

Fig. 7: Dispersion relation measured in ΓM direction of a hexagonal lattice PhC LED [11]. Data taken from [23]. The four lines crossing at $\omega a/2\pi c$=0.485 stem from diffraction of the same guided mode as sketched in Fig. 4b).

4.1. 2D Part: Lattice Type, Pitch and Filling Fraction

As band-bending effects can be neglected, only Bragg's law of diffraction $\boldsymbol{\beta}_d=\boldsymbol{\beta}_i+\mathbf{G}$ determines whether a guided mode with in-plane k-vector length $\beta_i>k_0$ gets folded above the light line by a reciprocal lattice vector **G**. In the following paragraphs, we will investigate properties of the PhC that have an impact on the diffraction process, like the pitch itself, the lattice type, the photonic strength of the lattice and the filling fraction. For the illustration of the diffraction process we will use a basic geometrical consideration as depicted in Fig. 8. Here, all resulting k-vectors $\boldsymbol{\beta}_d$ from diffraction of all guided modes of the degenerate set with in-plane k-vector length β_i by two different reciprocal lattice vector lengths G_1 and G_2 are depicted.

Apparently, the length of the reciprocal lattice vector determines whether a guided mode gets diffracted above the light line or not. As soon as $\beta_i-G<k_0$ an arc with half-angle φ of the blue circle lies within the extraction cone with radius k_0 and some part of the formerly guided mode gets extracted. The length $2\varphi\beta_i$ of this arc corresponds to the fraction of different in-plane direction $\boldsymbol{\beta}_i/\beta_i$ that gets diffracted to air. In order to extract as much in-plane directions as possible the reciprocal lattice vector should be chosen around $G\approx\beta_i$. In Fig. 9 the fraction of the in-plane directions diffracted to air with respect to all in-plane directions is shown as a function of the in-plane k-vector length β_i and assuming $G=\beta_i$. For small in-plane k-vector

lengths $\beta_i \approx k_0$ the arc within the extraction disk is almost one third of the circumference. In contrast, for the largest in-plane k-vector possible within the AlInGaP-material system, i.e. $\beta_i \approx 3.5k_0$, the fraction drops to only 9%.

Depending on the lattice type additional reciprocal lattice vectors are present with the same length $|\mathbf{G}|=G$ but different directions. For instance, a hexagonal lattice as shown in Fig. 10a) offers six reciprocal lattice vectors with length equal to the main reciprocal lattice vector length G_0. Thus, a larger fraction of the different in-plane directions of a guided mode can be diffracted to air. Assuming that these reciprocal lattice vectors are evenly distributed on a circle with radius G, Fig. 9 also shows the minimum number of reciprocal lattice vectors required for extracting all in-plane directions of the guided mode. Hence, all in-plane directions of guided modes with $k_0<\beta_i<1.9k_0$ can be extracted by the six main reciprocal lattice vectors of a hexagonal lattice. In contrast, for diffraction of guided modes with $\beta_i>1.9k_0$ a higher number of reciprocal lattice vectors with almost the same length is necessary. In the case of a hexagonal lattice higher order diffraction processes, i.e. diffraction by $G=\sqrt{3}\,G_0$ along with $G=2G_0$, can be used but as we will see later, diffraction by higher order processes is less efficient compared to diffraction by $G=G_0$.

To address the issue for large in-plane k-vectors, lattices with higher symmetry have been suggested, like Archimedean tilings [7], which are especially of interest for AlGaInP or AlGaAs based LEDs as their refractive index is rather high ($n_{SC}\approx 3.5$). The omni-directional diffraction properties of Archimedean lattices have been proven experimentally in [13] by measuring the dispersion above the light line. In order to investigate the properties of these lattices, hexagonal lattices with 1 atom per unit cell (the traditional hexagonal lattice), 7 atoms per unit cell (Archimedean tiling referred to as A7) and 13 atoms per unit cell (Archimedean tiling referred to as A13) along with their Fourier transform are shown in Fig. 10. For the hexagonal lattice the length of the main reciprocal lattice vector is $G_0=4\pi/3^{1/2}a$ with the pitch a; for the Archimedean tilings $G_0\approx 2\pi/a$. The lattices A7 and A13 offer twelve main reciprocal lattice vectors and therefore, extract all in-plane directions of guided modes with in-plane k-vector length of up to $3.8k_0$ according to Fig. 9. But apart from a more ring-like Fourier transform a significant reduction of the main Fourier peaks is observed for the A7 and A13 lattices. Therefore, one might expect that the extraction length of a specific guided mode $\boldsymbol{\beta}_i$ is increased as the index contrast is reduced. For convenience, we only compare the hexagonal lattice with the A13. The A7 was proven to yield almost the same results as the A13 tiling.

In order to take this effect into account we introduce an extraction coefficient κ that is proportional to the squared modulus of the amplitude of the Fourier transform of the lattice, $|\Delta\tilde{\varepsilon}_{\mathbf{G}}|^2$, [17][18] as a measure for the photonic strength of the lattice

$$\kappa(\boldsymbol{\beta}_i,\mathbf{G}) \propto \begin{cases} |\Delta\tilde{\varepsilon}_{\mathbf{G}}|^2 & \text{if } |\boldsymbol{\beta}_i-\mathbf{G}|<k_0 \\ 0 & \text{else} \end{cases}. \tag{7}$$

If the diffracted k-vector length $|\boldsymbol{\beta}_d|=|\boldsymbol{\beta}_i-\mathbf{G}|>k_0$ the extraction coefficient is zero. We further assume that diffraction of light from the extraction cone back to guided modes can be neglected as the confinement within the vertical cavity is weak. Therefore, light within the extraction cone gets extracted more rapidly than back-diffracted. In Fig. 11 the total extraction coefficient κ_{tot} of the whole guided mode is shown. To calculate κ_{tot}, all in-plane directions are taken into account by weighting each $|\Delta\tilde{\varepsilon}_{\mathbf{G}}|^2$ with the arc length $2\varphi\beta_i$ within the extraction cone. This length depends on the in-plane k-vector and the reciprocal lattice vector length, see Fig. 8. As a guided mode might be diffracted by more than one reciprocal lattice vector into the extraction disk, the whole Fourier transform of the lattices is considered by summation over all reciprocal lattice vectors.

$$\kappa_{tot}(\beta_i) \propto 2\beta_i \sum_G \varphi(\beta_i, G) \left|\Delta\tilde{\varepsilon}_{\mathbf{G}}\right|^2 \tag{8}$$

Thus, we take into account both, the photonic strength of the lattices and the in-plane diffraction behaviour.

Before focusing on the comparison between the different lattices, let's briefly investigate the main characteristics of the extraction coefficient in Fig. 11 for the hexagonal lattice. In the case of the guided mode with in-plane k-vector β_i=2.4k_0 diffraction to air by G_0<1.4k_0 only takes place by high order diffraction processes, i.e. diffraction by $G=\sqrt{3}\,G_0$, $2G_0$, $3G_0$ etc., as $|\boldsymbol{\beta}_d|=|\boldsymbol{\beta}_i-\mathbf{G}|<k_0$ only if $|\mathbf{G}|>G_0$. As the corresponding Fourier intensities are low, the extraction coefficient is small in this regime. The guided mode is significantly diffracted to air as soon as $|\boldsymbol{\beta}_d|=|\boldsymbol{\beta}_i-\mathbf{G}|<k_0$ for $|\mathbf{G}|=G_0$. Here, light gets diffracted by the main reciprocal lattice vectors having highest Fourier intensity. The optimum main reciprocal lattice vector is slightly smaller than β_i ($G_0\approx 2.1k_0$) as the fraction of in-plane directions extracted is maximized in this case. As soon as $G_0>\beta_i+k_0$, diffraction into the extraction disk is not possible because the hexagonal lattice supports no reciprocal lattice vectors with $|\mathbf{G}|<G_0$. The calculations for β_i=1.3k_0 in general show the same dependency except that also high order diffraction processes result in diffracted k-vectors with $\beta_d<k_0$ as the optimum main reciprocal lattice vector is $G_0\approx 0.7k_0$. Thus, small in-plane k-vectors get diffracted more efficient compared to longer ones.

From the reduced Fourier intensities of the A13 lattice compared to the hexagonal lattice a decreased extraction coefficient is observed despite the more omni-directional diffraction behaviour of the Archimedean tilings. But nevertheless almost the same amount of flux gets coupled out of the guided mode after some propagation distance. However, according to Fig. 9 the hexagonal lattice can only diffract 80% (56%) of the in-plane directions of the guided mode with β_i=2.4k_0 (β_i=3.4k_0) to air. Therefore, it empties these parts of the modes very rapidly while remaining the other parts unchanged. This light can only be recovered by diffraction processes between guided modes. But during this internal redistribution of light it is subject to absorption losses. In contrast, the higher symmetry of the Archimedean lattices enables direct extraction of the light as every in-plane direction gets diffracted to air.

Hence, three different regimes can be distinguished. If the absorption length resulting from the absorption present in the structure is comparable to the extraction length due to diffraction, the hexagonal lattice diffracts more light to air as the Archimedean lattices owing to its higher Fourier intensities. Especially guided modes are extracted faster by a hexagonal lattice, that are diffracted only by $|\mathbf{G}|=G_0$ into the extraction disk. If additionally higher order diffraction processes contribute to the extraction of a guided mode, both lattices perform equally. For systems with decreased absorption the Archimedean lattices can extract more light due to their omni-directionality regardless of the Fourier intensities. In the limit of vanishing absorption the gap in extraction between the hexagonal lattice and the Archimedean lattices decreases as the redistribution process is less prone to absorption.

The last parameter of this section – the filling fraction F of the lattice – determines the photonic strength and is easily optimised by calculating first the Fourier transform of the lattice and then using Eq. (8) to get the total extraction coefficient. Fig. 12a) shows the extraction coefficient κ_{tot} as a function of the filling fraction for the hexagonal lattice and the A13 tiling. In both limits $F \to 0$ and $F \to 1$ the PhC vanishes and the modes are not diffracted. Here, the main reciprocal lattice vector was chosen to yield maximum diffraction per length according to Fig. 11. The optimum filling fraction depends on the guided mode being extracted. If higher order diffraction processes do not result in diffraction within the extraction disk only the main reciprocal lattice vectors $G=G_0$ contribute to the diffraction process. According to Fig. 12b) these have maximum intensity for F=0.4. Please keep in mind, that the longer the in-plane k-vector of the guided mode being diffracted the longer the

optimum reciprocal lattice vector and consequently fewer high order diffraction processes result in diffracted k-vectors $\beta_d<k_0$. Thus, in the case of diffraction within the extraction disk by high order diffraction processes their Fourier intensity has also to be taken into account. The resulting summed Fourier intensity is maximum for F=0.5.

In summary, the optimum PhC lattice type depends on the in-plane k-vector length β_i of the guided mode that should get diffracted and on the losses present in the LED under study. In general, the larger the in-plane k-vector length, the higher the required number of reciprocal lattice vectors with the same length in order to diffract every in-plane direction of the guided mode. These reciprocal lattice vectors **G** should have the highest Fourier peaks $|\Delta\tilde{\varepsilon}_{\mathbf{G}}|^2$ of the PhC and length $G\approx\beta_i$. However, the need for higher symmetry lattices depends on the absorption losses. Maximized diffraction efficiency is achieved with a filling fraction of the lattices around $F\approx$0.45.

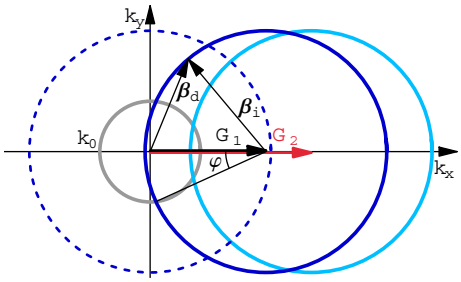

Fig. 8: Geometrical derivation of all diffraction processes according to Bragg's law of diffraction $\boldsymbol{\beta}_d=\boldsymbol{\beta}_i+\mathbf{G}$. The dashed blue line is a reminder of the guided mode with in-plane k-vector length β_i that gets diffracted. The dark blue (light blue) line depicts all diffraction processes from $\boldsymbol{\beta}_d=\boldsymbol{\beta}_i+\mathbf{G}_1$ ($\boldsymbol{\beta}_d=\boldsymbol{\beta}_i+\mathbf{G}_2$). The initial k-vector length β_i was chosen to be larger than k_0 (gray circle).

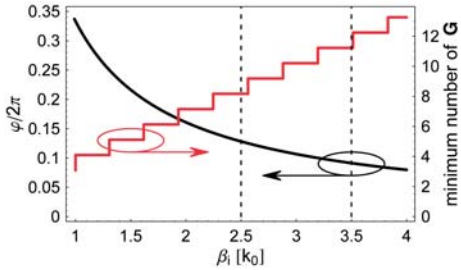

Fig. 9: Fraction of the in-plane directions diffracted to air (black) as a function of the in-plane k-vector. From a basic geometrical consideration the fraction of the guided mode diffracted to air by a reciprocal lattice vector **G** is given by $2\varphi/360°$ with $\cos\varphi=1-1/(2\beta_i^2/k_0^2)$ and $G=\beta_i$. In red the minimum number of reciprocal lattice vectors with length G is shown for extracting all in-plane directions to air. Here, it has been assumed that all **G** are homogenously spaced on a circle with radius G. The dashed vertical line at $\beta_i=2.5k_0$ ($3.5k_0$) indicates the maximum in-plane k-vector for GaN (AlGaInP or AlGaAs).

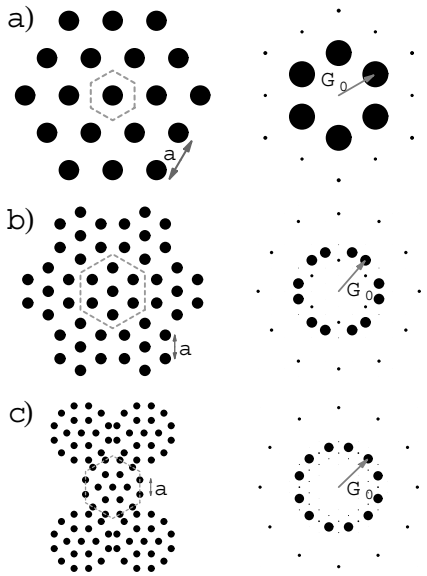

Fig. 10: Hexagonal lattices with a) 1 atom per unit cell (common hexagonal lattice) b) 7 atoms per unit cell (Archimedean tiling A7) and c) 13 atoms per unit cell (Archimedean tiling A13) with the corresponding Fourier transform. The diameter of the discs in the Fourier transform represents the amplitudes' squared modulus of the corresponding reciprocal lattice vector G. G_0 is referred to as the main reciprocal lattice vector length. In the case of the hexagonal lattice, G_0 is equal to the length of the primitive reciprocal lattice vectors.

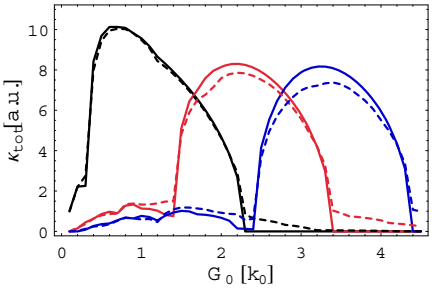

Fig. 11: Total extraction coefficient κ_{tot} as a function of the reciprocal lattice vector length of the main Fourier peak. The air filling fraction of the PhC is F=0.4. Black/red/blue lines correspond to guided modes with in-plane k-vector length β_i=1.3k_0, β_i=2.4k_0 (e.g. a highly guided mode in the GaN system) and β_i=3.4k_0 (AlGaInP or AlGaAs). The straight/dashed line corresponds to a hexagonal/A13 lattice. The A7 lattice shows nearly the same dependency as the A13 and is left out for clarity.

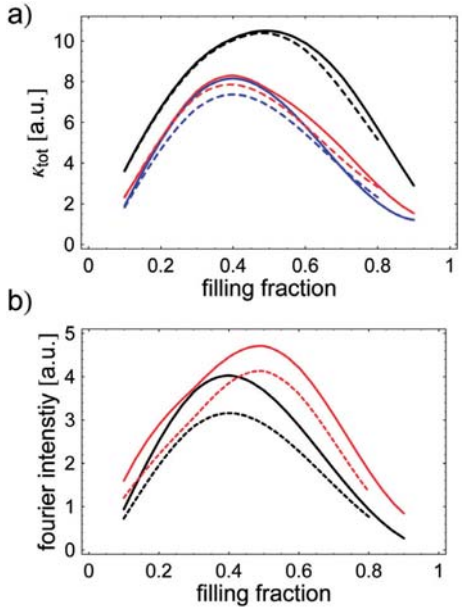

Fig. 12: a) Total extraction coefficient as a function of the filling fraction for the hexagonal (straight line) lattice and the A13 (dashed line). Black/red/blue lines correspond to guided modes with in-plane k-vector length β_i=1.3k_0, β_i=2.4k_0 and β_i=3.4k_0. The reciprocal lattice has been adjusted for maximum diffraction in each case. b) Sum over the Fourier intensities of all reciprocal lattice vectors with length G=G_0 (black) and $G\leq 2G_0$ (red) as a function of the filling fraction of the PhC.

4.2. 1D part: Vertical Layer Stack and Etch Depth

As we have seen in the last section, the choice of the reciprocal lattice vector length G relies on the in-plane k-vector length of the guided mode that should get diffracted. Typically, in real LEDs one is not in the lucky situation to have a layer stack that supports only a single guided mode, but one has to deal with a distribution of modes. In Fig. 13 the principal problem of several guided modes is depicted. The guided mode with in-plane k-vector length β_1 certainly gets diffracted very efficiently, whereas diffraction of guided mode β_2 mainly results in diffracted k-vectors in the vicinity of the edge of the extraction disk $\beta_d \approx k_0$. One has to mention here, that all guided modes with in-plane k-vector $\beta_i \in [G-k_0;G+k_0]$ get partially diffracted into the extraction disk. However, the question arises, which lattice pitch should be chosen in order to extract as much light as possible from the LED. Hence, what are the properties of the guided modes that determine how much light is diffracted to air before it is absorbed and how can we optimise these?

In Fig. 6 different types of modes are summarized. From these we will derive the main properties determining the extraction of a guided mode, namely the spontaneous emission into the guided mode, its interaction with the PhC, the absorption and the Fabry-Perot-Resonances of the radiating modes. Additionally, some limits for the optimisation due to technological feasibility and performance will be given along with results found in literature.

The first property that comes to one's mind that should influence the choice of the lattice constant, is the amount of light emitted into different modes. A guided mode carrying a large fraction of the active layer's emission should be diffracted instead of a guided mode which no light is emitted into. In general, the larger the in-plane k-vector length of the guided mode the more light is emitted into that mode[4]. From that point of view, guided modes with large in-

[4] From (3) we notice that the density of photonic states plays an important role for the spontaneous emission. As we know from quantum mechanics, a single state in k-space covers the area $(2\pi/L)^n$, with L some real length and n the dimensionality of k-space. With Fig. 4c) in mind we conclude that the "red" mode covers a larger area in k-space than the "blue" mode and thus offers a higher number of photon states. This number scales with β/k_{SC} and

plane k-vector are more preferable for diffraction than guided modes with smaller in-plane k-vector.

Now, how much light actually is emitted into the different guided modes heavily depends on the vertical position of the active layer with respect to the vertical mode profile (RCLED effect). As depicted in Fig. 6a) the guided mode labelled I has an anti-node at the position of the active layer and thus will carry away a lot of emission. The local electric field strength is maximum resulting in a high radiative rate, see Eq. (3). In contrast, no photons will be emitted into the guided mode II with a node at the position of the active layer. From this we conclude, that the vertical layer structure has to be optimised in order to reveal guided modes best suitable for diffraction by adjusting the cavity itself and the position of the active region. The guided mode carrying most emitted light should be chosen for diffraction. For a more detailed discussion regarding the layer optimisation the reader is referred to [61].

Secondly, the photons emitted into a guided mode have to interact with the PhC in order to couple with radiation modes above the light line. In [15] a thorough investigation reveals that the extraction coefficient κ of guided modes scales with t^{-3} – with t the thickness of the remaining un-etched core (see Fig. 6) – as long as the guided mode is confined within this core and evanescent in the PhC. It can be further shown, that the overlap of the guided mode with the PhC mainly attributes to this dependence. Therefore, we assume that the interaction depends in first order on the overlap of the guided mode with the PhC layer. Hence, along with the amount of emitted light into the guided modes a second property of the guided mode determines the choice of the optimum reciprocal lattice vector. For instance, mode I in Fig. 6a) has less overlap with the PhC compared to mode III. In general, guided modes with $1<\beta/k_0<n_{PhC}$ have good overlap with the PhC layer as they are not evanescent in the PhC layer. In contrast, guided modes with $\beta/k_0>n_{PhC}$ are evanescent in the PhC layer and therefore interact poorly with the PhC. But typically these carry the highest fraction of emitted light and thus, there is a need for extracting them.

From this consideration and according to the t^{-3}-dependence it seems preferable to etch through the whole LED in order to maximize the overlap of the guided modes with the PhC. But this implies perforation of the active region resulting in a decrease of the active area according to the filling fraction of the lattice. Furthermore, the non-radiative recombination of electron-hole-pairs is increased as the active region is prone to surface recombination processes. Thus, the active region should be embedded within the core having thickness $t>\lambda/2n_{SC}$. This lower boundary results from the cut-off thickness of the lowest order mode, i.e. mode I in Fig. 6a). Cores thinner than $\lambda/2n_{SC}$ do not confine any mode and thus, all the guided modes are mainly guided within the PhC. Opposed to a maximized overlap with the PhC, in this case a reduced recombination rate decreases the internal quantum efficiency, as none of the guided modes has significant field amplitude at the position of the active region, see e.g. mode III in Fig. 6a). Therefore, the optimum PhC LED consists of a core slightly thicker than $\lambda/2n_{SC}$ and a PhC with an etch-depth deeper than the attenuation length $1/\gamma$ of the guided mode, with $\gamma = \sqrt{n_{PhC}^2 k_0^2 - \beta_i^2}$. As this results in an overall thickness of the LED on the order of 100-300nm technological issues like current spreading and current injection become a severe problem. To accomplish reasonable current spreading while remaining with thin LEDs in [23] a transparent conductive oxide (TCO) was used. This has also been utilized in [24]. However, the absorption introduced by these TCOs has to be carefully considered.

Similar to the amount of spontaneous emission into a mode and its interaction with the PhC, the absorption of the mode relies on its overlap with the absorbing layers, like a TCO, the mirror, the contacts or the epitaxial layers themselves. In general, the vertical layer design should not support guided modes with both high spontaneous emission and high absorption,

---

is taken into account in (4) by the factor $\sin\theta=\beta/k_{SC}$. Therefore, more light is emitted into guided modes with large in-plane k-vector length compared to modes with smaller k-vector length.

as some of the light will probably be lost. If such modes cannot be avoided, the PhC should be adjusted to these in order to extract them as fast as possible.

An implementation of PhC LEDs explicitly addressing the issue of a thin core is given in [12]. The vertical layer stack of the presented GaN-on-sapphire LED is similar to the one shown in Fig. 6b) except that a low-refractive index layer of AlGaN is inserted between the active layer and the sapphire substrate. This layer along with the ~250nm deep PhC squeezes a single guided mode within a 350nm thick core. The remaining guided modes are mainly confined underneath the AlGaN layer and thus, only little light is emitted into them. With a back-mirror behind the sapphire substrate (mimicking a thin-film device) an enhancement of at least 70% compared to a flat LED is reported. The extraction efficiency is estimated to be 20%-24%. In [24] a adjustment of these layers results in a 2.3 times enhancement compared to a flat reference.

Also the PhC itself can be used to define the desired small cavity, as has been shown by embedding the PhC into the vertical layer structure of the LED [16][19] – in this case the core is sandwiched between the PhC layer and the semiconductor-to-air interface. This has been obtained by lateral epitaxial overgrowth, even though that this is a challenging task. In [16] a 500nm thick core showed twice as much light output compared to a ~1μm thick one. A 1.5 improvement of the extraction efficiency compared to an as-grown reference is reported in [19].

On the other, hand micro cavities only a few wavelengths thick could also be a solution as they only support a few guided modes and some of these modes can be chosen to have optimum properties for diffraction by adjusting the overall thickness and the position of the active layer inside the LED. In the case of AlGaInP-based PhC RCLEDs enhancement factors compared to a flat reference of 2.6 are possible [22]. For the GaAs material system the extraction efficiency of a RCLED with a metallic grating has been calculated as 43% [6]. For InGaN RCLEDs no realisations including a PhC have been published yet. However, thin PhC LEDs with a metallic back mirror have shown high extraction enhancements of 1.8 [23].

But even for thick LEDs supporting numerous guided modes enhancement factors compared to flat LEDs of 1.5 in the blue emission range [8], 2.5 in the UV [9] and 1.5 in the AlGaInP system [21] can be found.

Along with these extraction enhancements the influence of the lattice pitch on the emission pattern of the LED has been proven [8][23][24], as shown in Fig. 14. This can easily be seen by considering Fig. 8 and Fig. 4b). Imagine an emission wavelength of 450nm and pitch of 180nm. The leaky mode at a/λ=0.4 in Fig. 4b) is diffracted into the vicinity of the light line resulting in a rather flat emission pattern. In contrast, a pitch of 243nm causes diffraction into the vicinity of the Γ-point and therefore a strong forward emission.

Up to now we investigated properties of the guided modes but neglected the impact of the radiation modes ($\beta<k_0$). Apart from their contribution to the extraction efficiency that is optimised in RCLEDs (see section 2) their resonances also have an impact on the diffraction efficiency of guided modes [15]. Consider for instance, the radiation mode IV in Fig. 6a) and the radiation mode V. The difference between the two relies on their overlap with the PhC due to the Fabry-Perot-resonances. Thus, diffraction from guided modes into mode IV will be more efficient compared to diffraction into mode V.

In the case of substrate LEDs a detailed investigation is given in [15] and [18] revealing that the Fabry-Perot-resonances can suppress diffraction into the substrate. Diffraction into so-called substrate modes, e.g. modes labelled II and III in Fig. 6b) with $1<\beta/k_0<n_{subs}$, has to be omitted as this light is hardly recovered due to the low interaction of these modes with the PhC. The amount of power radiated into the substrate by the radiation modes, for instance mode IV and mode V in Fig. 6b), can be redirected by placing a mirror at the bottom side of the substrate.

In summary, the vertical layer stack of the LED should support guided modes with both a high fraction of the total emitted light and good interaction with the PhC. The reciprocal lattice vector length should be adjusted to that modes. Thus, a thin core containing the active region is most preferable, as the interaction of the guided modes with the PhC can be increased, and the total number of guided modes is reduced. In the case of substrate LEDs the range of guided modes for diffraction is limited to $n_{subs}<G/k_0<n_{SC}$ compared to the range of $1<G/k_0<n_{SC}$ in the case of thin-film LEDs, as substrate modes have only small interaction with the PhC and hence, cannot be recovered. Furthermore, the diffraction efficiency can be further improved by adjusting the Fabry-Perot-resonances. The latter requires a precise control over the thickness of the layers, especially that of the PhC layer.

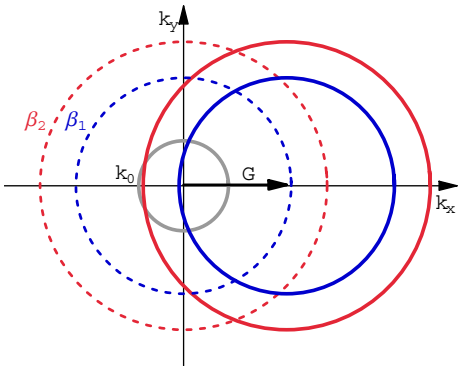

Fig. 13: Geometrical derivation of all diffraction processes for two guided modes with in-plane k-vectors $\boldsymbol{\beta}_1$ and $\boldsymbol{\beta}_2$ by one reciprocal lattice vector **G**. The dashed blue (red) line is a reminder of the guided mode that gets diffracted. The straight blue (red) line depicts all diffraction processes from $\boldsymbol{\beta}_d=\boldsymbol{\beta}_1+\mathbf{G}$ ($\boldsymbol{\beta}_d=\boldsymbol{\beta}_2+\mathbf{G}$).

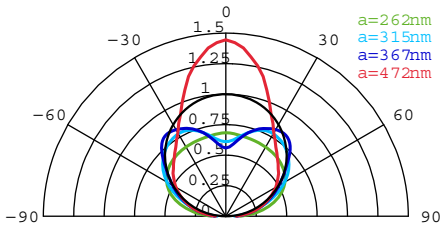

Fig. 14: Impact of the pitch of the PhC on the emission pattern of the LED. Azimuthal angle and wavelength averaged data taken from [17]; different colours represent different pitches. The overall flux is normalized to unity. A Lambertian emission profile is shown in black.

4.3. Set-ups for PhC LEDs

In general, two set-ups for PhC LEDs in the diffraction regime are possible, as shown in Fig. 15 [61]. In the scheme a) the whole LED area is used for light generation and extraction. This can be incorporated into thin-film LEDs and therefore has the advantages of scalability and a large light emitting area with only few dark regions due to contact shadowing. In addition, as the whole chip area is used for light generation the current density can be minimized. This is of great importance since the internal quantum efficiency tends to decrease with increasing current density because of carrier leakage and/or non-radiative recombination processes of electron-hole-pairs, like Auger recombination [62]. Decreased internal quantum efficiency results in stronger heating of the chip forcing a further increase of non-radiative processes. Of course, in this case etching through the whole LED is not favourable (see section 4.2 and 5).
In contrast, by separating the area of light generation and light extraction as depicted in Fig. 15b) etching through the active area has no disadvantages. As the light is generated within the un-perforated part the radiative recombination rate is not reduced and no active region is lost due to etching. However, the active area of the LED is limited as the light extraction area cannot be used for light generation. Thus, the efficiency decreases rapidly with increasing current due to current crowding and the resulting high non-radiative recombination rates.

Nevertheless, this set-up provides a good insight into the diffraction behaviour of the PhC, as only the guided light interacts with the PhC and the directly emitted light is either already coupled out or absorbed at the contact.
In both cases the LED area should be large enough to ensure complete light out-coupling. The extraction length of the fundamental guided mode in the case of GaN-on-sapphire LEDs has been calculated to be 80-200µm [11][12] and for GaN-based laser lift-off LEDs it has been estimated to be 5-10µm [14]. Therefore, thin-film LEDs offer stronger interaction of the guided modes with the PhC. It should be mentioned here, that these values do not include the extraction of all guided modes resulting in longer overall extraction lengths that have to be considered. In general, small extraction lengths are preferable as the light extraction has to compete with absorption processes at the mirror or inside the epitaxial structure being within the same length scale (see Fig. 3). Here, especially the reflectivity of the mirror plays an important role ([14] and section 8).

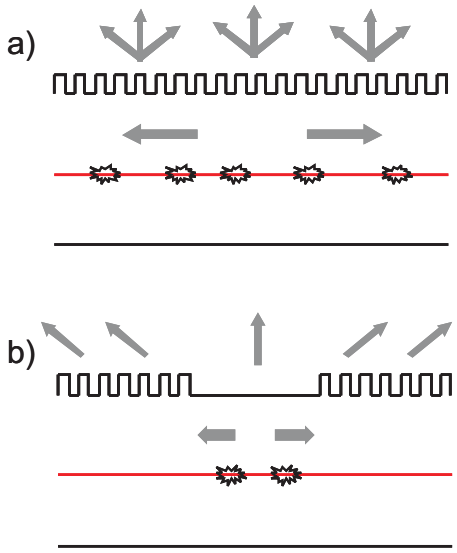

Fig. 15: Two possible set-ups for PhC LEDs (see text).

5. Strong PhCs – Molding the Flow of Light

In the regime of strong PhCs the impact on the dispersion relation goes beyond the pure band-folding and band-bending significantly alters the properties of light propagation. In principle, this set-up solves the fundamental problem of light extraction from LEDs: light emission into guided modes, as the emission into the guided modes is inhibited by the complete photonic band gap [2], as shown in Fig. 16. Thus light can only radiate into the ambient medium resulting in high extraction efficiencies. In the case of a photonic crystal slab in air nearly 100% extraction efficiency [4] has been calculated, if the emission wavelength overlaps with the photonic band-gap. Therefore, an enhanced vertical emission is observed [10]. On the other hand, this causes a significant reduction of the radiative recombination rate as the photon density of states is heavily reduced (see Eq. (3), [10] and [4]). This itself decreases the internal quantum efficiency of the devices as a consequence of the competition between radiative and non-radiative recombination, see Eq. (2). Additionally, etching of holes through the active layer enforces surface recombination of electron-hole-pairs leading to an increase of the non-radiative recombination rates and thus, to a further decrease of the internal quantum efficiency.
Therefore, instead of inhibiting spontaneous emission by a photonic band-gap it is more preferable to use both the enhancement of extraction due to Bragg-scattering and an increased density of photonic states [3]. This can be accomplished by adjusting the emission of the active layer to the flat bands of leaky modes, for instance for frequencies around 0.55 in Fig.

From the folding of the light line an interesting fact arises. In the case of a hexagonal lattice, for frequencies $a/\lambda>2/3$ all the modes lie above the light line. In this regime the 1. BZ fits completely within the extraction disk. Therefore, high extraction efficiencies of up to 90% could be achieved [2].
Apart from these approaches for enhancing the efficiency a combination of light generation and extraction as described in [5] results in 80% of the overall emission within a narrow escape cone of ±0.2°. Here, firstly the emission is collimated in-plane into the ΓK-direction of a hexagonal PhC slab (for instance emission around frequencies of 0.3 in Fig. 16). A second grating with twice the pitch of the first one is then used to redirect that light into the vicinity of the surface normal. However, this approach is extremely sensitive on the emission wavelength [18]. For shorter wavelength the emission falls into the band-gap and for longer wavelength the collimation of the emission is decreased.
Unfortunately, all of these encouraging results have only been demonstrated on free-standing PhC slabs with optical pumping. An electrically driven realisation of such PhC LEDs would probably suffer from weak current spreading and again from a loss of active area. Furthermore, as flat bands correspond to a low group-velocity of the Bloch modes absorption will have an impact on the performance of such PhC LEDs.

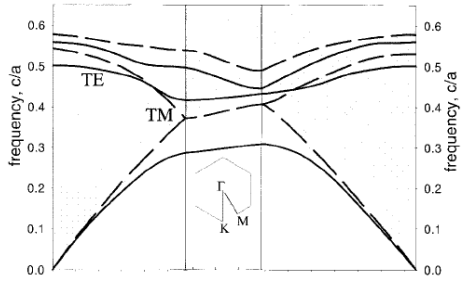

Fig. 16: Dispersion relation for a photonic crystal slab [3]. Emission around reduced frequencies of 0.35 is strongly inhibited due to a complete band-gap for TE-like polarized light. For frequencies of 0.5 to 0.6 emission occurs in leaky modes with a high density of states.

6. Special Cases for PhCs

6.1. Omni-directional Mirror

According to Fig. 3 the absorption within a LED plays an important role for the extraction efficiency. Especially in thin-film LEDs with a metallic back-mirror the losses introduced by the mirror limit the performance of these devices. Therefore, a loss-less omni-directional mirror based on a PhC could be a significant improvement. However, this could only be accomplished by a three-dimensional PhC with a photonic band-gap for every propagation direction and polarization. To the best of our knowledge no implementation of a three-dimensional PhC on LEDs has been reported so far that addresses this issue. In general, besides its reflectivity the PhC should also offer good heat dissipation, at least.
A first approximation is reported in [63]. Here, the mirror is formed by a low-index layer followed by a one-dimensional PhC (or Bragg reflector). Due to total internal reflection at the interface between the semiconductor and the low-index layer 100% reflection from the critical angle to glancing angles is achieved. The transmitted light within the critical angle is reflected back at the Bragg mirror. An overall angle and polarization averaged reflectivity of $R>99.95\%$

6.2. Metallic PhC

Depending on the dielectric and the metal the corresponding interface guides light, so called surface plasmons (SPs), i.e. the real part of the metal's permittivity ε_M has to be smaller than the negative permittivity of the dielectric ε_D: $\mathrm{Re}\{\varepsilon_M\}<\mathrm{Re}\{-\varepsilon_D\}$. Microscopically a SP is an oscillation of the electron plasma inside the metal. This oscillation can be expressed as a mode that is evanescent in both the semiconductor and the metal. The dispersion relation of a SP as shown in Fig. 17 reveals, that due to the flat band the SP offers a huge density of states and therefore, significantly enhances the radiative rate of an emitter placed into the vicinity of the metal-semiconductor interface [64]. The coupling of the emitter with the SP forms the surface plasmon polariton (SPP) [65]. But due to the confinement of the SP the light emitted to it never escapes and is absorbed in the metal. Here, a PhC is helpful as it scatters the light out of the SP into the semiconductor [65][66]. But the efficiency of a SPP coupled emitter is mainly limited by the efficiency of coupling light out of the SP [67][68]. This is determined by the absorption length within the metal and the extraction length due to scattering by the PhC and limits the application of SPPs to emitter with poor efficiency. In this case, the enhancement of internal quantum efficiency due to the Purcell factor overcomes the losses introduced by the metal.

Instead of a metallic PhC localized metallic particles have also been suggested to take advantage of the high Purcell factor [69]. But the main drawback of absorption in the metal still limits the efficiency. In addition, in a realistic device a lot of metallic particles should be incorporated, in order to use the whole chip area and therefore, get reasonable performance. Here, to maintain the properties of localized particle plasmons strong disorder has to be introduced [70].

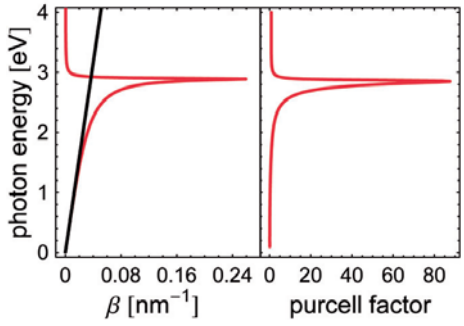

Fig. 17: Dispersion (red) of a surface plasmon at GaN-silver interface (n_{GaN}=2.5, silver from [71]). Light-line of GaN is shown in black. Right plot shows the Purcell factor for an emitter placed 10nm in front of the GaN-to-silver interface.

7. Patterning Techniques

As the periodicity of PhCs is in the order of the wavelength and LEDs emit from the near UV (360nm) up to the near IR (940nm), the patterning techniques have to be able to define holes in the same regime (100-1000nm) depending on the filling fraction and the lattice. But conventional patterning techniques (typ. contact lithography for semiconductors) are restricted to about a=1µm by the diffraction limit or are extremely expensive, like deep ultra-violet lithography. In this section, commonly used patterning techniques capable of realizing such dimensions are summarized.

7.1. Electron-Beam Lithography

Electron-beam lithography (e-beam) is probably the most widely used technique for patterning 1D and 2D PhC as it is an extended scanning electron microscope [72]. In this set-up an electron-beam scans across the resist covering the LEDs surface exposing the resist according to the PhC pattern. After selectively removing either the exposed or the un-exposed areas of the resist the pattern is etched into the semiconductor. With this method typical feature sizes down to 20nm are achieved. The scanning technique offers a huge flexibility on the patterns but limits the overall throughput. Therefore, e-beam is mostly applicable for low-volume production and especially for research and development.

7.2. Nano-Imprint

Nano-imprint could be thought of Gutenberg's invention transferred to the nano-scale [73]. First of all, a stamp is generated, typically e-beam-patterned material like quartz. As in the macroscopic world, the stamp is the inverse image of the one-dimensional or two-dimensional PhC and can be used several times. This stamp prints its pattern into a resist cast upon the LED's surface. By pressure and capillary forces the PhC lattice is transferred into the resist and after UV curing and/or heating (depending on the resist) the stamp is removed. Now, the resist can act as an etching mask transferring the pattern into the semiconductor. As first of all the stamp or master has to be generated it is not as flexible as e-beam lithography. But nano-imprint is applicable to mass-production as it offers high throughput (full wafer process) and reproducible results in the order of 10-20nm. And every possible pattern can be printed, so it is not limited to periodical ones. However, due to the stamping of the whole wafer, particles have to be avoided as these could damage the master. Transferring the pattern into the resist suffers from rough wafer surfaces and from a bow of the wafer, at least if an un-flexible master is used [74].

7.3. Laser Interference Lithography

In this technique two laser beams are used for interference and the resulting one-dimensional intensity profile defines the resist pattern [75]. By simply rotating this one-dimensional profile two-dimensional regular pattern are created, like rectangular or hexagonal lattices. Thus, this method is limited to regular patterns and is not capable of creating arbitrary lattices. The pitch of the lattice is varied by either the laser-wavelength or the angle between the two laser beams.

7.4. Natural Lithography

Here the natural affinity of spheres to pack to each other as close as possible is used [76]. Hence, with these techniques it is only possible to generate exactly these patterns, namely hexagonal in two dimensions and opal in three dimensions. Typically in two dimensions, spheres with diameter equal to the desired pitch are used to form the lattice upon a resist. These spheres are used as an etching mask in order to transfer the pattern into the resist. By a final etching process the pattern is transferred from the resist into the semiconductor. On one hand, this is an easy and cheap way of fabricating a hexagonal lattice. On the other hand, this method is limited by the availability of sphere diameters, to hexagonal patterns and by the reproducibility of the results. The latter is a result from multi-layer stacking of the spheres and a lack of long-range ordering.

7.5. Nano-Rods

Contrary to the techniques presented so far, here no material is removed but the LED is only grown on some defined areas [77]. In order to obtain a regular arrangement of the semiconductor pillars first of all one of the above techniques has to be used to define a pattern for the selective growth [78]. This results in an inverted PhC structure compared to the ones

8. Comparison between PhC LEDs and randomly textured LEDs

In this section we focus on the fundamental question for the application of PhC in LEDs: Does a PhC LED extract as much light as a state-of-the-art commercial LED? So far, commercial available thin-film LEDs typically include a random surface texturing as it is easy to fabricate and solves the problem of total internal reflection very efficiently. The benchmark presented in section 2 for realized LEDs already shows that this is a close competition. Here we shed light on both approaches using FDTD modelling and – first – a comparison of both schemes in the weak scattering model. For the latter the rough surface is modelled in analogy to the PhC, yet with the holes distributed in a random pattern.

From the point of view sketched in section 4.1 the Fourier amplitude of the random surface should give first information on the extraction efficiency. In Fig. 18 the real space image used for the random surface texture is shown along with its Fourier transform. Clearly, no discrete pattern is observed as for the lattices shown in Fig. 10. According to Eq. (7), Fig. 19 shows the extraction coefficient for a hexagonal lattice and the random surface texture. The random texture extracts less light from a single guided mode within a given propagation distance compared to the hexagonal lattice due to its lower Fourier amplitude – this is similar to the Archimedean lattices. In contrast, the random surface texture is less sensitive on the exact in-plane k-vector of the guided mode as for large reciprocal lattice vectors still all the modes get diffracted to air. This is especially helpful for thick LEDs with numerous guided modes. Furthermore, similar to the case of Archimedean lattices every in-plane propagation direction is diffracted to air as a huge number of reciprocal lattice vectors with $|\mathbf{G}|=G$ exists. In contrast to the Archimedean lattice, a rough surface offers omni-directional in-plane diffraction for every in-plane k-vector length of the guided mode not just for guided modes with $\beta_i \approx G_0$.

In order to compare a PhC LED with a standard LED in terms of absolute efficiency we resort now to full three-dimensional calculations using the FDTD method. As a vehicle we choose a GaN-based LED in thin-film configuration with a peak wavelength of 520nm. The shown modelling results represent a Gaussian average with a FWHM of 30nm including wavelengths from 470 to 570 with 71 supporting points. As the refractive index of GaN LEDs varies negligibly within the layer stack we assumed a constant index of n=2.4 for the whole 3µm thick LED, as depicted for instance in Fig. 6a). The active region is placed 160nm above an Ag-based mirror. The refractive index of this mirror was obtained by fitting a combined Plasma-Lorentz model [80] for the dielectric constant to the values of Ag from [71]. In order to take into account thin absorptive adhesion layers between the Ag and the GaN, we increased the damping constant within the Plasma-model by a factor of 10 and dropped the adhesion layer. Otherwise, the accurate description of such a thin layer within FDTD would result in a huge demand on RAM. The reflectivity of this mirror under normal incidence is ~90% compared to ~98% of the pure Ag mirror at 520nm. The surface roughness of the standard GaN-based LEDs typically consists of pyramidal structures defined by the crystallographic planes of GaN [81] with an average height of around 1µm.

For a first comparison we simply replaced the surface roughening by a hexagonal lattice with a typical etch-depth of 300nm and a lattice constant of a=600nm that has been optimised for

maximum extraction efficiency. As this lattice constant corresponds to a main reciprocal lattice constant of $G_0=k_0$ this PhC first of all diffracts guided modes with high overlap with the PhC and secondly, guided modes with higher in-plane k-vectors by high-order diffraction processes. Thus, we have chosen the filling fraction to be 50%. In order to investigate the dependency of the extraction on the propagation distance of light we calculate the Poynting flux through a disk parallel to the semiconductor-to-air interface in air with respect to the overall emitted flux by the dipole. By successively increasing the radius of this disk it is possible to compare different surface textures in terms of their extraction length.

In Fig. 20 the extraction efficiency for the PhC LED and the rough LED is shown as a function of the integration radius. Additionally, the extraction efficiency of an unstructured LED is depicted for comparison. First of all, the extraction efficiency of the unstructured LED is significantly higher than the 4% for an isotropic source. Here, the interference of the source with its mirror-image enhances the extraction efficiency (RCLED effect) [82]. Secondly, due to the higher extraction coefficient as shown in Fig. 19 the PhC LED indeed extracts more light within an integration radius of 5µm, although the etch-depth is only 300nm compared to 1µm of the random surface texture. But due to its discrete diffraction behaviour and its restricted in-plane omni-directionality it cannot compete with the rough surface. After an extrapolation of the extraction efficiency by an exponential function [17] we obtained an overall extraction efficiency of 45% for the PhC LED and 60% for the rough LED. The resulting enhancement factor of about 2.8 of the PhC LED compared to the unstructured reference is within the range of the reported enhancements summarized in section 4.2.

Of course, the chosen structure is not optimised for the implementation of the PhC as it is a rather thick LED supporting ~50 guided modes and the interaction of the PhC with the guided modes carrying most of the spontaneous emission is low. The interaction is increased by decreasing the overall thickness of the LED (remember the t^{-3} dependence of the overlap with the PhC). In order to demonstrate the potential of diffracting PhCs for light extraction we have chosen a LED with a GaN-thickness of 650nm. The refractive index profile of this demonstrator is shown in Fig. 21. The thick low-index layer (SiO_2 with n=1.5) pushes guided modes with $1.5k_0<\beta<2.4k_0$ away from the mirror [83] and reduces their absorption to a negligible amount. Therefore, we have chosen a main reciprocal lattice vector length $G_0=k_0$ and a hexagonal lattice in order to extract the mainly absorbed modes at first. The position of the active region guarantees high extraction of the directly emitted light. Additionally, the shallow PhC ensures to stay within the weak regime. The extraction efficiency of this PhC LED is extrapolated to 70% (Fig. 22), whereas a roughened LED with this SiO_2-mirror combination but an overall GaN thickness of 3µm has almost the same efficiency with 71%. The PhC in combination with the thin vertical structure extracts the light very rapidly, but still its efficiency is limited by the discrete diffraction behaviour as can be seen by the extrapolation of the data. A further reduction of the core thickness will probably enhance the extraction efficiency further. But this would also mean to leave the regime of weak coupling.

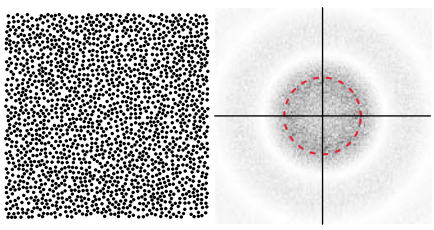

Fig. 18: (left) Real space image of a random distribution of holes. The image was generated on a area of $(40a)^2$ assuming the same filling fraction F=0.4 and the same number of holes per unit area as for the hexagonal lattice. (right) The Fourier transform of the rough surface along with the main reciprocal lattice vector defined by $G_0=4\pi/\sqrt{3}a$ (indicated by the red dashed circle).

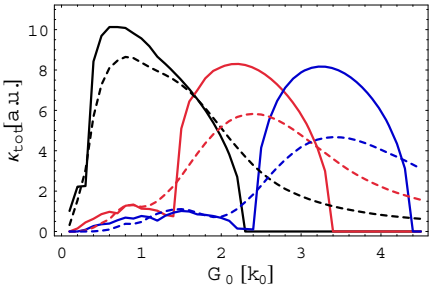

Fig. 19: Comparison of the extraction coefficient κ_{tot} for a hexagonal lattice (straight lines) and a random surface texture (dashed lines) as a function of the main reciprocal lattice vector. Black/red/blue lines correspond to β_i=1.3k_0, β_i=2.4k_0 and β_i=3.4k_0.

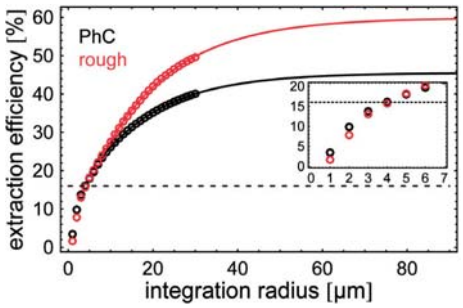

Fig. 20: Extraction efficiency as a function of the integration radius for a PhC LED (black) and a rough LED (red). The horizontal dashed line indicates the extraction efficiency of the unstructured LED. Symbols indicate the extraction efficiency calculated from the FDTD data for increasing integration radius. Straight lines represent the extrapolation with a function ~(1-exp(-α x)) starting from an integration radius x=8µm.

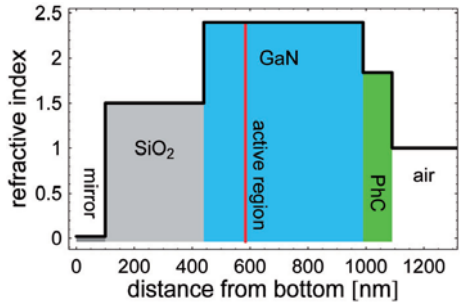

Fig. 21: Refractive index profile (black line) of the demonstrator for the potential of diffracting PhC LEDs.

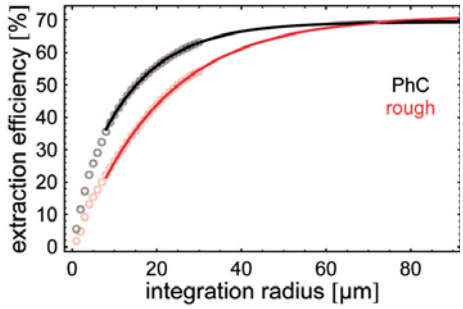

Fig. 22: Extraction efficiency as a function of the integration radius for the "optimal" PhC LED (black) and a rough LED (red) with the same SiO_2-mirror combination. Symbols indicate the extraction efficiency calculated from the FDTD data for increasing integration radius. Straight lines represent the extrapolation with a function ~(1-exp(-α x)) starting from an integration radius x=8µm.

9. Directional Emission

One certain advantage of PhC over rough surface LEDs is their capability to design the shape of the emission pattern. An example of the variation of the emission patter of a PhC LED with

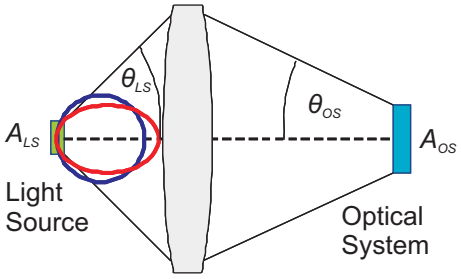

Fig. 23: Example of an étendue-limited system. The light emitted from the source is projected on the optical system with area A_{OS} and acceptance angle θ_{OS}. Depending on the source area A_{LS} only light emitted into a limited apex cone with angle θ_{LS} passes through the optical system. In blue a Lambertian emission profile is shown and in red a super-Lambertian one emitting more of its overall emission into the limited apex cone with angle θ_{LS}.

9.1. Étendue

The étendue or Huygen-Helmholtz invariant describes the phase space of light that can pass an optical component and is defined by

$$dE = n^2 \cos\theta \, d\Omega dA \tag{9}$$

with n the refractive index, θ the polar angle with respect to the optical axes, $d\Omega$ the solid angle and the surface area dA. Therefore, étendue is a limiting quantity for the functionality of a system. The performance of the whole set-up is determined by that optical component having the smallest phase space volume or étendue. In a projection based system the limiting component is the imager, e.g. a Digital Micromirror Device (DMD), liquid crystal display (LCD) or liquid crystal on silicon (LCoS). In the case of a DMD the étendue is given by the area of all micro-mirrors and half of the angle between on- and off-state – typically this angle is θ_{OS}=12°. For a 0.55" imager with an area of 93.7mm² the étendue is (with $d\Omega=\sin\theta d\theta d\varphi$ and n=1)

$$E_{OS} = \pi \, n^2 A_{OS} \sin^2 \theta_{OS} = 12.7 \, mm^2 sr \tag{10}$$

The limitation of the performance of the whole system by the étendue of the imager can be seen by considering the following example. Let's assume an ideal case, where all the light emitted into the entire hemisphere is collected by some optics and projected onto the DMD. From the étendue of the DMD of 12.7mm²sr and a source angle of θ_{OS}=90°, the source area is calculated to 4mm², where the étendue of the source matches the étendue of the optical system, $E_{LS}=E_{OS}$. Thus, by assuming some given radiant emittance of the source, the brightness on the imager can be enhanced by increasing the source area up to 4mm², as more source area simply generates more flux. For areas larger than 4mm² the étendue of the light source is larger than that of the DMD, and light will be wasted as it is emitted beyond the phase space of the imager. Thus, an increase of E_{LS} over and above E_{OS} by enlarging the source area starting from 4mm² does not enhance the brightness on the imager. In this case, the only way for increasing the brightness on the imager is to improve the radiant emittance from the surface.

In general, depending on the projection system only light emitted into a cone with apex angle $\theta_{LS}<90°$ is collected and projected onto the imager. In this case, the source area has to be adjusted depending on θ_{LS} in order to match the étendue of the optical system

$$A_{LS} = \frac{E_{OS}}{\pi \sin^2 \theta_{LS}}. \tag{11}$$

As we will see in the next section, a limited source angle enables to project more light onto the imager in combination with a more forward emission. On the one hand, this can be accomplished while remaining with constant radiant emittance or even with less radiant emittance. On the other hand, the required source area increases.
In Fig. 24 the required source area is illustrated as a function of the used source angle θ_{LS} for different ètendue values of the optical system. The smaller the apex angle the larger the chip area causing higher costs of the whole system as more and/or larger chips have to be used. Here, the total area of several mm² is not covered by a single chip but several. However, large chips are favourable in order to reduce the area occupied by the spacing between the individual chips. In terms of costs also the reduction of the étendue of the optical system is favourable, even though this is mainly because of the costs of large imagers. This reduction of the imager size additionally demands for a further increase of the performance of high-power LED devices.

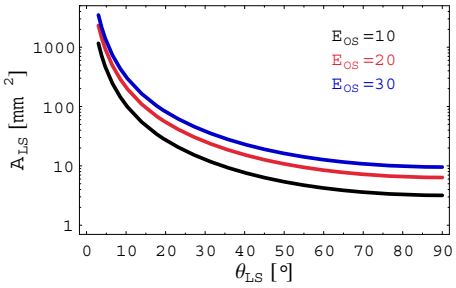

Fig. 24: Dependence of the required source area A_{LS} on the used apex angle θ_{LS} in order to match different values of étendue of the optical system E_{OS}, $E_{LS}=E_{OS}$.

9.2. Photonic Crystals and étendue

In this section we will discuss the benefit from PhC LEDs for étendue-limited applications due to a more forward emission. In order to quantify the collimation of the farfield profile we define the directionality as the amount of flux emitted into the apex cone θ_{LS} with respect to the overall emitted flux.
But before presenting results for PhC LEDs let's briefly investigate the amount of directionality achievable by applying diffracting PhCs. As every in-plane direction $\boldsymbol{\beta}_i/\beta_i$ of a guided mode gets diffracted by a reciprocal lattice vector $\mathbf{G}$, consider for instance the blue circle in Fig. 13, two groups of diffraction processes can be distinguished. Firstly, diffraction processes with in-plane k-vector β_d within the cone of accepted light, $0\leq\beta_d\leq k_0\sin\theta_{LS}$, enhance the directionality. In contrast, diffraction processes with $k_0\sin\theta_{LS}<\beta_d\leq k_0$ decrease the directionality. Therefore, by assuming constant diffracted intensity I_d from every guided mode of the degenerate set with $|\boldsymbol{\beta}_i|=\beta_i$ (and assuming $\beta_i\approx k_0$ with $\beta_i\approx G$) the directionality D resulting from diffraction of a single guided mode reads [17]

$$D = \frac{2I_d k_0 \sin\theta_{LS}}{2I_d k_0} = \sin\theta_{LS}. \tag{12}$$

Ignoring the impact of radiation modes on the farfield pattern and assuming a mono-mode LED – additional guided modes will reduce the directionality due to the mismatch between their k-vector and the reciprocal lattice vector – Eq. (12) describes a fundamental limit for the

directionality. A directionality within any θ_{LS}<90° of 100% cannot be achieved because besides diffraction into the limited apex cone diffraction outside this cone simultaneously takes place. In comparison, for a Lambertian emitter $\sin^2\theta_{LS}$ of the total emitted light is located inside an apex angle θ_{LS} – here the ratio between the area within $k_0\sin\theta_{LS}$ and the area within k_0 determines the directionality instead of a ratio of lengths as in Eq. (12). For an apex angle of θ_{LS}=30° diffraction of a guided mode results in the optimum case of 50% directionality, whereas only 25% of the Lambertian emission lies within the same cone.

In Fig. 25 four different LEDs are compared in terms of their emission profile, the flux within an apex angle θ_{LS} and the projected flux on the imager. As a reference (black dashed line) we choose the rough LED from Fig. 20 to have an efficacy of 100lm per electrical input power of 1W. For the other LEDs we assume the same internal quantum efficiency and the same electrical performance. Therefore, the overall efficiencies of these LEDs differ only owing to the individual extraction efficiency. Thus, the rough LED with SiO_2 in Fig. 22 (straight black line in Fig. 25) has an efficacy of 120lm/W. The emission profile of the rough LEDs is approximated by a Lambertian [25]. The third LED (red dashed line) is the same thick PhC LED as in Fig. 20 except that the main reciprocal lattice vector was adjusted (G_0=1.3k_0) to yield maximum forward emission. Thus, the extraction efficiency drops from 45% to 40% and the efficacy is about 68lm/W. The last example is the thin PhC LED from Fig. 22, but again with corrected main reciprocal lattice vector (G_0=1.6k_0) yielding an extraction efficiency of 64% and an efficacy of 106lm/W.

Due to the lower number of different guided modes the thin PhC LED shows a more pronounced forward emission compared to the thick PhC LED, as depicted in Fig. 25a). However, both have a super-Lambertian emission profile favourable for coupling their emission into an étendue-limited optical system. Apart from the emission profile the actual amount of flux within some apex angle θ_{LS} also depends on the total emitted flux, as shown in Fig. 25b). Due to its high efficacy and forward emission the thin PhC LED is superior to the other examples within an apex angle of θ_{LS}<65°. A more general remark should also be noted here: a limited apex angle decreases the efficiency of the system as light is wasted.

After this summary of the performance of the bare LEDs, in the following their impact on the performance of the DMD based projector will be investigated, that has already been used in the example of Eq. (10). Here, we assume that the area of a single chip is 1mm² having the efficacy as shown in Fig. 25b). If the whole emission can be collected, the maximum applicable source area for this example is 4mm². Thus, 480lm are generated on the imager by incorporation of four rough LEDs with SiO_2 driven at 1W electrical input power. For smaller apex angles θ_{LS}<90° still the same amount of flux can be coupled into the system, if the étendue of the imager is matched by increasing the source area according to Eq. (11). This stems from the Lambertian emission profile. In contrast, for limited apex angles more light is projected onto the imager by application of PhC LEDs due to the super-Lambertian emission profile. Even though the thin PhC LED has less radiant emittance compared to the rough LED with SiO_2, more flux is coupled into the projection system resulting in a peak flux of almost 800lm on the DMD. But even for rather large apex angles of about 40° the system with the thin PhC LED still projects 1.3 times more flux on the imager compared to the system with the thick rough LED and SiO_2. This enhancement is regardless of the actual source area as only the total flux scales with the chip area.

In summary, projection applications could benefit from the use of PhC LEDs due to their super-Lambertian emission profile and reasonable extraction efficiency. But the applicability of a more forward emission is limited owing to the required source areas and decreased efficiency. Furthermore, diffraction outside the desired apex angle restricts the amount of directionality achievable with diffracting PhC LEDs.

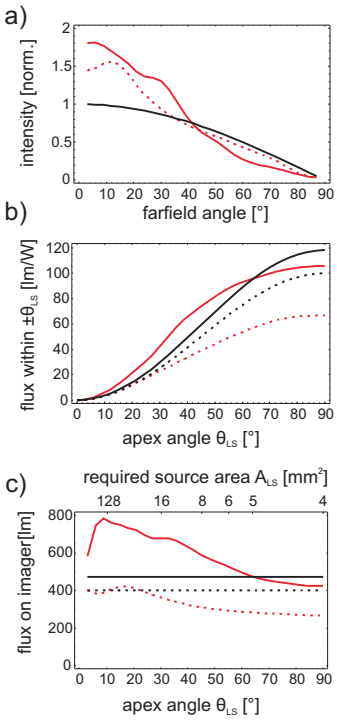

Fig. 25: a) Emission profiles of a Lambertian source (black), a thick PhC LED with G_0=1.3k_0 (red dashed) and a thin PhC LED with G_0=1.6k_0 (red straight). Overall emission of the three LEDs normalized to unity. b) Flux within apex angle θ_{LS} for the thick PhC LED (red dashed), the thin PhC LED (red straight), the rough LED (black dashed) and the rough LED with SiO_2 (black straight). c) Flux projected on the imager as a function of the apex angle θ_{LS} for the same LEDs as in b). The étendue of the imager is 12.7mm²sr and the required source area for matching this value is given on the upper x-axis.

10. Conclusions

We presented an overview about the application of PhCs in LEDs: extraction of light, improving the internal quantum efficiency by either band-effects or surface plasmon polaritons, and reduction of mirror losses. In order to reach high wall-plug efficiency, both electrical efficiency and internal quantum efficiency have to high in addition to extraction efficiency. This puts limits on the vertical layer stack of the LED, as e.g. current spreading has to be taken into account. In nearly all demonstrated designs the PhC is implemented as a scattering layer within the LED, acting as a weak perturbation to redistribute light from guided modes to the extraction cone. Thus, we focused on this regime and discussed the properties of PhCs determining the route for high-performance devices.

In general, the vertical layer structure determines the interaction of the guided modes with the PhC and the total number of guided modes, and its optimization is crucial to the PhC LED performance. Due to the discrete diffraction behaviour a low number of guided modes is most preferable. A reduction of absorption losses enhances the overall efficiency further. In the end, the extraction efficiency boils down to the two numbers extraction length and absorption length. We demonstrate, how a PhC LED can be optimized, staying within the weak perturbation limit, which provides insight into the physical processes and is still realistic enough to describe most cases of practical interest.

The freedom to design the angular distribution of the extracted light opens the road to enhance the performance of étendue-limited applications owing to the collimation of the farfield pattern. From a basic geometrical consideration a fundamental limit for the directionality achievable by diffracting PhCs is given.

Even though PhCs have demonstrated their potential for light extraction the benchmark is given by state-of-the-art devices, like thin-film LEDs with rough surfaces. Using FDTD we compare thin-film and PhC LEDs, each with an optimized vertical structure. The differences

are subtle and the overall extraction efficiency of the optimized structures is a close match. So for the now standard thin-film roughened or PhC LED, where the scattering layer is implemented as a thin layer – usually at the semiconductor surface – other criteria, like directionality, electrical performance and cost of production, are decisive.
This may be different for PhC LEDs which leave the regime of weak perturbation. From the authors' point of view the challenge of an electrically driven device along with a loss of active region restricts the application of strong PhCs showing the most impressive results. Here, radical new approaches, like core-shell growth of nano-rods, could offer new perspectives.

References

[1] J. M. Phillips, M. E. Coltring, M. H. Crawford, A. J. Fischer, M. R. Krames, R. Mueller-Mach, G. O. Mueller, Y. Ohno, L. E. S. Rohwer, J. A. Simmons, and J. Y. Tsao, "Research challenges to ultra-efficient inorganic solid-state lighting," Laser & Photon. Rev. **1**, 307 (2007).

[2] S. Fan, P. R. Villeneuve, J. D. Joannopoulos, and E. F. Schubert, "High extraction efficiency of spontaneous emission from slabs of photonic crystals," Phys. Rev. Lett. **78**, 3294 (1997).

[3] M. Boroditsky, R. Vrijen, T. F. Krauss, R. Coccioli, R. Bhat, and E. Yablonovitch, "Spontaneous emission extraction and purcell enhancement from thin-film 2-D photonic crystals," J. Lightwave Technol. **17**, 2096 (1999).

[4] R. K. Lee, Y. Xu, and A. Yariv, "Modified spontaneous emission from a two-dimensional photonic bandgap crystal slab," J. Opt. Soc. Am. B **17**, 1438 (2000).

[5] A.-L. Fehrembach, S. Enoch, and A. Sentenac, "Highly directive light sources using two-dimensional photonic crystal slabs," Appl. Phys. Lett. **79**, 4280 (2001).

[6] D. Delbeke, P. Bienstmann, R. Bockstaele, and R. Baets, "Rigorous electromagnetic analysis of dipole emission in periodically corrugated layers: the grating-assisted resonant-cavity light-emitting diode," J. Opt. Soc. Am. A **5**, 871 (2002).

[7] M. Rattier, H. Benisty, E. Schwoob, C. Weisbuch, T. F. Krauss, C. J. M. Smith, R. Houdre, and U. Oesterle, "Omnidirectional and compact guided light extraction from Archimedean photonic lattices," Appl. Phys. Lett. **83**, 1283 (2003).

[8] J. J. Wierer, M. R. Krames, J. E. Epler, N. F. Gardner, M. G. Craford, J. R. Wendt, J. A. Simmons, and M. M. Sigalas, "InGaN/GaN quantum-well heterostructure light-emitting diodes employing photonic crystal structures," Appl. Phys. Lett. **84**, 3885 (2004).

[9] J. Shakya, K. H. Kim, J. Y. Lin, and H. X. Jiang, "Enhanced light extraction in III-nitride ultraviolet photonic crystal light-emitting diodes," Appl. Phys. Lett. **85**, 142 (2004).

[10] M. Fujita, S. Takahashi, Y. Tanaka, T. Asano, and S. Noda, "Simultaneous inhibition and redistribution of spontaneous light emission in photonic crystals," Science **308**, 1296 (2005).

[11] A. David, C. Meier, R. Sharma, F. S. Diana, S. P. DenBaars, E. Hu, S. Nakamura, C. Weisbuch, and H. Benisty, "Photonic bands in two-dimensionally patterned multimode GaN waveguides for light extraction," Appl. Phys. Lett. **87**, 101107 (2005).

[12] A. David, T. Fujii, R. Sharma, K. McGroddy, S. Nakamura, S. P. DenBaars, E. L. Hu, C. Weisbuch, and H. Benisty, "Photonic-crystal GaN light-emitting diodes with tailored guided modes distribution," Appl. Phys. Lett. **88**, 061124 (2006).

[13] A. David, T. Fujii, E. Matioli, R. Sharma, S. Nakamura, S. P. DenBaars, C. Weisbuch, and H. Bensity, "GaN light-emitting diodes with Archimedean lattice photonic crystals," Appl. Phys. Lett. **88**, 073510 (2006).

[14] A. David, T. Fujii, B. Moran, S. Nakamura, S. P. DenBaars, C. Weisbuch, and H. Benisty, "Photonic crystal laser lift-off GaN light-emitting diodes," Appl. Phys. Lett. **88**, 133514 (2006).
[15] A. David, H. Benisty, and C. Weisbuch, "Optimization of light-diffracting photonic-crystals for high extraction efficiency LEDs," J. Disp. Technol. **3**, 133 (2007).
[16] A. David, B. Moran, K. McGroddy, E. Matioli, E. L. Hu, S. P. DenBaars, S. Nakamura, and C. Weisbuch, "Gan/InGaN light emitting diodes with embedded photonic crystal obtained by lateral epitaxial overgrowth," Appl. Phys. Lett. **92**, 113514 (2008).
[17] Ch. Wiesmann, K. Bergenek, N. Linder, and U. T. Schwarz, "Analysis of the emission characteristics of photonic crystal LEDs," Proc. SPIE **6989**, Light Emission I, 69890L (2008).
[18] H. Benisty, J. Danglot, A. Talneau, S. Enoch, J. M. Pottage, and A. David, "Investigation of extracting photonic crystal lattices for guided modes of GaAs-based heterostructures," IEEE J. Quantum Electron. **44**, 777 (2008).
[19] M.-K. Kwon, J.-Y. Kim, I.-K. Park, K. S. Kim, G.-Y. Jang, S.-J. Park, J. W. Kim, and Y. C. Kim, "Enhanced emission efficiency of GaN/InGaN multiple quantum well light-emitting diodes with an embedded photonic crystal," Appl. Phys. Lett. **92**, 251110 (2008).
[20] C.-F. Lai, J.-Y. Chi, H.-H. Yen, H.C. Kuo, C.-H. Chao, H.-T. Hsueh, J.-F. Trevor Wang, C.-Y. Huang, and W.-Y. Yeh, "Polarized light emission from photonic crystal light-emitting diodes," Appl. Phys. Lett. **92**, 243118 (2008).
[21] K. Bergenek, Ch. Wiesmann, R. Wirth, L. O'Faolain, N. Linder, K. Streubel, and T. F. Krauss, "Enhanced light extraction efficiency from AlGaInP thin-film light-emitting diodes with photonic crystals," Appl. Phys. Lett. **93**, 041105 (2008).
[22] K. Bergenek, Ch. Wiesmann, H. Zull, R. Wirth, P. Sundgren, N. Linder, K. Streubel, and T. F. Krauss, to be published.
[23] K. Bergenek, Ch. Wiesmann, H. Zull, R. Wirth, C. Rumbolz, N. Linder, K. Streubel, and T. F. Krauss to be published. LED consists of ~850nm GaN with >400nm PhC etched into it. PhC covered by ITO for current spreading.
[24] K. McGroddy, A. David, E. Matioli, M. Iza, S. Nakamura, S. DenBaars, J. S. Speck, C. Weisbuch, and E. L. Hu, "Directional emission control and increased light extraction in GaN photonic crystal light emitting diodes," Appl. Phys. Lett. **93**, 103502 (2008)
[25] V. Haerle, B. Hahn, S. Kaiser, A. Weimar, S. Bader, F. Eberhard, A. Plössl, and D. Eisert, "High brightness LEDs for general lighting applications using the new ThinGaN^{TM}-technology," Phys. Stat. Sol. (A) **201**, 2736 (2004).
[26] M. R. Krames, O. B. Shchekin, R. Mueller-Mach, G. O. Mueller, L. Zhou, G. Harbers, and M. G. Craford, "Status and future of high-power light-emitting diodes for solid-state lighting," J. Display Technol. **3**, 160 (2007).
[27] G. Harbers, S. J. Bierhuizen, and M. R. Krames, "Performance of high power light emitting diodes in display illumination applications," J. Display Technol. **3**, 98 (2008).
[28] A. Wilm, "Requirements on LEDs in étendue limited light engines," Proc. SPIE 7001, Laser and LED Projection, 70010F (2008).
[29] A. Taflove and S. C. Hagness, "Computational electrodynamics: the finite-difference time-domain method," (Artech House, Norwood, 2005).
[30] R. N. Hall, "Electron-hole recombination in Germanium," Phys. Rev. **87**, 387 (1952).
[31] W. Shockley and W. T. Read, "Statistics of the recombination of holes and electrons," Phys. Rev. **87**, 835 (1952).

[32] A. R. Beatti and P. T. Landsberg, "Auger effect in semiconductors," Proc. Roy. Soc. London **249**, 16 (1959).
[33] E. M. Purcell, "Spontaneous emission probabilities at radio frequencies," Phys. Rev. **69**, 681 (1946).
[34] W. N. Carr and G. E. Pittman, "One-watt GaAs p-n junction infrared source," Appl. Phys. Lett. **3**, 173 (1963).
[35] U. Zehnder, A. Weimar, U. Strauss, M. Fehrer, B. Hahn, H.-J. Lugauer, and V. Härle, "Industrial production of GaN and InGaN-light emitting diodes on SiC-substrates," J. Crystal Growth **230**, 497-502 (2001).
[36] M. R. Krames, M. Ochinai-Holocomb, G. E. Höfler, C. Carter-Coman, E. I. Chen, I.-H. Tan, P. Grillot, N. F. Gardner, H. C. Chui, J.-W. Huang, S. A. Stockman, F. A. Kish, and M. G. Craford, "High-power truncated-inverted-pyramid $(Al_xGa_{1-x})_{0.5}In_{0.5}P$/GaP light-emitting diode exhibiting >50% external quantum efficiency," Appl. Phys. Lett. **75**, 2365 (1999).
[37] I. Schnitzer, E. Yablonovitch, C. Caneau, T. J. Gmitter, and A. Scherer, "30% external quantum efficiency from surface textured, thin-film light-emitting diodes," Appl. Phys. Lett. **63**, 2174 (1993).
[38] R. Windisch, C. Rooman, S. Meinschmidt, P. Kiesel, D. Zipperer, G. H. Dohler, B. Dutta, M. Kuijk, T. Borghs, and P. Heremans, "Impact of texture-enhanced transmission on high-efficiency surface-textured light-emitting diodes," Appl. Phys. Lett. **79**, 2315 (2001).
[39] E. Yablonovitch, T. Gmitter, J. P. Harbison, and R. Bhat, "Extreme selectivity in the lift-off of epitaxial GaAs films," Appl. Phys. Lett. **51**, 2222 (1987).
[40] M. K. Kelly, O. Ambacher, R. Dimitrov, R. Handschuh, and M. Stutzmann, "Optical process for liftoff of group III-nitride films," Phys. Stat. Sol. (A) **159**, R3 (1997).
[41] W. S. Wong, T. Sands, and N. W. Cheung, "Damage-free separation of GaN thin-films from sapphire substrates," Appl. Phys. Lett. **72**, 599 (1998).
[42] R. Windisch, R. Butendeich, S. Illek, S. Kugler, R. Wirth, H. Zull, and K. Streubel, "100-lm/W InGaAlP thin-film light-emitting diodes with buried microreflectors," IEEE Photon. Technol. Lett. **19**, 774 (2007).
[43] S. Illek, I. Pietzonka, A. Plößl, P. Stauß, W. Wegleiter, R. Windisch, R. Wirth, H. Zull, and K. Streubel, "Scalability of buried micro-reflector light emitting diodes for high-current applications," Proc. SPIE LEDs: Research, Manufacturing and Applications VII, Vol. **4996**, 18-25 (2003).
[44] K. Tadatomo, H. Okagawa, Y. Ohuchi, T. Tsunekawa, Y. Imada, M. Kato, and T. Taguchi, "High output power InGaN ultraviolet light-emitting diodes fabricated on patterned substrates using metalorganic vapor phase epitaxy," Jpn. J. Appl. Phys. **40**, L583 (2001).
[45] E. F. Schubert, N. E. J. Hunt, M. Micovic, R. J. Malik, D. L. Sivco, A. Y. Cho, and G. D. Zydzik, "Highly efficient light-emitting diodes with microcavities," Science **12**, 943 (1994).
[46] H. Benisty, H. De Neve, and C. Weisbuch, "Impact of planar microcavity effects on light extraction – Part I: Basic concepts and analytical trends," IEEE J. Quantum Electron. **34**, 1612 (1998).
[47] H. Benisty, H. De Neve, and C. Weisbuch, "Impact of planar microcavity effects on light extraction – Part II: Selected exact simulations and role of photon recycling," IEEE J. Quantum Electron. **34**, 1632 (1998).
[48] R. Sharma, Y.-S. Choi, C.-F. Wang, A. David, C. Weisbuch, S. Nakamura, and E. L. Hu, "Gallium-nitride-based microcavity light-emitting diodes with air-gap distributed Bragg reflectors," Appl. Phys. Lett. **91**, 211108 (2007).

[49] R. Joray, M. Ilegems, R. P. Stanley, W. Schmid, R. Butendeich, R. Wirth, A. Jaeger, and K. Streubel, "Far-field radiation pattern of red emitting thin-film resonant cavity LEDs," IEEE Photon. Technol. Lett. **18**, 1052 (2006).
[50] C. Weisbuch, A. David, T. Fujii, C. Schwach, S. Denbaars, S. Nakamura, M. Rattier, H. Benisty, R. Houdré, R. Stanley, J. F. Carlin, T. F. Krauss, and C. J. M. Smith, "Recent results and latest views on microcavity LEDs," Proc. SPIE **5366**, 1-19 (2004).
[51] E. F. Schubert N. E. J. Hunt, R. J. Malik, M. Micovic, and D. L. Miller, "Temperature and modulation characteristics of resonant-cavity light-emitting diodes," J. Lightwave Technol. **14**, 1721 (1996).
[52] J. D. Joannopoulos, S. G. Johnson, J. N. Winn, and R. D. Meade, "Photonic crystals – Molding the flow of light," (Princeton University Press, Princeton, 2008).
[53] J.-M. Lourtioz, H. Benisty, V. Berger, J.-M. Gerard, D. Maystre, and A. Tchelnokov, "Photonic crystals: Towards nanoscale photonic devices," (Springer, Berlin, 2008).
[54] K. Sakoda, "Optical properties of photonic crystals," Springer Series in Optical Sciences Vol. 80 (Springer, Berlin, 2005).
[55] K. Busch, S. Lölkers, R. B. Wehrspohn, and H. Föll, "Photonic Crystals: advances in design, fabrication, and characterization," (Wiley-VCH, Berlin, 2004).
[56] K. Sakoda, "Optical properties of photonic crystals," Springer Series in Optical Sciences Vol. 80 (Springer, Berlin, 2005), pp. 175-179.
[57] M. J. Bergmann and H. C. Casey, "Optical-field calculations for lossy multiple-layer $Al_xGa_{1-x}N/In_xGa_{1-x}N$ laser diodes," J. Appl. Phys. **84**, 1196 (1998).
[58] J. D. Joannopoulos, S. G. Johnson, J. N. Winn, and R. D. Meade, "Photonic crystals – Molding the flow of light," (Princeton University Press, Princeton, 2008), chap. 2, p. 18.
[59] D. M. Whittaker and I. S. Culshaw, "Scattering-matrix treatment of patterned multiplayer structures," Phys. Rev. B **60**, 2610 (1999).
[60] S. G. Tikhodeev and A. L. Yablonskii, "Quasiguided modes and optical properties of photonic crystal slabs," Phys. Rev. B **66**, 045102 (2002).
[61] D. Delbeke, R. Bockstaele, P. Bienstmann, R. Baets, and H. Benisty, "High-efficiency semiconductor resonant-cavity light-emitting diodes: A review," J. Select. Topics in Quant. Electr. **8**, 189 (2002).
[62] P. Altieri, A. Jaeger, R. Windisch, N. Linder, P. Stauss, R. Oberschmid, and K. Streubel, "Internal quantum efficiency of high-brightness AlGaInP light-emitting devices," J. Appl. Phys. **98**, 086101 (2005).
[63] J.-Q. Xi, M. Ojha, J. L. Plawsky, W. N. Gill, J. K. Kim, and E. F. Schubert, "Internal high-reflectivity omni-directional reflectors," Appl. Phys. Lett. **97**, 031111 (2005).
[64] I. Gontijo, M. Boroditsky, E. Yablonovitch, S. Keller, U. K. Mishra, and S. P. DenBaars, "Coupling of InGaN quantum-well photoluminescence to silver surface plasmons," Phys. Rev. B **60**, 11564 (1999).
[65] K. Okamoto, I. Niki, A. Shvartser, Y. Narukawa, T. Mukai, and A. Scherer, "Surface-plasmon-enhanced light emitters based on InGaN quantum wells," Nat. Mat. **3**, 601 (2004).
[66] K. Okamoto, I. Niki, A. Shvartser, G. Maltezos, Y. Narukawa, T. Mukai, Y. Kawakami, and A. Scherer, "Surface plasmon enhanced bright light emission from InGaN/GaN," Phys. Stat. Sol. (A) **204**, 2103 (2007).
[67] G. Sun, J. B. Khurgin, and R. A. Soref, "Practicable enhancement of spontaneous emission using surface plasmons," Appl. Phys. Lett. **90**, 111107 (2007).

[68] J. Yoon, K. Choi, D. Shin, S. H. Song, H. S. Won, J. H. Kim, and J. M. Lee, "Enhanced external efficiency of InGaN/GaN quantum well light-emitting diodes by mediating surface plasmon-polaritons," J. Korean Phys. Soc **50**, 1018 (2007).
[69] S. Kühn, U. Håkanson, L. Rogobete, and V. Sandoghdar, "Enhancement of single-molecule fluorescence using a gold nanoparticle as an optical nanoantenna," Phys. Rev. Lett **97**, 017402 (2006).
[70] J. B. Khurgin, G. Sun, and R. A. Soref, "Electroluminescence efficiency enhancement using metal nanoparticles," Appl. Phys. Lett. **93**, 021120 (2008).
[71] P. B. Johnson and R. W. Christy, "Optical constants of the noble metals," Phys. Rev. B **6**, 4371 (1972).
[72] M. B. Stern, H. G. Craighead, P. F. Liao, and P. M. Mankiewich, "Fabrication of 20-nm structures in GaAs," Appl. Phys. Lett. **45**, 410 (1984).
[73] S. Y. Chon, P. R. Krauss, and P. J. Renstrom, "Imprint lithography with 25-nanometer resolution," Science **272**, 85 (1996).
[74] Y. Xia and G. M. Whitesides, "Soft lithography," Annu. Rev. Mater. Sci. 28, **153** (1998).
[75] S. Brueck, "Optical and interferometric lithography – Nanotechnology enablers," Proc. IEEE **93**, 1704 (2005).
[76] H. W. Deckmann and J. H. Dunsmuir, "Natural lithography," Appl. Phys. Lett. **41**, 377 (1982).
[77] W. Han, S. Fan, Q. Li, and Y. Hu, "Synthesis of gallium nitride nanorods through a carbon nanotube-confined Reaction," Science **277**, 1287 (1997).
[78] S. D. Hersee, X. Sun, and X. Wang, "The controlled growth of GaN nanowires," Nano Lett. **6**, 1808 (2006).
[79] F. Qian, S. Gradečak, Y. Li, C.-Y. Wen, and C. M. Lieber, "Core/multishell nanowire heterostructures as multicolor, high-efficiency light-emitting diodes," Nano Lett. **5**, 2287 (2005).
[80] http://www.lumerical.com/fdtd_online_help/ref_fdtd_matdb_models.php
[81] T. Fujii, Y. Gao, R. Sharma, E. L. Hu, S. P. DenBaars, and S. Nakamura, "Increase in the extraction efficiency of GaN-based light-emitting diodes via surface roughening," Appl. Phys. Lett. **84**, 855 (2004).
[82] Y. C. Shen, J. J. Wierer, M. R. Krames, M. J. Ludowise, M. S. Misra, F. Ahmed, A. Y. Kim, G. O. Mueller, J. C. Bhat, S. A. Stockman, and P. S. Martin, "Optical cavity effects in InGAN/GaN quantum-well-heterostructures flip-chip light-emitting diodes," APL **82**, 2221 (2003).
[83] T. Gessmann, E. F. Schubert, J. W. Graff, K. Streubel, and C. Karnutsch, "Omnidirectional reflective contacts for light-emitting diodes," IEEE Electron. Device Lett. **24**, 683 (2003).

Paper IV

Beam-shaping properties of InGaN thin-film micro-cavity light-emitting diodes with photonic crystals

K. Bergenek, Ch. Wiesmann, H. Zull, C. Rumbolz, R. Wirth, N. Linder, K. Streubel, T. F. Krauss

Proceedings of SPIE, Vol 7231, 72310C (2009)

Beam-shaping properties of InGaN thin-film micro-cavity light-emitting diodes with photonic crystals

K. Bergenek[a,b], Ch. Wiesmann[a], H. Zull[a], C. Rumbolz[a], R. Wirth[a], N. Linder[a], K. Streubel[a], T. F. Krauss[b]

[a] Osram Opto Semiconductors GmbH, Leibnizstr. 4, 93055 Regensburg, Germany
[b] University of St Andrews, School of Physics and Astronomy, St Andrews, Fife, KY16 9SS, United Kingdom

ABSTRACT

Photonic crystals (PhCs) are known to diffract guided modes in a light-emitting diode into the light extraction cone according to Bragg´s law. The extraction angle of a single mode is determined by the phase match between the guided mode and the reciprocal lattice vector of the PhC. Hence, light extraction by PhCs enables strong beam-shaping if the number of guided modes can be kept to a minimum. InGaN thin-film micro-cavity light-emitting diodes (MCLEDs) with photonic crystals (PhCs) emitting at 455 nm have been fabricated. The GaN layer thickness of the processed MCLEDs with a reflective metallic p-contact was 850 nm. One and two-dimensional PhCs were etched 400 nm into the n-GaN to diffract the guided light into air. The farfield radiation pattern was strongly modified depending on the lattice type and lattice constant of the PhC. Two- six- and twelve-fold symmetry was observed in the azimuthal plane from 1D lines, hexagonal lattices and Archimedean A7 lattices, respectively. The emission normal to the LED surface was enhanced by up to 330% compared with the unstructured MCLEDs. The external quantum efficiency was enhanced by 80% for extraction to air. The flux from PhC-MCLEDs in a radial lens was 15.7 mW at 20 mA and 36% external quantum efficiency was measured at 3 mA. High order diffraction was found to contribute significantly to the enhancements in efficiency and directionality. The experimental results are compared with FDTD simulations.
Keywords: light-emitting diodes, photonic crystal, cavity, InGaN

1. INTRODUCTION

The efficiency of light-emitting diodes (LEDs) in the visible range has been rapidly improving in the last few decades to emerge as one of the most efficient among all light sources. GaN is the dominating material system for ultra-violet, blue and green LEDs, whereas AlGaInP-based devices cover the remaining visible spectrum from green to hyper-red. The efficiency of LEDs is mainly limited by the internal quantum efficiency and the low light extraction efficiency. Most light in planar LEDs is captured within the semiconductor material (n=2.5 for GaN) due to total internal reflection at the air and substrate interface, respectively. Efficient light extraction requires an effective extraction mechanism while minimizing absorption losses at the electrical contacts, in a remaining growth substrate and in the semiconductor material itself. Highly efficient GaN LEDs utilize a flip-chip or a thin-film approach. In both cases a reflective metal contact/mirror is deposited on the epitaxial layers. For the thin-film approach, the growth substrate is subsequently removed by laser lift-off. The resulting layer structure is a thick GaN cavity between a metal mirror and air in which resonances in the optical field occur. Approximately $1\text{-}1/2n^2 = 92\%$ of the light emitted from the active region is caught in guided modes; a number that can be varied by placing the active region close to the bottom mirror. The light extraction can be enhanced considerably by a random surface texture[1]. This scatters the guided light arbitrarily at the GaN-air interface. In the absence of absorption in the GaN, in the electrical contacts and in the bottom mirror all light would eventually escape out of the LED after some round trips in the cavity. This approach has been proven to be very efficient and extraction efficiencies $\eta_{extr} \approx 75-80\%$ for GaN LED have been reported in encapsulation[2,3]. With these excellent values already achieved, there is little room for another great leap in extraction efficiency.

However, an improvement of the directionality of the emitted light while maintaining high light extraction efficiency may enhance the useful amount of light as it increases the coupling efficiency to étendue-limited optical systems such as projection applications[4]. The étendue E of an optical system reads[5]

Light-Emitting Diodes: Materials, Devices, and Applications for Solid State Lighting XIII, edited by Klaus P. Streubel, Heonsu Jeon, Li-Wei Tu, Proc. of SPIE Vol. 7231, 72310C

$$E = n \cdot \pi \cdot \sin^2 \theta \cdot A \quad (1)$$

The given E of the optical system determines the acceptance half-angle θ for a fixed emitting area A. Thus, the étendue sets the limit for how much light can be coupled to the optical system. For instance in the case of thin-film LEDs the random scattering of light at the rough surface leads to a Lambertian farfield pattern. This means that for an acceptance angle of 30°, only 25% of the emitted light can be coupled to the system as for a Lambertian emitter the relative fraction (referred to as directionality) of the totally emitted light within a given half-angle θ to the surface normal is given by $D(\theta) = \sin^2 \theta$. An equally efficient LED with a higher directionality would enhance the coupling to the optical system and therefore the efficiency of the whole system. It is worth mentioning that encapsulation in form of a lens does not necessarily increase the coupling to an étendue-limited system[3] despite its higher extraction efficiency. Therefore, directional emitters without encapsulation can be the most efficient choice for a light source, despite lower efficiency expressed in lm/W or a wall-plug efficiency.

Two directional light extraction schemes have been investigated thoroughly in the last 15 years: a modification of the spontaneous emission from the emitting layer in a micro-cavity[6] and diffraction of guided modes to air with shallow photonic crystals (PhC)[7]. Increased light extraction efficiency and higher directionality of the emitted light can be obtained in a micro-cavity LED (MCLED) if the active region is placed on a resonant site in a thin cavity with a single Fabry-Perot (FP) resonance and a low number of guided modes. Since the refractive index contrast between different AlInGaN material compositions is low, most realized GaN micro-cavity devices have only had a bottom metal mirror[11,12] but GaN MCLEDs with a dielectric distributed bragg reflector DBR[8,9] and GaN/air-gap DBR[10] have also been demonstrated. However, simulations have shown that close to ideal planar GaN MCLEDs with a highly reflecting metal mirror have η_{extr}<44% into epoxy[12]. The highest extraction efficiency from MCLEDs is also obtained for detuned cavities, which reduces the directionality. Since these numbers are much lower than realized values with surface roughening, it is not likely that bare GaN MCLEDs will ever outperform non-resonant devices for any acceptance angle.

Whereas the micro-cavity changes the spontaneous emission to minimize the fraction of light in guided modes, a shallow photonic crystal acts as a diffraction grating to extract these modes. It has been shown that PhC light extraction from LEDs can give a more directional farfield[13]. This effect is maximized in the single diffracted mode case, as discussed in Section 2. Attempts have been made to reach this regime with substrate LEDs[14,15] by trapping the fundamental guided mode between a low index layer and the PhC. However, the ideal case with only one mode can only be realised using a micro-cavity LED. This also gives the potential advantage of a directional background farfield from the FP resonance. It has recently been shown that the effect of improved directionality for light emitted in a micro-cavity and directional light extraction by a PhC can be combined[16]. Therefore, the PhC-MCLED is the most promising candidate to take up competition with random surface texturing devices for étendue limited systems.

As the optical losses at the contacts and the mirror are continuously being reduced in new chip designs, the difference in extraction efficiency between devices emitting to air and into encapsulation will also decrease. In a regime where the encapsulation can be omitted without efficiency loss or to offer the highest lm/$ ratio, the farfield shaping properties of PhCs can play an even more important role. Then, not only a directional farfield can offer advantages, also extremely flat farfields or farfields asymmetric in the azimuthal plane are preferable for applications such as backlighting of for an example liquid crystal displays. While Lambertian emitters would always have to rely on lenses to realize such farfields, a beam-shaping PhC-LED could manage without it. This would also increase the reliability of the devices since ageing of the encapsulant reduces the lifetime of the device[3,17]. A pre-requisite for such a future for PhC-LEDs is the ability to define the photonic crystal at a very low cost. Nano-imprint technology seems to be the most promising technology to achieve this to date.

We report on the characteristics of 850 nm thick thin-film GaN MCLEDs structured with >400 nm deep PhCs. The approach with a PhC applied on a MCLED has already been realized[18] and we show that it is possible to fabricate such devices with high efficiency and with greatly enhanced directionality. The impact of the lattice type and lattice constant is investigated in terms of general light extraction efficiency, directionality and beam-shaping flexibility. The symmetry of the different lattices can be identified from spectral farfield measurements.

2. PHOTONIC CRYSTAL LIGHT EXTRACTION

A PhC on the LED surface diffracts the light of a guided mode with an in-plane reciprocal vector $\vec{k}_i$ by the reciprocal lattice vector $\vec{G}$ of the PhC to the diffracted state $\vec{k}_d$ according to Bragg's law:

$$\vec{k}_d = \vec{k}_i - \vec{G} \tag{2}$$

with:

$$\vec{G} = G_0 \cdot (m \cdot \vec{b}_1 + n \cdot \vec{b}_2) \tag{3}$$

$$G_0 = \frac{2\lambda}{\sqrt{3}a} \tag{4}$$

$\vec{G}$ is the reciprocal lattice vector of the PhC with lattice constant a and $\vec{b}_1$ and $\vec{b}_2$ are the two normalized basis vectors of the lattice. For a hexagonal lattice, the relation between a and G_0 is given by Eq. (4). All vectors have been normalized by $k_0 = 2\pi / \lambda$. The light is extracted to air if $|\vec{k}_d| < 1$ and the extraction angle is given by $\theta = \text{asin}(|\vec{k}_d|)$. Using first order diffraction ($|\vec{G}| = G_0$), the extraction efficiency and directionality of the extracted light from a guided mode is maximized when $G_0 \approx |\vec{k}_i|$ as seen in the Ewald diagram in Fig. 1(a).

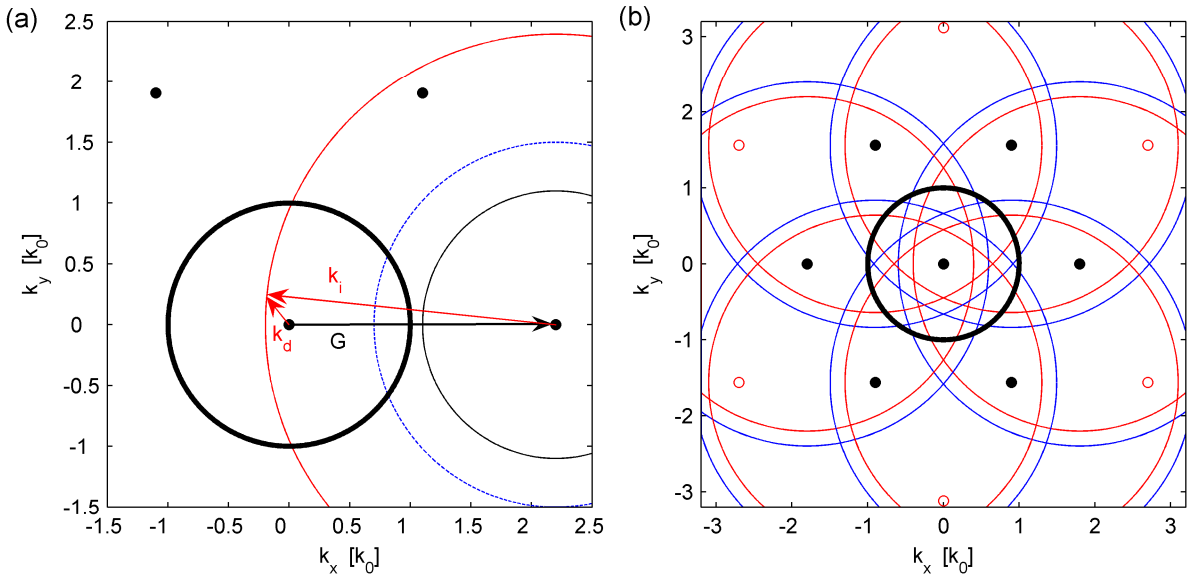

Fig. 1: Ewald diagrams (wave-vector diagrams[19]) illustrating light extraction of a mode with in-plane k-vector k_i diffracted by the reciprocal lattice vector G to the state k_d, which is inside the light extraction cone given by $|\vec{k}_{//}| < 1$ (thick black circle). A mismatch between k_i and G leads to a larger extraction angle (blue dashed line) or no diffraction at all into the light extraction cone (black line). Expected azimuthal farfield from first order diffraction of the two guided modes inside the light extraction cone (b).

Extraction of any additional mode with $k_i \neq G_0$ reduces the directionality within small extraction angles and the extraction efficiency of the additional mode is lower since the arc length of the circle within the light extraction cone is smaller as seen in Fig. 1(a). For $|k_i - G_0| > 1$ no light at all is diffracted to air from the nearest reciprocal lattice. As

long as $k_i > G_0$, the mode can still be extracted by higher order diffraction, but this is generally weaker since the diffraction strength (1/cm) for different diffraction orders is proportional to the square modulus of the Fourier transform of the photonic crystal[4,20]. The Fourier transform for first order diffraction (six nearest reciprocal lattice points in a hexagonal lattice) is roughly an order of magnitude larger than the second order depending on the air filling factor of the PhC. Therefore, the ideal case for light extraction and directionality would be a single diffracted mode containing a large fraction of the totally emitted light. This can be realised in a MCLED, which also offers the possibility to tune the farfield of the directly extracted light through the FP resonance. The other extreme is a LED with a quasi-continuum of guided modes with equal intensity. The diffracted states from this quasi-continuum would fill up the light extraction cone in Fig. 1 uniformly and result in a Lambertian farfield pattern. Hence, the beam-shaping properties of the PhC rely on the existence of a discrete set of guided modes.

The importance of the symmetry of the lattice for efficient light extraction has been discussed in recent years[4,20]. Three types of strictly periodic lattices are usually realised in the two-dimensional plane: 1D lines, square lattices and hexagonal lattices with a symmetry order of 2,4 and 6, respectively. The symmetry order tells how many nearest neighbour reciprocal lattice points the crystal has. Since spontaneous emission in LEDs is azimuthally omnidirectional, it has been argued that the symmetry order should be sufficiently high to extract light propagating in all in-plane directions by one diffraction order. High symmetry is needed for guided modes with a large effective index. A hexagonal lattice is sufficient for modes with $k_i<2$ but modes with higher effective index can not be extracted completely by one diffraction order. Quasi-crystals have higher symmetry and Archimedean tilings such as the A7 lattice[21] used in this study have twelve nearest reciprocal lattice points. This is more than sufficient for GaN LEDs for which $1<k_i<2.5$. Recent experimental results have shown however that the A7 lattice is not always more efficient than a hexagonal lattice[22,23].

3. FABRICATION

The GaN layers for our PhC-MCLEDs were grown by metal organic chemical vapour deposition on a sapphire substrate. The epitaxial layers consisted of a n-doped GaN buffer layer several microns thick followed by a single InGaN quantum well, a 20 nm thick $Al_{0.2}Ga_{0.8}N$ electron barrier and a 110 nm p-doped GaN layer. A silver-based mirror was deposited on the p-side and the wafer was then eutectically bonded to a new carrier. After laser lift-off of the sapphire substrate the n-GaN surface was cleaned in HCl and mechanically polished to obtain a smooth surface. Subsequently, the n-GaN buffer layer was dry etched to obtain the final GaN thickness of 850±50 nm. Some roughness on the chip surface can still be observed in Fig. 2(a). The PhCs (Fig. 2 (b) and (c)) were defined with electron beam lithography and etched at least 400 nm and possibly up to 550 nm into the epitaxial layers using a SiO_2 hard mask. The remaining GaN slab thickness is therefore 375±125 nm, typically corresponding to a 2-λ cavity. The lattice constant of the hexagonal PhC was varied between 226 nm and 700 nm, corresponding to a reciprocal lattice constant G_0 between 2.3 and 0.74. For comparison, Archimedean A7 lattices were also fabricated with G_0 between 2.1 and 1. The mesas were etched followed by the deposition of a 135 nm thick ITO layer to enable current spreading in the absence of the etched n-doped buffer GaN layer. A comparison of the PhC with just GaN (Fig. 2 (b) and (c)) with Fig. 2(d) shows that the ITO-layer reduces the air filling factor of the PhC as it is deposited at the sidewalls. The n-contact was deposited before the wafer was diced into square chips of 250 μm side length. The PhC-MCLEDs and bare MCLED references were mounted on TO18 headers for characterization.

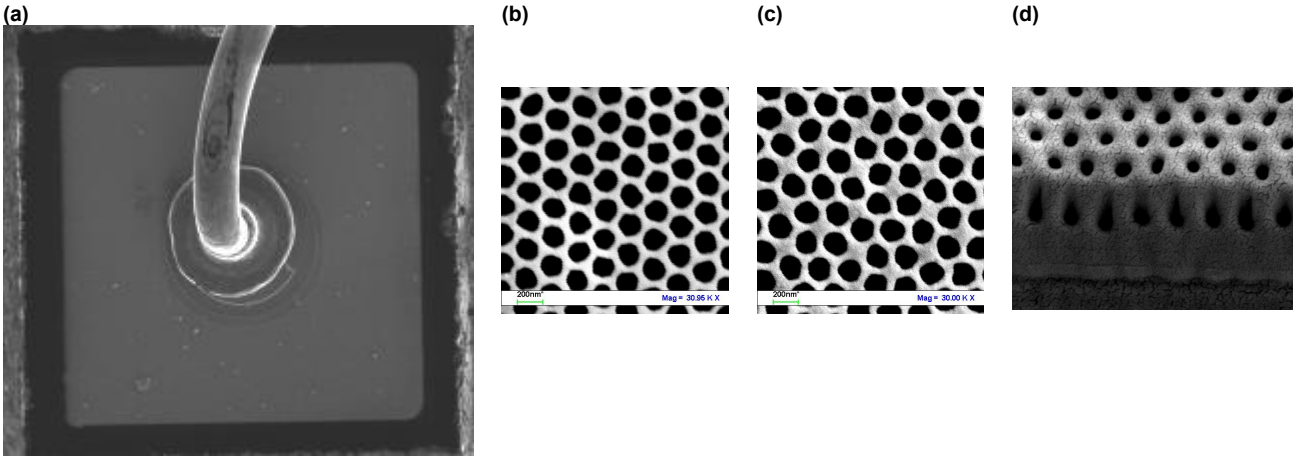

Fig. 2: SEM images: MCLED chip with 250 µm side length (a), hexagonal lattice a=224 nm (b), A7 lattice a=250 nm (c), vertical cross section of a PhC-MCLED with ITO deposited on the surface (d)

4. RESULTS

4.1 Light extraction

The emitted flux of the LEDs was measured under DC operation in an integrating sphere. The emitted flux for the PhC-MCLEDs measured at 20 mA is plotted in Fig. 3 as a function of the reciprocal lattice constant G_0. We consider first the devices with the hexagonal lattices. 10.7 mW is emitted from a hexagonal PhC-MCLED with G_0=1.7 (a=304 nm), an enhancement of 81% compared to the 5.9 mW from the best bare MCLED. The variation in flux between the different lattice constants is surprisingly small. Even the largest lattice constant with G_0=0.74 is only slightly less efficient despite the fact that no guided modes exist that can be extracted in the vertical direction by first order diffraction. The difference between hexagonal and A7 lattices is also small – whereas the hexagonal lattices are most efficient for most lattice constants, the highest flux among all PhC-MCLEDs (10.9 mW) comes from an A7 lattice with G_0=1.5. The very similar performance of the two lattices is in accordance with recent results in Refs. 22-23, suggesting that the use of quasi-crystals does not bring any advantage over the hexagonal lattice regarding light extraction efficiency.

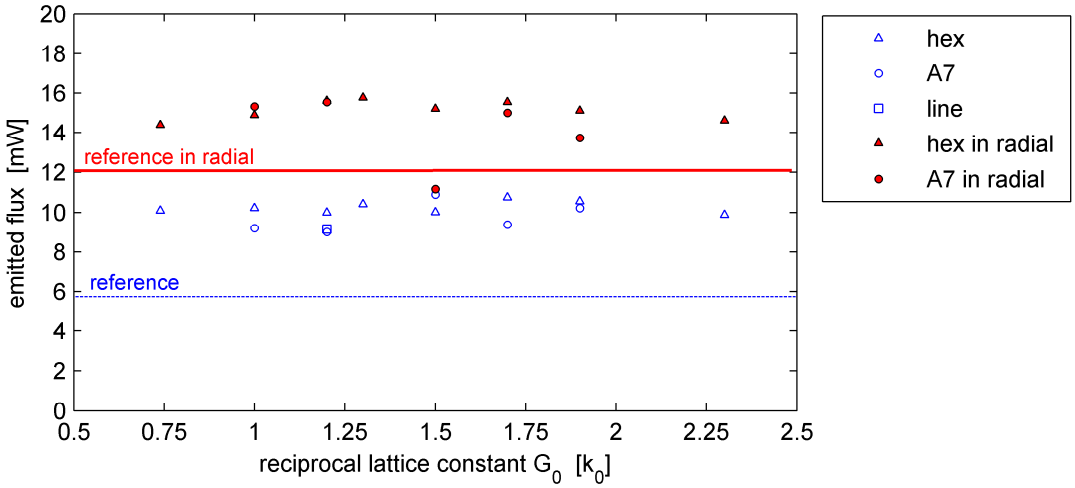

Fig. 3: Emitted flux at 20 mA as a function of the reciprocal lattice constant for hexagonal, A7 and line lattices for emission to air (open marks) and in a radial lens (filled marks). Dashed and solid lines correspond to the emitted flux from the reference devices to air and in a radial lens, respectively.

To compare the efficiency of our PhC-MCLEDs with commercial LEDs with surface roughening, we also mounted devices in a 5 mm radial epoxy lens for integrating sphere measurements. The emitted flux at 20 mA (Fig. 3) is 15.8 mW for a device with G_0=1.3 and the peak external quantum efficiency $\eta_{QE} = 36\%$ is measured at 3 mA. The variation between different lattice constants is very small also in epoxy. The emitted flux at 20 mA is lower than for standard processed LEDs with surface roughening. The emitted flux from such devices with similar epitaxial quality as for our devices is typically 20 mW. The 20% loss in extraction efficiency can partially be attributed to absorption in the top ITO layer: We simulate the extraction efficiency for the bare MCLED into epoxy with the 1D method given in Ref. 24. The spontaneous emission from the quantum well is assumed to radiate only into horizontal dipoles. The extraction efficiency η_{extr} is 37% when we include absorption in the ITO-layer. The same simulation but without ITO absorption yields a 16% increase to η_{extr} =43%. A similar efficiency drop can be expected for the PhC-MCLED devices and this explains to a large extent the worse performance compared to the commercial type devices. We conclude that the extraction strength of PhCs is close to but not superior to the extraction strength of surface roughening. Hence, the only potential advantage with PhC light extraction lies in its beam-shaping properties in the farfield.

To estimate the light extraction efficiency of the PhC-MCLEDs, 3D FDTD simulations with horizontal dipoles are used as described in Ref. 4. A 30 µm large integration radius was used for the calculation and the final values were then extrapolated with an exponential function. The GaN is assumed to be free of absorption whereas experimental values are used for the ITO absorption. A very conservative estimation of the mirror reflectivity to 90% under normal incidence was assumed. The extraction efficiency to air is then 31% for G_0= 1.7 and 32% for G_0=1.2. Considering the experimental peak efficiency $\eta_{QE} = 25\%$ to air at 3 mA and an internal quantum efficiency well below estimated top efficiencies[3] $\eta_{\text{int}} < 70\%$ for GaN LEDs, the simulated extraction efficiencies are clearly too low. This can be attributed to the low mirror reflectivity assumed in the simulation. The interesting result here is that – just as for the experimental results - the extraction efficiency is almost equal despite the large change in reciprocal lattice constant.

4.2 Beam-shape of the emitted light

We now turn to the beam-shape of the light emitted from the PhC-MCLEDs. The radiant intensity I of the LEDs on TO18 headers was measured in a radiant tube that collects the emitted light within 0.01sr to the surface normal. Additionally, spectrally resolved farfields were collected with an optical fibre mounted on a rotating arm connected to a spectrometer. The step size was $\Delta\theta = 1°$.

Directionality

The radiant intensity I is plotted as a function of G_0 in Fig. 4(a). In contrast to the emitted flux, there is a strong variation depending on the lattice constant and the lattice type. 4.35 mW/sr is measured at 20 mA for a hexagonal lattice with G_0=1.2 (a=432 nm) corresponding to an enhancement factor 4.3 compared with the bare MCLEDs. The decline for larger reciprocal lattice constants is quite steep and G_0=1.5 has the lowest radiant intensity among the fabricated hexagonal devices. The dependency on G_0 for the A7 devices is similar but the variation is smaller. The radiant intensity for G_0=1.2 is 3.28 mW/sr, which is less than for the corresponding hexagonal PhC-MCLED.

Most LED applications however have a much larger acceptance angle than ~3° that is collected for the radiant intensity measurement. We use the farfield measurements to obtain the directionality of the emitted light within different angles. The integrated intensity within the acceptance angle θ was calculated as

$$P(\theta) = 2\pi \cdot \int_0^{\theta} I(\theta') \cdot \sin\theta' \cdot d\theta' \approx 2\pi \sum_{\theta' < \theta} I(\theta') \cdot \sin\theta' \cdot \Delta\theta' \qquad (5)$$

where I(θ') is the mean farfield intensity measured at the angle θ' (step size $\Delta\theta' = 1°$) for ten azimuthal angles spread between the symmetry directions of the lattices. We compare the structured devices with the bare reference and plot the PhC gain $P_{PhC}(\theta) / P_{ref}(\theta)$ as a function of the acceptance angle in Fig. 4(b) for a few lattice constants. Clearly, the optimal lattice constant depends on the acceptance angle with a shift to larger G with increasing acceptance angle. For the hexagonal lattices, highest integrated intensity within small acceptance angles θ<18° is obtained for G_0=1.2, a

slightly larger G_0=1.3 is optimal between 18° and 30° (not shown for figure clarity) and G=1.5 between 30° and 55°. The PhC gain declines with increasing acceptance angle from a value between 1.9 and 4.4 at θ=1° to less than 2 for the total emitted light at θ=90°. It should be noted that the high gain factors for small acceptance angles are partially caused by an anti-directional reference farfield from the bare MCLED. The FP is strongly detuned with a peak at 50°-60° for λ=455 nm. The peak angle of the FP resonance is dominantly determined by the optical length between the active quantum well and the bottom mirror. Simulations show that a 10-20 nm thinner p-side would be ideal for directional light extraction in the micro-cavity regime. The anti-directional FP resonance caused by the detuned p-side is present also for the devices with PhC and it causes an anti-directional background farfield to the diffracted light. Therefore the relative directionality gain compared to a Lambertian emitter is relatively small. It is given by $D(\theta)/D_{Lam}(\theta)$, where $D(\theta)=P(\theta)/P(90°)$ and it is plotted in Fig. 4(c). The directionality improvement over a Lambertian radiation pattern for small angles is larger than 40% but it declines quickly to below 20% for θ>20°. The PhC gain and directionality gain for the A7 devices depend similarly on the acceptance angle as the hexagonal MCLEDs but with slightly varying amplitude.

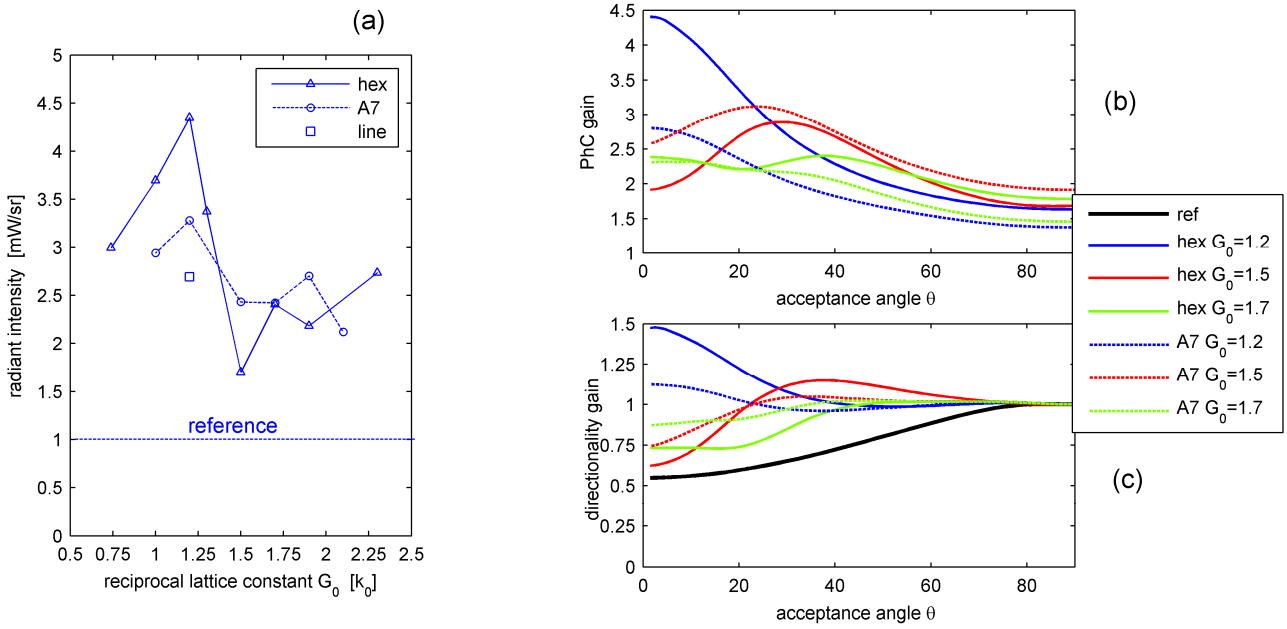

Fig. 4 Radiant intensity as a function of G_0 (a); PhC gain within acceptance angle θ compared to the flat MCLEDs (b) and directionality gain within the acceptance angle θ compared to a Lambertian emitter.

Azimuthal uniformity of the farfields

The azimuthal farfield is of particular interest for PhC-LEDs since it is influenced by the symmetry of the lattice. Monochromatic azimuthal farfields with $\Delta\varphi=3°$ for hexagonal and A7 PhC-MCLEDs are seen in Fig. 5 (a)-(b).

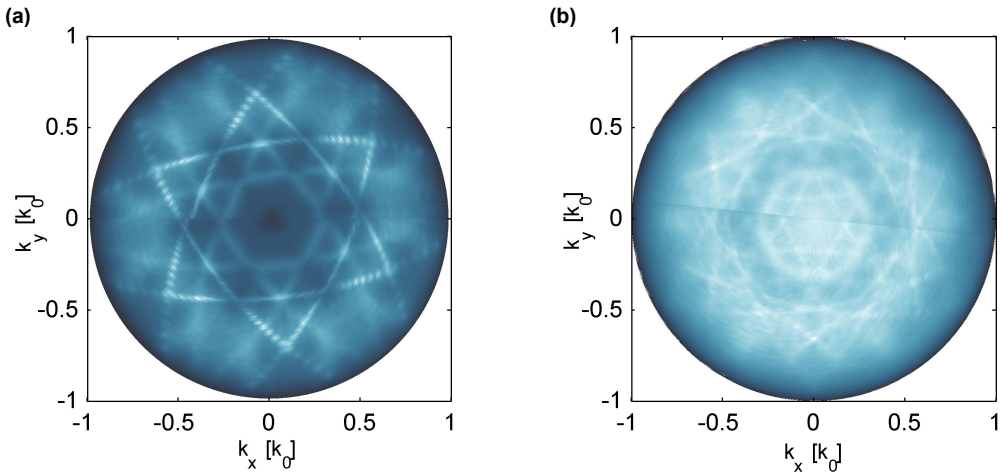

Fig. 5: Azimuthal monochromatic farfields showing the symmetry of the lattices: hexagonal, $a/\lambda=0.59$ (a) and A7, $a/\lambda=0.58$ (b)

Two sets of diffraction lines in Fig. 5(a) form two stars with hexagonal symmetry. These diffraction lines correspond to the extraction of two guided modes with $k_i=2.4$ and 2.2, respectively, in excellent agreement with the expected pattern from two guided modes diffracted by a hexagonal lattice as shown in the Ewald diagram in Fig. 1(b). Twelve-fold symmetry is observed for the A7 lattice in Fig. 5(b). The line intensity is lower and smeared out compared to the lines from the hexagonal lattice. This is understandable since roughly the same diffraction strength is distributed over twelve reciprocal lattice points instead of six points for the hexagonal lattice. The azimuthal farfield from a 1D lattice in Fig. 6(a) has only got two diffraction lines as expected and it is therefore very asymmetric. This device with $G_0=1.2$ was fabricated together with the two-dimensional lattices. The corresponding farfields parallel and orthogonal to the lattice are plotted in Fig. 6(b).

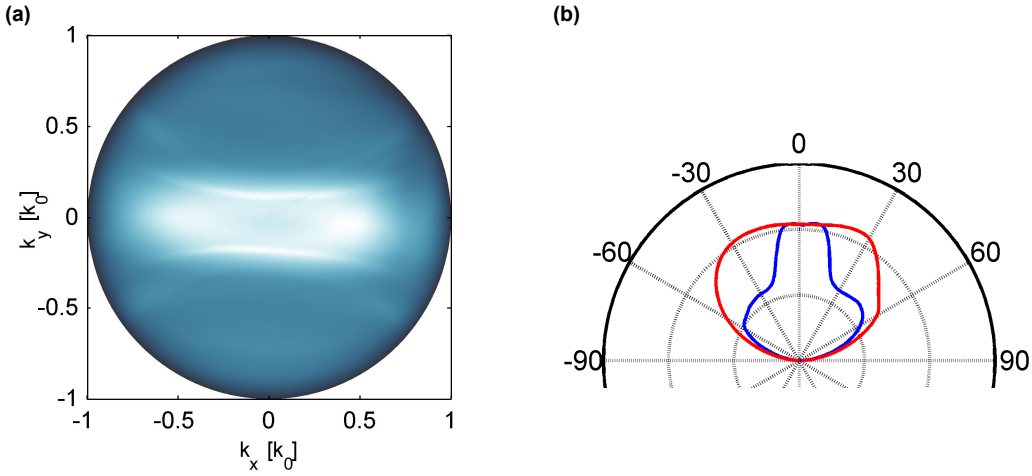

Fig. 6: Azimuthal monochromatic farfield ($a/\lambda=0.79$) of a PhC-MCLED with a 1D lattice with $G_0=1.2$ (a) and farfield measured parallel and orthogonal to the lattice (b).

In order to measure the azimuthal uniformity we calculated the azimuthal contrast C_φ as:

$$C_\varphi(\theta) = \frac{I(\theta)^{\max} - I(\theta)^{\min}}{I(\theta)^{\max} + I(\theta)^{\min}} \quad (5)$$

The highest azimuthal contrast of 20-27% is measured between θ=20° and θ=40° for the 1D grating. For comparison, the azimuthal contrast for the 2D lattices is at least a factor 2 lower and the A7 lattices have the lowest contrast for most lattice constants as for an example seen in Fig. 5 (a)-(b). Despite the lack of omnidirectional extraction for the 1D lattice, the emitted flux at 20 mA is very close the hexagonal PhC-MCLED and even better than the A7 device (Fig. 3). The radiant intensity on the other hand (Fig. 4(a)) is lower than for both two-dimensional lattices.

In conclusion, the farfield shape is determined by the Fabry-Perot resonance given by the micro-cavity and the lattice of the PhC. By correctly tuning these two parameters, directional or flat farfields can be designed at the cost of only marginal changes in the light extraction efficiency. The impact of the FP resonance was found to be large also for the MCLEDs with PhCs. Whereas the farfield shaping from the FP resonance and the PhC diffraction counteracted each other for the presented devices, even more extreme farfields could in principle be achieved if the corresponding contributions constructively interact. The coupling to an external optical system with a limited acceptance angle can be optimized by choosing the correct lattice constant as shown in Fig. 4(b). For our devices, G_0=1.2 is optimal for very small acceptance angles but larger reciprocal lattice constants should be used for applications with typical acceptance angles between 30-45°. The symmetry order of the lattice changes the azimuthal uniformity of the farfield but the overall extraction efficiency changes just marginally. Non-symmetric azimuthal farfields can therefore be realized with a 1D grating.

4.3 High order diffraction

As mentioned in Section 2, it is generally assumed that only first order diffraction contributes substantially to the light extraction of guided modes. Fig. 7 shows the azimuthal farfield for the most efficient hexagonal PhC-MCLED with G_0=1.7 and λ=475 nm. Two sets of six lines are rotated by 30° relative to another, corresponding to the azimuthal angle shift between the ΓM- and ΓK-direction of the hexagonal lattice. This suggests that not only first order diffraction occurs (six nearest reciprocal lattice points) but also second order diffraction (second nearest set of points)

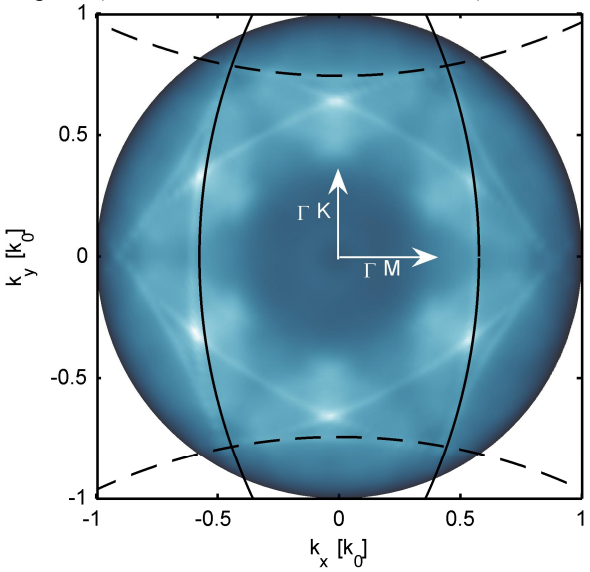

Fig. 7: Azimuthal farfield (a/λ=0.64) for a hexagonal PhC-MCLED with G_0=1.7. Predicted lines for first (solid) and second order (dashed) diffraction are super-imposed.

By extracting the effective index $|\vec{k}_i|$ from any first order line in the ΓM-direction using Eq. 2, the line for the second order diffraction can be predicted. The first and second order lines with the same effective index are super-imposed in Fig. 7. They are in excellent agreement with the measured azimuthal farfield, which proves that the same guided mode is diffracted by the first as well as the second diffraction order. As seen in the figure, the line intensity is similar for the two diffraction orders. This is very unexpected since it is not conform to the diffraction strength argument in Section 2. Further analysis of the farfield patterns to explain this result will be published elsewhere.

5. CONCLUSIONS AND PERSPECTIVES

A very large fraction of the spontaneously emitted light in a planar LED is caught in guided modes. Photonic crystals extract these modes to air in a predictable way and the extraction angle can be calculated by Braggs´s law in Eq. (2). It is therefore possible to design the farfield emission pattern by changing the lattice constant of the photonic crystal, its symmetry and the vertical layer stack of the LED. Devices with a directional farfield are of particular interest since they can couple more light to étendue limited optical systems. The possibility to shape the farfield declines with an increasing number of guided modes. Therefore, the strongest effects can be expected from micro-cavity LEDs with photonic crystals.

Aiming towards the optimal PhC-MCLED, we reported on the characteristics of 850 nm thick thin-film GaN MCLEDs structured with >400 nm deep PhCs. Since only a few guided modes dominated the farfields, a strong variation of the farfield shape was observed as the PhC parameters were varied. It was shown that the optimal choice of lattice constant depends on the acceptance angle of the optical system collecting the light. The radiant intensity could be enhanced by a factor of 4.3 compared to MCLEDs without the photonic crystal. It was also shown that a 1D lattice can be used to obtain a farfield pattern with high azimuthal contrast with only a small efficiency loss compared to that of a hexagonal lattice. The efficiency of the PhC devices was lower than for state-of-the-art LEDs with surface roughening but still on a comparable level. Simulations showed that the lower efficiency was to a large extent caused by the introduction of an absorbing ITO contact layer. The low number of extracted modes in the farfields unexpectedly allowed us to identify strong diffraction of the second order for the most efficient hexagonal PhC-MCLED. Further analysis is needed to evaluate the role of high order diffraction in the micro-cavity regime.

ACKNOWLEDGEMENTS

Part of the processing work was done at MC2 Nanofabrication Laboratory, Chalmers University of Technology, Göteborg, Sweden and was financed by the FP6-Research Infrastructures program MC2ACCESS with Contract No: 026029.

REFERENCES

[1] Schnitzer, I, Yablonivitch, E., Caneau, C., Gmitter, T. J., Scherer, A., "30% external quantum efficiency from surface textured, thin-film light-emitting diodes", Appl. Phys. Lett. 63, 2174-2176 (1993).

[2] Haerle, V., Hahn, B, Kaiser, S., Weimar, A., Bader, S., Eberhard, F, Plössl, A., Eisert,D., "High brightness LEDs for general lighting applications Using the new ThinGaNTM-Technology", Phys. Stat. Sol. (A) 201(12), 2736-2739 (2004).

[3] Krames, M. R., Shcekin, O. B., Mueller-Mach, R., Mueller, G. O., Zhou, L., Harbers, G., Craford, M. G., "Status and Future of High-Power Light-Emitting Diodes for Solid-State Lighting", IEEE J. Display Technol. 3(2), 160-175 (2007).

[4] Wiesmann, Ch., Bergenek, K., Linder, N., Schwarz, U. T., "Photonic crystal LEDs - designing light extraction", Laser & Photon. Rev., DOI: 10.1002/ lpor.200810053 (2008).

[5] Harbers, G., Bierhuizen, S. J., Krames, M. R., "Performance of High Power Light Emitting Diodes in Display Illumination Applications", IEEE J. Display Technol. 3(2), 98-109 (2007).

[6] Schubert, E. F., Wang, Y.-H., Cho, A. Y., Tu, L.-W., Zydzik, G. J., "Resonant cavity light-emitting diode", Appl. Phys. Lett. 60, 921 (1992)

[7] Erchak, A. A., Ripin, D. J., Fan, S., Rakich, P., Joannopoulos, J. D., Ippen, E. P., Petrich, G. S., Kolodziejski, L. A., "Enhanced coupling to vertical radiation using a two-dimensional photonic crystal in a semiconductor light-emitting diode", Appl. Phys. Lett. 78, 563-565 (2001)

[8] Huang, G. S., Lu, T. C., Kuo, H. C., Wang, S. C., Chen, H-G., "Fabrication of Microcavity Light-Emitting Diodes Using Highly Reflective AlN-GaN and Ta_2O_5-SiO_2 Distributed Bragg Mirrors", IEEE Photonics Tech. L. 19(13), 999-1001 (2007).

[9] Rizzi, F., Edwards, P. R., Betjka, K., Semond, F., Kang, X. N., Zhang, G. Y., Gu, E., Dawson, M. D., Watson, I. M., Martin, R. W., "(In,Ga)N/GaN microcavities with double dielectric mirrors fabricated by selective removal of an (Al,In)N sacrificial layer," Appl. Phys. Lett. 90, 111112 (2007) .

[10] Sharma, R., Choi, Y-S. , Wang, C-F., David, A., Weisbuch, C., Nakamura, S, Hu, E. L., "Gallium-nitride-based microcavity light-emitting diodes with air-gap distributed Bragg reflectors", Appl. Phys. Lett. 91, 211108 (2007).

[11] Fujii, T., David, A., Schwach, C., Pattison, P. M., Sharma, R., Fujito, K., Margalith, T., DenBaars, S. P., Weisbuch, C., Nakamura, S., "Micro Cavity Effect in GaN-Based Light-Emitting Diodes Formed by Laser Lift-Off and Etch-Back Technique", Jpn J Appl. Phys. 43(3B), L411-413 (2004).

[12] Weisbuch, C, David, A, Fujii, T., Schwach, C., DenBaars, S. P., Nakamura, S., Rattier, M., Benisty, H., Houdré, R., Stanley, R. P., Carlin, J. F., Krauss, T. F., Smith, C. J. M., "Recent results and latest views on microcavities LED", Proc. SPIE 5366, 1-19 (2004).

[13] Wierer, J. J., Krames, M. R., Epler, J. E., Gardner, N. F., Craford, M. G., Wendt, J. R., Simmons, J. A., Sigalas, M. M., "InGaN/GaN quantum-well heterostructure light-emitting diodes employing photonic crystal structures", Appl. Phys. Lett. 84, 3885-3887 (2004).

[14] David, A., Fujii, T., Sharma, R., McGroddy, K., Nakamura, S., DenBaars, S. P., Hu, E. L., Weisbuch, C., Benisty, H., "Photonic-crystal GaN light-emitting diodes with tailored guided modes distribution", Appl. Phys. Lett. 88, 061124 (2006).

[15] McGroddy, K., David, A., Matioli, E., Iza, M., Nakamura, S., DenBaars, S., Speck, J. S., Weisbuch, C. & Hu, E. L., "Directional emission control and increased light extraction in GaN photonic crystal light emitting diodes", Appl. Phys. Lett. 93, 103502 (2008)

[16] Bergenek, K., Wiesmann, Ch., Zull, H., Wirth, R., Sundgren, P., Linder, N., Streubel, K., Krauss, T. F., "Directional light extraction from thin-film resonant cavity light-emitting diodes with a photonic crystal" Appl. Phys. Lett. 93(23), 231109 (2008).

[17] Narendran, N., Gu, Y., Freyssinier, J. P., Yu, H., Deng, L., "Solid-state lighting: Failure analysis of white LEDs", J. Cryst. Growth 268, 449-456, (2004).

[18] David, A., Fujii, T., Moran, B., Nakamura, S., DenBaars, S. P., Weisbuch C., Benisty, H., "Photonic crystal laser lift-off GaN light-emitting diodes", Appl. Phys. Lett. 88, 133514 (2006) .

[19] Delbeke, D., Bienstman, P., Bockstaele, R., Baets, R., "Rigorous electromagnetic analysis of dipole emission in periodically corrugated layers: the grating-assisted resonant-cavity light-emitting diode", J. Opt. Soc. Am. A 19, 871-880 (2002).

[20] David, A., Benisty, H., Weisbuch, C., "Optimization of Light-Diffracting Photonic-Crystals for High Extraction Efficiency LEDs", IEEE J Display Technol. 3(2), 133-148 (2007).

[21] Rattier, M., Benisty, H., Schwoob, E., Weisbuch, C., Krauss, T. F., Smith, C. J. M., Houdré, R. and Oesterle, U., "Omnidirectional and compact guided light extraction from Archimedean photonic lattices", Appl. Phys. Lett. 83, 1283-1285 (2003).

[22] Bergenek, K., Wiesmann, Ch., Wirth, R., O'Faolain, L., Linder, N., Streubel, K. & Krauss, T. F, "Enhanced light extraction efficiency from AlGaInP thin-film light-emitting diodes with photonic crystals", Appl. Phys. Lett. 93, 041105 (2008).

[23] Benisty, H., Danglot, J., Talneau, A., Enoch, S., Pottage, J.M., David, A., "Investigation of Extracting Photonic Crystal Lattices for Guided Modes of GaAs-Based Heterostructures", IEEE J. Quantum Electronics 44, 777-789 (2008).

[24] Wasey, J. A. E., Barnes, W. L., "Efficiency of spontaneous emission from planar microcavities", J Mod Optics 47(5), 725-741 (2000).

Paper V

Strong high order diffraction of guided modes in micro-cavity light-emitting diodes with hexagonal photonic crystals

Krister Bergenek, Christopher Wiesmann, Heribert Zull, Christian Rumbolz, Ralph Wirth, Norbert Linder, Klaus Streubel and Thomas F. Krauss

Accepted for publication in IEEE Journal of Quantum Electronics
on 23 April 2009

Strong high order diffraction of guided modes in micro-cavity light-emitting diodes with hexagonal photonic crystals

Krister Bergenek, Christopher Wiesmann, Heribert Zull, Christian Rumbolz, Ralph Wirth, Norbert Linder, Klaus Streubel and Thomas F. Krauss

***Abstract*—Photonic crystals (PhCs) have now been firmly established as an efficient means for light extraction from light emitting diodes (LEDs). We analyze the diffraction properties from thin GaN micro-cavity LEDs with hexagonal lattices that feature three guided TE modes only. In contrast to common design rules, we find that high order diffraction contributes significantly to the light extraction and increases the directionality of the emitted light. The implementation of the PhC leads to an enhancement in light extraction by a factor of up to 1.8 and the directionality of the light is greatly improved with a radiant intensity enhancement factor of 4.3, which can only be explained by the higher order diffraction that has been hitherto neglected. Furthermore, we show that higher order diffraction contributes significantly to the high azimuthal extraction uniformity we observe, suggesting that the use of quasi-crystal lattices is not necessary. We use a model including mode absorption where each in-plane angle of the guided modes is treated separately in order to explain the experimental results.**

***Index Terms*— light-emitting diode, microcavity, InGaN, photonic crystal, diffraction**

I. Introduction

Over the last twenty years, solid state light emitting diodes (LEDs) have emerged as one of the most efficient light sources [1]. The efficiency of LEDs is mainly limited by the internal quantum efficiency and the low light extraction efficiency due to total internal reflection at the interface between the high-index semiconductor and air. Photonic crystals can enhance the light extraction from light emitting diodes in two ways. Firstly, the spontaneous emission rate from the radiating quantum wells can be changed by modifying the optical density of states available to the emitter. By operating the device at a frequency with a photonic bandgap, the emission into guided modes can then be suppressed [2],[3]. In this way the light is forced into radiating modes that escape the high-index semiconductor. A complete band gap can only be obtained if the emitting layers are within the photonic crystal, which requires deep etching. Since etching through the emitting layer induces non-radiative loss channels, this effect has only been demonstrated at cryogenic temperatures [4]. Alternatively, a shallow photonic crystal can be applied to the surface of the semiconductor slab to enable diffraction of guided light into air [5]-[6]. In this latter case, the spontaneous light emission and the light extraction can be considered as two separate problems. The light diffraction is described by Bragg`s law, where the initial and diffracted state of the light are denoted by their in-plane k-vectors in the reciprocal space:

$$\vec{k}_d = \vec{k}_i - \vec{G} \qquad (1)$$

$\vec{k}_i$ and $\vec{k}_d$ are the initial and diffracted k-vectors, respectively, after diffraction by a reciprocal lattice vector $\vec{G} = G_0 \cdot (m \cdot \vec{b}_1 + n \cdot \vec{b}_2)$. $\vec{G}$ is a reciprocal lattice vector of the PhC and for a hexagonal lattice $G_0 = \frac{2\lambda}{\sqrt{3}a}$, a is the lattice constant and $\vec{b}_1 = (1,0)$ and $\vec{b}_2 = (1/2, \sqrt{3}/2)$. All vectors have been normalized by $k_0 = 2\pi/\lambda$. The light is extracted to air if $|\vec{k}_d| < 1$ and the extraction angle is given by $\theta = \mathrm{asin}(|\vec{k}_d|)$. Hence, the light extraction angle for diffracted light from a guided mode can be controlled and a more directional farfield can be obtained than for Lambertian emitters [7]-[9]. The corresponding diffraction strength β (1/cm) for different diffraction orders is proportional to the square modulus of the Fourier transform of the photonic crystal. With an air filling factor 0.5 of the PhC, the diffraction strength ratio between the first and second order is $\beta_1 / \beta_2 = 8.0$. The calculation of the diffraction strength is described in Appendix A. Often, a smaller air filling factor is used [7], [10], which results in even larger ratios. It is therefore generally assumed that higher order diffraction can be neglected for light extraction from LEDs [10]. Using first

Manuscript received February x, 2009.

Part of the processing work was done at MC2 Nanofabrication Laboratory, Chalmers University of Technology, Göteborg, Sweden and was financed by the FP6-Research Infrastructures program MC2ACCESS with Contract No: 026029.

Krister Bergenek is with Osram Opto Semiconductors GmbH, Leibnizstr. 4, 93055 Regensburg, Germany and University of St Andrews, School of Physics and Astronomy, St Andrews, Fife, KY16 9SS, United Kingdom, phone: +49-15115012451; fax: +49-941 8501090; e-mail: krister.bergenek@osram-os.com.

Christopher Wiesmann, Heribert Zull, Christian Rumbolz, Ralph Wirth, Norbert Linder and Klaus Streubel are with Osram Opto Semiconductors GmbH, Leibnizstr. 4, 93055 Regensburg, Germany

Thomas F. Krauss is with University of St Andrews, School of Physics and Astronomy, St Andrews, Fife, KY16 9SS, United Kingdom

order diffraction ($|\vec{G}| = G_0$), the extraction efficiency and directionality of the extracted light from a guided mode is maximized when $G_0 \approx |\vec{k}_i|$. The existence of additional modes with $k_i \neq G_0$ reduces the light extraction efficiency and the directionality within small extraction angles, so a single diffracted mode regime is desirable. A concentration of much spontaneous emission into one mode has been demonstrated also with very thick cavities like GaN-LEDs with a thick sapphire substrate [11]. This was achieved by optimizing the vertical layer stack composition and the emitting layer position. However, the existence of empty modes, such as substrate modes, offers competing diffraction channels to the radiating modes. Hence, the highest light extraction is achieved when no other guided modes exist and diffraction to air is the only loss channel together with material absorption. Recent simulations with the finite difference time domain (FDTD) method in [12] have shown that the extraction efficiency to air can be increased to 70% by reducing the cavity thickness to 650 nm.

Aiming towards the single diffracted mode PhC-LED, we report on the diffraction properties of 850 nm thick GaN micro-cavity LEDs (MCLEDs) structured with >400 nm deep hexagonal PhCs with different lattice constants. Spectral resolved farfield measurements reveal that high order diffraction contributes substantially to the light extraction and that the highest extraction efficiency is obtained when G_0 allows both first and second order diffraction. This somewhat surprising result is explained by a model where absorption is included and where the in-plane degeneracy of the guided mode has been lifted.

II. Fabrication

The GaN layers were grown by metal organic chemical vapour deposition on a sapphire substrate. The epitaxial layers consisted of a several microns thick n-doped GaN buffer layer followed by a single InGaN quantum well, a 20 nm thick $Al_{0.2}Ga_{0.8}N$ electron barrier and a 110 nm p-doped GaN layer. An Ag-based mirror was deposited on the p-side and the wafer was then eutectically bonded to a Ge-carrier. After laser lift-off of the sapphire substrate, the n-GaN surface was cleaned in HCl and mechanically polished to remove crystal defect induced surface roughness. Subsequently, the n-GaN buffer layer was dry etched to obtain the final GaN thickness of 850±50 nm. The hexagonal PhC on the surface was defined with electron beam lithography and etched to a depth of 400-550 nm (depending on hole size) using a SiO_2 hard mask. The thickness of the remaining GaN slab - containing the emitting quantum well - is therefore 375±125 nm, corresponding to a 2λ cavity. The lattice constant of the hexagonal PhC was varied between 226 nm and 700 nm, corresponding to a reciprocal lattice constant G_0 between 2.3 and 0.74. Mesas were etched followed by the deposition of a 135 nm thick ITO layer to enable current spreading in the absence of the etched n-doped buffer GaN layer. This resulted in a homogenous current distribution on the chip, but the non-optimized contact led to a high forward voltage around 4.5V at 20 mA - much more than for state-of-the-art LEDs. The ITO was to some extent also deposited on the PhC side-walls, thus reducing the air filling factor. The n-contact was deposited before the wafer was diced into square chips with 250 µm side length. The PhC-MCLEDs and bare MCLED references were mounted on TO18 headers for characterization.

III. Experimental Results

The emitted flux of the LEDs was measured under DC operation in an integrating sphere. The emitted flux for PhC-MCLEDs measured at 20 mA is plotted in Fig. 1(a) as a function of G_0.

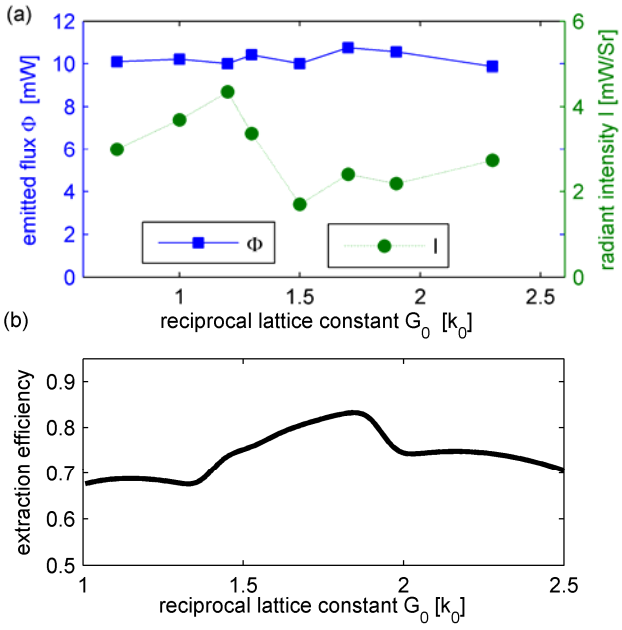

Fig. 1: Emitted flux (squares) and radiant intensity (circles) for PhC-MCLEDs with different reciprocal lattice constants measured at 20 mA (a). Simulated extraction efficiency of mode I as a function of G_0 (b).

10.7 mW is emitted from a PhC-MCLED with G_0=1.7 (a=304 nm), an enhancement larger than 80% compared to the 5.9 mW from the best bare MCLED. The variation in flux between the different lattice constants is small, which is surprising considering the large range of lattice constants. The radiant intensity in the direction vertical to the LED surface, on the other hand, varies strongly with the lattice constant as also seen in Fig. 1(a) and 4.35 mW/sr is measured at 20 mA for G_0=1.2 (a=432 nm) which is a 330% increase compared to the bare MCLED. This high enhancement is achieved because the MCLED itself has a flat farfield. In conclusion, the extraction efficiency depends only weakly on the lattice constant but the farfield radiation pattern from the PhC-MCLEDs varies strongly.

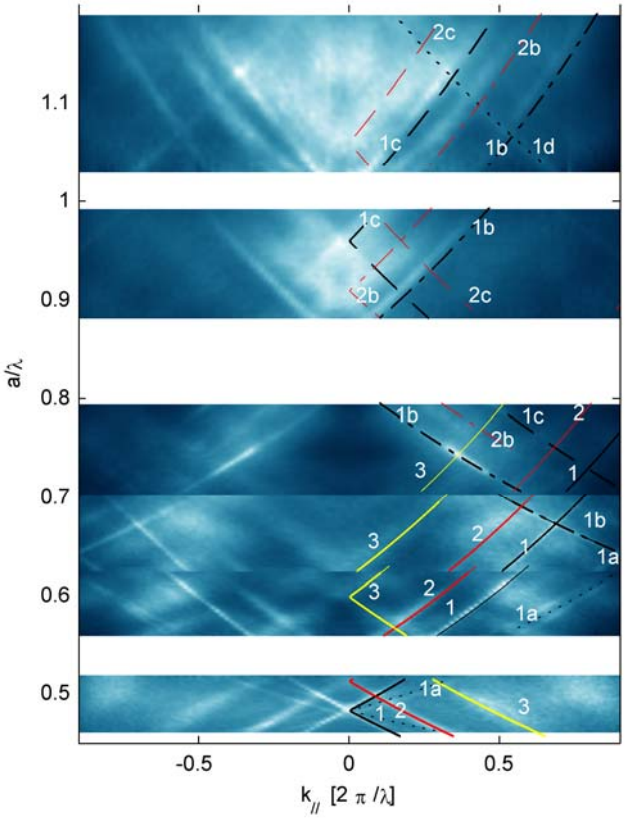

Fig. 2: "Photonic band diagram": Spectral resolved farfields for TE polarized light collected in the ΓM-direction for different lattice constants. Three modes are detected altogether. Predicted diffraction lines from modes I-III are superimposed. b-,c- and d-lines are caused by diffraction of second, third and fourth order, respectively.

Spectral resolved farfield measurements are used to analyze the mode dispersion in the PhC-MCLEDs [13]. The farfields were collected with an optical fibre mounted on a rotating arm connected to a spectrometer and the in-plane k-vector was calculated as $k_{//} = \sin\theta$. The large spread in fabricated lattice constants allows us to put their farfields together to mimic a photonic band diagram for the ΓM-direction on a large frequency range as shown in Fig. 2. A polarizer was used to detect only TE polarized modes in the waveguide sense. Small line offsets between the farfields from different PhC-MCLEDs are observed because the vertical dimensions of the structure do not scale with a/λ as in a conventional band diagram. Analysis of the band diagram reveals that only three guided modes (I, II and III) with $k_i \approx 2.4$, 2.2 and 1.9, respectively, cause the observed diffraction lines labelled 1-3 in Fig. 2. The vertical mode profiles of these modes are plotted in Fig. 3.

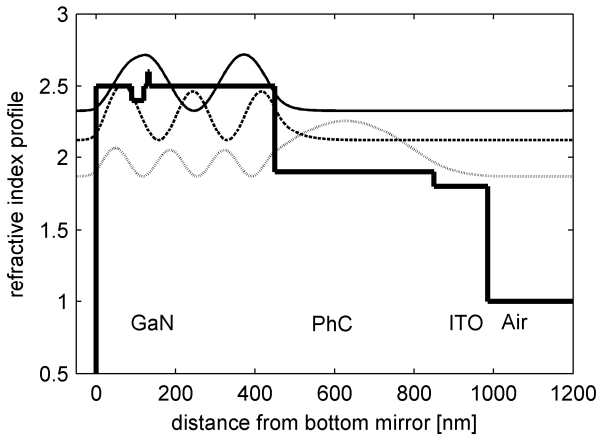

Fig. 3 Refractive index profile for the PhC-MCLED and calculated vertical mode profiles of the modes 1-3 (solid, dashed and dotted, respectively) causing the diffraction lines in Fig. 2. The vertical offset of the mode profiles corresponds to the calculated effective indices of the modes.

The dispersion of the modes is extracted from one farfield and by using Eq. 1 all other diffraction lines can be predicted. The predicted lines are superimposed in Fig. 2. At low frequencies a/λ~0.45-0.62 only first order diffraction is allowed and we observe line 1-3 caused by mode I-III together with line 1a. The latter line is caused by light in mode I diffracted by the nearest reciprocal lattice points ±60° off the measurement axis, also referred to as a B-type Bloch mode in [13]. Line 1b can be seen in a large frequency range from 0.62 to 1.2. This line is caused by second order diffraction (e.g. by $\vec{G} = G_0 \cdot (\vec{b}_1 + \vec{b}_2)$) with $|\vec{G}| = \sqrt{3} G_0$. Fig. 4 shows the azimuthally resolved farfield at a/λ~0.64. The shift of 30° of line 1b relative to line 1 proves that the former is caused by second order diffraction of the same mode I. In the same way it can be shown that line 1c, which appears at a/λ~0.95, is shifted 30° in the plane relative to line 1b (not shown) and that it is caused by third order diffraction with $|\vec{G}| = 2 \cdot G_0$, e.g. by $\vec{G} = G_0 \cdot 2 \cdot \vec{b}_1$. Finally, line 1d is identified as mode I diffracted by the fourth order with $|\vec{G}| = \sqrt{7} \cdot G_0$, e.g. by $\vec{G} = G_0 \cdot (2 \cdot \vec{b}_1 + \vec{b}_2)$. Second and third order diffraction of mode II can be observed for some frequencies (line 2b and 2c) whereas no high order diffraction is seen for mode III.

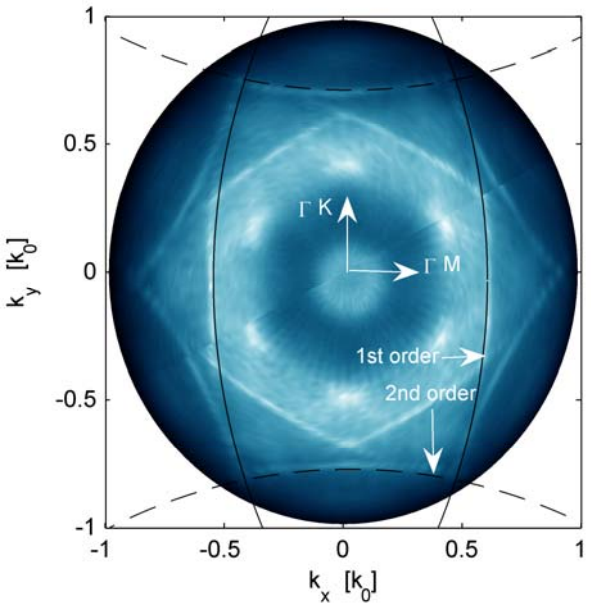

Fig. 4 Azimuthally resolved farfield of the emitted light (λ=475 nm) for a PhC-MCLED with a/ λ=0.644 nm (G =1.7) measured with a polarizer. Diffraction lines from first order and second order diffraction are shifted by 30°. For simplicity, only two predicted lines for each diffraction order are superimposed.

The identification of strong high order diffraction lines is very surprising because of its lower diffraction strength β (1/cm) given by the squared modulus of the Fourier transform of the PhC. To isolate the extraction efficiency of mode I by first and second order diffraction, respectively, we evaluate the farfield at a/λ=0.666 and θ=47° without using a polarizer. This exercise is indeed delicate, since every mode induces six diffraction lines per diffraction order into the azimuthal farfields as seen in Fig. 4 and Fig. 5. In order to get a reasonable comparison between the two diffraction orders, i.e. line 1 and line 1b, the line intensities have been measured for the same extraction angle θ as shown in Fig. 4, so that the effect of the Fabry Perot resonance is averaged out. At the frequency and extraction angle mentioned above, two first order lines cross each other exactly in the ΓK-direction and two second order lines cross each other in the ΓM direction as seen in Fig. 5. The doubled intensity at these points makes it easier to extract the line intensity from the background farfield. The extraction efficiency ratio between the first and second order lines is determined to be $\eta_1/\eta_2 = 1.6 \pm 0.2$ in favour of first order diffraction. There is a significant discrepancy between this measured extraction efficiency ratio and the theoretical diffraction strength ratio $\beta_1/\beta_2 = 8.0$.

IV. Theoretical Model

We explain this discrepancy with a model describing all losses of one guided mode where the in-plane degeneracy has been lifted. Each in-plane angle φ must be treated separately since the different diffraction orders are shifted by 30°. The extraction efficiency η_i by diffraction order i of the guided mode with an absorption coefficient α (1/cm) propagating in a sufficiently large photonic crystal is:

$$\eta_i(\varphi) = \frac{\beta_i}{\beta_i + \beta_j + \alpha} \tag{2a}$$

$$\eta_i(\varphi) = \frac{\beta_i}{\beta_i + \alpha} \tag{2b}$$

Eq. (2a) applies if two diffraction orders i and j are possible for one in-plane angle φ whereas Eq. (2b) applies if only one diffraction order i is possible for φ. The two different cases are shown in an Ewald diagram in Fig. 6. Using Eq. 2(a) we get the common assumption $\eta_i/\eta_j = \beta_i/\beta_j$ for light propagating with an in-plane angle where both diffraction orders are allowed. In the case where only one of the diffraction processes is allowed, however, Eq. (2b) applies and the extraction efficiency with order i does not depend on the diffraction strength of order j anymore. Despite its lower Fourier intensity, higher diffraction orders can then contribute substantially to the light extraction in a low absorption regime where $\beta_i > \alpha$. It should be noted that Eqs. 2 (a)-(b) are only valid as long as the net diffraction between different guided modes can be neglected, which is the case in our experiment where only three guided modes are present. In a substrate LED, on the other hand, there is a quasi-continuum of substrate modes and diffraction to these modes competes with diffraction to the radiating modes. Eq. 2(a) will always apply in the latter case and consequently, high order diffraction will play a minor role. Eqs. 2 (a)-(b) are valid only if the length scales (i.e $1/\alpha$ and $1/\beta_i$) are much smaller than the chip side length.

With the theoretical relation $\beta_1/\beta_2 = 8.0$ and the experimentally measured ratio $\eta_1/\eta_2 = 1.6$ applied to Eq. (2b), the absorption is calculated to be $\alpha = 0.75 \cdot \beta_2 = 0.09\beta_1$.

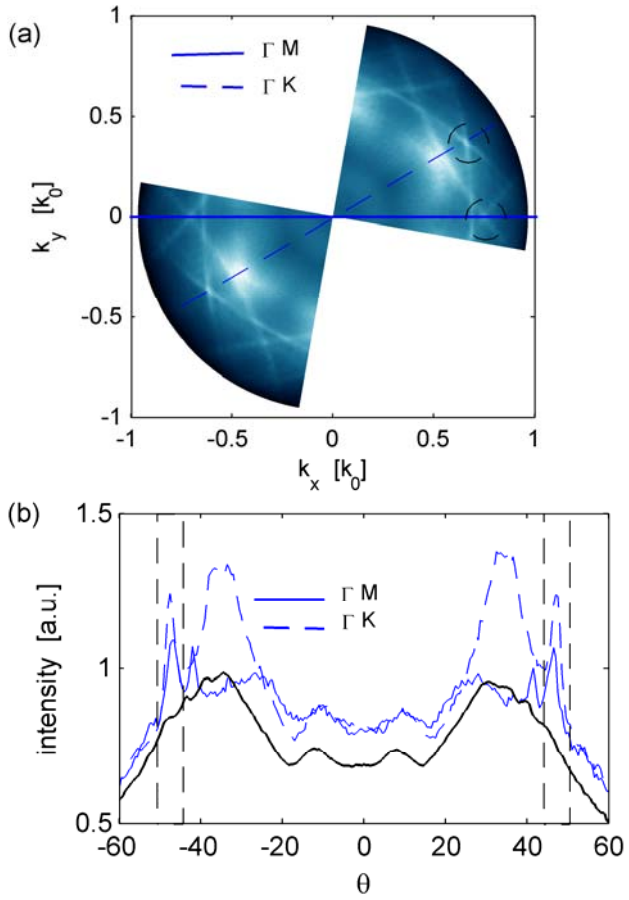

Fig. 5 : Slice of azimuthal farfield at λ=459 nm measured without a polarizer (a). The dashed and solid line shows the measurement axis used in b): Farfield in the ΓK-direction (dashed, 1st order) and ΓM-direction (solid, 2nd order). First and second order diffraction intensity is extracted by subtracting the background farfield (black) around θ=47° where two 1st order lines and two 2nd order lines intersect, see (a).

The use of Eq. (2b) is correct since the extracted line intensities were measured for φ for which only one of the two diffraction orders is allowed. The total extraction efficiency of the mode is then calculated by integrating over φ and we get $\eta_{mode} = 81\%$. This value is sensitive to variations in air filling factor of the PhC since the air filling factor changes the diffraction strength ratio between first and second order diffraction: a relative error of ±20% giving an $\eta_{mode} = 67 - 87\%$. Considering the overall efficiency of our devices, a number at the lower end of this range seems plausible. With the given ratio between the absorption coefficient and the diffraction strengths, the extraction efficiency of mode I is calculated as a function of G_0 with the help of Eqs. 1 and 2 (a)-(b) and is plotted in Fig. 1(b). The optimum is reached for G_0=1.7-1.9 for which all in-plane angles φ of the mode can be extracted by either first or second order diffraction or both of them. Accordingly, the two most efficient PhC-MCLEDs in Fig. 1(a) have G_0 within this range. Hence, the inherent lack of omnidirectionality of a hexagonal lattice for modes with $k_i > 2$ can be overcome by using two diffraction orders. From Fig. 1 (a) (G_0=1.2) and Fig. 2 (a/λ=0.95) we see that highest directionality is obtained experimentally when G_0 allows for both second and third order diffraction. The small difference in $|\vec{G}|$ between these diffraction orders results in omnidirectional diffraction into a smaller angle range, at the cost of a slightly lower efficiency as predicted in Fig. 1(b). These findings are summarized in Fig. 7. The calculated extraction efficiency of this mode in different propagation directions is plotted for three lattice constants. First order diffraction is maximized when the lattice constant is matched to the effective index of the mode (left) but cannot extract the light propating near the ΓK-direction. The use of two diffraction orders (center and right) enables omnidirectional light extraction.

Finally, the model is used to consider the two remaining modes. Only first order diffraction is observed for mode III in Fig. 2, since the hexagonal lattice diffracts omnidirectionally for $k_i = 1.9$. Hence, Eq. 2(a) applies and no second order diffraction is observed since $\eta_1 / \eta_2 = \beta_1 / \beta_2 = 8.0$. Second order diffraction of mode II (line 2b) is observed for a/λ>0.75. Below this frequency, also first order diffraction can extract this in-plane angle and accordingly, line 2b vanishes. The disappearance of line 2b is a strong indication of the validity of Eqs. 2 (a)-(b).

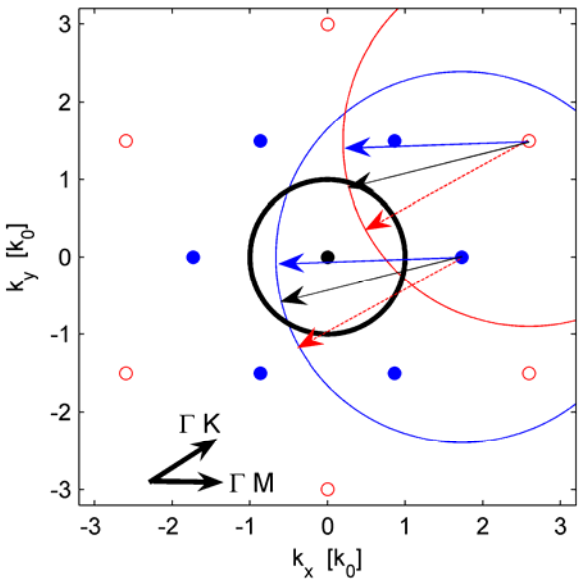

Fig. 6 Ewald diagram showing omnidirectional light extraction of mode I (k_i=2.4 and G=1.7) from the nearest (filled) and second nearest (open) reciprocal lattice points. In-plane k-vectors within the light extraction cone given by |k|<1 are extracted. The solid (dashed) k-vector is only extracted by first order diffraction (second order diffraction), i.e. Eq. 2(b) applies, whereas the black k-vector is diffracted by both the first and the second order and thus Eq. 2(a) applies.

The very small variation in emitted flux for different lattice constants (Fig. 1a) can now easily be understood. The contribution from second and third order diffraction results in

a rather weak dependency on the lattice constant as already seen in Fig. 1b for mode 1. Similar curves for mode 2 and 3 can be expected but with a minor shift of the maximum towards smaller lattice constants due to the lower effective index of these modes. The shifted maxima for the three modes weaken the dependency on the lattice constant even more.

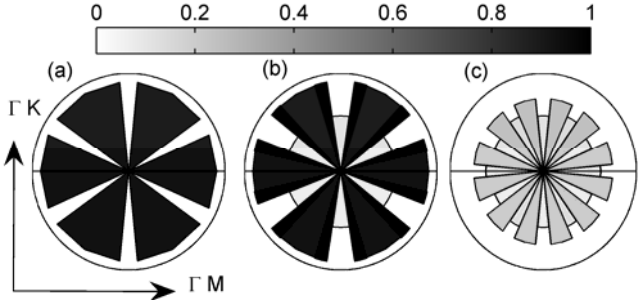

Fig. 7 Extraction efficiency of mode 1 with k_1=2.4 in the azimuthal plane for photonic crystals with G_0=2.4 (a), 1.7 (b) and 1.2 (c). The lengths of the pie slices are proportional to the extraction efficiency. The gray-scale corresponds to the relative diffraction strength β that depends on the extracting diffraction orders. The diffraction strength is strongest for the first diffraction order (a) and (b). Extraction of light propagating in the ΓK-direction requires second order diffraction (b) and (c).

V. AZIMUTHAL UNIFORMITY OF FARFIELDS

The omnidirectional diffraction with two diffraction orders should also result in a farfield with higher azimuthal uniformity than when only one diffraction order dominates. When first order diffraction dominates, local in-plane maxima for a fix θ are found in the ΓM-direction at in-plane angles, for which only one diffraction line exists. Additional maxima occur for larger extraction angles in the ΓM- or ΓK-direction where first order diffraction lines intersect. The situation is different at frequencies where second and third order diffraction dominate. In this case, diffraction occurs to approximately the same extraction angle θ from both symmetry directions. One could therefore expect a smaller contrast between the two symmetry directions. The combination of the first and the second order diffraction is less advantageous in this respect, since the two diffraction orders extract to different extraction angles. The azimuthal contrast $C_\varphi(\theta)$ is calculated as:

$$C_\varphi(\theta) = \frac{I(\theta)_{\Gamma K} - I(\theta)_{\Gamma M}}{I(\theta)_{\Gamma K} + I(\theta)_{\Gamma M}} \qquad (3)$$

Where $I(\theta)_{\Gamma K(\Gamma M)}$ is the measured farfield intensity at the angle θ along the ΓK direction (ΓM). We compare C_φ between G_0=1.9 where only first order diffraction is allowed and G_0=1.2 where the second and third order dominate. For the first order lattice $C_\varphi \in [-12,+12]\%$ depending on θ. For the PhC-MCLED with G_0=1.2 the azimuthal contrast is considerably reduced to $C_\varphi \in [0,+8]\%$. In conclusion, the use of a lattice constant between the second and third order gives high directionality of the emitted light in combination with omnidirectional light extraction and a more uniform farfield in the azimuthal plane.

VI. CONCLUSION

We have studied the PhC diffraction properties from thin GaN MCLEDs in which we observe only three guided TE modes. The implementation of the PhC leads to an enhancement in light extraction with a factor up to 1.8 and the directionality of the light is greatly improved with a radiant intensity enhancement factor 4.3.

By analyzing farfields with different lattice constants, we can identify diffraction lines of one mode from four diffraction orders and show that extraction of a guided mode with a hexagonal PhC is most efficient for a lattice constant where both first and second order diffraction contribute to the light extraction. This general conclusion holds for modes with $k_i > 2$ and a low absorption coefficient. A combination of second and third order diffraction gives almost equally efficient light extraction with higher directionality. The trends from the experimental results are explained by a model including absorption losses and where each in-plane angle of the guided modes is considered separately. The presented results point out a new direction in the choice of lattice towards the ideal single diffracted mode photonic crystal light-emitting diode.

During the review process, very high extraction efficiency to air with PhC-MCLEDs quite similar to ours was published in [14]. Considering these high extraction values, the mode absorption must be very low. According to our analysis, high order diffraction should then be able to contribute strongly to the light extraction efficiency. We note with interest that second order diffraction is visible also in their azimuthal farfields and that the highest extraction efficiency was achieved with devices near the second and third diffraction order for the low order modes.

APPENDIX A: CALCULATION OF THE FOURIER TRANSFORM OF THE PHOTONIC CRYSTAL

The diffraction strength β is proportional to the squared Fourier transform of the photonic crystal dielectric map [10]:

$$\beta \propto \tilde{\varepsilon}(G)^2 \qquad (4)$$

For circular holes, the Fourier transform can be calculated with Bessel functions:

$$\tilde{\varepsilon}(G) = F \cdot \frac{J_1(GR)}{GR} \qquad (5)$$

Here, F is the air filling factor of the PhC, J_1 is the first Bessel function of the first kind, G is the reciprocal wave-vector length and R is the radius of the holes. For a hexagonal lattice, the filling factor is given by:

$$F = \frac{2 \cdot \pi}{\sqrt{3}} \left(\frac{R}{a} \right)^2 \quad (5)$$

The relation between the lattice constant a and the reciprocal lattice constant G_0 is given by:

$$G_0 = \frac{4\pi}{\sqrt{3} \cdot a} \quad (5)$$

First (ΓM), second (ΓK) and third order ($2 \cdot \Gamma M$) diffraction corresponds to the reciprocal lattce vector lengths G_0, $\sqrt{3}G_0$ and $2 \cdot G_0$, respectively. The relative diffraction strength for the first three diffraction orders is shown in Fig. 8 as a function of the filling factor. The first order (ΓM) is eight times stronger than the second diffraction order (ΓK) at the filling factor 0.5. The first order is maximized for $F = 0.4$.

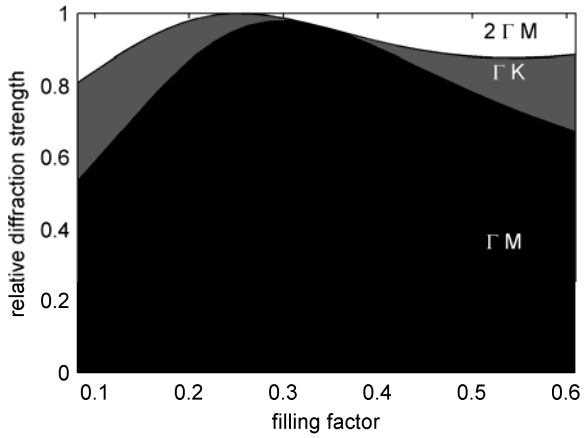

Fig. 8 Relative diffraction strength between the first three diffraction orders as a function of the air filling factor of the photonic crystal.

REFERENCES

[1] J. M. Phillips, M.E. Coltrin, M. H. Crawford, A. J. Fischer, M. R. Krames, R. Mueller-Mach, G. O Mueller, Y. Ohno, L. E. S. Rohwer, J. A. Simmons, J. Y. Tsao; "Research challenges to ultra-efficient inorganic solid-state lighting", Laser & Photon. Rev. 1 No 4, 307-333 (2007)

[2] S. Fan, P. R. Villeneuve, J. D. Joannopoulos ; "High extraction efficiency of spontaneous emission from slabs of photonic crystals", Phys. Rev. Lett. Vol. 78, No 17 (1997)

[3] R. K. Lee, Y. Xu, A. Yariv; "Modified spontaneous emission from a two-dimensional photonic bandgap crystal slab", J. Opt. Soc. Am. B 17(8), 1438-1442 (2000)

[4] M. Fujita, S. Takahashi, Y. Tanaka, T. Asano, S. Noda ; "Simultaneous Inhibition and Redistribution of Spontaneous Light Emission in Photonic Crystals", Science, Vol 308 1296-1298 (2005)

[5] M. Rattier, H. Benisty, E. Schwoob, C. Weisbuch, T. F. Krauss, C. J. M. Smith, R. Houdré, U. Oesterle, "Omnidirectional and compact guided light extraction from Archimedean photonic lattices", Appl. Phys. Lett. 83(7), 1283-1285 (2003)

[6] H. Benisty, J. Danglot, A. Talneau, S. Enoch, J. M. Pottage, A. David, "Investigation of Extracting Photonic Crystal Lattices for Guided Modes of GaAs-based Heterostructures", IEEE J. Quantum Electron. 44(8), 777-789 (2008)

[7] A. A. Erchak, D. J. Ripin, S. Fan, P. Rakich, J.D. Joannopoulos, E.P. Ippen, G. S. Petrich, L. A. Kolodziejski, "Enhanced coupling to vertical radiation using a two-dimensional photonic crystal in a semiconductor light-emitting diode", Appl. Phys. Lett. 78, 563-565 (2001)

[8] K. Bergenek, Ch. Wiesmann, H. Zull, R. Wirth, P. Sundgren, N. Linder, K. Streubel, T. F. Krauss, "Directional light extraction from thin-film resonant cavity light-emitting diodes with a photonic crystal", Appl. Phys. Lett. 93 231109 (2008)

[9] J. J. Wierer, M.R. Krames, J. E. Epler, N. F. Gardner, M. G. Craford, J. R. Wendt, J. A. Simmons and M. M. Sigalas, "InGaN/GaN quantum-well heterostructure light-emitting diodes employing photonic crystal structures", Appl. Phys. Lett. 84, 3885-3887 (2004)

[10] A. David, H. Benisty, C. Weisbuch, "Optimization of Light-Diffrating Photonic-Crystals for High Extraction Efficiency LEDs", J Display Technology Vol 3, No 2 (2007)

[11] A. David, T. Fujii, R. Sharma, K. McGroddy, S. Nakamura, S. P. DenBaars, E. L. Hu, C. Weisbuch and H. Benisty, "Photonic-crystal GaN light-emitting diodes with tailored guided modes distribution" , Appl. Phys. Lett. 88, 061124 (2006)

[12] C. Wiesmann, K. Bergenek, N. Linder, and U. T. Schwarz, "Photonic crystal LEDs - designing light extraction", Laser & Photon. Rev. 3(3), 262-286 (2009)

[13] A. David, C., Meier, R. Sharma, F.S. Diana, S. P. DenBaars, E. Hu, S. Nakamura, C. Weisbuch, H. Benisty; "Photonic bands in two-dimensionally patterned multimode GaN waveguides for light extraction", Appl. Phys. Lett., 87, 101107 (2005)

[14] J.J. Wierer, A. David, M. M. Megens, "III-nitride photonic crystal light-emitting diodes with high extraction efficiency", Nature Photon. 3, 163-169 (2009)

Krister Bergenek received the masters degree in engineering physics from Chalmers University of Technology, Göteborg, Sweden in 2006. He is with Osram Opto Semiconductors GmbH, Regensburg, Germany and he is working towards a Ph. D. degree at the University of St Andrews, St Andrews, Scotland. His research interests include modeling, design and fabrication of photonic crystal light-emitting diodes in the GaN and AlGaInP material system.

Christopher Wiesmann received the diploma in physics, in 2004 from University Regensburg, Regensburg, Germany. He was a PhD student working at Osram Semiconductors GmbH, Regensburg, Germany, from 2004 to 2008. Currently he is holding a position as development engineer at Osram OS. His research focuses on the simulation and design of photonic crystal light-emitting diodes.

Heribert Zull was born in Werneck, Germany, on February 7, 1967. He received the Dipl. Phys. and Ph.D. degrees in physics from the University of Wuerzburg, Germany, in 1993 and 1997, respectively. His graduate studies included device physics of quantum well/wire/box and microcavity structures, and the fabrication technologies of mesoscopic- and nano-structures using plasma etching with electron beam technology.
In 1996 he joined the opto semiconductor department of Siemens Semiconductors. Since 1999 he has been a development engineer at OSRAM Opto Semiconductors GmbH in Regensburg, Germany. His current work includes fabrication technologies for the development and manufacturing of LEDs and semiconductor lasers.
Dr. Zull is a member of the German Physical Society (DPG e.V.).

Christian Rumbolz received his physics diploma in 2003 from the University of Stuttgart. The diploma thesis dealt with the interaction of heavy, high-energetic ions with metal-silicon interfaces.
In 2004 he joined OSRAM Opto Semiconductors GmbH in Regensburg, Germany working on the development of blue laser diodes. Since 2007 he works for the process engineering department at Osram OS dealing with plasma etch and deposition processes.

Ralph Wirth received the diploma and doctor's degree in physics from University of Stuttgart, Germany, in 1996 and 1999, respectively.
In 1999 he joined OSRAM Opto Semiconductors, Regensburg, Germany, where he has been engaged in the development of light-emitting-diodes mainly in the red and yellow wavelength range, including thin-film LEDs and

resonant-cavity LEDs. Recently, he is focussing on the pre-development of new LED components for solid-state lighting and automotive applications.

Norbert Linder graduated in physics in 1990 and earned his Ph.D. degree in physics in 1996, both from the University of Erlangen-Nuremburg, Germany. From 1996 to 1998 he held a Feodor-Lynen fellowship from the Alexander-von-Humboldt foundation, Germany, and worked as a postgraduate researcher at the Physics department of the University of California, San Diego, investigating electron spin dynamics in semiconductor structures.
In 1998 he joined the R&D department at OSRAM Opto Semiconductors in Regensburg, Germany. Since then, he held various positions as project manager for the development of high-brightness LEDs and semiconductor lasers. In 2004, Dr. Linder became head of the device modelling group, which supports all R&D activities in OSRAM OS. His current interests are focused on the research and design of Nitride and Phosphide LEDs and laser diodes, with special emphasis on the application of nano-optical structures for light extraction and beam shaping. He has authored or co-authored more than 40 publications in scientific journals and numerous conference presentations. Dr. Linder is a member of the German Physical Society (DPG).

Klaus Streubel is Senior Director R&D at Osram Opto Semiconductors and head of the Conceptual Engineering department. He is responsible for the research and pre-development activities in the area of LEDs and Lasers at Osram OS. Dr. Streubel received his diploma and his PhD degree in Physics from the University in Stuttgart. For his PhD, he developed MOPVE systems and growth processes for InGaAs semiconductors. He spent two years as a post doc at the Swedish Institute of Microelectronics in Stockholm, where he was involved in the development of semiconductor lasers. In 1993, Dr. Streubel took a permanent position at the Royal Institute of Technology (KTH) in Stockholm, where he received a lecturer certificate and was appointed as adjunct professor. At KTH he led and grew the long wavelength vertical cavity laser group and started a successful collaboration with the University of California in Santa Barbara.
In 1997, Dr. Streubel switched from academic to industrial research. The following two years, he developed vertical cavity lasers and resonant-cavity LEDs at Mitel Semiconductors in Järfälla, before he joined Osram Opto Semiconductors in Regensburg, Gemany in 1999. At Osram he took the responsibility for the development of AlGaInP devices and initiated the implementation of thin-film technology for high-brightness LEDs. Since 2006, Dr. Streubel is heading the Conceptual Engineering department at Osram OS, where he is responsible for all aspects of research and development in the field of LEDs and Lasers. In 2004 Dr. Streubel and his team were awarded with the Osram Innovation Award for his work on AlGaInP LEDs. In December 2007, he was awarded with the German Future Price of the German Federal President for the innovation of thin-film LEDs.

Thomas F. Krauss obtained a Dipl.-Ing. in Photographic Engineering (FH Koeln, Germany) in 1989 based on a diploma thesis conducted at IBM, Yorktown Heights, USA in the area of Excimer Laser Ablation. Following a PhD in the area of semiconductor ring lasers at the University of Glasgow (1992), he initiated the field of semiconductor photonic crystals in the UK. He gained SERC (1993) and Royal Society (1995) Research Fellowships in support of this work and has since established a reputation worldwide, as evidenced by the large number of invited talks he presents at international level (10-12 such presentations per year) He is grant holder of several EPSRC, EU and industrially sponsored research projects, coordinated EU-FP5 "PICCO" and leads the current EU-FP6 "SPLASH", both studying fundamental and applied aspects of photonic crystals.
His research interest is the study of optical nanostructures and how they can be used to control the emission and propagation of light. This includes studying microemitters for optical interconnects in "SpeckNets", slowing down light to enhance nonlinear effects, using diffractive optics for enhanced emission from LEDs as well as optically trapping bioparticles in photonic nanoresonators.
He collaborates strongly in Europe, especially through the EU-FP6 "epixnet" network and overseas, with the Australian CUDOS consortium. His 15-strong group operate the nanofabrication facility at St. Andrews, including electron beam and photolithography, wet and dry etching, thin film deposition as well as a characterisation suite for active and passive microphotonic devices. Prof Krauss was elected a Fellow of the IoP (2001) and the Royal Society of Edinburgh (2002).

Paper VI

Theoretical Investigation of the Radiation Pattern from LEDs Incorporating Shallow Photonic Crystals

Christopher Wiesmann, Krister Bergenek, Romauld Houdré, Ross P. Stanley, Norbert Linder and Ulrich T. Schwarz

Accepted for publication in IEEE Journal of Quantum Electronics
on 14 May 2009

Theoretical Investigation of the Radiation Pattern from LEDs Incorporating Shallow Photonic Crystals

Christopher Wiesmann, Krister Bergenek, Romuald Houdré, Ross P. Stanley, *Member*, *IEEE*, Norbert Linder, and Ulrich T. Schwarz

***Abstract*—A theoretical approach based on coupled mode theory is presented in order to determine the radiation pattern of light emitting diodes (LEDs) incorporating a shallow photonic crystal (PhC). From this, a fundamental limit for the directionality of the diffraction of a single guided mode is given. Additionally, the Fabry-Perot resonances are shown to have significant impact on the directionality of diffracted light. For a realistic green emitting InGaN LED in thin-film configuration the optimum reciprocal lattice vector is derived in terms of absolute diffracted intensity and directionality within a limited acceptance angle. The latter can be as high as 1.8 times the directionality of a Lambertian emitter. Furthermore, the spontaneous emission distribution between guided modes heavily influences the diffracted intensity.**

***Index Terms*—Coupled mode theory, diffraction, light emitting diodes, photonic crystals.**

I. INTRODUCTION

IN recent years considerable work has been carried out to enhance the low extraction efficiency of semiconductor light emitting diodes by using photonic crystals [1]-[12]. The extraction efficiency of LEDs is limited to 2-4% per facet – depending on the material system – due to total internal reflection occurring at the planar semiconductor-to-air interface. Commercially, two solutions are typically used to overcome this limitation. Firstly, light is coupled out of all six facets of the chip. For highly transparent substrates and tilted angles between the facets extraction efficiencies of up to 50% have been demonstrated [13]. Secondly, roughening the top facet enables extraction of light regardless of its incident angle and additionally, redistributes the reflected light. Along with a mirror on the opposite side [14] high extraction efficiencies of up to 75%-80% have been realized [15], [16] in this so called thin-film configuration.

By applying photonic crystals (PhCs), light extraction enhancements of about 2.6 have been achieved [11]. Furthermore, shaping of the LED's radiation pattern by PhCs with different lattice constants has been demonstrated [3]. Thereby, the directionality can be improved, where directionality refers to the amount of light being emitted into an angle θ to the surface normal with respect to the overall emitted light. This is of particular interest for coupling the light of a LED into an optical system with limited acceptance angle, e.g. a light engine of projection devices or automotive headlamps [17].

The presented theoretical approach determines the radiation pattern resulting from diffraction of guided modes while taking into account the properties of the PhC such as lattice type, pitch, filling fraction and etch depth. As the demand on computation time is low, a wide range of parameter variations can be carried out. Additionally, a clear insight into the basic mechanisms determining the radiation pattern is possible.

We start in section II from Bragg's Law and consider the diffraction of a single guided mode based on an Ewald-like geometrical construction. This allows us to estimate some limits for the directionality. Then the influence of additional guided modes on the far field is studied. In section III, coupled mode theory is used to derive the factors determining the radiation pattern of a PhC LED while taking into account cavity effects. Afterwards, results from our model are compared to other methods and references are summarized containing a comparison between our model and experimental data. In section V, we investigate the impact of radiative modes and calculate the far field of a GaN-based green emitting LED incorporating a hexagonal PhC in dependence of the primitive reciprocal lattice vector and the distribution of spontaneous emission between the guided modes.

For our study, we choose a green emitting InGaN LED in thin-film configuration as depicted in Fig. 1 for two reasons. On the one hand, the variations of the refractive index in

Manuscript received January 22, 2009.

Ch. Wiesmann is with OSRAM Opto Semiconductors, 93055 Regensburg, Germany and University Regensburg, 93040 Regensburg, Germany (e-mail: christopher.wiesmann@osram-os.com).

K. Bergenek is with OSRAM Opto Semiconductors, 93055 Regensburg, Germany and University of St Andrews, St. Andrews, Fife KY16 9SS, United Kingdom.

R. Houdré is with Institut de Photonique et Electronique Quantique, Faculté des Sciences de Base, Station 3, EPFL, CH 1015 Lausanne, Switzerland.

R. P. Stanley is with Centre Suisse d'Electronique et de Microtechnique SA, CH-2002 Neuchâtel, Switzerland.

N. Linder is with OSRAM Opto Semiconductors, 93055 Regensburg, Germany.

U. T. Schwarz is with University Regensburg, 93040 Regensburg, Germany.